

THE UNIVERSITY OF HULL  
DEPARTMENT OF CHEMISTRY

**Antiferroelectricity and Related Chirality Induced Frustrations  
in Smectic Liquid Crystals: Effect of Molecular Structure**

Being a Thesis submitted for the Degree of Doctor of Philosophy

in the University of Hull

by

Alexey S Petrenko, MSc (Kharkov National University, Ukraine)

October 2002

## Summary

This work was devoted to synthesis of new antiferroelectric liquid crystalline materials in series of chiral 1-methylheptyl 4'-(4-n-alkyloxybenzoyloxy)biphenyl-4-carboxylates. 9 new types of materials were synthesised and their chemical, mesomorphic and electrooptical properties were investigated in the homologous series.

The chemical structure of each material synthesised was proved through <sup>1</sup>HNMR and IR spectroscopy studies, mass spectrometry, optical rotation measurements and analytical HPLC technique.

The mesomorphic properties of the final products were investigated by the DSC method and textural observations in polarising light microscope. The electrooptical experiments were done in thin planar cells by applying AC triangular wave field of various voltages and frequencies. The electrooptical response measured was plotted as a function of the external voltage and the resulting curves were analysed in detail.

Apart from the investigation into mesomorphic behaviour of the compounds prepared, the effect of V-shaped switching was described for some of the homologues. The switching parameters were determined and conclusions were reached on the origins of the V-shaped electrooptical response.

The studies on a new type of the twist grain boundary phase with local antiferroelectric structure were described in separate chapter.

### Acknowledgements

I would like to express my sincere gratitude to Professor J. W. Goodby for his most inspired supervision during my time at the University of Hull.

I wish to thank Dr M. Hird for his advice on liquid crystal synthesis. My thanks also go to Professor K Toyne, Dr A Hall and Dr RA Lewis for the fruitful discussions on solving most difficult synthetic problems. I would like to thank Mrs Julie Haley and Mrs Brenda Worthington for providing technical assistance, chromatography and spectral analyses.

I am most grateful to my friends at the University of Hull who were supportive, helpful and really enjoyable company over all these years: Mark Godber and Jon West. I also would like to mention my fellow students Tim Bilson, Dr Simon Lumsdon, Dr A Eastwood, Dr C Ledger and Dr G Cosquer. I wish you all the very best.

Special thanks go to Mrs Aileen Partanen who became my UK-based auntie.

I wish to express my appreciation to the University of Hull and DERA (Malvern) for their financial support.

Finally, I thank my wife and my parents for their love.

## Contents

<b>1</b>	<b>Introduction.....</b>	<b>6</b>
1.1	<i>Solid antiferroelectrics.....</i>	6
1.2	<i>Ferroelectric and antiferroelectric properties of liquid crystals.....</i>	14
1.2.1	Symmetry and spontaneous polarization in the chiral smectic C* phase.....	14
1.2.2	Soft-mode and Goldstone mode.....	16
1.2.3	Antiferroelectric smectic C <sub>A</sub> * phase.....	18
1.2.3.1	Experimental observations.....	18
1.2.3.2	Ferrielectric sub-phases.....	20
1.2.3.3	“Forbidden” reflections in the antiferroelectric and ferrielectric smectic C phases.....	23
1.2.3.4	Symmetry of the antiferroelectric smectic C <sub>A</sub> * phase.....	25
1.3	<i>Microscopic origins of anticlinic and synclinic ordering in smectic phases.....</i>	27
1.3.1	Stabilization of the alternating tilt between smectic layers.....	27
1.3.2	Molecular theories of the smectic C phases.....	34
1.3.2.1	Introduction.....	34
1.3.2.2	Model of transverse dipoles.....	36
1.3.2.3	Wulf’s steric model.....	40
1.3.2.4	Comparison of the theory with experiment.....	42
1.3.2.5	Model of induced dipoles interaction.....	46
1.3.2.6	Concept of the ordered electricity in the quadrupole systems.....	49
	References (sections 1.1 – 1.3).....	51
1.4	<i>Structures of compounds, which exhibit antiferroelectric phases.....</i>	56
	<i>References (section 1.4).....</i>	69
<b>2</b>	<b>Aims.....</b>	<b>71</b>
<b>3</b>	<b>Experimental and synthetic methods.....</b>	<b>76</b>
3.1	<i>Description of the techniques and apparatus.....</i>	76
3.1.1	General synthetic procedures.....	76
3.1.2	Characterization of materials.....	77
3.2	<i>Preparation of the materials.....</i>	79
3.2.1	Preparation of 4- <i>n</i> -alkoxy and 4- <i>n</i> -alk- $\omega$ -enylbenzoic acids <b>3-11</b> .....	79
3.2.2	Preparation of 2,3-difluoro-4- <i>n</i> -alkyl or 4- <i>n</i> -alk- $\omega$ -enylbenzoic acids <b>19-26</b> .....	81
3.2.3	Preparation of the key intermediates.....	86
3.2.3.1	Synthesis of the ( <i>R</i> )-1-methylheptyl 4'-hydroxybiphenyl-4-carboxylate <b>31</b> .....	86
3.2.3.2	Preparation of ( <i>S</i> )-1-methylheptyl 2-(4-hydroxyphenyl)pyrimidine-5-carboxylate <b>41</b> .....	89
3.2.3.3	Preparation of ( <i>S</i> )-1-methylheptyl 2,3-difluoro-4-hydroxybiphenyl-4'-carboxylate <b>47</b> and ( <i>S</i> )-1-methylheptyl 2-(2,3-difluoro-4-hydroxyphenyl) pyrimidine-5-carboxylate <b>51</b> .....	94
3.2.4	Preparation of final products.....	99
3.2.4.1	Preparation of compounds of general structure 1: ( <i>R</i> )-1-methylheptyl 4'-(4- <i>n</i> -alkoxy benzoyloxy)biphenyl-4-carboxylates <b>52-54</b> .....	99
3.2.4.2	Preparation of compounds of general structure 2: ( <i>R</i> )-1-methylheptyl 4'-(4-alkoxy-2,3-difluorobenzoyloxy)biphenyl-4-carboxylates <b>56-60</b> .....	101
3.2.4.3	Compounds of general structure 3: ( <i>S</i> )-1-methylheptyl 4'-(4-alk- $\omega$ -enyloxybenzoyl oxy)biphenyl-4-carboxylates <b>61-63</b> .....	102
3.2.4.4	Preparation of compounds of general structure 4: ( <i>S</i> )-1-methylheptyl 4'-(4-alk- $\omega$ -enyloxy-2,3-difluoro benzoyloxy)biphenyl-4-carboxylates <b>64-66</b> .....	103
3.2.4.5	Preparation of compounds of general structure 5: ( <i>S</i> )-1-methylheptyl 4'-{4-[ $\omega$ -(1,1,3,3,3-pentamethyldisiloxanyl)- or ( $\omega$ -1,1,3,3,5,5-heptamethyl)trisiloxanyalkoxy]benzoyl oxy} biphenyl-4-carboxylates <b>67-71</b> .....	104
3.2.4.6	Preparation of compounds of general structure 6: ( <i>S</i> )-1-methylheptyl 4'-{4-[ $\omega$ -(1,1,3,3,3-pentamethyldisiloxanyl)alkoxy]benzoyloxy} biphenyl-4-carboxylates <b>72-74</b> .....	106
3.2.4.7	Preparation of compounds of general structure 7: ( <i>S</i> )-1-methylheptyl 2-[4-(4-alkoxybenzoyloxy)phenyl]pyrimidine-5-carboxylates <b>75-79</b> .....	107

3.2.4.8	Preparation of compounds of general structure 8: ( <i>S</i> )-1-methylheptyl 4'-(4-alkoxybenzoyloxy)-2', 3'-difluorobiphenyl-4-carboxylates <b>80-84</b> .....	108
3.2.4.9	Preparation of compounds of general structure 9: ( <i>S</i> )-1-methylheptyl 2-[4-(4-alkoxybenzoyloxy)-2,3-difluorophenyl] pyrimidine-5-carboxyates <b>85-88</b> .....	109
	<i>References (Section 3)</i> .....	110
<b>4</b>	<b>Results and discussion</b> .....	<b>111</b>
4.1	<i>Aromatic cores based on the biphenyl fragment</i> .....	111
4.1.1	Compounds of general structure 1: ( <i>R</i> )-1-Methylheptyl 4'-(4- <i>n</i> -alkoxybenzoyloxy) biphenyl-4-carboxylates, <b>52-54</b> .....	111
4.1.2	Compounds of general structure 2: ( <i>R</i> )-1-methylheptyl 4'-(4-alkoxy-2,3-difluoro benzoyloxy)biphenyl-4-carboxylates, <b>56-60</b> .....	119
4.2	<i>Introduction of the terminal double bond/siloxane unit into the non-chiral alkyl chain</i> .....	124
4.2.1	Compounds of general structure 3, ( <i>S</i> )-1-methylheptyl 4'-(4-alk- $\omega$ -enyloxybenzoyl oxy)biphenyl-4-carboxylates <b>61-63</b> , and general structure 4, ( <i>S</i> )-1-methylheptyl 4'-(4-alk- $\omega$ -enyloxy-2,3-difluorobenzoyloxy) biphenyl-4-carboxylates <b>64-66</b> .....	124
4.2.2	Compounds of general structure 5 ( <i>S</i> )-1-methylheptyl 4'-{4-[ $\omega$ -(1,1,3,3,3-pentamethyl disiloxanyl)alkoxy-2,3-difluoro]benzoyloxy} biphenyl-4-carboxylates <b>67-71</b> and general structure 6 ( <i>S</i> )-1-methylheptyl 4'-{4-[ $\omega$ -(1,1,3,3,3-pentamethyl disiloxanyl)alkoxy-2,3-difluoro] benzoyloxy} biphenyl-4-carboxylates <b>72-74</b> .....	131
4.3	<i>Modifications of the central part of the aromatic core</i> .....	136
4.3.1	Compounds of general structure 7: ( <i>S</i> )-1-methylheptyl 2-[4-(4-alkoxybenzoyl oxy)phenyl] pyrimidine-5-carboxylates <b>75-79</b> .....	136
4.3.2	Compounds of general structure 8: ( <i>S</i> )-1-methylheptyl 4'-(4-alkoxybenzoyloxy)-2',3'-difluorobiphenyl-4-carboxylates <b>80-84</b> and general structure 9 ( <i>S</i> )-1-methylheptyl 2-[4-(4-alkoxybenzoyloxy)-2,3-difluoro phenyl] pyrimidine-5-carboxyates <b>85-88</b> .....	141
	<i>References (section 4)</i> .....	148
<b>5</b>	<b>V-shaped electrooptical response in the smectic C* phase</b> .....	<b>149</b>
5.1	<i>Theoretical description of the problem</i> .....	149
5.2	<i>Results of the electrooptical studies in selected homologues of compounds of general structure 1-9</i> .....	166
	<i>References (section 5)</i> .....	182
<b>6</b>	<b>Twist grain boundary phase with local antiferroelectric structure</b> .....	<b>184</b>
6.1	<i>Introduction</i> .....	184
6.2	<i>Transition temperatures</i> .....	187
6.3	<i>Differential scanning calorimetry</i> .....	188
6.4	<i>Defect textures</i> .....	189
6.5	<i>Miscibility studies</i> .....	192
6.6	<i>Electrical field studies</i> .....	194
6.7	<i>The model</i> .....	196
	<i>References (section 6)</i> .....	198
<b>7</b>	<b>Conclusions</b> .....	<b>199</b>

# 1 Introduction

## 1.1 Solid antiferroelectrics

The conventional definition of an **antiferroelectric** in solid state physics is given as an antipolar crystal where the free energy is comparable to that of the ferroelectric modification<sup>1</sup> of the same crystal, and which therefore may be switched from an antipolar state to ferroelectric state by the application of the electric field [1]. The antipolar arrangement of charged particles in a crystal lattice was first discussed by Kittel [3] and latter observed experimentally in lead circonate ( $\text{PbZrO}_4$ ) [4]. According to Kittel an antiferroelectric is a crystal in which ionic chains are polarized spontaneously, and in which adjacent chains of ions of the opposite kind are polarized in the opposite direction, so that the bulk spontaneous polarization is zero. A typical feature of antiferroelectric materials is a characteristic shape of polarization response to an applied electric field, as shown in figure 1.1c. Unlike most dielectrics that show a Langevin-type response to an external electric field [5] (figure 1.1a), antiferroelectric and ferroelectric materials possess a spontaneous polarization (**Ps**) which gives rise to a non-linear shape of the P-E response, which is called hysteresis (see figure 1.1b and c).

In the absence of an electric field, typically the structure of a ferroelectric material is broken into two types of the domains where the polarization vectors point in opposite directions. Therefore, the total **Ps** of the bulk structure is zero (see figure 1.1b, point **O**)<sup>2</sup>. An electric field applied reverses the direction of the opposing polarization domains giving rise to a uniform structure with a finite **Ps** value (point **A**). At the point **B** the saturation value of polarization is reached as all domains are aligned along the

---

<sup>1</sup> A material is said to be ferroelectric when it has two or more orientational states in the absence of an electric field and can be shifted from one to another of these states by an electric field. Any two of orientational states are identical in crystal structure and differ only in electric polarization vector at null electric field [2].

<sup>2</sup> It should be noted that a multidomain system will also have zero polarization, this is generally the case for most materials

electric field. The single domain structure remains thermodynamically stable even when the electric field is switched off (point **H**). At this point the polarization is said to be spontaneous and it is defined to be in a positive direction. This point is thus the retained or remnant polarization ( $P_r$ ) at zero applied field. Its sign can be reversed by applying a negative electric field and reorienting all the domains (at point **D**). The hysteresis loop formed by this process passes through points **C** and **F** at zero polarization. This point is called the coercive field  $E_c$  and is measure of the stability of the ferroelectric structure.

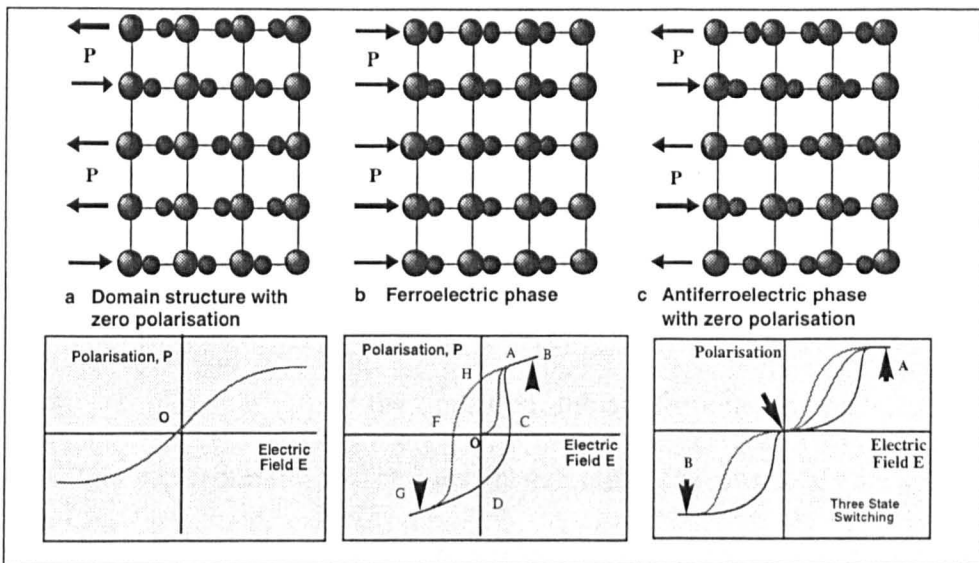


**Figure 1.1** Different shapes of P–E function.

In the case of antiferroelectrics at zero electric field the antipolar arrangement of the domains again produces a zero macroscopic polarization (figure 1.1c). It is different from the random domain structure of a ferroelectric in a sense that the latter is a macroscopic phenomenon [1]. It is still possible to produce a spontaneous polarization by reorienting all the domains along an electric field. However, relaxation processes lead to a transition to the initial antipolar structure. The corresponding hysteresis loop of the **P–E** response is shifted from the origin **O** and duplicates when both directions of the electric field are considered.

Antiferroelectric can be thus regarded as consisting of two ferroelectric sub-lattices with their spontaneous polarizations pointing in opposite directions, and which penetrate each other thereby forming a macrostructure with zero bulk spontaneous polarization. The spontaneous polarizations of the sub-lattices are proposed to be produced by the same groups or dipoles as those in the sub-lattices of the ferroelectric phase of similar energy [1].

Analogous with ferroelectrics, antiferroelectrics are classified by the type of the phase transition which it is formed from on cooling the high temperature paraelectric phase. A *proper* antiferroelectric is classified by a transition where the spontaneous polarization associated with the sub-lattices is the order parameter (or the driving force for the transition). Alternatively, when  $P_s$  passively follows some other order parameter or is a part of more complex make up of the transition, the antiferroelectric phase is said to be *improper*. The experimental difficulties in detecting the onset of the spontaneous polarization in the sub-lattices of an antiferroelectric do not allow for the construction of a theory in which the spontaneous polarization,  $P_s$ , plays a primary role. From this point, proper antiferroelectrics are still to be discovered and until now remain an elegant model [6].

Generally, antiferroelectrics can be divided into *displacive* and *order-disorder* classes, again with analogy to ferroelectrics [6]. In displacive ferroelectrics the spontaneous polarization is a result of the displacement of ions from their equilibrium positions in the paraelectric phase. This class of compounds is represented by crystals, which have a strong ionic bond between, as well as within, the constituent particles. In turn, when a substance consists of molecules containing dipolar groups, which are connected by covalent bonds within the molecule and by ionic bonds to the dipole groups of other

molecules, the displacive mechanism may not operate. Crystals of this type have several equilibrium positions of the permanent dipoles, which are all random in the paraelectric phase. At the transition to the ferro- or antiferroelectric phase the dipole re-organisation takes place, giving rise respectively to a polar or antipolar macroscopic structure. This type of phase transition is called order-disorder transition (order-disorder antiferroelectrics).

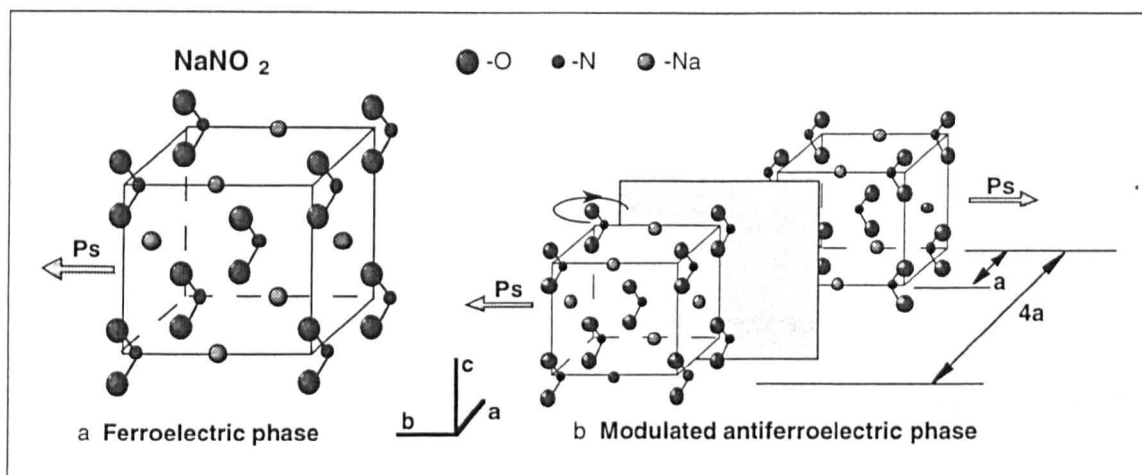


**Figure 1.2** Anti- and ferro-electric phases of sodium nitrite

A good example, that demonstrates the onset of ferroelectricity and antiferroelectricity in solids via an order-disorder transition, is crystalline sodium nitrite. In the paraelectric phase the orientation of  $\text{NO}_2^-$  groups are random along the polar  $b$ -axis shown in figure 1.2 [7]. At  $164.7^\circ\text{C}$  the paraelectric phase transforms to a modulated antiferroelectric phase in which the spontaneous polarization continuously changes its direction when passing from one unit cell to another along the  $a$ -axis as shown in figure 1.2b. The period of such modulated structure is  $8a$ , so the sign of spontaneous polarization alternates every  $4a$  step along  $a$ . The transition from the antiferroelectric to ferroelectric phase occurs at  $163.4^\circ\text{C}$ , at which point all of the nitrite ions align along  $b$  direction, see figure 1.2a. The fact that the transition is not governed by the condensation of any vibrational modes present, was confirmed by IR and Raman spectroscopy [7]. Flipping nitrite ions alone, which are statistically distributed in the paraelectric phase and highly

ordered in the ferroelectric and antiferroelectric phases, is responsible for the appearance of the spontaneous polarization.

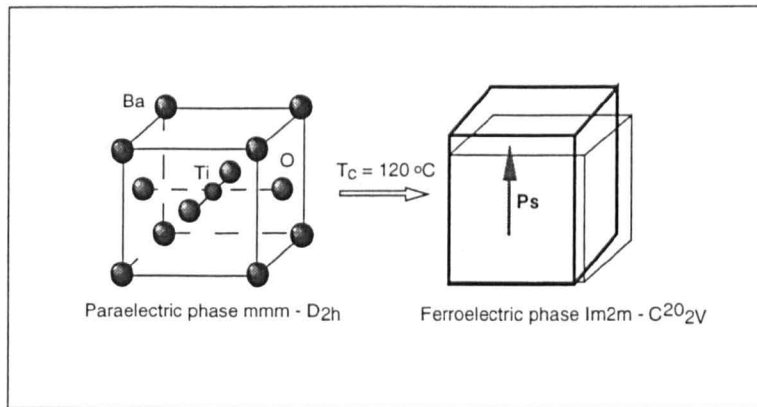


**Figure 1.3** Structure of ferroelectric BaTiO<sub>3</sub>.

The transition to the ferroelectric phase belongs to the group of *ferroic* transitions [8] for which the symmetry group of the high temperature phase does not coincide with the symmetry group of the low-temperature ordered phase. Both displacive and order-disorder transitions are always accompanied by a lowering of the symmetry. In the case of order-disorder ferroelectricity found for sodium nitrite the symmetry of the paraelectric phase, mmm or D<sub>2h</sub>, is reduced to Im2m (C<sup>20</sup><sub>2v</sub>) in the ferroelectric phase [9]. As the symmetry does not change continuously at the phase transition, it is said to become spontaneously broken. For example, during the displacive transition from the paraelectric phase found in barium titanate to the ferroelectric phase which is schematically shown in figure 1.3 the symmetry of the structure changes abruptly from cubic to tetragonal as a result of the condensation of the polar soft-mode [10].

In general, the association of a particular physical property with the symmetry of a crystal can be determined in terms of two fundamental concepts. First, the Curie principle is related to field forces such as electric field or mechanical deformation. It states that a crystal acted upon by an external force retains only those symmetry

elements, which are compatible with the symmetry of that force. Any effects, which occur in a crystal as a result of application of an external force, should also be a subject of this principle [11]: when certain actions produce certain effects, the symmetry elements of the actions must be found in the effects produced.

The second principle developed by Neumann last century [12] says that object will possess an intrinsic property only if its symmetry is the same or lower than that of the physical property. The schematic representation of the last statement is depicted in figure 1.4. Both principles are complementary to each other and together establish the symmetry relationships between a property, the object possessing this property, and a force, which induces the property.

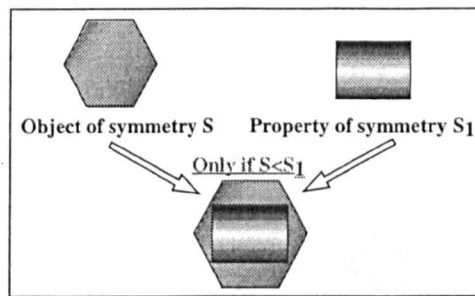


**Figure 1.4** Visualisation of Neumann's principle.

A physical property as well as an external force, which produces it, can be visualised as an object of certain symmetry. The 32 crystal classes are not applicable here as they describe discrete lattices. Forces like stress or electric field belong to continuous symmetries and are described by the seven continuous Curie groups shown in figure 1.5 [13]:

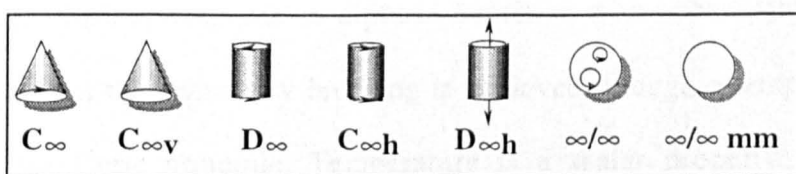


**Figure 1.5** Graphic re-presentation of the seven Curie groups

An electric field has the symmetry of a polar vector,  $C_{\infty v}$  and according to the Curie principle the corresponding polarization induced in a material should belong to the same symmetry group. Thus, to exhibit a spontaneous polarization the symmetry of the material should include a polar axis along which a physical property shows directionality [14]. A polar axis is incompatible with centre of symmetry and, thus, only non-centrosymmetric groups have the possibility of a spontaneous polarization "built in" to their structures. This conclusion can also be reached by applying Neumann's principle to the 32 crystal point groups. Only those with symmetries lower, or the same as  $C_{\infty v}$ , allow for the possibility of possessing a spontaneous polarization. Ten out of 32 space groups satisfy Neumann's condition and, not surprisingly, all of them do not possess a centre of symmetry, see figure 1.6.

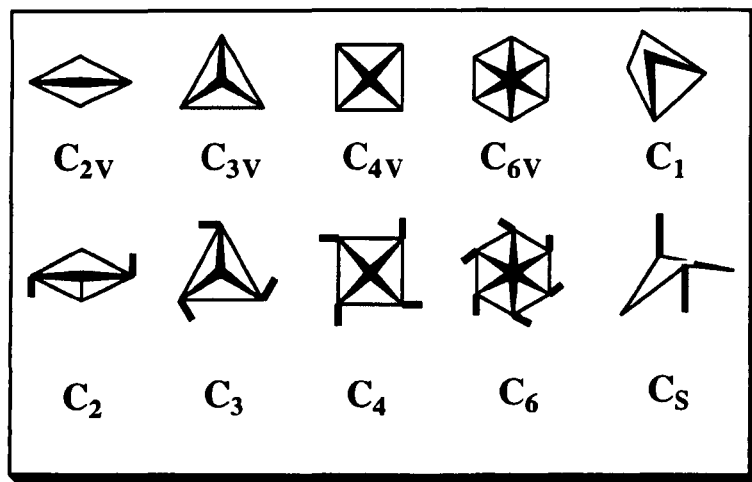


**Figure 1.6** The point groups with a "built-in" spontaneous polarization.

Non-centrosymmetric point groups constitute the class of pyroelectric materials. A spontaneous polarization can appear in a material below a certain temperature (Curie temperature), which corresponds to a phase transition with accompanying symmetry breaking. The fact that symmetry breaking is achieved through a temperature change contradicts the Curie principle. Temperature is a scalar property with spherical symmetry ( $\infty/m\infty$ ) [15], so therefore it cannot cause any symmetry lowering which is

incompatible with its own symmetry. This paradox is resolved by the well-known phenomenon of domain formation, which accompanies any symmetry breaking phase transition. The symmetry of each domain formed at the transition is lower than in the high temperature phase, however the arrangement of the domains occurs along the symmetry elements lost at the transition [16]. Hence, the symmetry of the whole material remains unchanged. When the polarization associated with each domain is switched by an external electric field the material becomes ferroelectric and Curie principle is fully satisfied. The single domain structure has symmetry elements, which are lower than that of an applied electric field ( $C_{\infty v}$ ).

## 1.2 Ferroelectric and antiferroelectric properties of liquid crystals

### 1.2.1 Symmetry and spontaneous polarization in the chiral smectic C\* phase

Symmetry considerations were a starting point in the theoretical prediction of ferroelectric properties in liquid crystals [17]. Simple liquid crystal phases represent a special type of continuous medium and their symmetry is described using the Curie groups [18], e.g. nematic and smectic A belong to  $D_{\infty h}$  group. The tilted phases possess somewhat more complex structures and their symmetry may be related to one of the crystal point groups. The symmetry of smectic C phase belongs to the  $C_{2h}$  point group, which includes the following symmetry elements: a centre of symmetry,  $C_2$  axis and a mirror plane perpendicular to the two-fold axis.

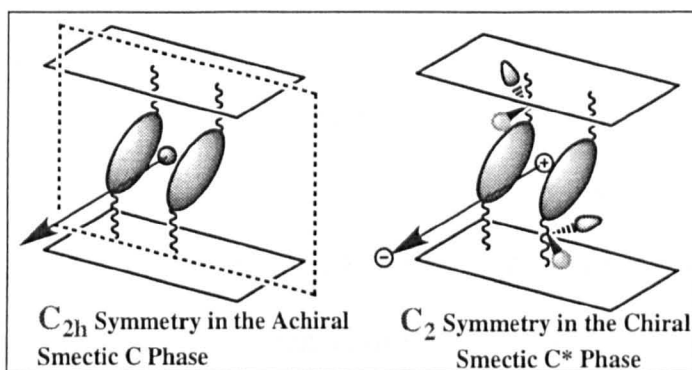


**Figure 1.7** Symmetry elements of the non-chiral and chiral smectic C phases

This phase is neither ferroelectric nor pyroelectric. However, when the molecules, which constitute the phase, are chiral the symmetry of the phase is lowered and the centre of symmetry and the mirror plane are no longer allowed operations, see figure 1.7. Hence, the chiral smectic C phase may have a spontaneous polarization, which develops in either direction along the  $C_2$  axis, thus Neumann's principle is then satisfied. The same is essentially true for other chiral tilted smectic phases, e.g. smectic I\* and F\*.

In order to exhibit a spontaneous polarization the lateral components of the molecular dipoles parallel to the layer planes should couple with one another. It is believed that in

the chiral smectic C phase rotation of molecules around their long axes is restricted<sup>3</sup> [19]. Therefore, the distribution of the transverse components of the molecular dipoles is not statistical and thus produces a significant dipolar component along the  $C_2$  axis. When an external electric field is applied to the sample of the chiral smectic C liquid crystal the dipoles align along the field in all smectic layers and the whole structure is polarised. Switching the direction of the field produces the state with an opposite sign of both the polarization and the molecular tilt. As in the crystalline ferroelectrics, the spontaneous polarization exists within the material at zero field, however, its comparable magnitude is 100 and even 1000 times smaller than the corresponding values found in solid materials. The molecular dipoles remain aligned only over a short period of time and the relaxation processes lead to the spontaneous polarization promptly fading away. In order to maintain spontaneous polarization and the uniform tilted structure effective alignment techniques are required. Consequently, special conditions are applied with respect to the boundary layers of the liquid crystal in order to prevent formation of a modulated helical structure (see below).

Strictly speaking, liquid crystalline ferroelectrics only partly satisfy the definition of the ferroelectricity. It is more appropriate to relate chiral smectic C phase to the broader class of **electrets** in which spontaneous polarization arises from the field-induced alignment of molecular dipoles [21]. Still, regardless of the many doubts over its true ferroelectric nature, the chiral smectic C phase is nevertheless related to the class of improper ferroelectrics as the spontaneous polarization is not the primary order parameter of the phase transition from the paraelectric phase, e.g. SmA, and passively follows the change in the magnitude of the tilt angle. It also should be ascribed to the order-disorder ferroelectric class, though this classification cannot be applied simply to liquid crystals due to the absence of rigid bonding between molecules.

---

<sup>3</sup> The rotation is hindered only slightly. The dipole order parameter remains rather small. However, its non-zero value implies that the opposite orientations of molecular dipoles are non-equivalent [22].

### 1.2.2 Soft-mode and Goldstone mode

In the paraelectric smectic A phase the molecules rotate freely around their long axes, so the dipoles are randomly distributed. The molecules are also involved in vibrational motions, which are expressed as short-time stabilisations of the molecular tilt, see figure 1.8a. This motion is called the soft-mode of the smectic A phase. Its condensation may be achieved applying an electric field along the short molecular axis (for positive dielectric anisotropy materials) even in the non-chiral smectic A phase [22]. Otherwise, it naturally occurs at the smectic A-smectic C phase transition [23] leading to the formation of the thermodynamically stable tilted structure. As shown in section 1.3 the microscopic origins of such a stabilisation include various sorts of molecular interactions with a special role given to dipolar and high order polar interactions. Thus, the presence of dipoles in the molecular structure of the mesogen is not only an important prerequisite of ferroelectricity in the chiral smectic C phase, but is also one of the conditions necessary for the smectic C phase to be formed.

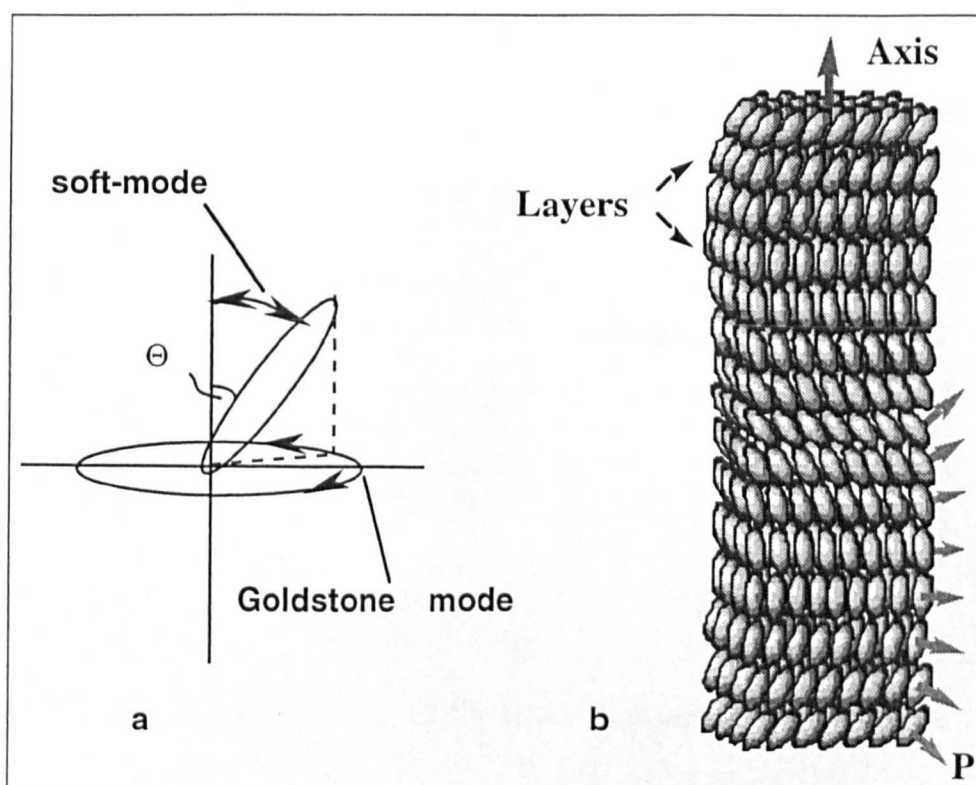


**Figure 1.8** Stabilisation of helical structure in the chiral smectic C phase

A remarkable feature of smectic A\*-smectic C\* phase transition is breaking of the continuous symmetry of the smectic A phase from  $D_{\infty V}$  to  $C_2$ . When the continuous symmetry breaks an additional vibrational mode should appear in the structure, restoring continuous symmetry [24]. This is realised in the chiral smectic C phase in a form of the macroscopic helical structure. The azimuthal direction of the molecular tilt changes continuously from layer to layer as a result of the instability called the Goldstone mode, see figure 1.8. The helical smectic C structure represents an example of modulated ferroelectrics where the spontaneous polarization varies along a certain direction [25].

The change of the sign of molecular chirality produces a helix of opposite handedness with the same value of the helical pitch. In an analogy with solids where two ferroelectric sub-lattices combined together give rise to an antiferroelectric structure, two opposite helices of the smectic C\* phase may be expected to produce an antiferroelectric liquid crystalline phase, see figure 1.9.

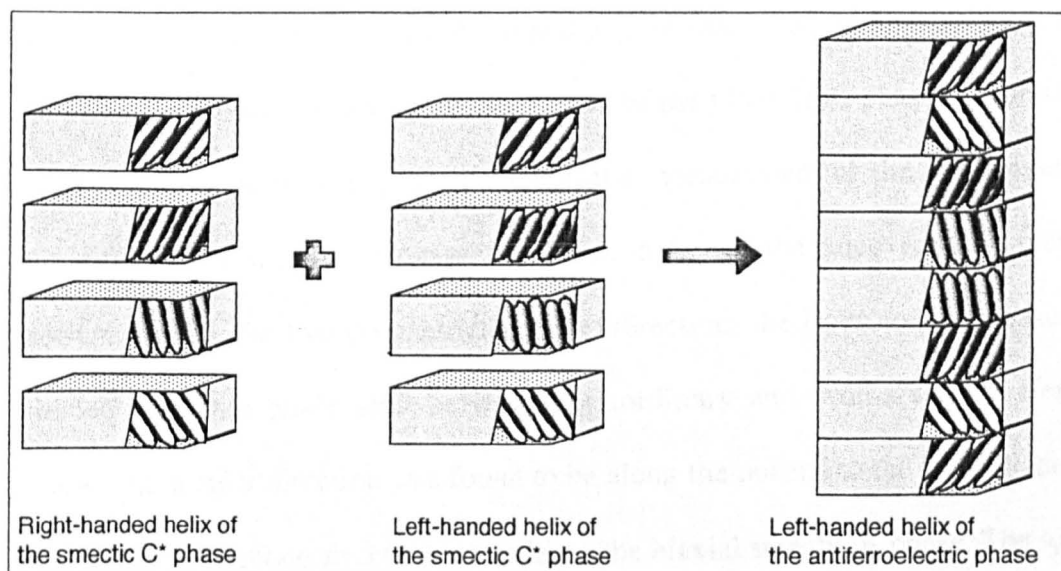


**Figure 1.9** Hypothetical picture of the formation of an antiferroelectric phase

### 1.2.3 Antiferroelectric smectic $C_A^*$ phase

#### 1.2.3.1 Experimental observations

One of the first experimental observations of the liquid crystalline phase, which later was recognized as the  $SmC_A^*$  phase, described a chiral tilted mesophase that appeared below the ferroelectric smectic  $C^*$  phase in a mixture of esters of 4-alkoxybenzoic acids incorporating chiral L-4-alkoxybenzylidene-4'-amino-2-chloropropyl cinnamate [26]. The tilted nature of the phase was manifested by a high magnitude of the pyroelectric coefficient, though it showed no spontaneous polarization after an external electric field was applied to it. At the same time, the absence of an electrooptical response at low fields was typical feature of orthogonal phases, harder to resolve this controversy the phase structure was suggested to be of an herringbone type. According to the proposed model the molecules were tilted in opposite directions in each layer. The magnitude of tilt angle remains constant in all layers, however the azimuthal angle varies discontinuously from 0 to  $\pi$  (figure 1.10) passing from one layer to another. A year later a similar structure was suggested for the  $SmO$  phase that was found in the phase sequence of chiral 1-methylheptyl-terephthalidene-bis-amino cinnamate [27]. Despite the phase behaviour being very similar to that of the tilted  $SmC$  phase, the herringbone arrangement of layers was proved through the measurement of the birefringence in a thin film of the smectic  $O$  phase formed on a top of the uncovered droplet of the isotropic liquid. For two symmetrically tilted directions the layer normal measurements yielded the same phase shift between extraordinary and ordinary rays. Hence, the average molecular direction was found to be along the normal to the layer plane. In this sense, the herringbone structure is similar to the biaxial smectic  $A$  phase. The technique used also allowed an accurate control of the number of layers in the film. The odd and even numbered films behaved differently, for example, odd and even domains had different colours [28].

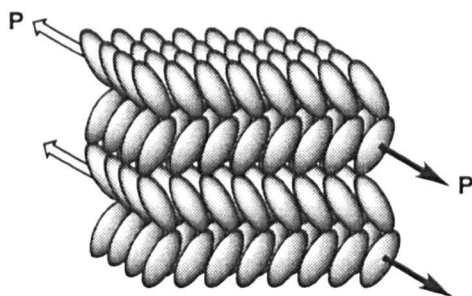


**Figure 1.10** Structure of the antiferroelectric smectic C phase

Even though these two early reports indicated that the molecules were tilted in opposite directions on passing from one smectic layer to the next, the reports did not confirm the presence of antiferroelectricity.

The report by Goodby et al. [29] showed that the chiral compounds (*R*)- and (*S*)-methyl pentyl 4-decyloxybenzoyloxybiphenyl-4'-carboxylates possess two extra ferroelectric phases ( $X_1$  and  $X_2$ ) in comparison to the racemic modification. The transitions to and from these phases had extremely small enthalpies. The phases disappeared by mixing of one of the chiral substances and its racemic modification at percentages below 78 and 70%.

The discovery of the antiferroelectricity in the mesomorphic state was completed when the detailed analysis of electrooptical behaviour of chiral 4-(1-methylheptyloxy carbonyl) phenyl 4'-octyloxybiphenyl-4-carboxylate (**MHPOBC**) [30, 31] revealed that there was a chiral tilted smectic phase with zero spontaneous polarization. Its antiferroelectric properties arose from the fact that the phase may undergo a field-induced transition to the ferroelectric smectic C phase. The alternating tilt structure mentioned above was adopted here as the only possibility to account for zero spontaneous polarization of the phase. As anticipated in the theoretical treatment, at the transition from the ferroelectric smectic  $C^*$  phase to the antiferroelectric phase the

structure remains helical with the helical pitch showing a discontinuous jump. It is still unclear why the pitch handedness reverses its sign at the transition to or from the antiferroelectric smectic C phase [32]. Like any other helical structure the antiferroelectric smectic phase selectively reflects light of the wavelength [33]:

$$\lambda_0 = nP,$$

where  $n$  is the mean refractive index of the medium and  $P$  is a helical pitch.

Remarkably, at the oblique incidence of light the spectrum of the phase does not possess full-pitch band, which was found in the smectic C phase [30]. This result is in agreement with the proposed herringbone structure and its helical version is similar to the cholesterics in a sense that both structures have half-pitch reflections.

### 1.2.3.2 Ferrielectric sub-phases

Apart from the antiferroelectric phase there is a number of sub-phases which were discovered in the temperature interval lying between the  $\text{SmC}^*$  and  $\text{SmC}_A^*$  phases [34]. The sub-phases are believed to form as a result of a frustration between ferro- and antiferroelectricity in liquid crystals [35]. To account for the phases' structure the Ising model of the magnetic phase transition [13] was adopted here treating the configuration of two successive smectic layers as an Ising variable. The model denoted as ANNNI (Axial Next Nearest Neighbour Ising) [36] takes into account interactions between molecules in a particular layer and their neighbours in the nearest and next nearest layers. Ferroelectric and antiferroelectric orderings are designed as  $\mathbf{F}$  and  $\mathbf{A}$  variables respectively and the different structures allowed can be characterised by the parameter  $q_T = F/(F+A)$  which denotes the fraction of ferroelectric ordering  $\mathbf{F}$  to the total ordering in a periodic structure. Resulting arrays of structures constitute a temperature-induced Devil's staircase [37] with both synclinic (ferroelectric) and anticlinic (antiferroelectric) arrangements of the tilted layers being present in the phase structures at the same time,

see figure 1.11. Thus, the phases exhibit ferrielectric behaviour and are analogous to solid ferrielectrics whose structure possesses ferroelectric properties in one direction and antiferroelectric properties along the other [38].

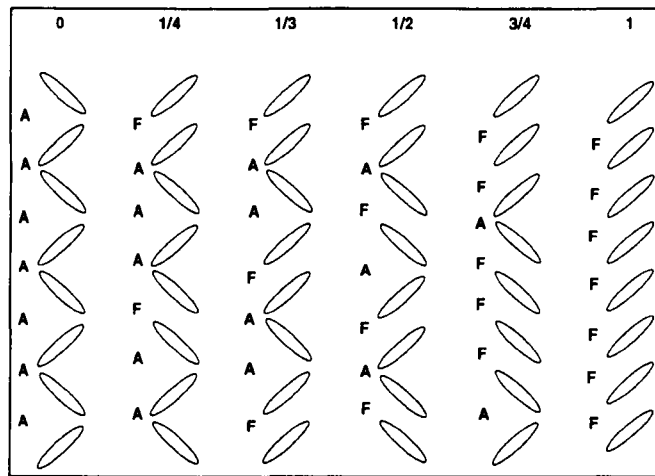


**Figure 1.11** Temperature-induced devil's staircase between ferroelectric and antiferroelectric smectic C phases.

In the Ising model treatment the molecular orientation within the layers is confined to the tilt plane. The azimuthal angle of each layer changes abruptly from 0 to  $\pi$  and its variation due to chirality is neglected despite the fact that all ferrielectric sub-phases were found to be helical [35]. In this sense, the Ising model approximation appears slightly unrealistic, especially, in the case of the  $\text{SmC}_\alpha$  phase, which is a high temperature member of the ferrielectric phase family and was shown to have a very short helical pitch [36]. To resolve this inconsistency Cepic and Blinc [39] built the ANN model with a variation of the azimuthal angle being incorporated into the model order parameter. The order parameter (and consequently the azimuthal angle) gains a discrete value different from zero or  $\pi$  and, as a result, molecular orientation in the successive layers is neither parallel nor anti-parallel. In this case the nearest and next nearest interactions are of comparable value and its competition produces a helical structure, which is spread over few layers. The tilt of molecules is constant throughout

the bulk and so is the phase difference between the two nearest layers. Slight precession of the later value with the temperature accounts for why the  $\text{SmC}_\alpha$  phase has ferrielectric characteristics at the low temperatures but antiferroelectric properties at the vicinity of the  $\text{SmA-SmC}_\alpha$  transition. At higher temperatures, the phase difference of the azimuthal angle between two layers become close to  $\pi/2$  thereby giving rise to the antiferroelectric structure having four layers periodicity with zero spontaneous polarization.

Though a four layer periodic structure was later (see section 1.2.3.3) found in the  $\text{SmC}_{\text{FI2}}$  phase and not in the  $\text{SmC}_\alpha$  phase, the approach itself known as an *XY* or *discrete* model was proved to be quite fruitful in the general description of the smectic ferrielectric sub-phases [40]. For all of them a variation of the azimuthal angle produces a short pitch helix, which has a value of the phase difference between successive layers, which is unique for any particular phase.

The nomenclature used to describe new phases emphasises their structural similarity to the parent smectic  $\text{C}^*$  phase. Antiferroelectric phase is denoted with the symbol  $\text{SmC}_\Lambda^*$  which reads: antiferroelectric smectic  $\text{C}^*$  phase. Its non-chiral version is the alternating tilt phase  $\text{SmC}_{\Lambda\text{H}}$  [41]. Ferrielectric sub-phases are described by a common symbol  $\text{SmC}_{\text{FI}}$  and various modifications are denoted with an additional number in the symbol index. Sometimes,  $\alpha$ ,  $\beta$ , and  $\gamma$  indices are used next to the  $\text{SmC}^*$  symbol to describe the non-commensurate smectic C phase [ $\text{SmC}_\alpha^*$ ], the ferroelectric phase [ $\text{SmC}_\beta^*$ ] and ferrielectric phases [ $\text{SmC}_\gamma^*$ ] respectively. This nomenclature is confusing as it does not introduce a similar style notation for the antiferroelectric phase and a number of other less known smectic C sub-phases [42]. Also, it is restricted to the chiral phases and, therefore, is avoided where possible in this discussion.

### 1.2.3.3 “Forbidden” reflections in the antiferroelectric and ferroelectric smectic C phases

The structure of the antiferroelectric and ferroelectric smectic C phases was recently proved by X-ray diffraction experiments [43]. The conventional small angle X-ray scattering from oriented samples readily revealed differences in degree of orientational and positional order realised in various liquid-crystalline phases [44]. Rather diffuse reflections due to a weak correlation between the long molecular axes found in the nematic phase are replaced with intensive sharp spots in the smectic A and C phases indicating presence of extensive layer-like ordering along the layer normal. It is described by a sinusoidal distribution function and the diffraction peaks are centred near the integer values of the scattering vector  $Q = 2\pi/d$  where  $d$  is a layer spacing. In the case of the smectic C phase, the molecular tilt in the smectic layers may be observed directly in the diffraction pattern or calculated from the value of the layer spacing [45].

The diffraction from tilted layers in the antiferroelectric smectic C\* phase also occur at integer  $Q$  values corresponding to the layer spacing. The difference of the phase structure from those of smectic A\* and smectic C\* phases may be described in terms of a two-fold screw axis which is responsible for the alternating direction of molecular tilt in adjacent layers. The  $180^\circ$  rotation of the molecules in any layer is accompanied by an  $a/2$  translation along the layer normal ( $a$  - is the length of the unit cell which includes two layers). Such a fractional translation within a unit cell causes destructive interference of the X-rays, and reflections from corresponding planes are systematically absent in the diffraction pattern [46]. X-ray radiation propagating along the layer normal only estimates the electron density distribution in layers and does not reveal the variation of azimuthal angle due to a screw axis or a glide plane present in the chiral and non-chiral smectic C alternating phases respectively. The resulting X-ray pattern is very similar to that of the smectic A phase [47].

Absent or "forbidden" reflections imply that all layers in the antiferroelectric smectic C\* phase (or its non-chiral analogue) are crystallographically equivalent. They consist of the similar molecules, which are tilted at the same angle from the layer normal and occupy the same conformational energy levels. Still, there is a factor, which may distinguish them. It is the directionality of certain physical properties due to the anisotropic nature of the molecules of the mesophase. For example, the electric susceptibility, which links the molecular polarization with an external electric field is given by:

$$4\pi\mathbf{P} = \chi\mathbf{E}$$

which is described by a second-rank tensor. Its anisotropy can be neglected in conventional X-ray experiments where the scattering is considered to be elastic in a sense that there is no significant energy exchange between the radiation and the substance [47]. However, at the sufficiently high energies the absorption processes start to contribute to the interactions. The amount of the energy absorbed depends on the orientation of the susceptibility tensor, and consequently, the molecular orientation relative to the polarization of the incident beam. Apparently, in the antiferroelectric smectic C\* phase, the molecules having opposite orientations of their long axes in two subsequent layers absorb different amount of the X-ray radiation if its energy is close to the maximum in the absorption spectrum of the material. It leads to the non-equivalence of two layers and "forbidden" ATS (anisotropy of the tensor of susceptibility) reflections occur with a measurable intensity [48]. These reflections were observed in the diffraction patterns of various smectic C\* phases for a compound containing sulphur which absorption maximum lies in the X-ray region (2475 eV) [43]. In both chiral and non-chiral alternating smectic C phases the presence of half-integer ATS peaks indicates presence of a two-layer super-lattice in which molecules flip at 180° passing from one layer to another.

In the ferroelectric phases, ATS peaks appear at quarter-integer ( $\text{SmC}_{\text{F}2}$ ) or third-integer ( $\text{SmC}_{\text{F}1}$ ) values of  $Q^4$ . Corresponding structures include four- and three lattice periodicities as predicted in the *clock*-model (section 1.2.3.2). The helical structure of the  $\text{SmC}_\alpha$  phase was found to be incommensurate. The azimuthal angle varies randomly in the nearest and next nearest layers so the phase difference is not constant.

#### 1.2.3.4 Symmetry of the antiferroelectric smectic $C_A^*$ phase

The  $\text{SmC}_A^*$  phase may appear at the transition from the ferroelectric smectic  $C^*$  phase or directly from the paraelectric smectic A phase. In both cases the resulting structure is an infinite lattice [49] of smectic layers with alternating direction of the molecular tilt. As mentioned above, the phase symmetry includes non-integer translations and, hence, the structure cannot be fully described by one of the thirty two point groups [50]. Using a space group notation the symmetry is defined as  $D_2^2$  ( $P222_1$ ) [51]. The operations include two  $C_2$  axes and one screw two-fold axis [52] parallel to the layer normal, see figure 1.12.

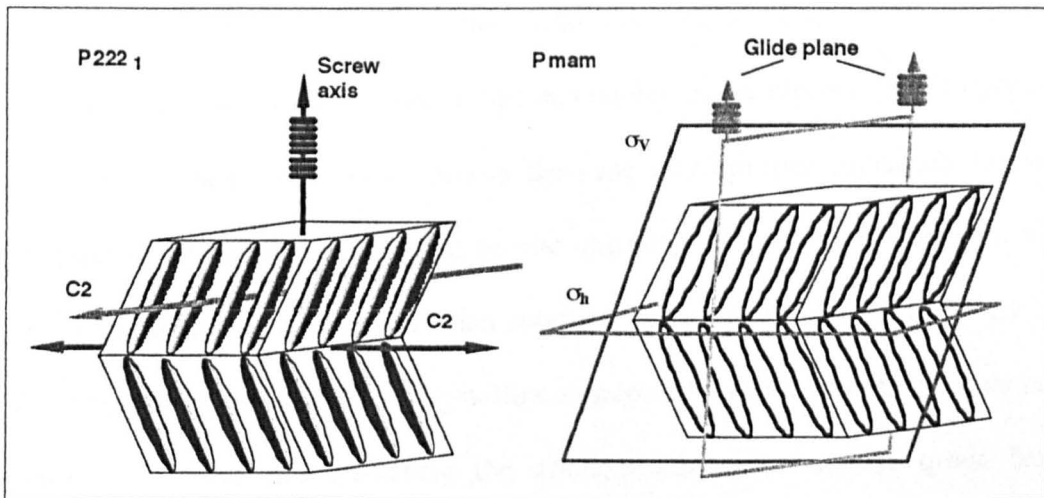


**Figure 1.12** Symmetry of the chiral and non-chiral antiferroelectric phases.

<sup>4</sup> Most recent X-ray studies on the structure of the ferroelectric phases demonstrated that the layer periodicity in F12 and F11 phases is somewhat more complex and may have a variable phase difference between adjacent layers [90].

The  $C_2$  axes are not intersecting, so the choice of the origin to determine the phase symmetry is not arbitrary and depends on which of the  $C_2$  axes is considered [53]. The phase does not possess a centre of inversion, however, the symmetry is still higher than that of the spontaneous polarization in a way that the polar properties along one axis are compensated by a simple two-fold rotation along any other axis.

When an electric field is applied along one of the axes the transition to the ferroelectric smectic  $C^*$  phase takes place. The symmetry is reduced to  $C_2$  and the spontaneous polarization appears along the selected axis by the direction of the applied field. The magnitude of the field, which drives the transition, is relatively small indicating a small energy difference between antiferro- and ferroelectric phases. Nevertheless, this action constitutes a field induced phase transition. The full cycle of alternating current changing from  $-E$  to  $+E$  and back produces a double hysteresis response from the spontaneous polarization, as it does in solid antiferroelectrics. The molecular chirality is an essential factor here as only in the chiral phase organisation the transverse dipoles are retained in each layer and which can be coupled to the electric field to give rise to a ferroelectric state. In a sense, this is the case of improper transition (spontaneous polarization is strongly dependent on the chirality of the system), though there is a growing amount of experimental data showing that proper antiferroelectricity may also be realised in non-chiral liquid crystalline systems. Among them are the banana shaped molecules, which are attracting the greatest attention because quasi ferro- and antiferroelectric behaviour has been found in some compounds [54, 55]. However, it is thought that they represent a special case in liquid crystalline behaviour, which has little in common with the smectic phases of calamitic molecules to which this discussion is restricted.

### 1.3 Microscopic origins of antclinic and synclinic ordering in smectic phases

#### 1.3.1 Stabilization of the alternating tilt between smectic layers

As described previously in the ferroelectric smectic C\* phase the spontaneous polarization develops along the C<sub>2</sub> axis perpendicular to the tilt plane. In general its magnitude grows with temperature on cooling from the Curie point. At some point, it may reach a critical value when the system should rearrange itself in order to diminish the electrostatic contributions to the total energy. The optimal way to compensate strong lateral spontaneous polarization is a pairing of transverse molecular dipoles between two neighbouring layers. For the whole compensation of dipoles to occur the molecules in adjacent layers must be tilted in the opposite directions [56] thereby giving rise to the antiferroelectric structure. There are three reasons why the alternation of molecular tilt occurs [57]:

1. The effective transverse dipoles become antiparallel when they form a pair. In the chiral smectic C phase it is only possible when the direction of molecular tilt is changed.
2. The pairing can emerge equally between one layer and both top and bottom adjacent layers because of the head-tail equivalence of molecules within a layer.
3. The change of the dipole orientation in one layer relatively to the other results in the reversal of the sign of spontaneous polarization. It must be accompanied by the reversal of the tilting sense according to the fundamental equation [58]

$$\vec{P} = P \frac{\vec{z} \times \vec{n}}{|\vec{z} \times \vec{n}|}$$

where  $\vec{z}$  is a unit vector parallel to the smectic layer normal and  $\vec{n}$  is the director.

The majority of the antiferroelectric liquid crystals known to date have a transverse dipole moment represented by the carbonyl group placed between the rigid mesogenic

core and flexible chiral alkyl chain. For the electrostatic interaction to be most effective the alkyl chains should not obstruct the intermolecular interaction between carbonyl groups in adjacent layers; even though the former have a considerable fraction of *gauche* conformers in the liquid crystalline state [59], they still present a significant structural barrier between two layers.

Experimentally, it was found for compounds that exhibit an antiferroelectric phase, the chiral chain is bent as much as  $43^\circ$  away from the direction of long molecular axis [36]. Some evidence was found in X-ray experiments for almost L-shape of the molecules [60]<sup>5</sup>. Such a bent molecular shapes may serve as a way of supporting the pairing model as in these cases the distance of approach between carbonyl groups of molecules in adjacent layers is considerably shortened. Still, the disruption at the layer interfaces caused by the packing of L-shaped molecules negates this model as being practical.

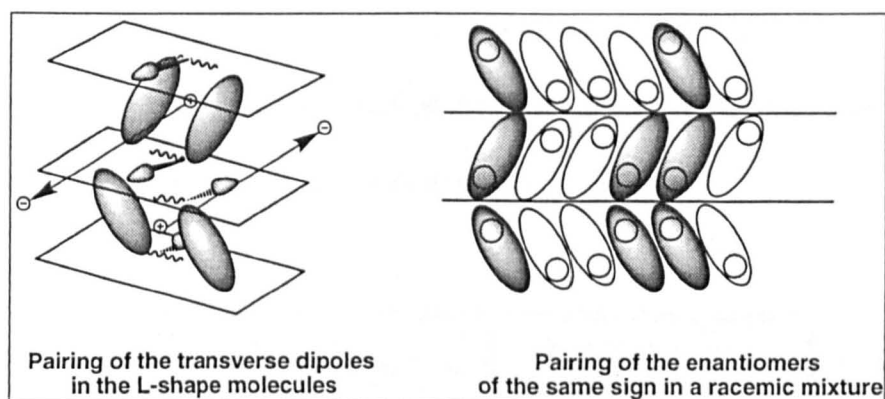


**Figure 1.13** Formation of the alternating tilt structure

The necessary condition for the pairing of transverse molecular dipoles is the presence of molecular chirality. In the chiral smectic phase rotation of the transverse dipoles around long molecular axis is statistically restricted so the components along  $C_2$  axis are not averaged out and may create a significant electrostatic field within each smectic

<sup>5</sup> There are also experimental evidences that contradict this fact and imply that the layer spacing is approximately the same as the molecular length [91].

layer [36]. On a microscopic scale this process may well occur in the racemic mixtures of smectic C\* materials in which the molecular domains of the same chirality were shown to form spontaneously [61]. Self-recognition of optical isomers of the same sign in a liquid crystalline racemate takes place similar to the process of the spontaneous optical resolution of enantiomers during crystallisation. The same isomers in adjacent smectic layers form a pair and, if the transverse dipoles have a significant magnitude, their compensation requires molecules to tilt in the opposite directions thereby stabilising the herringbone-tilted structure, see figure 1.13. Thus, the model of pairing dipoles (see section 1.3.2.2) may be extended to explain formation of the non-chiral antiferroelectric phase in the racemic mixtures [62]. However, it remains useless for the case of compounds, which do not contain chiral centre and yet still exhibit an alternating tilt smectic C phase. For example, certain swallow-tail compounds, see figure 1.14 were found to form herringbone smectic structures on cooling from the smectic A phase [56]. In this case it was suggested that a steric interaction across the layer interface between the swallow-tail of the molecule in one layer and straight alkyl chain of the molecule in another produces a molecular dimer.

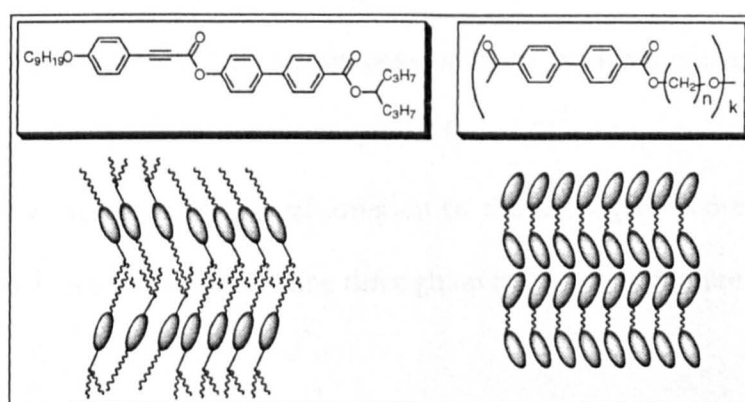


**Figure 1.14** Stabilisation of the alternating tilt between layers formed by dimers and zig-zag shaped polymers

Similar zig-zag shaped structures can be obtained in certain types of the non-chiral main-chain polymers, see figure 1.14. The steric nature of the interactions leading to the stabilisation of herringbone tilts in layers is rooted in the fact that only compounds with the middle alkyl chain having an odd number of carbons form an anticlinic, antiferroelectric-like arrangement [63]. For even numbers a synclinic structure is preferred.

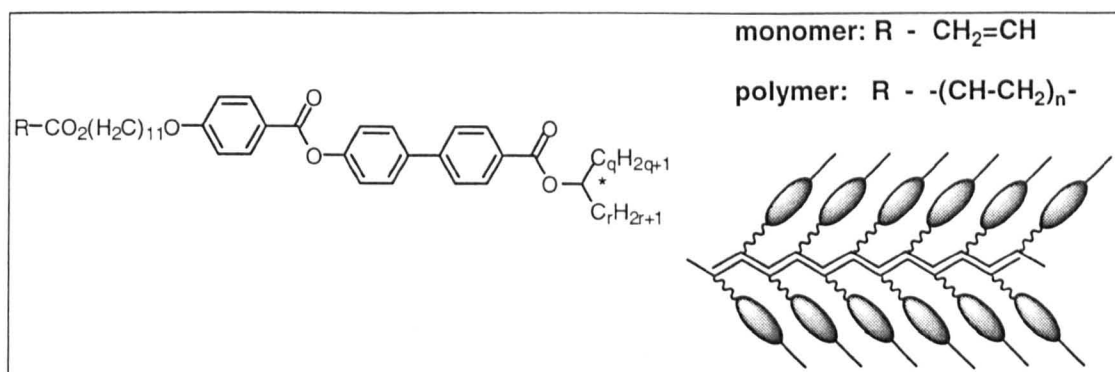


**Figure 1.15** Formation of the antiferroelectric phase in the side-chain polymers

Chiral side-chain polymers were also shown to favour herringbone molecular packing, see figure 1.15. While the chiral monomer exhibits a whole range of the smectic phases including the chiral smectic A\* and smectic C\* phases the polymerised compound forms an antiferroelectric phase at the expense of any other smectic structure. Despite the presence of the chiral centre and the possibility to realise a pairing mechanism of transverse dipoles it is believed that the phase is stabilised by steric effects [64]. The zig-zag shape is ensured by the conformation of the mesogenic cores relative to the backbone chain which remains the same throughout the whole structure.

In a similar manner, the stabilisation of antiferroelectric ordering is achieved in non-chiral side-chain polymers, which also were found to exhibit the alternating tilt phase. Though non-chiral this phase can undergo a field-induced transition to the ferroelectric smectic C phase thereby possessing truly antiferroelectric properties. The symmetry of

the structure is  $C_{2v}$  and low enough to allow appearance of a spontaneous polarization along the polar  $C_2$  axis which lies at each layer boundary and parallel to the tilt plane as shown in figure 1.16. If one considers the molecular dipole being parallel to the long molecular axis, its projection on the tilted plane is not affected by free rotation, in other words it is not dependent on chirality.

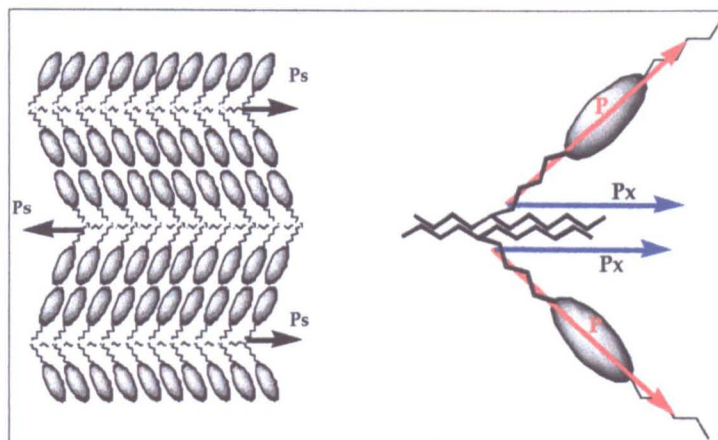


**Figure 1.16** Formation of an antiferroelectric-like ordering in non-chiral side-chain polymer

As a result, in each layer (on one side of the backbone chain) all of the dipolar components are aligned along the  $C_2$  axis producing a local spontaneous polarization. On the other side of the chain, the dipole projections on tilt plane have the same magnitude but opposite direction so they bring a positive contribution to the interlayer  $P_s$ . Passing from one layer boundary to another the direction of  $P_s$  changes to the opposite and the phase is antiferroelectric [65].

The results explicitly show that chirality is not a driving factor that necessitates appearance of the alternating tilt layered structure and, moreover, it is not the only means to break the phase symmetry allowing the spontaneous polarization in a material. The originality of the herringbone smectic ordering brings in the possibility of the spontaneous polarization developing along  $C_2$  axis at the layer boundary which is

present in both chiral and non-chiral phases. Though the dipolar alignment along interlayer axis becomes important only in the chiral phase (or polymer structure shown in figure 1.16) where a mirror plane perpendicular to the axis is absent, it still seems to occur in the non-chiral phase.

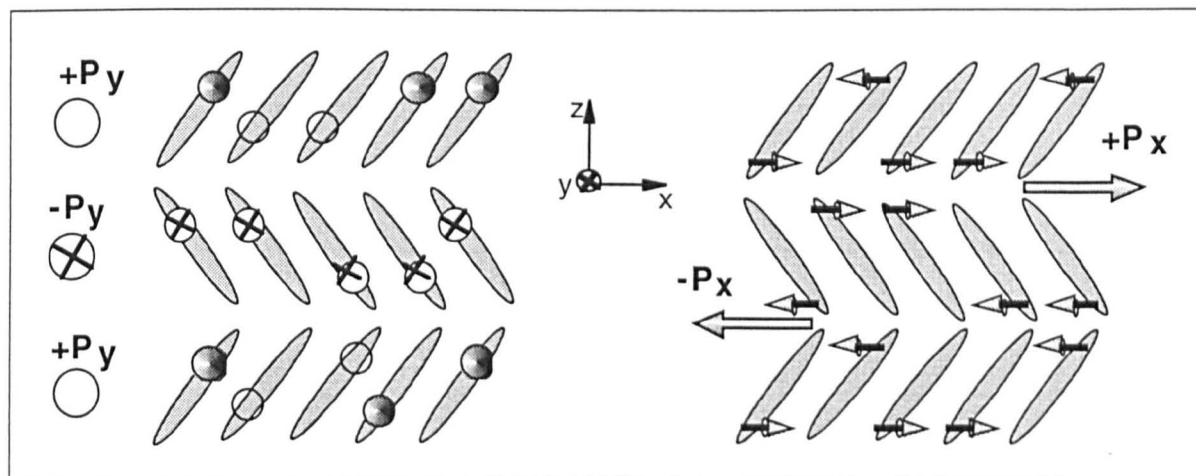


**Figure 1.17** Pairing of molecular dipoles along the transverse  $y$  and in-plane  $x$ - axes in the antiferroelectric phase

As at the layer boundary all dipole components parallel to the tilt plane (figure 1.17,  $x$ -axis) should point in the same direction, we can speculate about the nature of the pairing of these components of molecular dipoles giving rise to the opposite tilt in adjacent layers [58]. In the contrast to the model of pairing of transverse dipoles along  $y$ -axis, the "X-model" can be applied to the non-chiral alternating smectic C phase, as there is no requirement for hindered rotation about the long molecular axis.

Non-chiral molecules were also shown to form herringbone smectic C structure in the molecular simulations [66]. The model takes into account only hard-core repulsion forces between mesogenic molecules represented by the three segment flexible structure ignoring any polar or chiral effects. The corresponding interaction potential was constructed as a function of molecular conformation and the resulting solutions give three possible molecular arrangements as follows:

1. When molecular interactions are invariant to translation and any  $180^\circ$  rotation the smectic A phase is formed.
2. The smectic C phase is stable when the potential is not symmetric with respect to the flips of the molecular orientation about the layer normal.
3. Finally, a herringbone ordering is realised when an asymmetry of the solution derived at in respect to flipping about layer normal is dependent on translation parameter. The energy difference between anticlinic and synclinic orderings is found to be small (especially when the layer spacing is not much smaller than the molecular length). Therefore, additional interactions could readily shift the thermodynamic stability in favour of one type of ordering to another.

Both smectic C and alternating smectic C phases were experimentally observed in Langmuir monolayers of fatty acids providing a good opportunity to compare experimental results and the theoretical model mentioned above [67]. Density functional theory designed specially for the monolayer systems found that the smectic C ordering is stabilised by the anisotropic dispersion intermolecular interaction [68]. This result is consistent with the molecular model of the smectic C phase given by Van der Meer and Vertogen (see section 1.3.2.5). The antiferroelectric phase is found to exist when the molecules constituting the phase possess large quadrupole moments. Quadrupole-quadrupole types of interaction compete with the anisotropic dispersion giving rise to one type of ordering or another. The stability of the alternating tilt phase above the smectic C phase appears to be extremely sensitive to the peculiarities of molecular structure and, in particular, to presence of the polar groups which can be combined to form a spatial quadrupole unit.

## **1.3.2 Molecular theories of the smectic C phases.**

### **1.3.2.1 Introduction**

The description of the liquid crystalline state still remains a challenging problem of fundamental science. It has been addressed from the various approaches in phenomenological physics, for example, by the continuum theory [72] which models the static and dynamic behaviour of liquid crystals, the Landau-de Gennes theory of phase transitions [73], and the molecular statistical theories of simple liquid-crystalline phases [74]. The latter are of particular interest for synthetic chemists as they challenge the most controversial question of structure-property relationships - what features concerned with molecular structure and molecular interactions are responsible for the stability of the different LC phases.

The history of molecular theories of the mesomorphic state goes back to the fifth decade of the last century when Onsager developed his pioneering work on hard-core repulsion interactions in nematics [75]. Onsager's intermolecular potential did not include any attractive terms, so his model, at least qualitatively, may be applied only to the lyotropic systems.

The first attempt to build a molecular theory of thermotropic liquid-crystalline phases was by Meier and Saupe [76]. Constructing a simple anisotropic attraction potential, i.e. an electrostatic interaction between molecules, they described the transition from the isotropic liquid to the nematic phase in the frame of a mean-field approximation. This approach was extended further by McMillan who included the possibility of translational ordering in his calculations for the orthogonal smectic phases [77].

In general, the mean-field approximation proved to be a simple and often successful method for describing liquid crystal phases. As far as the McMillan's theory of the smectic A phase was concerned, the theory provided a good qualitative and sometimes even quantitative description of the nematic-smectic A transition. However, there are still some peculiarities of the smectic A phase to be explained. The important question that was left unanswered was which type of molecular interaction was important, and which interactions force the director to be normal to the smectic planes. Also, the theory does not consider hard-core repulsion effects between molecules, which were recently proved on their own to stabilise a layered ordering [78]. The recent attempts to include hard-core repulsions in the McMillan theory had the coupling between the molecular long axis and the intermolecular vector as a term in the energy expression [79]. What seems to be an important result of these calculations is that the energy is minimised when the molecules are packed together with their long axes being parallel to the layer normal.

Having developed such a detailed but still vulnerable description of the molecular origins of the orthogonal liquid-crystalline phases, the next step was to understand the forces which induce the molecular tilt which accompanies the transition from the smectic A (or nematic) phase to the smectic C phase. It should be noted that the resulting tilted structure was considered to be unfavourable from the packing point of view. Tilted molecules were believed to occupy more area in the smectic plane and, therefore, there is more excluded area in the layer than in the smectic A phase<sup>6</sup>. This means that hard-core repulsions on their own, which were used to describe nematic and smectic A ordering, can not be used here as the driving force for the molecular tilt.

---

<sup>6</sup> This is found to be in contradiction with the results of molecular modelling that showed molecule packing in the tilted structure would improve the electronic and dipolar distribution within the molecular layers [80].

Some additional interaction was required to be found which would reduce an increasing energy of the system at the transition to the smectic C phase.

The models mentioned in the following sections offer various mechanisms to balance the energy increase due to the molecular tilt. Some of them were experimentally proved to be unrealistic but still are worth discussing as they provide a good background for the understanding of molecular interactions, which occur between molecules in liquid-crystalline phases.

### 1.3.2.2 Model of transverse dipoles

In this model the primary role in the formation of the SmC phase is played by hindered molecular rotation around its long axis [81]. In the SmA phase the rotation is free and it is frozen out in the SmC phase. It is assumed that molecular order in the SmA phase is well established. The molecules form the orthogonal structure with allowed free rotation and translation along any axis. Also, the molecules are of cylindrical shape and have a permanent dipole located at the molecular centre. Two outboard dipoles anti-parallel to each other<sup>7</sup> sit at the distance  $d/2$  above and below the central dipole (figure 1.18a).

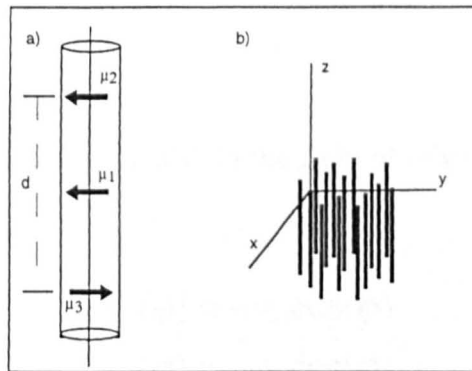


**Figure 1.18** a) Schematic representation of molecule in the McMillan's model. b) a smectic layer in three dimensions considered without any interactions with neighbouring layers.

<sup>7</sup> The situation when outboard dipoles are parallel to each other is considered to be less favourable for the formation of the smectic C phase. The molecules are believed to be in their all trans conformations to facilitate the tilt, which put the outboard dipoles in the opposite directions.

The dipole-dipole interactions are considered to be a driving force of the SmA-SmC transition with the interaction potential:

$$U = \sum_{i < j} \frac{\bar{\mu}_i \cdot \bar{\mu}_j}{\epsilon_\infty r_{ij}^3} - \frac{3\bar{\mu}_i \cdot \bar{r}_{ij} \bar{\mu}_j \cdot \bar{r}_{ij}}{\epsilon_\infty r_{ij}^5}$$

$r_{ij}$  is a distance between dipoles and  $\epsilon_\infty$  is the high-frequency dielectric constant of the medium.

McMillan's model predicts formation of three phases depending on the counter balance of the outboard and central dipoles. The calculations are largely simplified by considering one smectic layer and ignoring interlayer interactions. Molecules lie with their centres on the  $xy$  plane and long axes being parallel to the  $z$  axis. They are free to rotate, turn up side down and translate in  $xy$  plane thereby being a two dimensional liquid (figure 1.18b).

Two possible configurations of molecular dipoles are considered. The first one is where the upper outboard dipole is parallel to the central dipole, this configuration is denoted as (+). The second is the opposite as the lower dipole is parallel to the central one (configuration (-)).

The potential, which a molecule "feels" in the field of other molecular dipoles is thus defined for both configurations:

$$V_+(\varphi) = -v_+ \cos(\varphi)$$

$$V_-(\varphi) = -v_- \cos(\varphi)$$

where  $\varphi$  is an angle between molecular dipole and  $x$ -axis.

To describe molecular orientation a single-particle distribution function is introduced as a function of  $V$  and  $\varphi$ .

$$f_+(\varphi) = (1/N)e^{v_+ \cos \varphi / kT}$$

$$f_-(\varphi) = (1/N)e^{v_- \cos \varphi / kT}$$

With these distribution functions the average central dipole moment can be written:

$$\mu_1 \alpha = \mu_1 \int_0^{2\pi} d\varphi \cos \varphi [f_+(\varphi) + f_-(\varphi)]$$

The same operation is applied for the average upper (or lower dipole):

$$\mu_2 \beta = \mu_2 \int_0^{2\pi} d\varphi \cos \varphi [f_+(\varphi) - f_-(\varphi)]$$

Another assumption of the model is that the dipole-dipole interactions on different levels are considered negligible. So the electric field at the central dipole of one molecule will be determined by the average central dipoles of the others:

$$E_1 = \frac{\mu_1 \alpha (\pi n_2)^{3/2}}{\epsilon_\infty}$$

Similarly, the electric field on the upper (lower) dipole is:

$$E_2 = \frac{\mu_2 \beta (\pi n_2)^{3/2}}{\epsilon_\infty}$$

where  $n_2$  is the number of molecules per unit area.

According to the model, we assume at the transition to the SmC phase the rotation around long molecular axes becomes hindered, or at least the rotation of the molecular fragments that carry dipoles. As a result of dipole-dipole interaction each particular dipole will experience a torque in the electric field of the dipoles of neighbouring molecules with the general expression for a potential:

$$\bar{V}_+(\varphi) = -(\mu_1 E_1 + 2\mu_2 E_2) \cos \varphi$$

$$\bar{V}_-(\varphi) = -(\mu_1 E_1 - 2\mu_2 E_2) \cos \varphi$$

If the field is strong enough, the dipoles on the same level become aligned. When  $2\mu_2 > \mu_1$  the outboard dipoles become aligned and the central dipoles remain random. If the outboard dipoles are not exactly perpendicular to the long molecular axis (as it is in the reality), but have their component  $d$  along the  $z$  axis, there is a torque of  $3kT_c d\beta$  ( $T_c$  - the Curie temperature,  $\beta$  - order parameter), which will tilt the molecules over to the  $x$  axis to keep the outboard dipoles aligned. The tilted phase produced is a SmC phase. It is not a ferroelectric phase as initially the antiparallel orientation of the outboard dipoles was assumed. It should be noticed that the tilt angle is not the primary property of the phase, but instead it passively follows the order parameter  $\beta$  i.e. the alignment of the outboard dipoles [82].

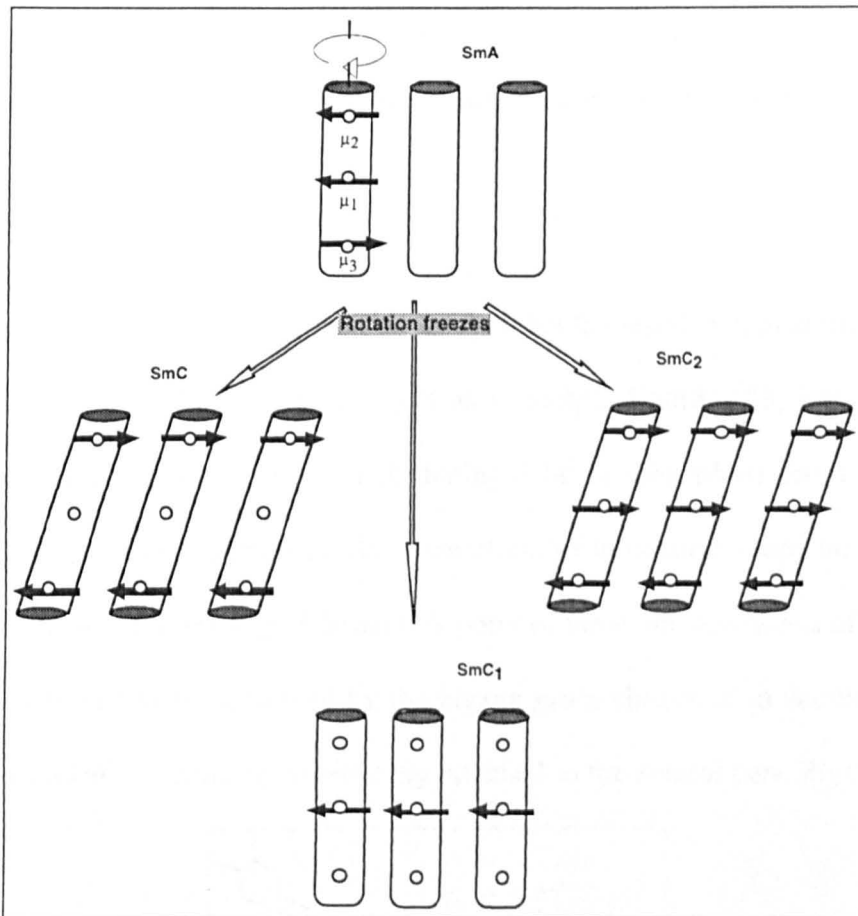


**Figure 1.19** Formation of three tilted smectic phases from the smectic A phase. The phases are stabilised by various contribution of the central and outboard dipoles.

When the central dipole value is somewhat larger than  $2\mu_2$  the  $\text{SmC}_1$  phase appears with only the central dipoles aligned ( $\alpha \neq 0$ ,  $\beta = 0$ ). This phase is orthogonal and ferroelectric.

When the outboard and central dipoles are of similar magnitude another ferroelectric phase,  $\text{SmC}_2$ , is produced. This time it is tilted with all three dipoles aligned, see figure 1.19.

Thus, according to this model to produce a  $\text{SmC}$  phase a molecule should possess an approximate centre of symmetry. Large outboard dipoles are preferred to lie at approximately the same distance from the centre. Also, a zigzag trans gross shape of molecule is found to be necessary to produce an anti-parallel orientation of the outboard dipoles.

### 1.3.2.3 Wulf's steric model

In Wulf's model the emphasis is made on the fact that the repulsive, or steric forces play a predominant role in liquid crystals, just as in simple liquids [83, 84]. That is the characteristic orientational order, which distinguishes a mesophase from an ordinary liquid is assumed to be mainly a result of the effect of molecular shape on the packing problem encountered in the liquid. From this point of view, the formation of the smectic C phase is believed to be promoted by the zigzag gross shapes of molecules, which is provided by end alkyl chains symmetrically attached to the central core (figure 1.20).

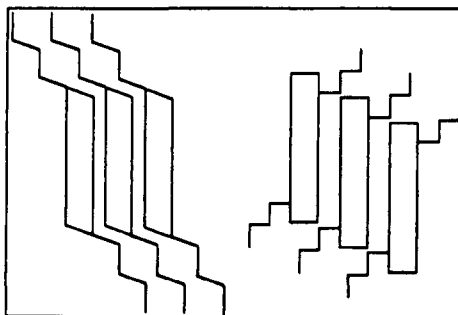


**Figure 1.20** Suggested models of molecular zigzag shape proposed by Wulf [83].

Correspondingly, the molecules are assumed to have a centre of symmetry, a property, which seemed to be common for all smectic molecules at the time the theory was developed. As required for symmetrical molecules the interaction between such molecules is unchanged by the combined operation  $v^3 \rightarrow -v^3, v^2 \rightarrow -v^2$  (reversal of the molecular axes 3 and 2 of a molecule, see figure 1.21), but not by the first or the second operation alone. The model calculation starts by writing down an effective interaction potential between the molecules that simulates the effect of the molecular zigzag gross shape:

$$-A_1(r)[\bar{v}^3(1) \cdot \bar{v}^3(2)][\bar{v}^2(1) \cdot \bar{v}^2(2)] - [A_2(r)/r_2^2][\bar{v}^3(1) \cdot \bar{r}\bar{v}^2(1) \cdot \bar{r} + \bar{v}^3(2) \cdot \bar{r}\bar{v}^2(2) \cdot \bar{r}]$$

The first term describes the alignment of the long ( $v^3$ ) and short molecular axes ( $v^2$ ). At this point the model becomes similar to the McMillan's as the free rotation around the long molecular axis is also not allowed here. The second term is responsible for the tilt with respect to the intermolecular vector  $\mathbf{r}$  in order to achieve optimal packing (figure 1.21).

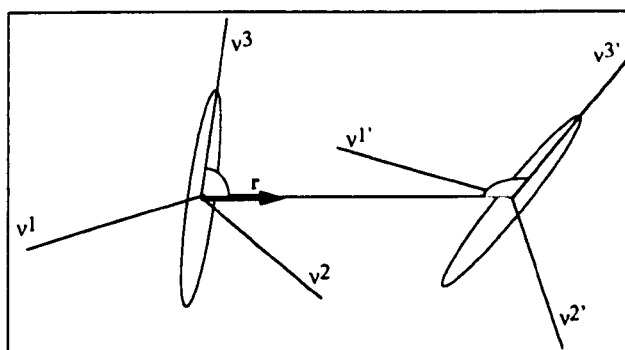


**Figure 1.21** Mutual orientation of the molecules in Wulf's representation.

If the order in the SmA phase is well established and all interactions apart from orientational ones are neglected the formation of the smectic C phase could be explained in following manner. Assume that the  $z$  axis is parallel to the long molecular

axes in the SmA phase and perpendicular to the smectic planes. If there is any kind of force applied in the Y direction it will result in a uniform shearing deformation with the Y axis perpendicular to the shearing planes. In order to produce new ordering keeping the thermodynamical volume of the system constant as well as all molecular axes aligned, the molecular centres of mass should be shifted thereby resulting in a smectic phase where molecules tilt over from the z axis, see figure 1.22.

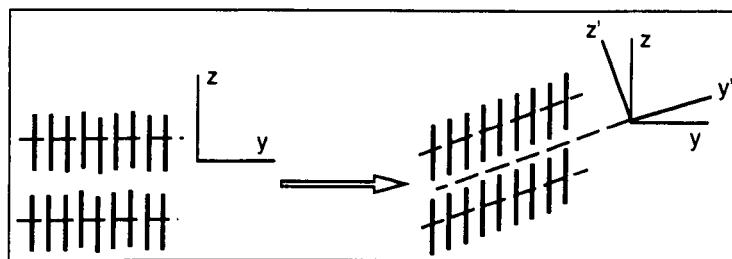


**Figure 1.22** Transition to the tilted smectic phase

The actual increase of the molecular volume and its effect on the energy can be neglected as shown in the model's calculations. The interaction potential is also calculated in a mean field approximation. As a result a second order phase transition, SmA-SmC, is found with a tilt angle growing constantly from zero at the transition and always remaining smaller than  $\pi/4$ .

#### 1.3.2.4 Comparison of the theory with experiment

Wulf's steric model and McMillan's model of transverse dipoles were put in serious doubt in the experimental work by Goodby and de Jeu [84, 85]. At the same time they reported synthesis of new compounds exhibiting SmA and SmC phases and provided the detailed analysis of their structures, effect on mesomorphic behaviour, and formation of the SmC phase in particular.

In the work by de Jeu four types of compounds depicted in figure 1.23 were under investigation.

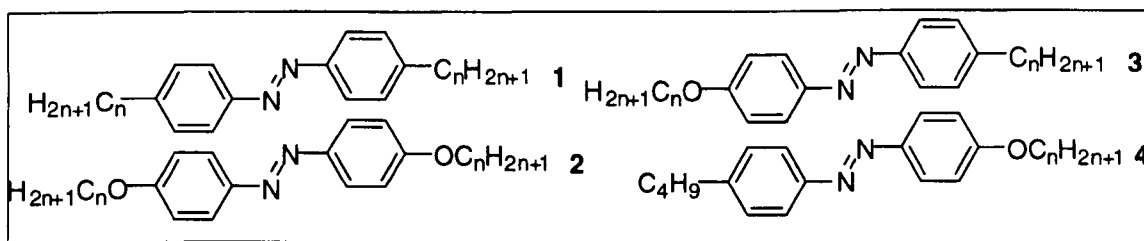


**Figure 1.23** Molecular structures discussed in reference 84

The phase sequence of compounds **1** includes a nematic phase and for long alkyl substituents - SmA and SmB phases. In type **2** compounds an ether linkage was introduced to the terminal alkyl chains thereby producing a dipole moment of about 1.3 D at an angle of about  $72^\circ$  with the p,p'-axis of the adjacent aromatic ring. Remarkably, the magnitude of the dipole component along long molecular axis is not affected by substitution of one alkyl carbon with an ether oxygen and remains *ca.* 0.4 D. Hence, the dipole components along the long molecular axis are very similar for the compounds of general structure **1** and **2**. Furthermore their molecular shape does not change much with introduction of an ether oxygen because its size is somewhat smaller than a  $\text{CH}_2$  group and makes the molecules of series **2** about only 0.5 Å longer than the corresponding values in series **1**.

The zigzag shape of molecules of general structure **1** having the  $\text{C}_{\text{Ar}}\text{-C-C}$  angle of  $108^\circ$  (tetrahedral value) is more pronounced than that of molecules of general structure **2** with a  $\text{C}_{\text{Ar}}\text{-O-C}$  angle of  $120^\circ$ . It is also stabilised in structures **1** by less flexible alkyl chains. Nevertheless, the SmC phase was found in compounds **2**. There is no SmA phase present between the N and the SmC phases. As soon as the layered structure is established the phase takes the form of a SmC phase with a relatively large tilt angle.

In series **2** two outboard dipoles (as mentioned above) are introduced into molecular structure. Hence, the results are in agreement with McMillan's dipole model of the SmC phase. The fact that central dipole moment has no influence on the type of the smectic phase which appeared requires free rotation of the central aromatic cores in these systems. It is only the rotation of the dipoles of the ether groups that is not allowed.

The absence of the SmC phase in the phase sequence of compounds **1** shows that repulsion between zigzag shaped molecules are hardly responsible for the formation of the tilted structure, at least for the compounds under consideration.

An interesting test of the transverse dipole model is provided by the compounds of general structure **3**, which exhibit a small tendency to form the SmC phase. They contain only one dipole moment at one molecular end, though the molecular shape is retained similar to that of molecules of general structure **1** and **2**. Assuming that there is no preference in molecular orientation (up or down) McMillan model could still be applied (figure 1.24).

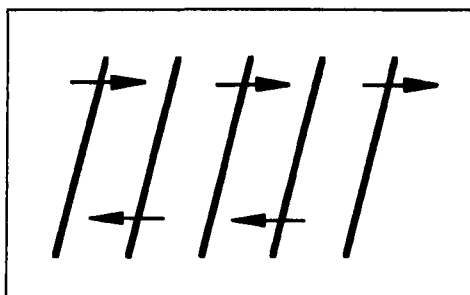


**Figure 1.24** Packing of molecules with one transverse dipole

In this case the distances between the dipoles would be longer and they would affect the McMillan calculations of SmA-SmC transition temperature by the factor  $2 \cdot 2^{-1/2}$  thereby reducing the transition temperature more than twice that of its initial value. That reduction could be avoided if one considers transverse polarizabilities instead of the

transverse dipoles. For simplicity, the transverse polarizability could be assumed to be represented by two point polarizabilities at the positions  $\pm d/2$ . Including polarizability into McMillan's equation increases the transition temperature by about 50% thereby compensating for the absence of a second dipole.

Another conclusion drawn from de Jeu's work is that the symmetrical shape of molecules is not always an essential factor for the SmC phase formation. Comparison of compounds of general structure **3** and **4** that have the same length shows the tendency to form the SmC phase is greater in case of non-symmetrical molecules of general structure **4**. Generally, there was no evidence found to support McMillan's and Wulf's ideas of molecular symmetry playing the main part in SmC phase formation. However, the tendency to form smectic phases of some other type increases more strongly for the non-symmetrical molecules than the tendency to form a SmC phase.

Another experimental study, which opposed the models of transverse dipoles and steric repulsion was provided by Goodby et al [85] (figure 1.25). Comparing mesomorphic behaviour of compounds **1** and **2** (figure 1.25) highlights that the smectic C phase may appear when the transverse dipoles are not present in the molecular structure. This contradicts the idea that transverse dipoles are necessary to tilt the molecules over in the smectic layers. Though it was also found that such dipolar properties do appear to stabilise the SmC phase, i.e. give higher SmC-SmA transition temperature and broader interval of the mesophase.

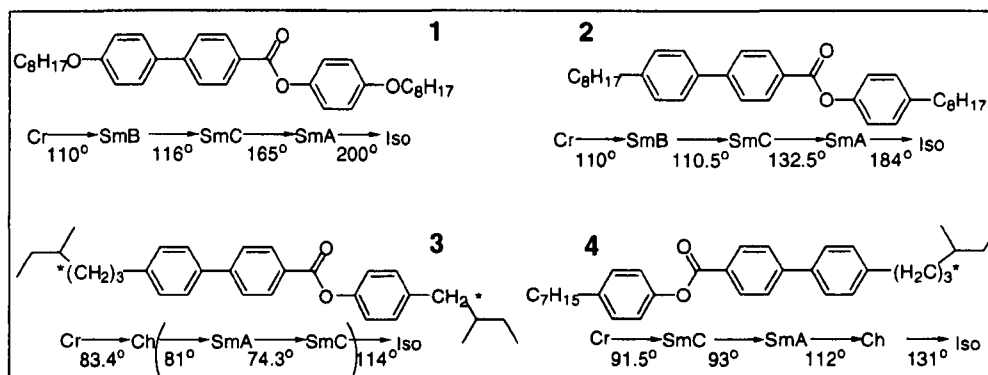


**Figure 1.25** Structures of compounds described in reference 85

The structures **3** and **4** have the branched alkyl chains at the both molecular ends that move molecular conformation away from the zigzag shape. The fact that they still exhibit the SmC phase does not support the Wulf's idea of zigzag packing being an essential feature of molecular self-organisation to form a SmC phase. These experimental data essentially demonstrate that transverse dipoles still play significant role in formation of the SmC phase. However, as used by McMillan dipole-dipole interactions cannot be responsible for the molecular tilt.

### 1.3.2.5 Model of induced dipoles interaction

In order to overcome the shortfalls of the dipole model some specific type of interaction, independent of the rotation around long molecular axis, was to be found for the description of the SmC phase. One of the attempts to produce a reliable equation for intermolecular potential was made by Van Der Meer and Vertogen [86, 87].

The model by Van Der Meer and Vertogen takes into consideration dipole - induced dipole interaction between molecules, namely the interaction of a permanent dipole moment of one molecule and the polarizable core of the neighbouring molecule, figure 1.26. This interaction is quadratic and hence is independent of the rotation around long molecular axis.

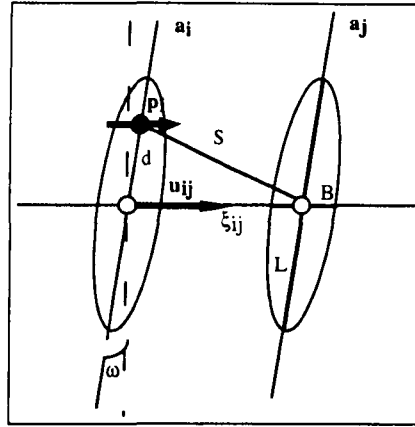


**Figure 1.26** Representation of molecular model by Van Der Meer and Vertogen.

Firstly, the orientational part of the interaction potential is determined. It is assumed that orientational dependence of the potential is largely due to the coupling between van der Waals forces and anisotropic hard repulsions. The interactions between two molecules  $i$  and  $j$  can be considered to be only dependent upon the nearest neighbour distance or the closest distance of approach  $\xi(i, j)$ . The distance varies between the molecular breadth  $B$  and length  $L$ . It is also a function of the orientations of the long molecular axes as defined by  $\mathbf{a}_i$  and  $\mathbf{a}_j$ , and the direction of intermolecular vector  $\mathbf{u}_{ij}$  that points from the centre of  $i$  to the centre of the molecule  $j$ .

The expression for the orientational part of the potential is derived and expanded in series of  $\omega$ :

$$V(\omega) = -V_0 + V_2 \sin^2 \omega + V_3 \sin^4 \omega$$

$V_0$  is a coefficient describing an interaction between parallel molecules in the SmA phase.  $V_2$  and  $V_3$  are the interactions when the molecules are tilted with a tilt angle of  $\omega$ . The equation states clearly that in the absence of any additional interaction the SmA ordering is the most favoured. The only way to produce a tilt without increasing the energy is to introduce an additional interaction, which will change the sign of the second term of the equation. The third term is small compared to other two.

When a molecular dipole is introduced onto the axis of one of the molecules, it induces a dipole in the centre of the neighbouring molecule. The energy of the attraction between the dipole and the centre of another molecule is found to be a function of  $\mathbf{d}$  (the distance from the dipole to the molecular centre),  $B$  (breadth), and  $L$  (length),  $(\mathbf{a}_i \cdot \mathbf{p}_i)$  (the angle between the dipole and long molecular axis) and can be expressed as:

$$V_{\alpha\mu} = -1/3\alpha\mu^2 B^{-6}(1+x^2)^{-6}[7x^4 + 6x^2 - 1 + (7x^4 - 12x^2 + 1)P_2(\bar{\mathbf{a}}_i \cdot \bar{\mathbf{p}}_i)](\bar{\mathbf{a}}_i \cdot \bar{\mathbf{u}}_{ij})^2$$

where  $\alpha$  is the central polarizability,  $\mu$ - dipole moment,  $x = d/B$ . The coefficient  $(\mathbf{a}_i \cdot \mathbf{u}_{ij})^2$  has the following properties:

for  $P_2(\mathbf{a}_i \cdot \mathbf{p}_i) = 1$  (longitudinal dipole) its optimal value is  $-0.1 \alpha\mu^2 B^{-6}$  at  $x = 1$ .

for  $P_2 = 0$  (the angle between the dipole and the long axis is  $54.7^\circ$ ) its optimal value is  $0.31 \alpha\mu^2 B^{-6}$  at  $x = 0.7$ .

for  $P_2 = -1/2$  (transverse dipoles) its optimal value is  $-0.5 \alpha\mu^2 B^{-6}$  at  $x = 0.6$ . Thus, an acentral dipole and, particularly, an acentral transverse dipole placed somewhere in between the centre and one of the ends of the molecule induces the highest tendency for the long axis to tilt towards the direction of the line connecting the centre of the molecule and that of the neighbour.

The final interaction can be summarised as follows:

$$V(\omega) = -V_0 + (V_2 - 2V_{\alpha\mu})\sin^2 \omega + V_3 \sin^4 \omega$$

The coefficient  $2$  appears to describe the effect of the dipole of the second molecule on the first one. If  $V_{\alpha\mu}/V_2 < 1/2$ , the energy is minimal for  $\omega = 0$ . This situation corresponds to the smectic A phase. If  $V_{\alpha\mu}/V_2 > 1/2$  the energy is minimal for  $\omega \neq 0$  and the smectic C phase is formed.

To sum up, it should be noticed, once again, that an important role in the formation of the SmC phase is played by transverse dipole moments situated at the optimal location in the molecular structure. In this case its contribution to the dipole-induced dipole interaction is maximised and the forces, which oppose the tilt, can be overcome. The estimated magnitudes of the two competing interactions are of the same order and if there are strong enough dipoles present in the molecules the SmC phase may appear.

### **1.3.2.6 Concept of the ordered electricity in the quadrupole systems**

Finally, the most recent approach to the problem of molecular tilt in smectics should be mentioned. The interaction potential in the Van Der Meer and Vertogen model is independent of molecular rotation and hence is not in contradiction with experiment. At the same time, its mathematical form looks similar to the expression found for the model, which considers quadrupolar interactions between the molecules in a mesophase as the driving force of the molecular tilt [88]. This model is a further development of the method used by Barbero and Durand [89] who argue that molecular tilt is an intrinsic property of any layered quadrupole structure.

In their attempt to explain nematic – smectic C and smectic A smectic C phase transition the authors consider nematic liquid crystals as uniform quadrupole oriented systems. There is a possibility for macroscopic spatial modulation, which is realised in form of a layered structure (such a modulation also leads to the formation of twist in chiral nematics). As soon as such a structure of layered quadrupoles is present a gradient of quadrupole moment,  $\nabla Q$ , appears throughout the material. This is due to the electrostatic interaction between the same parts of different molecules which are in most cases have electron-rich hard core and flexible alkyl chains with low electron density on both sides.

A gradient of quadrupole moment gives rise to an electric polarization, which will contribute into the energy of the system in terms of dielectric part with general expression:

$$2\pi P_Z^2 / \epsilon_{ZZ} = (1/2)a^2(\cos^2 \theta - 1/3)^2$$

Parameter  $a$  includes all of the functions which appear in the model. It could be seen that to suppress this contribution the molecules should tilt over at the “magic” angle,  $\cos^2 \vartheta = 1/3$ ,  $\vartheta = 54^\circ$ . Thus, it is a geometrical property of a quadrupolar layered system that a tilt at the “magic” angle suppresses the dielectric energy, by aligning the dipoles normal to the order gradient. The bigger the quadrupolar moment of the molecules the more ordered they become and the tendency to tilt is more pronounced. This concept of ordered electricity in nematics can also be used to explain the formation of tilted phases in the lyotropic systems.

In conclusion, it should be noted that models of induced dipolar and quadrupolar interactions use similar mathematical expressions for the interaction potential. In general, the quadrupolar type of potential appears to be a good model potential for the theory of nematic or smectic A – smectic C transitions. It will be important in the future to find more general correlation of molecular structure with appearance of the tilt in smectics. Also, all of the models discussed, neglect the biaxiality of the smectic C phase which is always induced by the tilt. Corresponding contributions to the free energy, however small, still deserve a further attention.

**References (sections 1.1 – 1.3)**

1. GA Smolenski, "Ferroelectrics and Related Materials", Gordon and Breach Science Publishers, 1984
2. ME Lines, AM Glass, "Principles and Applications of Ferroelectrics and Related Materials", Oxford, Clarendon Press, 1977, p. 8
3. C Kittel, *Phys Rev*, **82**, 1951, 729
4. G Shirane, *Phys Rev*, 1951, **84**, 476
5. RJ Coelho, "Physics of Dielectrics for the Engineer", Oxford: Elsevier, 1979
6. ref 1 p. 236, p. 310
7. ref 2, p.328
8. YA Izyumov, VN Syromyatnikov, "Phase Transitions and Crystal Symmetry", Kluwer Academic Publishers, 1990
9. International Union of Crystallography, "International Tables of Crystallography", Birmingham: Kynoch P, 1959
10. F Jona, G Shirane, "Ferroelectric Crystals", New York: Doven Publications Inc, 1993, p. 110
11. Colloque Pierre Curie, "Symmetries and Broken Symmetries in Condensed Matter Physics: Proceedings of the Colloque Pierre Curie", ed. by N Boceara, Paris: IDSET, 1981
12. RE Newnham, "Structure-Property Relations", Springer-Verlag, 1975, p.19
13. ST Lagerwall in "Handbook of Liquid Crystals", ed D Demus, JW Goodby, GW Gray, H.-W Spiess, V Vill, Wiley-VCH, 1998, Vol 2B, p. 552
14. JP Glusker, M Lewis, M Rossi, "Crystal Structure Analysis for Chemists and Biologists", 1994, VCH, p. 169
15. ref 14, p. 15
16. ref 10, p. 82

17. RB Meyer, L Liebert, L Strzelecki and P Keller, *J de Physique*, 1975, **36**, L69
18. PG de Gennes and J Prost, "Physics of Liquid Crystals", Oxford: Clarendon Press, 2<sup>nd</sup> ed, 1993
19. R Blinc in "Advances in Liquid Crystal Research and Applications" ed. L Bata, Pergamon Press Akademiai Kiado, 1981, Vol 1, p. 328
20. SA Pikin and MA Osipov in "Ferroelectric Liquid Crystals" ed JW Goodby et al., Gordon and Breach Science Publishers, 1991, p. 288
21. ref 2, p. 546
22. LM Blinov in "Physical Properties of Liquid Crystals", Wiley-VCH, 1999, p.376
23. I Musevic, B Zeks and R Blinc in "Liquid Crystals in the Nineties and Beyond" ed. S Kumar, World Scientific, 1995, p. 205
24. J Goldstone, A Salam and S Weinberg, *Phys Rev*, 1962, **127**, 965
25. R Blinc, *Ferroelectrics*, 1999, **220**, 105
26. LA Beresnev, LM Blinov, VA Baikalov, EP Pozhidayev, GV Purvanetskas and AI Pavluchenko, *Mol Cryst Liq Cryst*, 1982, **89**, 327
27. A.-M Levelut, C Germain, P Keller, L Liébert and J Billard, *J Phys (Paris)*, 1983, **44**, 623
28. Y Galerme, L Liébert, *Phys Rev Lett*, 1990, **64**, 8, 906
29. JW Goodby and E Chin, *Liq Cryst*, 1988, **3**, 1245
30. ADL Chandani, T Hagiwara, Y Suzuki, Y Ouchi, H Takazoe, A Fukuda, *Jpn J Appl Phys*, 1988, **27**, L729
31. ADL Chandani, E Gorecka, Y Ouchi, H Takezoe and A Fukuda, *Jpn J Appl Phys*, 1989, **28**, L1265
32. Y Takanishi, H Takezoe, A Fukuda, H Komura and J Watanabe, *J Mat Chem*, 1992, **2**, 1, 71

33. KA Suresh in "Liquid Crystals in the Nineties and Beyond" ed. S Kumar, World Scientific, 1995, p. 225
34. ADL Chandani, Y Ouchi, H Takazoe, A Fukuda, K Terashima, K Furukawa and A Kishi, *Jpn J Appl Phys*, 1989, **28**, L1261
35. H Takazoe, J Lee, A Fukuda, *Mol Cryst Liq Cryst*, 1991, **202**, 85
36. T Nakai, S Miyajima, Y Takanishi, S Yoshida and A Fukuda, *J Phys Chem B*, 1999, **103**, 406
37. ref 10, p. 329
38. ref 1, p.104
39. M Cepic and B Zeks, *Mol Cryst Liq Cryst*, 1995, 263, p. 61
40. A Roy and NV Madhusudana, *Eur Phys J E*, 2000, **1**, p. 319
41. JW Goodby and GW Gray in "Physical Properties of Liquid Crystals", Wiley-VCH, 1999, p. 17
42. A Fukuda and T Matsumoto, *Mol Cryst Liq Cryst*, 1999, 328, p. 1
43. P Mach, R Pindak, AM Levelut, P Barois, HT Nguyen, H Baltes, M Hird, K Toyne, A Seed, J Goodby, CC Huang, L Furenid, *Phys Rev E*, 1999, **60**, 6793
44. AJ Leadbetter in "Thermotropic Liquid Crystals" ed. GW Gray, John Wiley and Sons, 1987, p. 1
45. AJ Leadbetter in " The Molecular Physics of Liquid Crystals" ed. GR Luckhurst and GW Gray, Academic Press, 1979, p. 285
46. ref 16, p 131
47. JM Seddon in "Handbook of Liquid Crystals", ed D Demus, J Goodby, GW Gray, H.-W Spiess, V Vill, Wiley-VCH, 1998, Vol 2B, p. 655
48. VE Dmitrienko, *Acta Cryst*, 1983, **A39**, 29
49. S Bhagavantam "Crystal Symmetry and Physical Properties", Academic Press, 1966, p. 62

50. JC Burfoot, "Ferroelectrics: An Introduction to the Physical Principles", London: D. Van Nostrand Company Ltd, 1967, p. 23
51. P Toledano, AM Figueiredo Neto, AA Boulbitch and A Roy, *Phys Rev E*, 1999, **59**, 9, p. 6785
52. HF Franzen "Physical Chemistry of Solids", World Scientific, 1994, p. 59
53. HD Megaw, "Crystal Structures: A Working Approach", Philadelphia: Saunders, 1973
54. G Heppke and D Moro, *Science*, 1998, **279**, 1872
55. SA Pikin, *Mol Cryst Liq Cryst*, 1999, **328**, 31
56. I Nishiyama and JW Goodby, *J Mater Chem*, 1992, **2**, 1051
57. A Fukuda, Y Takanishi, T Isozaki, K Ishikawa and H Takazoe, *J Mater Chem*, 1994, **4**, 997
58. K Miyachi and A Fukuda in "Handbook of Liquid Crystals", ed D Demus, J Goodby, GW Gray, H.-W Spiess, V Vill, Wiley-VCH, 1998, Vol 2B, 665
59. BI Ostrovski in "Liquid Crystals I" ed. DMP Mingos, Springer, 203
60. H Allouchi, HT Nguyen and M Cotrait, *Mol Cryst Liq Cryst*, 1999, **328**, 375
61. T Kasumoto, K Sato, H Matsutani, A Yoshizawa, N Ise, J Umezawa, Y Takanishi, H Takazoe, T Hiyama, *Mol Cryst Liq Cryst*, 1999, **330**, 1471
62. DD Parghi, SM Kelly, and JW Goodby, *Ferroelectrics*, 1998, **212**, 349
63. J Watanabe and M Hayashi, *Macromolecules*, 1989, **22**, 4083
64. I Nishiyama and JW Goodby, *J Mat Chem*, 1993, **3**, 2, 169
65. EAS Bustamante, SV Yablonskii, BI Ostrovski, LA Beresnev, LM Blinov and W Haase, *Liq Cryst*, 1996, **21**, 6, 829
66. AG Vanakaras, DJ Photinos and ET Samulski, *Phys Rev E*, 1998, **57**, 5, p. 4875
67. VM Kaganer, JR Peterson, RU Kenn, MS Shih, M Durbin, P Dutta, *J Chem Phys*, 1995, **102**, 23, p. 9412
68. VM Kaganer, MA Osipov, *J Chem Phys*, 1998, **109**, 7, p. 2600
69. A Fukuda and T Matsumoto, *Mol Cryst Liq Cryst*, 1999, **328**, p.1
70. W Cochran "The Dynamics of Atoms in Crystals", Edward Arnold, 1973, p.138

71. JW O'Sullivan, YP Panarin, JK Vij, AJ Seed, M Hird and JW Goodby, *J Phys: Condens Matter*, 1996, **8**, L551
72. FM Leslie, in *Continuum Theory for Liquid Crystals* in "Physical Properties of Liquid Crystals", ed. D Demus et al., Wiley-VCH, 1999, pp 25-39.
73. G Vertogen, WH de Jeu, *Thermotropic Liquid Crystals, Fundamentals*, Springer-Verlag, 1988, pp 221-244.
74. MA Osipov, *Molecular Theories of Liquid Crystals* in "Physical Properties of Liquid Crystals", ed. D Demus et al., Wiley-VCH, 1999, pp 40-71.
75. L Onsager, *Ann. N. Y. Acad. Sci.*, 1949, **51**, 627.
76. W Maier, A Saupe, *Z. Naturforsch.*, 1960, **15a**, 287.
77. WL McMillan, *Phys. Rev. A*, 1971, **4**, 1238.
78. JAC Veerman, D Frenkel, *Phys. Rev. A*, 1990, **41**, 3237.
79. L Mederos, DE Sullivan, *Phys. Rev. A*, 1989, **39**, 854.
80. JW Goodby, "Smectic Liquid Crystals", *PhD thesis*, 1977
81. WL McMillan, *Phys Rev A*, 1973, **8**, No 4, 1921.
82. KC Chu and WL McMillan, *Phys Rev A*, 1977, **15**, No 3, 1181.
83. A Wulf, *Phys Rev A*, 1975, **11**, No 1, 365.
84. WH de Jeu, *J de Phys (Paris)*, 1977, **38**, 1265.
85. JW Goodby, GW Gray, DG McDonnell, *Mol. Cryst. Liq. Cryst.*, 1977, **34**, 183
86. BW Van Der Meer and G Vertogen, *de Phys Colloq (Paris)*, 1979, **40**, C3-222
87. MA Osipov, *Izv. Acad. Nauk, Physical series*, 1989, **53**, 1915.
88. E Velasco, L Mederos and TJ Sluckin, *Liq. Cryst.*, 1996, **20**, 399.
89. G Barbero, G Durand, *Mol. Cryst. Liq. Cryst.*, 1990, **179**, 57
90. LS Hirst, SJ Watson, HF Gleeson, P Cluzean, P Barois, R Pindak, J Pitum, A Cady, PM Johnson, CC Huang, AM Levelut, G Strajer, J Pollmann, W Caliebe, A Seed, MR Herbert, JW Goodby, M Hird, *Phys. Rev. E*, 2002, **65**, art no 041705, part 1
91. JT Mills, HF Gleeson, JW Goodby, M Hird, A Seed, P Styring, *J. Mat. Chem.*, 1998, **8**, 2385

### 1.4 Structures of compounds, which exhibit antiferroelectric phases

The majority of smectic liquid crystalline materials synthesised to date belong to the class of aromatic esters [1]. Well-chosen positions of carboxylic groups within an appropriate mesogenic core in most cases produces desirable liquid crystalline properties. Esters are made via simple synthetic routes and are characterised by a relatively high chemical stability. The preparation of such materials was intensified during the last two decades due to the recognition of ferroelectric properties exhibited by the smectic C\* phases. This promoted a comprehensive search for chiral materials possessing room temperature smectic behaviour and thereby room temperature ferroelectric properties. The search not only resulted in the optimisation of the smectogenic molecular structure but also led to the discovery of the antiferroelectric, the related smectic C sub-phases, the frustrated twist grain boundary phases [2] and blue smectic phases [3].

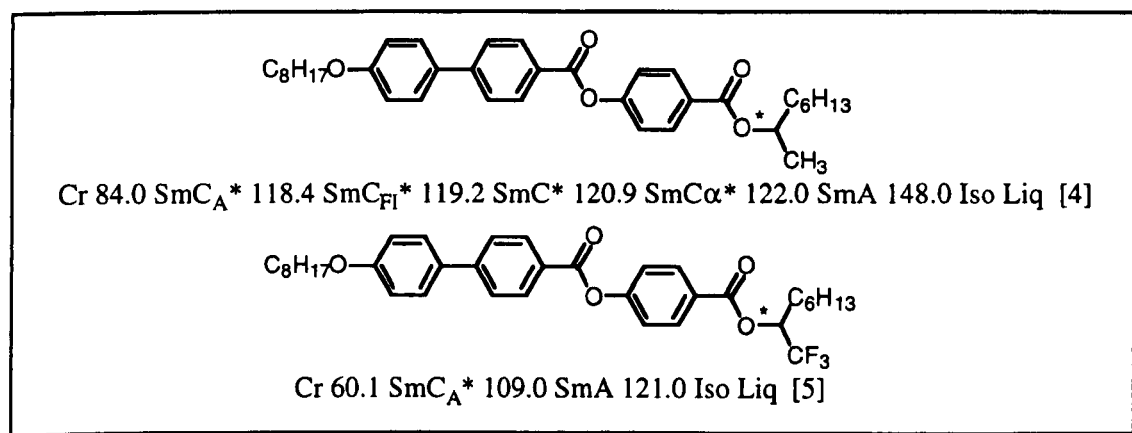


**Figure 1.27** The structures of MHPOBC and TFMHPOBC

The forerunners of most antiferroelectric liquid crystals were the aromatic diesters, *1-methylheptyl 4-(4'-octyloxybiphenyl-4-carboxyloxy)benzoate* and *1-trifluoromethyl heptyl 4-(4'-octyloxybiphenyl-4-carboxyloxy)benzoate* (MHPOBC and TFMHPOBC) [4, 5], see figure 1.27. Approximately 400 antiferroelectric liquid crystal compounds that followed have similar molecular structures to those of MHPOBC and TFMHPOBC.

The presence of an ester group in these compounds was proved to be an essential factor for the antiferroelectric phase to appear at relatively low temperatures and broad temperature ranges. Even slight structural modification to the carboxylic group, for instance, substitution of the ether oxygen with nitrogen substantially reduces the temperature interval of the  $\text{SmC}_A^*$  phase, see figure 1.28 [6]. In similar fashion, replacement of the central ester function with simple ether link in structure of MHPOBC leads to the high temperatures of the  $\text{SmC}_A^*$  phase together with shortening of the phase interval [7].

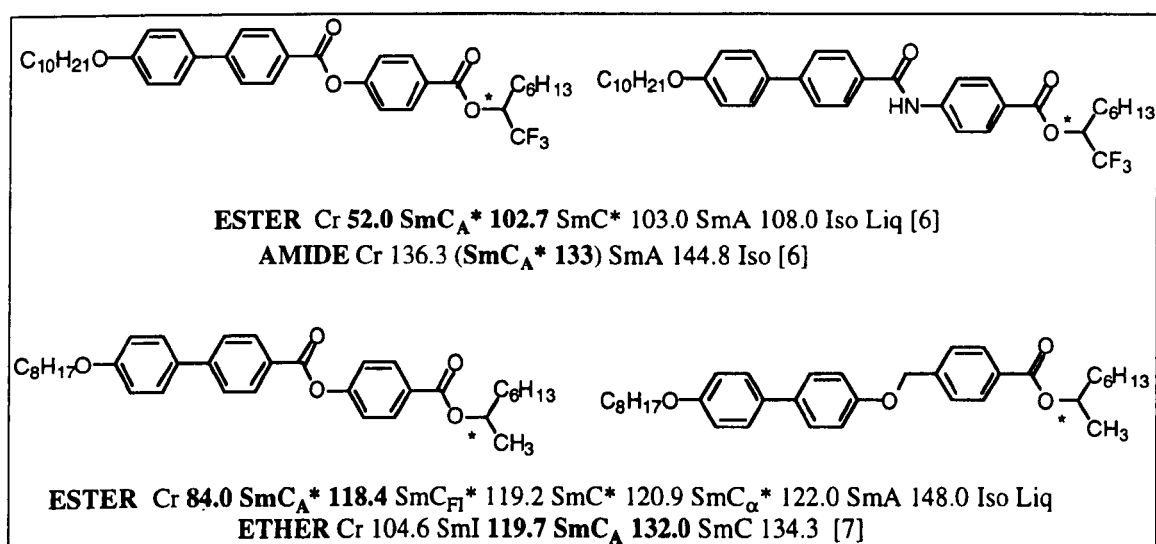
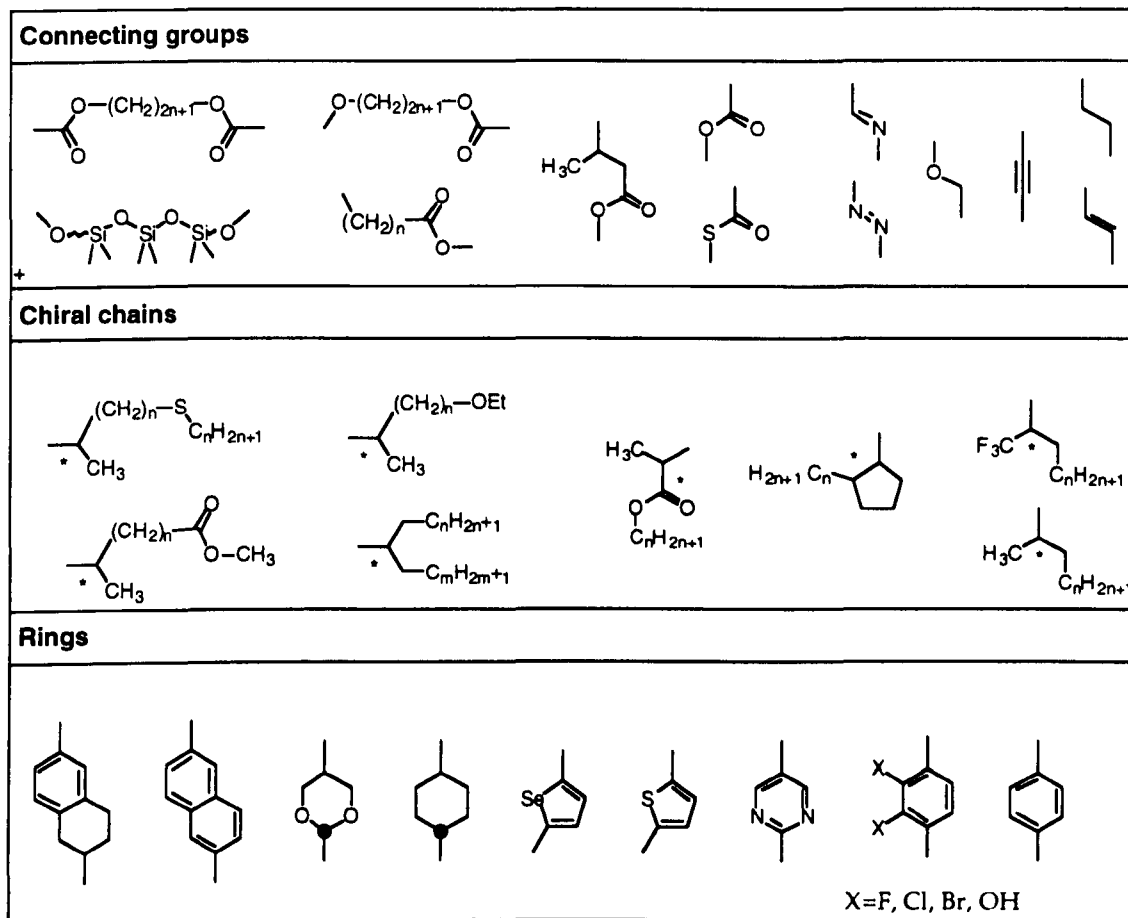


Figure 1.28 Replacement of ester functions with amide and ether connectors.

Typically, molecules that exhibit  $\text{SmC}_A^*$  phase, consist of three structural sub-units: the chiral chain, a central core and a non-chiral chain [8]. These units are combined with linking groups, which may also play a vital role in the stabilisation of the antiferroelectric properties of the material. Most commonly used structural units in the antiferroelectric materials are shown in the figure 1.29 below.



**Figure 1.29** Composite units of structures, which exhibit antiferroelectric smectic C phases.

The core is the central part of the molecular structure providing the molecule with rigidity and high geometric anisotropy. In general, it consists of at least two aromatic and/or alicyclic rings. Antiferroelectric liquid crystal compounds containing only one ring are not yet known. The optimal core dimension is believed to have three six-membered rings. Increasing the number of rings generally results in the raising of transition temperatures above 100 °C. There are examples of four- or even six-ring systems which still show the antiferroelectric phase at temperatures around 80 °C [8, 9], though in the latter case the same number of ester groups are required to provide flexibility to the structure and, as a consequence, lower melting and clearing points (figure 1.30). At the same time the presence of so many ester groups makes those

compounds more viscous which in turn affects their switching characteristic in applied electric fields.

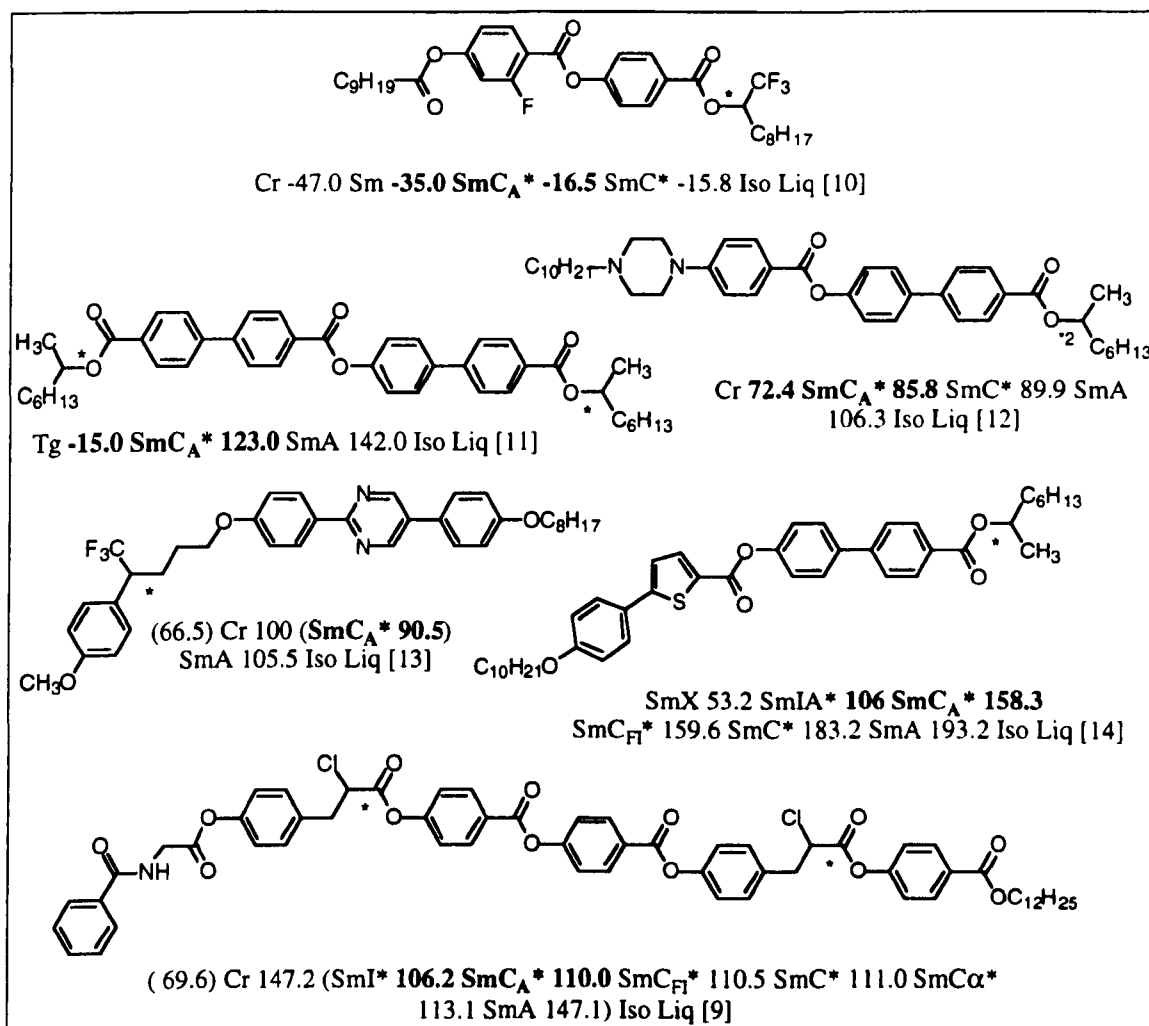


**Figure 1.30** Stability of the antiferroelectric smectic C<sub>A</sub>\* phase as a function of structure of the aromatic core.

The rings used in the core are based on benzene, cyclohexane, tetraline, 1,3-dioxane, piperidine, pyrimidine, etc, with some examples shown in the figures 1.30 and 1.31. Rings may be joined with a connector or directly thereby forming biphenyl and similar fragments or fused aromatic systems such as naphthalene. The linearity of molecular structure is not essential. For example, incorporation of the thiophene ring into a mesogenic core produces a bend shaped core without suppression of the SmC<sub>A</sub>\* phase (figure 1.31).

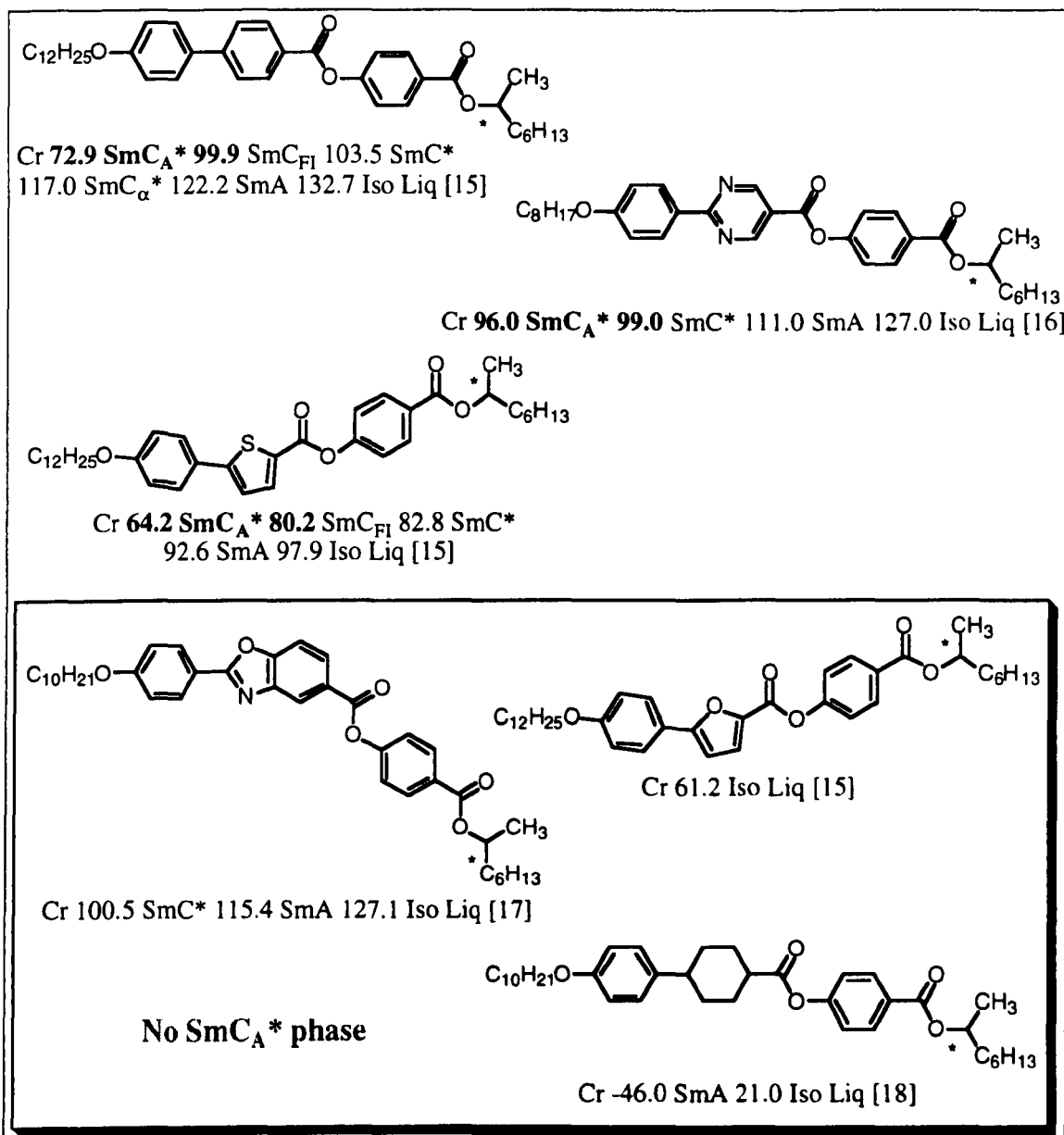


**Figure 1.31** Examples of molecular structures that have positive and negative effect on stability of the SmC<sub>A</sub>\* phase

Some exceptions should also be mentioned. The last three compounds in the figure 1.31 do not exhibit the antiferroelectric phase and the reasons for that are not yet clear.

A concise analysis of the effect of various rings on the stability of the SmC<sub>A</sub>\* phase could be offered as summarised in the diagram below, see figure 1.32. Rings appearing in the generic structure shown above the diagram are arranged horizontally according to

the index of  $\text{SmC}_A^*$  phase stability  $\text{St}$  (axis  $x$ ) determined for each compound as following:

$$\text{St} = \Delta T_{\text{CA}} / \Delta T_{\text{LC}}$$

where  $\Delta T_{\text{CA}}$  is a temperature interval of the antiferroelectric phase and  $\Delta T_{\text{LC}}$  is whole mesophase temperature range. When  $\text{St}$  equals 1 the antiferroelectric phase is the only mesophase in the phase sequence.

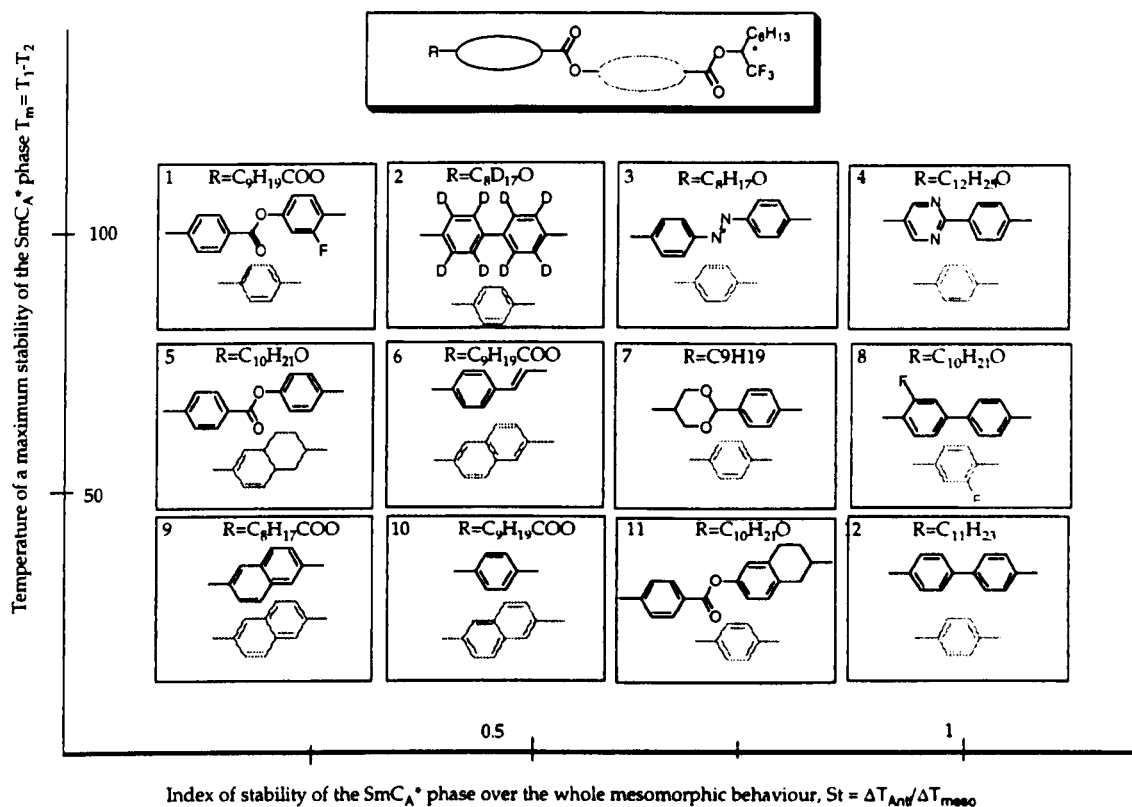


**Figure 1.32** An approximate estimation of stability of the  $\text{SmC}_A^*$  phase as a function of the structure of molecular core [19]

Along the vertical axis the average temperature of the  $\text{SmC}_A^*$  phase  $T_m$  is considered:  $T_m = (T_2 + T_1) / 2$  where  $T_1$  and  $T_2$  are top and bottom temperature limits of the antiferroelectric phase. Thus, MFPOBC is placed in the right bottom corner of the diagram as it exhibits an antiferroelectric phase at the expense of any other phase at the temperature interval centred around 20-30 °C. Being one of the first antiferroelectric liquid crystals MFPOBC still remains by far the one the most studied. The greatly

reduced stability of the  $\text{SmC}_A^*$  phase of its deuterium analogue demonstrates how the slightest change in molecular structure affects the stability of the  $\text{SmC}_A^*$  phase.

In general, a high degree of the aromaticity of the core appears an essential structural feature of the  $\text{SmC}_A^*$  phase. The core is also required to be more or less flat. For example, the dioxanyl ring, structure 7 (figure 1.32), slightly sticks out from the plane of the core destabilising intralayer interactions. In similar fashion, extra flexibility associated with the molecular core, e.g. provided with ester, azo or alkene linking groups (structures 1,3 and 6 respectively) does not enhance the antiferroelectric phase stability in comparison to the simple biphenyl structure 12. Introducing the pyrimidine ring (structure 4) increases the  $T_m$  value and the stability index remains at a fairly high level, close to 1.

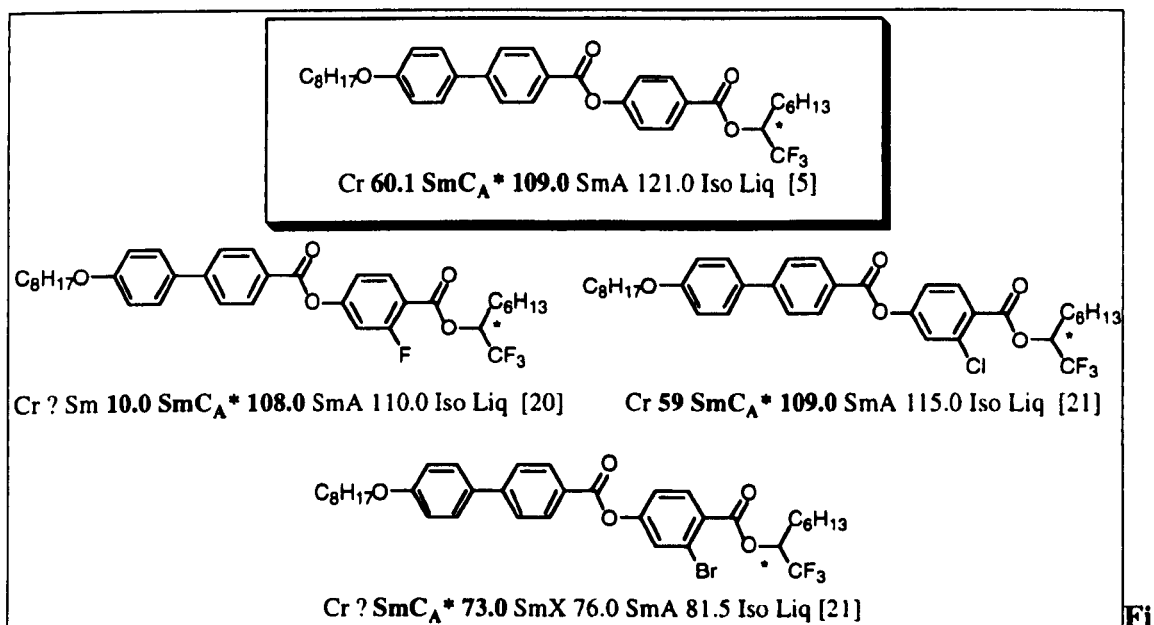
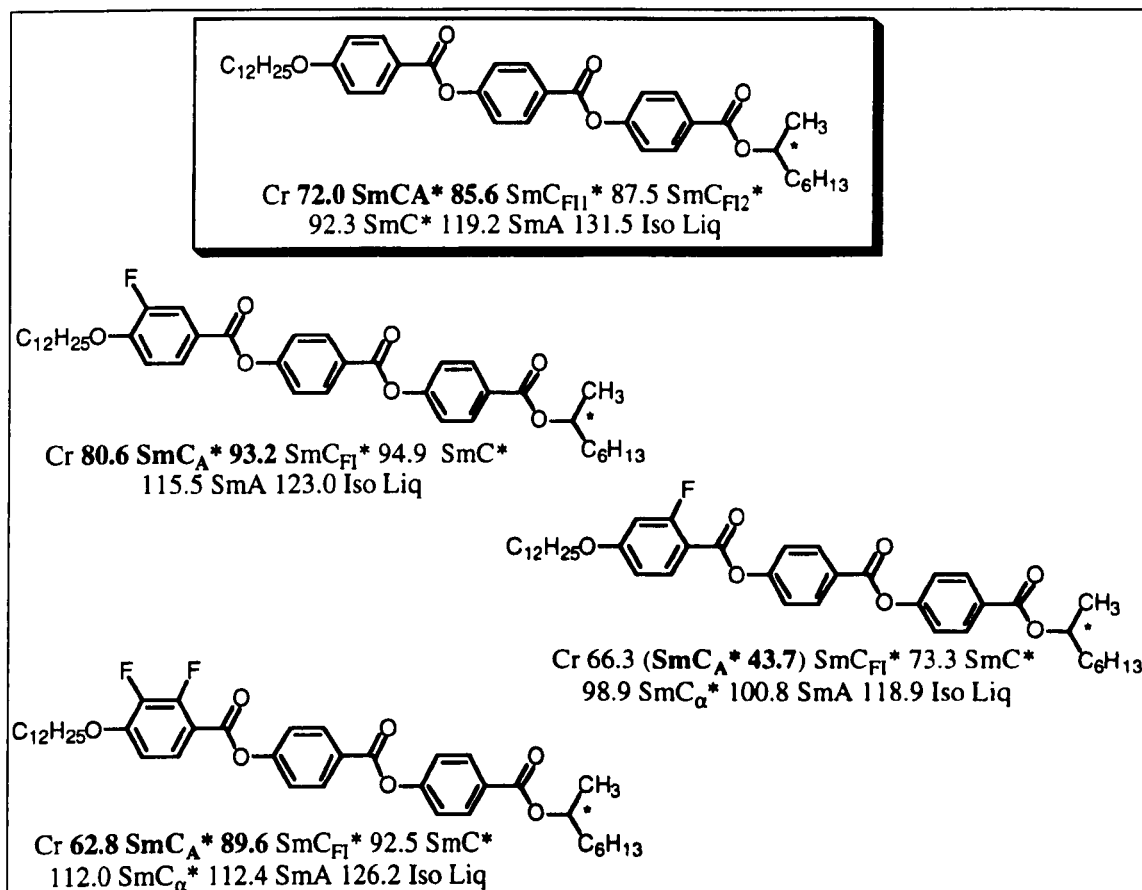


Figure 1.33 Effect of halogen atoms introduced into the molecular core

The incorporation of different substituents in the ortho- and meta-positions to the bridge, or linking group may substantially affect the mesomorphic behaviour depending on the size and polarity of the substituent. The most commonly used substituents are

halogen atoms with fluorine substituent being most studied commonly due to its small size (figure 1.33).

Fluorine substituted within the core is also important as well as the number of fluorine atoms that are introduced (figure 1.34).



**Figure 1.34** Effect of fluorine atoms and their number introduced into molecular core

[21]

In determining the stability of the antiferroelectric phase an important role is played by the structure of the chiral chain, which should favour the self-assembly of layers with an alternating tilt direction. Generally, the chiral chain possesses two alkyl groups in a branched aliphatic moiety. The main branch may contain an alkoxy, ester, alicyclic or aromatic group at the terminus. The most common structure of the chiral chain is  $-CH^*(CH_3)C_nH_{2n+1}$ , though  $-CH^*(CF_3)C_nH_{2n+1}$  moiety is known to stabilise

antiferroelectricity much better, see for example transition temperatures of MHPOBC and MFPOBC. In turn, it is also believed that when the branching occurs at the second carbon in the chain, e.g.  $-\text{CH}_2\text{CH}^*(\text{CH}_3)\text{C}_n\text{H}_{2n+1}$  the antiferroelectric phase is suppressed totally. The polarity of the C-F bond introduces a significant dipole moment to the molecular structure at the chiral centre. Its orientation related to the rest of the structure determines whether the CF dipole contributes to the total dipole moment of molecular structure or counteracts it. Alternatively, instead of cancelling the effect of other polar groups fluorine may be part of the more complex quadrupole structure, which is known to have a stabilising effect on the alternating tilt of molecules (see section 1.3 of this introduction).

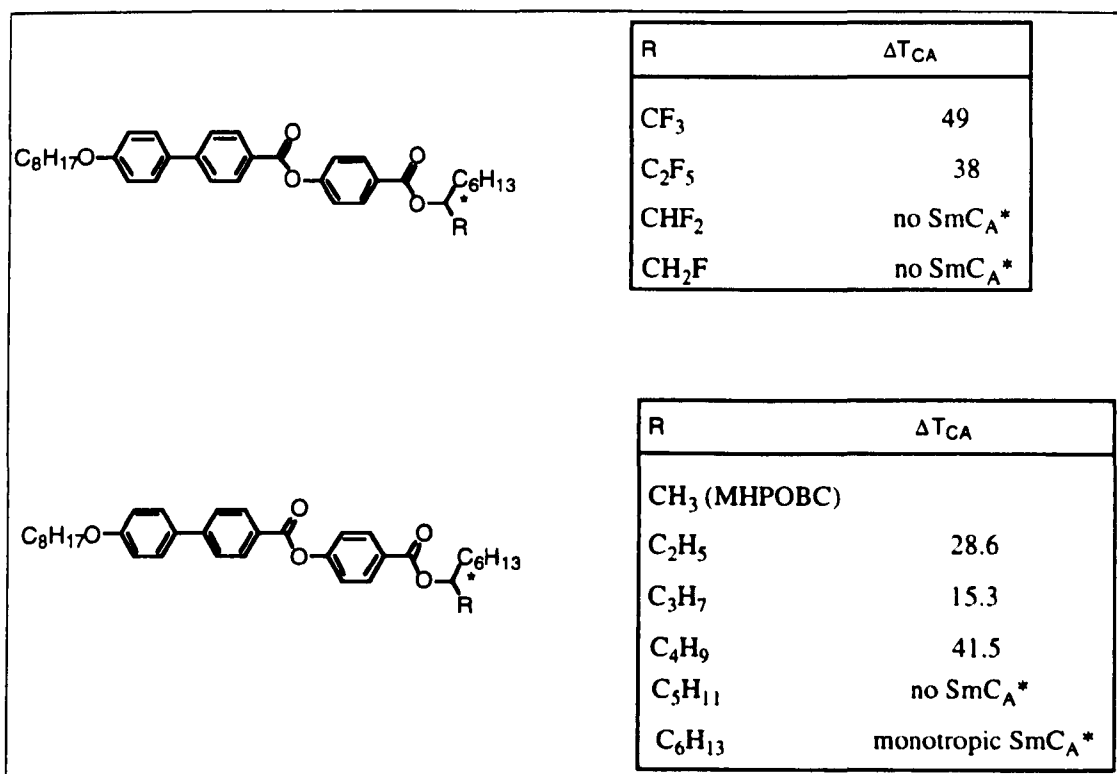


**Figure 1.35** Dependence of antiferroelectric phase stability with respect to the length of lateral branch [23, 24]

It can be clearly seen in figure 1.35 that fully fluorinated short end of the chiral chain stabilises the SmC<sub>A</sub>\* and partial substitution favours the SmC\* phase. In the former case the polarity and, more important, orientation of the CF<sub>3</sub> dipole adds to the dipoles

of the carbonyl groups and forms a quadrupole with them. In contrast, contribution of  $\text{CHF}_2$  or  $\text{CH}_2\text{F}$  groups is only enough to produce a synclinal tilted structure of the  $\text{SmC}^*$  phase. The lateral branch of the chiral chain may include more than two atoms of carbons. In general the branch longer than butyl may destabilise the antiferroelectric phase with an odd-even effect being observed (figure 1.35).

In the case of the 1-alkylheptyl 4'-(4''-nonyloxyphenylpropiolyloxy)biphenyl-4-carboxylates (figure 1.36) the antiferroelectric phase is stabilised via suppression of the  $\text{SmC}^*$  phase as the length of lateral branch is increased. Replacement of the methyl with a propyl group leads to complete disappearance of  $\text{SmC}^*$  phase and the transition to the  $\text{SmC}_A^*$  phase occurs directly from the  $\text{SmA}^*$  phase. This effect has been coined the "propyl effect" [25].

p	Iso to A*	A* to C*	A* or C* to C*anti	Recryst
1	92.7	65.8		54.0
2	68.9	46.2	45.3	<RT
3	59.8		42.6	<RT

*The transition temperatures (°C) for the (R) and (S)-1-alkylheptyl 4'-(4''-nonyloxyphenylpropiolyloxy)biphenyl-4-carboxylates.*

**Where <RT denotes a transition occurring below room temperature.**

**Figure 1.36** Demonstration of the "propyl" effect for the series of chiral 1-alkylheptyl 4'-(4''-nonyloxyphenylpropiolyloxy)biphenyl-4-carboxylates

Lastly, the structures of the non-chiral chain stabilising the antiferroelectric phase should be mentioned. The length of the alkyl chain in antiferroelectric compounds directly connected to the aromatic core may broadly vary from 6 to 16 atoms of carbons. Substitution of the alkyl chain with alkoxy radical generally broadens the  $\text{SmC}_A^*$  temperature interval though it is also accompanied with a slight increase in transition temperatures. The ester linkage placed between the core and the alkyl chain has a similar effect [27].

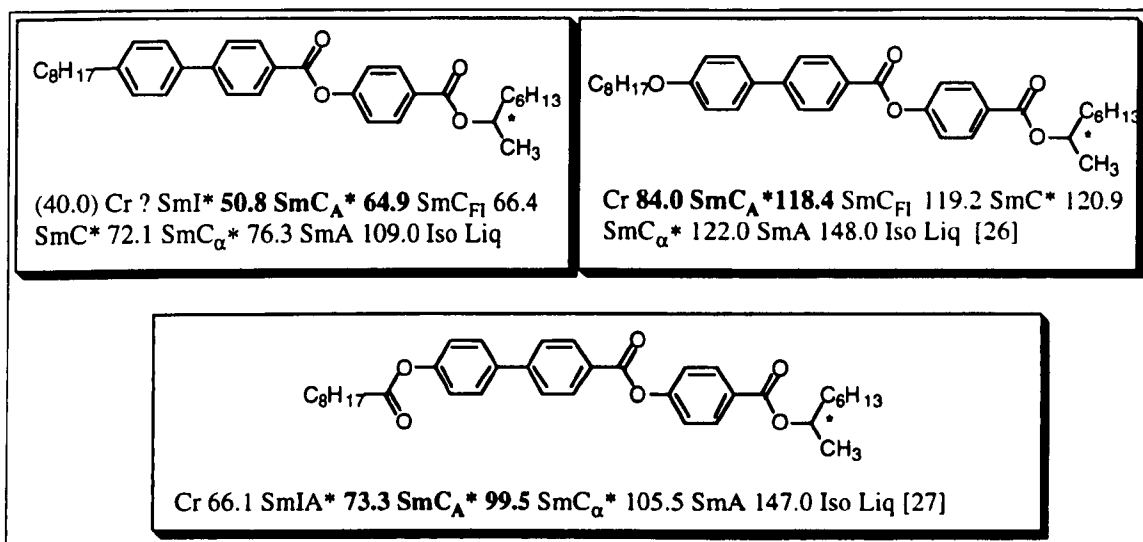


**Figure 1.37** Variations in the non-chiral chain structure

Minor structural changes at the terminus of the non-chiral chain generally do not affect the stability of the antiferroelectric phase, see figure 1.38. However, they may suppress other mesophases allowing the alternating arrangement of tilted layers to dominate the structure of the liquid crystal over a broad temperature range. For instance, both methoxyl and double bonded termini introduced instead of the methyl group for the structures shown in figure 1.38 suppress the formation of the orthogonal SmA phase thereby producing materials, which exhibit only antiferroelectric phases.

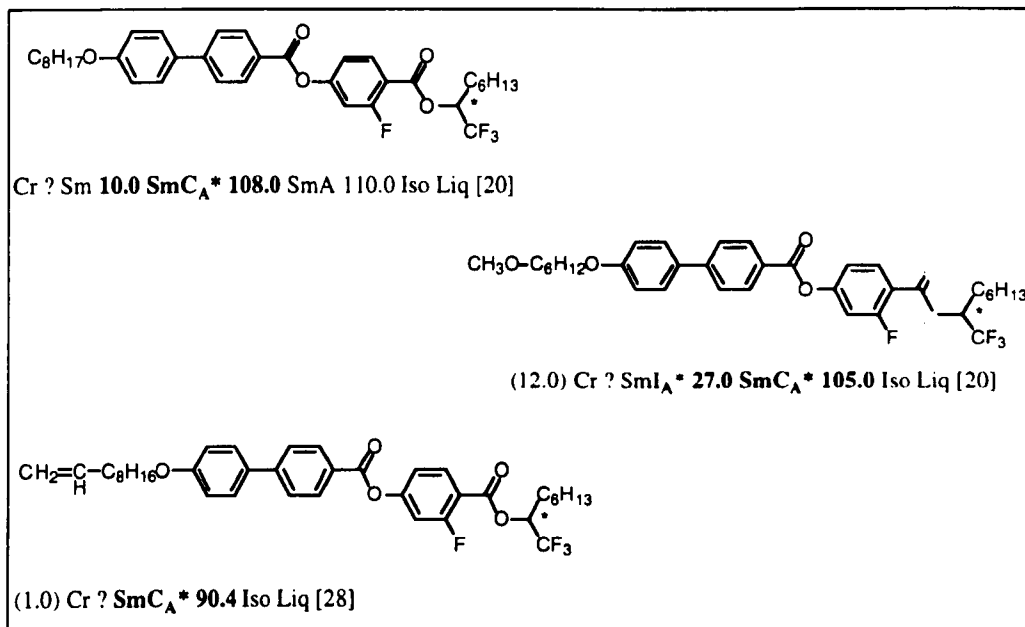


**Figure 1.38** Effect of the terminal group attached to the non-chiral chain

Often non-chiral chains are used as a link between two aromatic cores in polymeric compounds, e.g. twins, trimers etc. Polymeric compounds form the SmC<sub>A</sub>\* phase when the linking chain has an odd number of carbons according to the proposed mechanism described in section 1.4. The mesogenic groups may be the same thereby creating a symmetrical molecule (twin) or they may have two different mesogenic units as shown in figure 1.39.

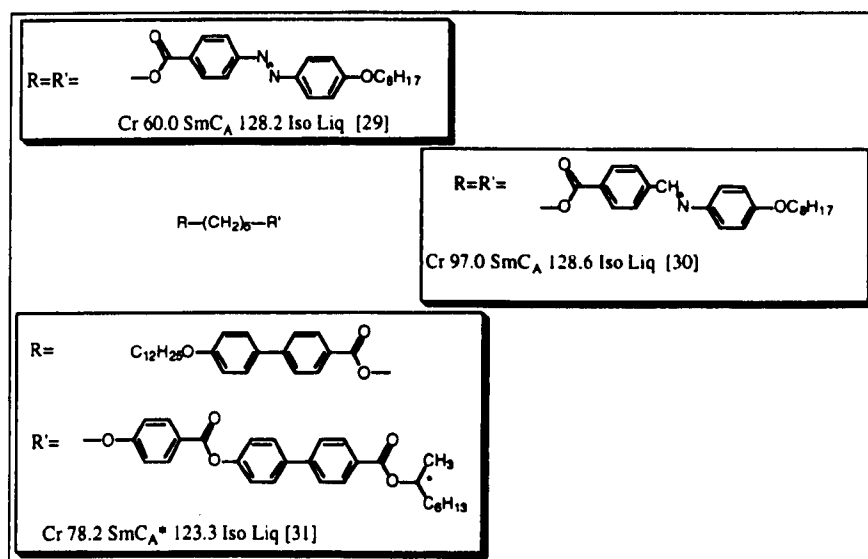


**Figure 1.39** Structures of bimesogens which promote formation of the SmC<sub>A</sub>\* phase

The mesogenic cores may be attached with their non-chiral chains to a bridging group such as a cyclohexane ring. Trimesogen in figure 1.40a is an example of an antiferroelectric liquid crystal with low shape anisotropy. The most commonly used bridging group to construct bimesogens is a siloxane unit (figure 1.40b). In this case the number of silicon atoms constituting the bridge determines whether the  $SmC_A^*$  dominates over synclincic smectic C phase. It was found that siloxanes with odd number of silicon atoms in the chain promote antiferroelectric phases while the even members do not [33].

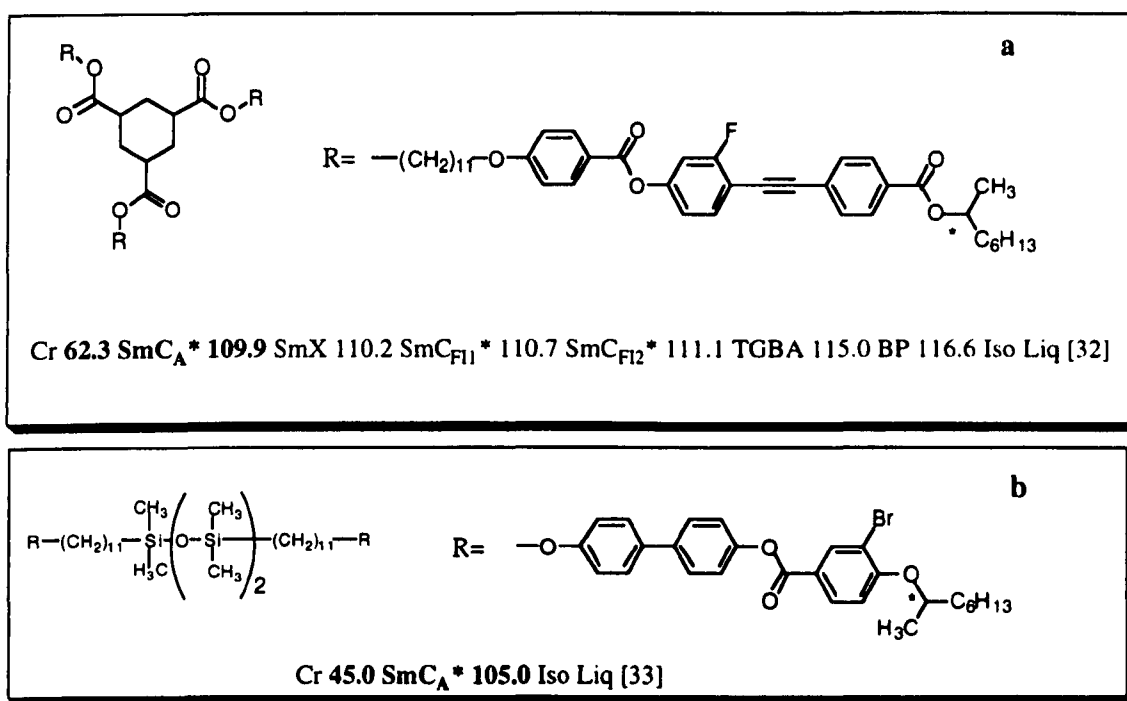


**Figure 1.40** Trimesogenic and siloxane containing structures which promote formation of the  $SmC_A^*$  phase

### 1.5 References (section 1.4)

1. JW Goodby in " Ferroelectric Liquid Crystals" ed. JW Goodby et al., vol 7, Gordon and Breach Scientific Publishers, 1991
2. JW Goodby, MA Waugh, SM Stein, E Chin, R Pindak and JS Patel, *Nature*, 1989, **337**, 449.
3. B Pansu, MH Li, HT Nguyen, *J Phys II*, 1997, **7**, 751
4. K Hiraoka, A Taguchi, Y Ouchi, H Takazoe, A Fukuda, *Jpn J Appl Phys, Part 2*, 1990, **29**, L103
5. Y Suzuki, T Hagiwara, Y Aihara, Y Sadamune, I Kawamura, N Okamura, T Kitazume, M Kakimoto, Y Imai, Y Yamada, N Yamamoto and K Mori, *Abst. 15<sup>th</sup> Jpn Liq Cryst Conf (Ekisho-Tohronkai)*, Osaka, 1989) p 304
6. Y Suzuki, T Ohde (Showa Shell Sekiyu), EP 571.277
7. J Szydłowska, D Pocięcha, E Gorecka., *J Mater Chem*, 1999, **9**, 361
8. M Nakata, Y Takanishi, K Ishikawa, H Takazoe, Y Aoki, H Nohira *Jpn J Appl Phys*, 2000, **39**, L42
9. PA Kumar, M Srinivasulu, VGKM Pisipati, *Liq Cryst*, 1999, **26**, 6, 859
10. Y Suzuki, (Showa Shell Sekiyu), EP 422.996
11. D Bennemann, G Heppke, AM Levelut, D Lotzsch, *Mol Cryst Liq Cryst*, 1995, A260, 351
12. NF Cooray, Y Suzuki, I Kawamura, *Liq Cryst*, 1999, **26**, 8, 1197
13. Y Aoki and H Nohira, *Liq Cryst*, 1999, **26**, 1, 97
14. AS Matharu, C Grover, L Komitov, G Andersson, *J Mat Chem*, 2000, **10**, 1303
15. AJ Seed, M Hird, P Styring, HF Gleeson, JT Mills, *Mol Cryst Liq Cryst*, 1997, A299, 19
16. MY Mizukami, (Mitsubishi Gas Chemical Company), EP 568. 246, 1993

17. T Takiguchi, T Iwaki, T Togano, Y Yamada, S Nakamura (Canon), EP 462.578 (18.06.91)
18. T Shimizu, K Taniguchi, S Nishiyama, S Miyakoshi, T Yamanaka, N Doi, H Hama (Mitsui Petrochemical Industries): EP 467.662 (17.07.91)
19. V Vill, Computer database *LiqCryst 3.01*, LCI Publisher, 1998
20. Y Arai, (Mitsubishi Chemical Company), EP 585.032, 1993
21. Y Suzuki, T Hagiwara, Y Aihara, Y Sadamune, I Kawamura, N Okamura, T Kitazume, M Kakimoto, Y Imai, Y Yamada, N Yamamoto and K Mori, *Abst 15<sup>th</sup> Jpn Liq Cryst Conf*, 1989, 302
22. V Laux, N Isaert, V Faye, HT Nguyen, *Liq Cryst*, 2000, **27**, 1, 81
23. Y Suzuki, T Hagiwara, Y Aihara, Y Sadamune, Y-S Negi, I Kawamura, Y Yamada, N Yamamoto and K Mori, *Abst 15<sup>th</sup> Jpn Liq Cryst Conf*, 1989, 304
24. Y Ouchi, Y Yoshioka, H Ishii, K Seki, M Kitamura, R Noyori, Y Talanishi and I Nishiyama., *J Mat Chem*, 1995, **5**, 12, 2297
25. I Nishiyama and JW Goodby, *J Mat Chem*, 1992, **2**, 10, 1015
26. K Hiraoka, A Taguchi, Y Ouchi, H Takazoe, A Fukuda, *Jpn J Appl Phys, Part 2*, 1990, **29**, L103
27. Y Takanishi, H Takezoe and A Fukuda, *Ferroelectrics*, 1993, **147**, 135
28. NF Cooray, M Kakimoto, Y Imai, Y Suzuki, *Macromolecules*, 1994, **27**, 1592
29. T Noiri, S Adachi, J Watanabe, *Liq Cryst*, 1995, **19**, 139
30. J Watanabe, T Izumi, T Niori, M Zennyoji, Y Takanishi, H Takazoe, *Mol Cryst Liq Cryst*, 2000, **346**, 77
31. V Faye, A Babeau, F Placin, HT Nguyen, P Barois, V Laux, N Isaert, *Liq Cryst*, 1996, **21**, 485
32. MH Li, L Detre, P Cluzeau, N Isaert, HT Nguyen, *Liq Cryst*, 1998, **24**, 3, 347
33. WK Robinson, PS Kloess, C Carboni, HJ Coles, *Liq Cryst*, 1997, **23**, 309

## 2 Aims

Since the discovery of antiferroelectricity in phase sequences of MHPOBC and TFHPOBC, a worldwide extensive study has been undertaken on the design and optimisation of inexpensive materials that would exhibit a broad antiferroelectric  $\text{SmC}_A^*$  phase at ambient temperatures with a view of using them in tristate display devices. A major part of the synthetic work reported over the last ten years has been focused on modification to the structures of MHPOBC. More than 300 compounds have been prepared in the exploration of new bridging groups, chirality bearing units, and various rings in the central cores of the molecules [1]. Though there was little progress achieved in the synthesis of commercially available individual compounds that possess a broad  $\text{SmC}_A^*$  phase at the room temperature, nevertheless, the synthetic library created was sufficiently large so as to produce a few multi-component liquid crystalline mixtures which exhibit antiferroelectric behaviour over a practical temperature range [1].

Over recent years it was shown that antiferroelectricity is a universal phenomenon in liquid crystals and not just a property of the MHPOBC family of compounds. Nowadays, the family of the antiferroelectric liquid crystals extends from polymer networks and oligomers to multi-ring systems, and to the so-called banana-shaped molecules, as described in section 1.4. One of the first attempts to prepare a non-MHPOBC type of an antiferroelectric liquid crystalline material was synthesis of chiral 1-methylheptyl 4-alkoxybenzoate biphenyl 4-carboxylates (MHBBC) [2]. Similar to MHPOBC, the molecular skeleton of the MHBBC series contains three phenyl rings, however, the relative positions of the two ester groups is altered, see figure 1. It was found that the “2+1” core of MHBBC stabilised the antiferroelectric smectic  $\text{C}_A^*$  phase

at lower temperatures and also favoured a richer phase polymorphism, thereby

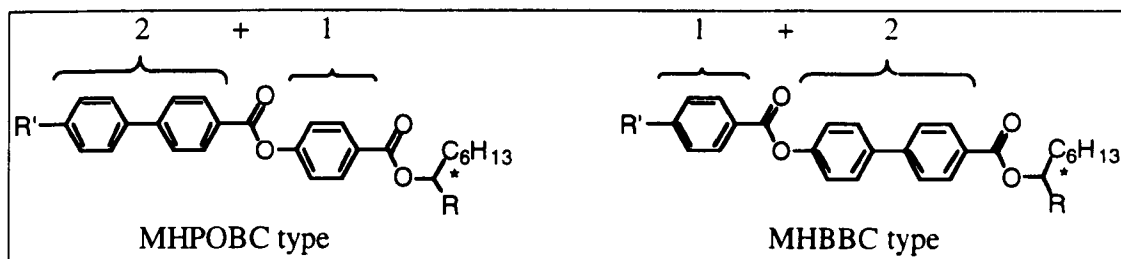


**Figure 1** Schematic representation of molecular skeletons of MHPOBC and MHBBC

presenting excellent alternatives to the MHPOBC analogues. However, until recently this class of structures remained largely unexplored, and in 2000 there were only 10 compounds of MHBBC type registered in the LiqCryst database [3]. It seemed that more extensive research on structure-property relationships was required for this new series of molecular structures. It is, thus, of great interest to establish the relation between the stability of a particular type of the smectic C\* phase, and which aspects of the molecular design affect it.

*The objective of this work was therefore to investigate the effect of the structural modifications of 1-methylheptyl 4'-(4-alkoxybenzoyloxy)biphenyl 4-carboxylates (compounds of general structure 1, figure 2) on the thermal stability of the smectic C\* phases, especially the SmC\* antiferroelectric phase, and other chirality induced frustrated phases. As the effect of substitutions in the chiral chain was studied in the series in some detail previously [2], it was most important to examine the substitutions incorporated into the central molecular core as well as into the terminus of the non-chiral chain.*

The general synthetic strategy to the target materials is shown in the figure 1.2. Compounds of general structure 1 were subjected to various structural modifications,

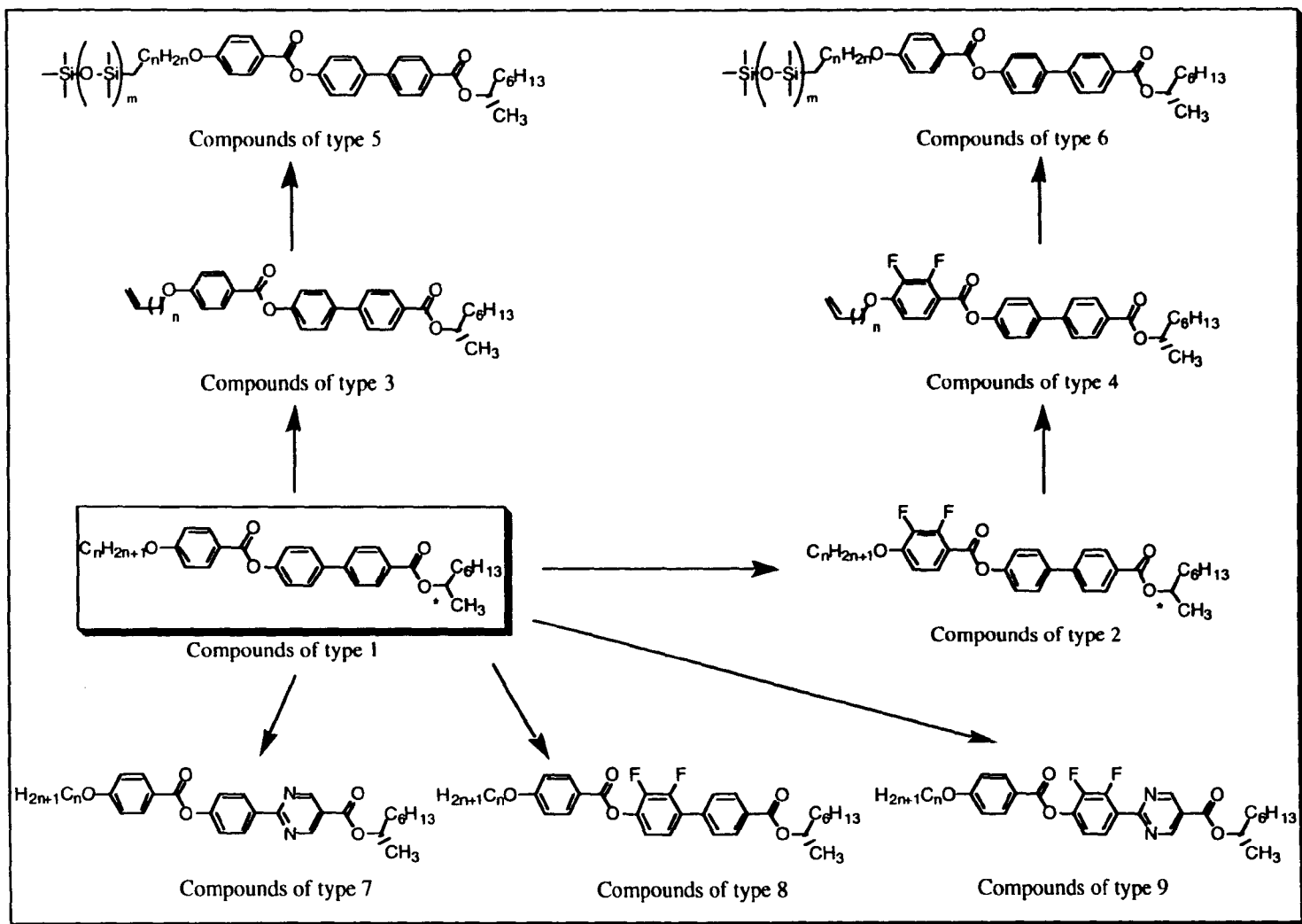


**Figure 2** The plan of synthesis undertaken in the course of this project

giving rise to 8 novel types of materials in the MHBBC family. The mesomorphic behaviours of compounds of general structure **1** served as reference sources, for which the liquid crystalline properties of the materials derived were compared, and a judgement was made as to whether the structural modification was “successful” in respect of the stability of the  $\text{SmC}_A^*$  phase versus other modifications of the  $\text{SmC}^*$  phase.

Changes in molecular structure involved introduction of lateral fluorine substituents into the benzoyl fragment (compounds of general structure **2**) and biphenyl unit (compounds of general structure **8** and **9**) of the parent compounds of general structure **1**. Highly electronegative fluorine substituents were expected to increase the transverse component of the molecular dipole moment and, consequently, alter the strength of the lateral intermolecular interactions. The effect of the laterally attached fluorine substituents on mesomorphic behaviour was also compared with the impact of the introduction of a pyrimidine ring. The 2-phenylpyrimidine fragment was introduced into compounds of general structure **7**. The combination of both fluorine substituents and a 2-phenylpyrimidine fragment was realised in compounds of general structure **9**. In total, different combinations of fluorine substitution with biphenyl or 2-phenylpyrimidine fragments provided 4 new examples of molecular cores, which have never been investigated before.

The variations in molecular core were accompanied with modification of the non-chiral chain. Firstly, a terminal double bond was introduced into the non-chiral chain of compounds of general structure **1** and **2** giving rise to new compounds of general structure **3** and **4**. In the following step it was planned to replace the double bond with the siloxane chain thereby producing two more new types of materials **5** and **6**. It was

also interesting to investigate an odd-even effect, that was described for siloxane chains (see chapter 1.4), within the series **5** by varying the number of siloxane units (-Si-O-Si), and how it influences stabilisation of either synclinic or anticlinic ordering in the SmC phase.

## References

1. K Miyachi and A Fukuda in "Handbook of Liquid Crystals", ed D Demus J Goodby, GW Gray, H-W Spiess, V Vill, Willey-VCH, 1998, **2B**, 665
2. JW Goodby, JS Patel and E Chin, J Mat Chem, 1992, **2**, 1997
3. V Vill, LiqCryst 3.5, LCI Publisher, 2000

### 3 Experimental and synthetic methods

#### 3.1 Description of the techniques and apparatus

##### 3.1.1 General synthetic procedures

Unless stated, the starting materials and reagents were purchased from either Aldrich or Lancaster Chemical Companies and used without purification. Diethyl ether was dried over sodium wire. Tetrahydrofuran was distilled from sodium and benzophenone. Palladium tetrakis(triphenylphosphine) was prepared according to the procedure described in [1]. High purity palladium acetate (99%) was purchased from Aldrich. 1,1,1,3,3-Pentamethyldisiloxane and 1,1,1,3,3,5,5-heptamethyltrisiloxane (93%) were bought from Fluorochem. Low quality of the commercial 1,1,1,3,3,5,5-heptamethyltrisiloxane was not improved either by distillation or preparative HPLC giving rise to the loss of purity in the final trisiloxane compounds of general structure **5** (see section 3.2.4.5). As determined by the <sup>1</sup>HNMR spectroscopy the main contamination in the commercial material came from the isomeric trisiloxanes, whose polar properties and boiling points are close to those of the major component.

The purities of the intermediates and final products were examined by TLC using Silica gel 60 F254 (Merck, Darmstadt). Detection of the materials was achieved using UV irradiation ( $\lambda = 254$  and  $365$  nm). HPLC was used to check the purity of the final compounds and various intermediates using chromatographic system that comprised a Kontron 420 pump, a Must Multi-port Stream Switch, a Perkin-Elmer ISS-100 Auto Sampler, a Dynamax microsorb C18 Reverse Phase column ( $5 \mu\text{m}$  particle size,  $25 \times 0.46$  cm), and a Spectroflow 757 Absorbance Detector ( $\lambda = 254$  nm) using an 80/20 % mixture acetonitrile/chloroform as the eluent. Proton nuclear resonance (<sup>1</sup>HNMR) spectroscopy was carried out using a Jeol JNM-LA 400 FT NMR spectrometer. Infrared spectroscopy was carried out using a Perkin-Elmer 882 infrared spectrometer. Mass

spectra were recorded using a Finnigan-MAT 1020 automated GC/MS spectrometer. Optical rotations of chiral materials were determined using an AA10 Automatic polarimeter. Values were measured in chloroform at the sodium D-line ( $\lambda = 589 \text{ nm}$ ) and at  $27.5 \text{ }^\circ\text{C}$ .

### 3.1.2 Characterization of materials

Phase identifications and determination of phase transition temperatures were carried out together by thermal polarised light microscopy using a Zeiss Universal transmitted polarized light microscope equipped with a Mettler FP52 microfurnace in conjunction with an FP5 Central Processor. Homeotropic sample preparations suitable for phase characterisation were prepared by using cleaned glass microscope slides (washed with water, acetone, water, concentrated nitric acid, water and dry acetone), whereas homogeneous defect textures were obtained by not using specially cleaned slides. Photomicrographs were taken using a Zeiss Universal polarising light microscope equipped with a Zeiss M35 Camera and MC63 Processor. The scale to the actual size of the exposed object was 1:100.

Differential scanning thermographs (aluminium pans and scan rate of  $2$  and  $10 \text{ }^\circ\text{C min}^{-1}$ ) were obtained using a Perkin Elmer DSC 7 PC system operating on UNIX or Windows (Pyrex) software. The results obtained were standardised relative to indium (measured onset  $156.7 \text{ }^\circ\text{C}$ , DH  $28.5 \text{ J g}^{-1}$ , literature value [2]  $156.6 \text{ }^\circ\text{C}$ , DH  $28.45 \text{ J g}^{-1}$ ).

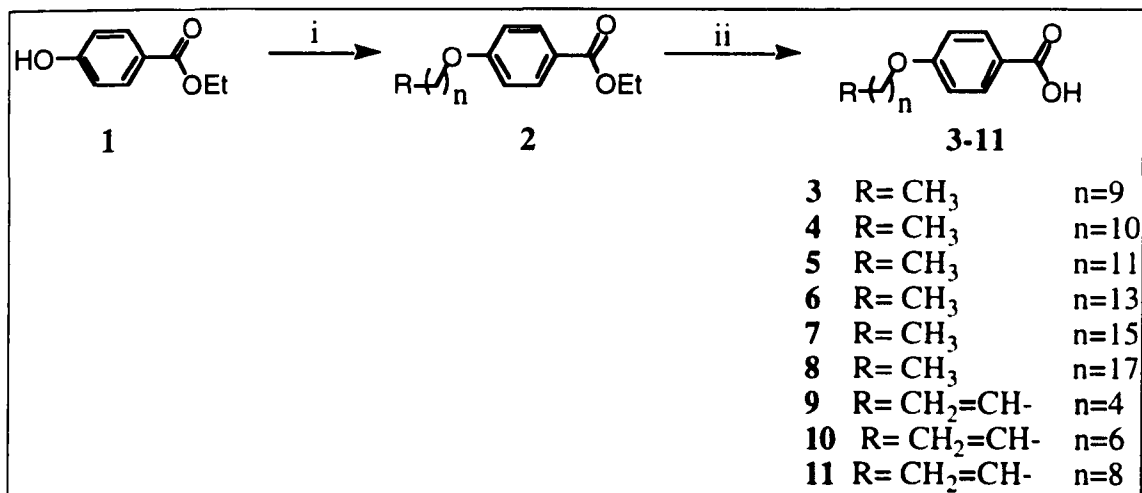
Electrooptical measurements were carried out using homogeneously aligned cells (Linkam) which were constructed from electrically-conducting indium tin oxide (ITO) coated glass, treated with antiparallel-buffed polyimide (PI) coated layers so as to give sites for planar, homogeneous growth of the liquid-crystalline phase. The cell gap (*ca.*  $5 \text{ }\mu\text{m}$ ) maintained by glass spacers was verified by UV-VIS interferometry using a Philips

PU H720 UV-VIS scanning spectrometer. The effective electrode areas of the cells used were  $0.9 \text{ cm}^2$ . The temperature was controlled using a Linkam THM 600 that was attached to a Linkam TP91 central processor. The cells were filled by capillary action at atmospheric pressure, with the liquid-crystalline materials in the isotropic liquid state. Good alignment was achieved by cooling slowly ( $< 0.1 \text{ }^\circ\text{C min}^{-1}$ ) from the isotropic liquid into the required liquid-crystalline phase while applying an electric field (square wave form,  $V = 20 \text{ V cm}^{-2}$ , 200 Hz). Typically, spontaneous polarization values were measured by the triangular wave method. The triangular waveform for the electric field was generated by a Hewlett Packard 33120A 15 MHz function generator with a maximum amplitude of  $\pm 10 \text{ V}$  and a  $32 \pm 0.2 \text{ ns}$  rise time. The output signal was amplified by a fixed gain ( $\times 50$ ) amplifier with a maximum amplitude of  $\pm 175 \text{ V}$ ,  $16.5 \pm 0.3 \text{ ms}$  rise time and 1 kHz waveform capability. A triangular voltage with 5-100  $\text{V cm}^{-2}$  at 20 Hz was applied to the cell. An optical polarizing microscope was used for observing textural changes during the measurements. The current was measured by detecting the voltage change across a resistor of 100 kW, which was sufficiently small compared with the impedance of the cell connected in series, and amplified by the means of a variable gain operational amplifier with an input impedance  $\gg 100 \text{ kW}$ , therefore the current loss for the measurement is negligible. The voltage was digitised using a Hewlett Packard 54600B 100 MHz, 1 M digitising oscilloscope. The data was analysed on a 486 SX 40 MHz microcomputer using acquisition and analysis software.

## 3.2 Preparation of the materials

### 3.2.1 Preparation of 4-*n*-alkoxy and 4-*n*-alk- $\omega$ -enylbenzoic acids 3-11

The synthesis of the acids 3-11 was performed according to the procedure described in [3] and outlined in Scheme 3.1.



**Scheme 3.1** Preparation of 4-substituted benzoic acids 3-11. i – K<sub>2</sub>CO<sub>3</sub>, *n*-alkyl or *n*-alk- $\omega$ -enyl bromide, butanone; ii – KOH, EtOH

A mixture of ethyl benzoate (0.1 mol), *n*-alkyl or *n*-alk- $\omega$ -enylbromide (0.12 mol) and potassium carbonate (0.2 mol) in 100 ml of butanone was heated under reflux overnight. The white precipitate was filtered and washed with butanone. The solvent of the filtrate was removed *in vacuo* to give an off-white solid, e.g. ethyl 4-alkoxybenzoate 2. Compound 2 and a solution of potassium hydroxide (0.2 mol) in water were mixed in ethanol (200 ml) and the mixture was refluxed for three hours. Ethanol was removed *in vacuo*, water was added and the mixture was acidified with 5N HCl. The precipitate was filtrated and re-crystallised from ethanol<sup>8</sup> to give a white crystalline solid (3-11).

<sup>8</sup> The mesomorphic behaviour and phase transition temperatures were investigated for all of the acids prepared and found in good agreement ( $\pm 2$  °C) with the reference data [4, 5].

Data of  $^1\text{H}$ NMR, IR spectroscopies and mass spectrometry and synthetic yields for compounds **3-11** are shown in tables 3.1 and 3.2.

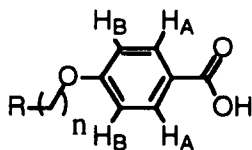


**Table 3.1** Data  $^1\text{H}$ NMR spectroscopy for acids **3-11**

No	n	R	$^1\text{H}$ NMR, 400 MHz, $\text{CDCl}_3$ , $\delta$ , ppm							
			$\text{H}_A$ d	$\text{H}_B$ d	$\text{CH}_2=\text{CH}$ m	$\text{CH}_2=\text{CH}$ m	$\text{CH}_2-\text{O}$ t	- $\text{CH}_2$ -		$\text{CH}_3$ t
								- $\text{CH}_2$ - m	$\text{CH}_2-\text{CH}_2$ quint	
<b>3</b> <sup>9</sup>	9	$\text{CH}_3$	7.85	6.98	-	-	4.01	1.5-1.2 14H	1.70	0.84
<b>4</b> <sup>9</sup>	10	$\text{CH}_3$	7.85	6.97	-	-	4.01	1.5-1.1 16H	1.74	0.82
<b>5</b> <sup>9</sup>	11	$\text{CH}_3$	7.81	6.93	-	-	3.97	1.5-1.1 18H	1.68	0.80
<b>6</b> <sup>9</sup>	13	$\text{CH}_3$	7.81	6.94	-	-	3.97	1.6-1.1 22H	1.9	0.81
<b>7</b> <sup>9</sup>	15	$\text{CH}_3$	7.85	6.97	-	-	4.02	1.5-1.2 26H	1.74	0.81
<b>8</b>	17	$\text{CH}_3$	7.85	6.98	-	-	4.01	1.5-1.1 30H	1.74	0.82
<b>9</b>	4	$\text{CH}_2=\text{CH}$	8.05	6.93	5.00	5.83	4.04	1.6 2H	1.83	-
<b>10</b>	6	$\text{CH}_2=\text{CH}$	8.05	6.95	4.98	5.82	4.04	1.5-1.2 6H	1.83	-
<b>11</b>	8	$\text{CH}_2=\text{CH}$	8.04	6.93	4.97	5.81	4.02	1.5-1.2 12H	1.81	-

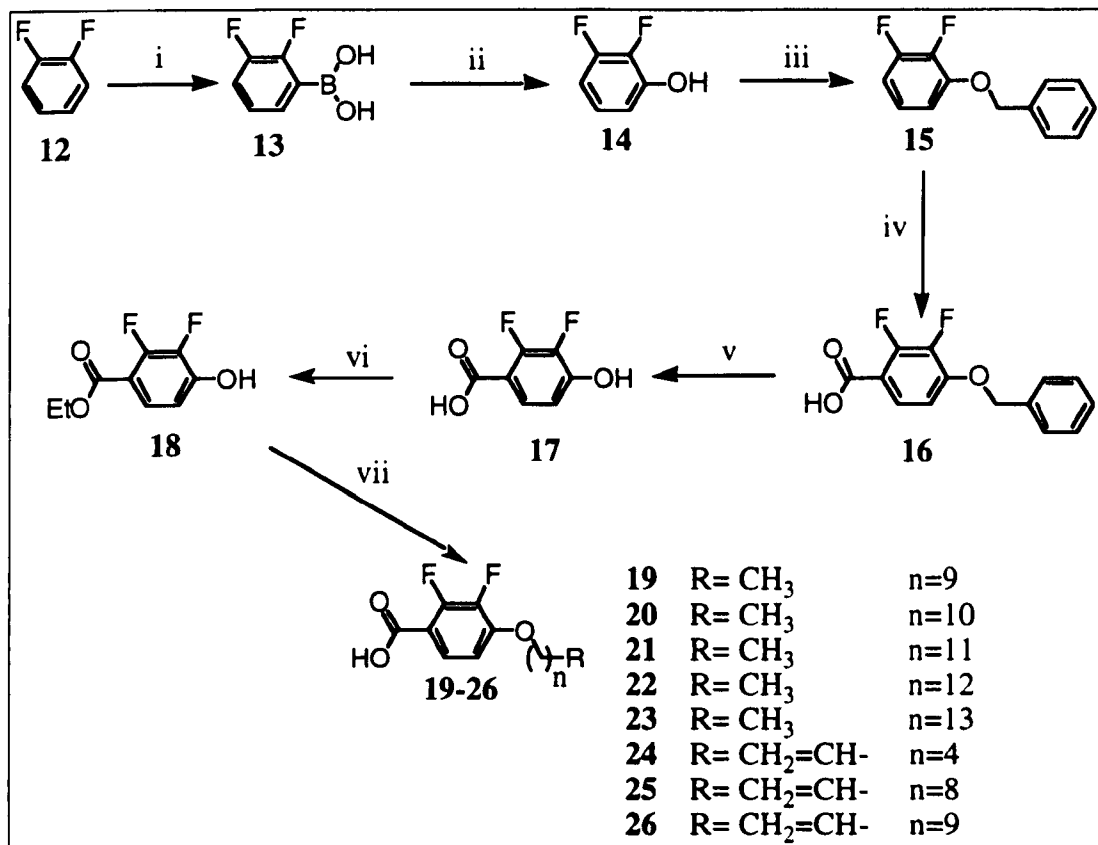
**Table 2** Data of the infrared spectroscopy, mass spectrometry and preparative yields for acids **3-11**.

No	n	R	IR, KBr disc, $\nu$ , $\text{cm}^{-1}$					Mass	Yield, %
			C=O	C=C	C=C <sub>Ar</sub>	C-H	O-H		
<b>3</b>	9	$\text{CH}_3$	The infra-red spectra for acids <b>3-7</b> were not determined					278	86
<b>4</b>	10	$\text{CH}_3$						292	88
<b>5</b>	11	$\text{CH}_3$						306	81
<b>6</b>	13	$\text{CH}_3$						334	74
<b>7</b>	15	$\text{CH}_3$						362	74
<b>8</b>	17	$\text{CH}_3$						1693	1515
<b>9</b>	5	$\text{CH}_2=\text{CH}$	1676	1513	1609	2935 2860	-	248	74
<b>10</b>	7	$\text{CH}_2=\text{CH}$	1690	1581	1609	2927 2857	3440	-	54
<b>11</b>	8	$\text{CH}_2=\text{CH}$	1677	1551	1608	2928 2858	3435	339	45

<sup>9</sup>  $(\text{CD}_3)_2\text{SO}$  was used as a solvent

### 3.2.2 Preparation of 2,3-difluoro-4-*n*-alkyl or 4-*n*-alk- $\omega$ -enylbenzoic acids 19-26

The synthetic procedures in preparation of the 2,3-difluoro-substituted acids were adapted from reference 6. The synthetic pathway is outlined in the scheme 3.2.



**Scheme 3.2** Preparation of the 2,3-difluoro-4-*n*-alkyl or 4-*n*-alk- $\omega$ -enylbenzoic acids 19-26: i - a. BuLi, -78 °C b. B(OMe)<sub>3</sub> c. H<sup>+</sup>, room t; ii - H<sub>2</sub>O<sub>2</sub>; iii - BnCl, K<sub>2</sub>CO<sub>3</sub>, butanone, reflux; iv - a. BuLi, -78 °C b. CO<sub>2</sub> c. H<sup>+</sup>, room t; v - Pd(C) 10%, EtOH; vi - H<sub>2</sub>SO<sub>4</sub> (cat amounts), EtOH; vii - a. *n*-alkyl or *n*-alk- $\omega$ -enylbromide, K<sub>2</sub>CO<sub>3</sub>, butanone, reflux. b. KOH, EtOH

#### 2,3-difluorophenylboronic acid 13

Solution of 1,2-difluorobenzene **12** (20 g, 0.18 mol) in dry tetrahydrofuran (200 ml) was stirred at -78 °C under nitrogen atmosphere. A solution of the butyllithium in hexanes (10M, 20 ml) was added dropwise during one hour. The mixture was stirred for other 30 minutes at -78 °C and 50% solution of the trimethylborate (37.4 g, 0.36 mol) in

tetrahydrofuran was added keeping temperature below  $-75\text{ }^{\circ}\text{C}$ . A white suspension was formed and left stirring overnight. A solution of the hydrochloric acid (18%) was added to produce a clear solution. The product was extracted into ether, washed with water and dried ( $\text{MgSO}_4$ ). The solvent was removed *in vacuo* to give an off-white solid. Yield: 28 g (98 %).

To perform spectral characterisation 1 g (6.3 mmol) of the boronic acid was converted into its cyclic ester by reaction with an equimolar amount of the ethylene glycol in 50 ml of pentane at room temperature. After two hours stirring the white suspension cleared indicating completion of the formation of the ester.  $\text{MgSO}_4$  was added to absorb the water formed in the course of the reaction. The solution was filtered and pentane was removed *in vacuo* to give colourless oil.

Yield: 1g (62%)

$^1\text{H}$ NMR 400Hz,  $\text{CDCl}_3$ ,  $\delta$ , ppm: 7.49 (1H, m), 7.27 (1H, m), 7.10 (1H, m), 4.42 (4H, s).

IR (neat),  $\nu\text{ cm}^{-1}$ : 2986, 1474, 1363, **1270**, 1141, 735.

### ***2,3-difluorophenol 14***

A solution of the hydrogen peroxide (100 Vol/Vol) was added dropwise to a stirred solution of **13** (28 g, 0.18 mol) in 150 ml of tetrahydrofuran. After the vigorous reaction was over the mixture was gently heated for 12 hours<sup>10</sup>. The product was extracted into dichloromethane, washed with water to remove peroxides and dried ( $\text{MgSO}_4$ ). After removal of the solvent the product was distilled *in vacuo* to give colourless liquid. Bp  $83\text{-}84\text{ }^{\circ}\text{C}$  (20 mm Hg).

Yield: 18.7 g (80%).

$^1\text{H}$ NMR 400 MHz,  $\text{CDCl}_3$ ,  $\delta$ , ppm: 6.93 (1H, m), 6.73 (2H, m), 6.15 (1H, broad s). IR

(neat),  $\nu\text{ cm}^{-1}$ : **3400** (broad), 1630, 1515, 1254, 1022, 773

---

<sup>10</sup> Heating under reflux led to the oxidation of the tetrahydrofuran to the  $\gamma$ -butyrolactone, which makes the purification of the target 2,3-difluorophenol difficult.

***1-benzyloxy-2,3-difluorobenzene 15***

A mixture of **14** (8.6 g, 0.07 mol), benzyl chloride (8.8 g, 0.07 mol), K<sub>2</sub>CO<sub>3</sub> (21.2 g, 0.15 mol) in butanone was heated under reflux for 24 hours. After cooling to room temperature the precipitate was filtered and the solvent was removed *in vacuo*. The residue was purified over silica gel by continuous extraction into hexane to give white crystalline solid. Yield: 12 g (78%) Mp 32-34 °C

<sup>1</sup>HNMR 400 MHz, CDCl<sub>3</sub>, δ, ppm: 7.38 (5H, m), 6.93 (1H, m), 6.76 (20H, m), 5.14 (2H, s).

***4-benzyloxy-2,3-difluorobenzoic acid 16***

A solution of **15** (20.2 g, 92 mmol) in dry tetrahydrofuran (200 ml) was stirred at -95 °C<sup>11</sup> under a nitrogen atmosphere. A solution of the butyllithium in hexanes (10 M, 10 ml) was added dropwise over one hour. The mixture was stirred for 30 min at -100 °C and poured onto a slurry of solid carbon dioxide in tetrahydrofuran. A white suspension was formed which was left stirring overnight. An aqueous solution of the hydrochloric acid (18%) was added to produce a clear solution. The product was extracted into ether, washed with water and dried (MgSO<sub>4</sub>). The solvent was removed *in vacuo* to give an off-white solid, which was washed several times with warm hexane, filtered and dried in air.

Yield: 10 g (41 %)

To perform spectral characterisations of the acid **16** a small amount was converted into ethyl ester by reaction in ethanol in presence of catalytic amounts of H<sub>2</sub>SO<sub>4</sub>.

Yield 87%. Mp 74-75 °C

<sup>1</sup>HNMR, 400 MHz, CDCl<sub>3</sub>, δ ppm: 7.66 (m, 1H), 7.38 (m, 5H), 7.29 (m, 1H), 6.80 (m, 1H), 5.21 (s, 2H), 4.37 (2H), 1.38 (3H). IR, KBr disc, ν cm<sup>-1</sup>: 2985, **1719**, 1635, 1521, 1469, 1371, 1305, 1214, 1093, 819, 735. M<sup>+</sup>: 292

---

<sup>11</sup> Temperatures below -90 °C were maintained using the mixture of ethanol-liquid nitrogen as coolant.

**2,3-difluoro-4-hydroxybenzoic acid 17**

Compound **16** (10 g, 37.8 mmol) was dissolved in ethanol (200 ml). A catalytic amount of 10% palladium on carbon was added and the mixture was stirred under a hydrogen atmosphere. After TLC analysis revealed reaction completion, the catalyst was filtered off and the solvent removed *in vacuo*. The residue was used in the next step without further purification. Yield: 6.3 g (97%); <sup>1</sup>HNMR, 400 MHz, DMSO,  $\delta$  ppm: 11.45 (s, 1H), 7.53 (m, 1H), 6.83 (t, 1H); IR,  $\nu$  cm<sup>-1</sup>, KBr disc: **3478**, 2842, 2589, **1683**, 1628, 1605, 1253, 933, 849. M<sup>+</sup> 174

**ethyl 2,3-difluoro-4-hydroxybenzoate 18**

A solution of **17** (2.5 g (14.4 mmol)) and few drops of H<sub>2</sub>SO<sub>4</sub> (conc.) in ethanol was refluxed for two days. Then the mixture was neutralised by addition of NaHCO<sub>3</sub> (sat. aq. solution). The precipitate was filtered off and purified by sublimation at 100 °C.

Yield: 1.5 g (52%), mp 104-105 °C; <sup>1</sup>HNMR, 400 MHz, CDCl<sub>3</sub>,  $\delta$  ppm: 7.66 (m 1H), 6.83 (m, 1H), 6.02 (s, 1H), 4.38 (q, 2H), 1.39 (t, 3H); IR  $\nu$  cm<sup>-1</sup>: 3258, 1698, 1632, 1217, 955, 832; M<sup>+</sup> 202

**4-n-alkyl or 4-n-alk- $\omega$ -enyl- 2,3-difluorobenzoic acids 19-26**

A mixture of **18** (1 mmol), *n*-alkyl or *n*-alk- $\omega$ -enylbromide (0.12 mol), potassium carbonate (0.2 mmol ) in butanone (20 ml) was heated under reflux overnight. The white solid was filtrated and washed with butanone. The filtrate was evaporated to dryness to give an off-white solid, which was mixed with a solution of the potassium hydroxide (2 mmol) in aqueous ethanol (200 ml). The resulting mixture was refluxed for 3 h. Ethanol was removed *in vacuo*, water was added and the mixture was acidified with 5N HCl. The precipitate was filtrated and recrystallised from ethanol. Data for

<sup>1</sup>HNMR, IR, mass spectral analyses and preparative yields are shown in Tables 3.3 and 3.4<sup>12</sup>.

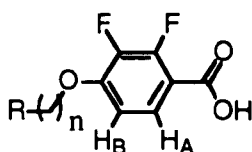


**Table 3.3** <sup>1</sup>HNMR data recorded for 2,3-difluoro-4-n-alkyl or 4-n-alk- $\omega$ -enylbenzoic acids 19-26

No	n	R	1HNMR, 400 MHz, CDCl <sub>3</sub> , $\delta$ , ppm							
			H <sub>B</sub>	H <sub>A</sub>	CH <sub>2</sub> =CH	CH <sub>2</sub> =CH	CH <sub>2</sub> -O	-CH <sub>2</sub> -		CH <sub>3</sub>
			m	m	m	m	t	-CH <sub>2</sub> - m	CH <sub>2</sub> -CH <sub>2</sub> Quintet	t
19	9	CH <sub>3</sub>	7.76	6.78	-	-	4.11	1.5-1.2 14H	1.85	0.88
20	10	CH <sub>3</sub>	7.75	6.78	-	-	4.11	1.5-1.2 16H	1.85	0.88
21	11	CH <sub>3</sub>	7.76	6.78	-	-	4.11	1.5-1.2 18H	1.85	0.88
22 <sup>13</sup>	12	CH <sub>3</sub>	7.70	6.76	-	-	4.09	1.5-1.2 20H	1.84	0.88
23	13	CH <sub>3</sub>	7.72	6.75	-	-	4.09	1.5-1.2 22H	1.84	0.88
24	4	CH <sub>2</sub> =CH	7.77	6.78	5.03	5.82	4.13	1.60 2H	1.88	-
25	8	CH <sub>2</sub> =CH	7.77	6.79	4.97	5.81	4.11	1.5-1.3 12H	1.85	-
26	9	CH <sub>2</sub> =CH	6.92	8.02	4.97	5.81	4.02	1.5-1.3 14H	1.85	-

**Table 3.4** Infrared spectroscopy, mass-spectrometry data and preparative yields for acids 19-26

No	n	R	IR, KBr disc, n, cm <sup>-1</sup>						M+	Yield, %
			C=O	C=C	C=C <sub>Ar</sub>	C-H	O-H	C-F		
19	9	CH <sub>3</sub>	1698	-	1625	2946 2857	3440	1090	314	75
20	10	CH <sub>3</sub>	1698	-	1625	2925 2858	3480	1089	328	88
21	11	CH <sub>3</sub>	1694	-	1626	2925 2856	3480	1087	342	70
22	12	CH <sub>3</sub>	1695	-	1627	2925 2859	-	1087	356	46
23	13	CH <sub>3</sub>	1693	-	1629	2925 2855	-	1089	370	75
24	4	CH <sub>2</sub> =CH	1694	1579	1627	2948	-	1087	256	79
25	6	CH <sub>2</sub> =CH	1694	1585	1626	2927 2856	3430	1087	312	71
26	8	CH <sub>2</sub> =CH	1693	1580	1626	2930 2856	3440	1087	326	92

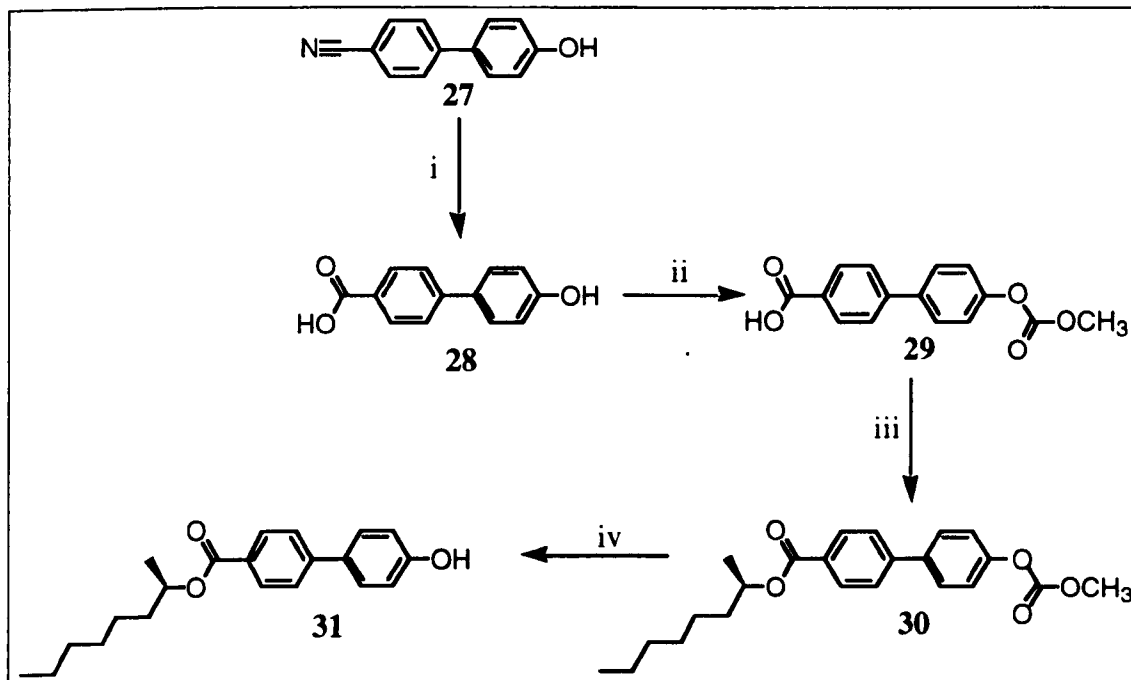
<sup>12</sup> The mesomorphic behaviour and phase transition temperatures were investigated for all of the 2,3-difluorobenzoic acids prepared and found to be in good agreement ( $\pm 2$  °C) with the reference data [6].

<sup>13</sup> The spectra were recorded in (CD<sub>3</sub>)<sub>2</sub>SO

### 3.2.3 Preparation of the key intermediates

#### 3.2.3.1 Synthesis of the (*R*)-1-methylheptyl 4'-hydroxybiphenyl-4-carboxylate **31**

The synthesis of the compound **31** was carried out utilising conventional synthetic methods [7] and according to the procedures described in reference 8.



**Scheme 3.3** Preparation of (*R*)-1-methylheptyl 4'-hydroxybiphenyl-4-carboxylate **31**.

i. HOAc, H<sub>2</sub>SO<sub>4</sub>, H<sub>2</sub>O, reflux; ii. NaOH, CH<sub>3</sub>OCOCl, -5 °C; iii. (+)-*S*-octanol, DEAD, PPh<sub>3</sub>, THF; iv. EtOH, NH<sub>3</sub> (35% solution)

#### 4'-hydroxybiphenyl-4-carboxylic acid **28**

A mixture of 4-cyano-4'-hydroxybiphenyl **27** (5 g, 25.6 mmol), acetic acid (100 ml), H<sub>2</sub>SO<sub>4</sub> (conc.) (10 ml), and H<sub>2</sub>O (10 ml) was heated under reflux for 8 h. After reaching room temperature the mixture was poured onto ice. The white precipitate was filtered off, washed with water and dried in air. The product was re-crystallised from acetic acid to give a white powder.

Yield: 4.6 g (84%). Mp >300 °C

<sup>1</sup>HNMR, 400 MHz, CDCl<sub>3</sub>+DMSO, δ, ppm: 8.58 (s, 1H), 8.08 (d, 2H), 7.55 (dd, 4H), 6.95 (2H); IR, KBr disc, ν cm<sup>-1</sup>: 3376, 2919, 2551, 1679, 1604, 1298, 1239, 1196.

***4'-Methoxycarbonyloxybiphenyl-4-carboxylic acid 29***

Methyl chloroformate (1.3 g, 14 mmol) was added dropwise to the solution of **28** (1.5 g, 7 mmol) in 0.2M NaOH at -4 °C. After 4 hours stirring 5N HCl was added and the mixture was poured into water. The precipitate was filtered off and the product was recrystallised from acetic acid.

Yield: 1.7g (90%). Cr 258.7 °C N >300 °C Iso

<sup>1</sup>HNMR, 400 MHz, CDCl<sub>3</sub>, δ, ppm: 8.00 (d, 2H), 7.66 (dd, 4H), 7.20 (d, 2H), 3.85 (s, 3H); IR, KBr disc, ν cm<sup>-1</sup>: 2972, 1772, 1679, 1611, 1265 cm. M<sup>+</sup> 272

***(R)-1-Methylheptyl 4'-methoxycarbonyloxybiphenyl-4-carboxylate 30***

Diethylazodicarboxylate (DEAD) (0.6 g, 3.4 mmol) was added dropwise to the stirred solution of **29** (0.9 g, 3.3 mmol), *S*-(+)-octanol<sup>14</sup> (0.5 g, 3.6 mmol) and triphenyl phosphine (0.9 g, 3.4 mmol) in 50 ml of dried tetrahydrofuran. After the addition of DEAD the clear, colourless solution was produced and stirred for 24 h. Tetrahydrofuran was removed *in vacuo* to give a yellowish oil, which was used in the next stage without further purification.

Yield: 0.9 g (71%)

<sup>1</sup>HNMR, 400 MHz, CDCl<sub>3</sub>, δ, ppm: 8.10 (d, 2H), 7.62 (d, 4H), 7.32 (d, 2H), 5.17 (sex, 1H), 3.93 (s, 3H), 1.76 (m, 1H), 1.62 (m, 1H), 1.50-1.20 (m, 8H), 1.35 (d, 3H), 0.88 (t, 3H);

***(R)-1-Methylheptyl 4'-hydroxybiphenyl-4-carboxylate 31***

To a solution of **30** (0.9 g) in ethanol (20 ml), a 10 ml solution of ammonia (26%) was added dropwise. The mixture was stirred for one hour at room temperature, neutralised by the addition of HCl (20% aq sol) and poured into water. The product was extracted

---

<sup>14</sup> In some cases *R*-isomer of 2-octanol was used giving rise to the inverse configuration of the chiral centre in some of the final products

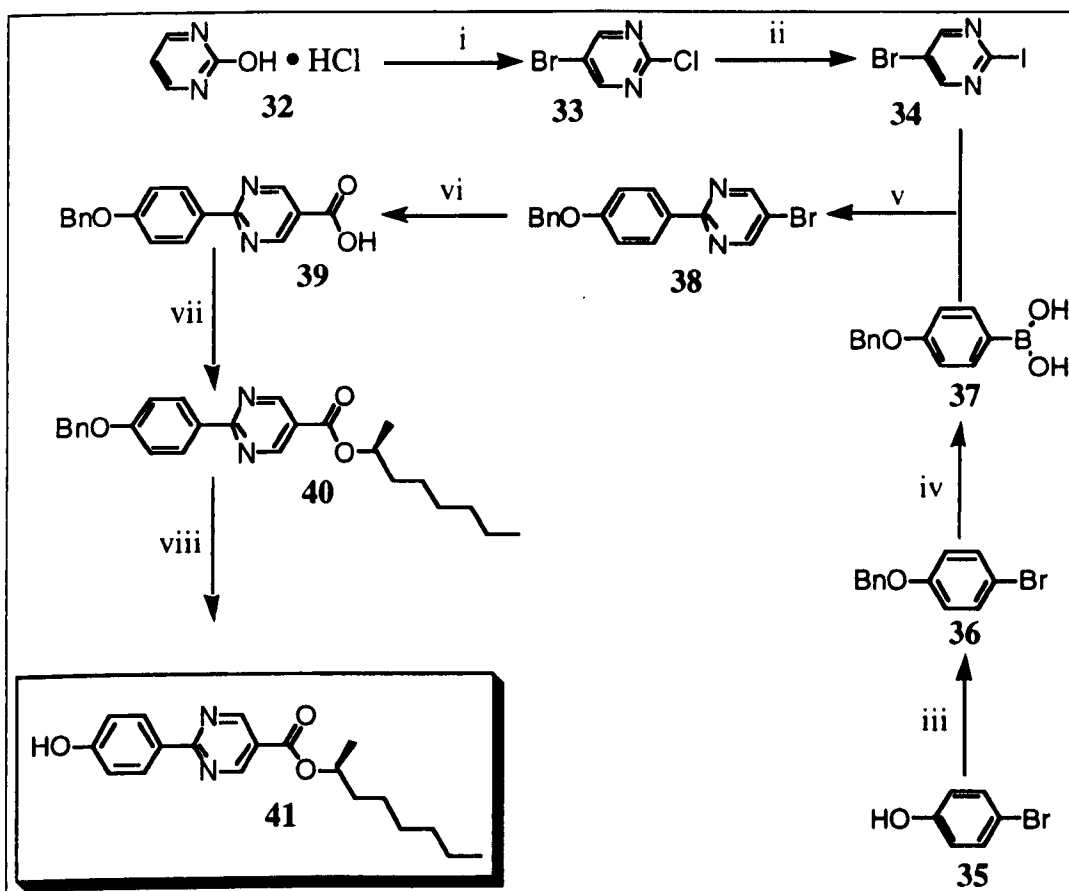
into ether (twice), the organic layer was washed with water and dried over  $\text{MgSO}_4$ . The solvent was removed *in vacuo* and the residue was purified by flash-chromatography over silica gel using a mixture of EtOAc – petroleum spirit (bp 60-80 °C) (1:1).

Yield: 0.7 g (93%). Mp 84-85 °C

$^1\text{H}$ NMR, 400 MHz,  $\text{CDCl}_3$ ,  $\delta$ , ppm: 8.07 (d, 2H), 7.56 (dd, 4H), 6.93 (dt, 2H), 5.17 (sec, 1H), 5.05 (s, 1H), 1.75 (m, 1H), 1.63 (m, 1H), 1.35 (m, 8H), 0.88 (t, 6H); IR, KBr disc,  $\nu$   $\text{cm}^{-1}$ : **3363**, 2963, 2855, 1689, 1605, 1229, 1062, 835;  $M^+$  326

### 3.2.3.2 Preparation of (*S*)-1-methylheptyl 2-(4-hydroxyphenyl)pyrimidine-5-carboxylate **41**

The synthetic pathways in the preparation of (*S*)-1-methylheptyl 2-(4-hydroxyphenyl)pyrimidine-5-carboxylate **41** are shown in the scheme 3.4. The synthesis of 5-bromo-2-iodopyrimidine **34** was carried out as described in ref 9. Selective palladium-catalysed Suzuki coupling of **34** with boronic acid **37** was achieved following the procedure described in reference 10.



**Scheme 3.4** Preparation of (*S*)-1-Methylheptyl 2-(4-hydroxyphenyl)pyrimidine-5-carboxylate **41**. i. a)  $\text{Br}_2$ ,  $\text{H}_2\text{O}$  b)  $\text{POCl}_3$ , *N,N*-dimethylaniline. c) ice; ii.  $\text{HI}$ ,  $\text{CH}_2\text{Cl}_2$ , 0-5 °C; iii. benzyl chloride,  $\text{K}_2\text{CO}_3$ , acetone, reflux; iv. a)  $\text{BuLi}$ , -78 °C, THF b)  $\text{B}(\text{OMe})_3$ . c)  $\text{H}^+$ ; v.  $\text{Pd}[\text{PPh}_3]_4$ ,  $\text{Na}_2\text{CO}_3$ , DME vi. a)  $\text{BuLi}$ , -100 °C, THF. b)  $\text{CO}_2$ . c)  $\text{H}^+$ ; vii. DEAD,  $\text{PPh}_3$ , *R*-2-octanol ; viii.  $\text{Pd}(\text{C})$ ,  $\text{H}_2$ , EtOAc

**5-Bromo-2-chloropyrimidine 33**

Bromine (67 g, 0.42 mol) was added dropwise to the solution of compound **32** (50 g, 0.38 mol) in water (200 ml) at room temperature. The mixture was stirred for 1 h, then water and excess bromine were removed and the solid was dried *in vacuo* ( $P_2O_5$ ). Phosphorus oxychloride (500 ml) and *N,N*-dimethylaniline (20 ml) were added and the mixture was heated under reflux for 6 h. The mixture was allowed to cool and was slowly poured onto ice (extreme care required), and the product was isolated by extraction into ether (2 x 200 ml). The ethereal extract was washed with water and dried ( $MgSO_4$ ), and the solvent was removed *in vacuo* to yield an off-white solid which was dissolved in hexane and purified by continuous hot filtration through silica gel.

Yield: 33.8 g (52%); mp 77-78 °C;  $^1H$ NMR, 400 MHz,  $CDCl_3$ ,  $\delta$ , ppm: 8.69 (s, 2H); IR, KBr disc,  $\nu$   $cm^{-1}$ : 1534, 1396, 1164, 1008, **934, 757**

**5-Bromo-2-iodopyrimidine 34**

Cold hydriodic acid (57%, 0.60 mol, 79 ml) was added dropwise to a stirred pre-cooled (-5 °C) solution of compound **33** (22.8 g, 0.12 mol) in dichloromethane (100 ml). The mixture was stirred at 0 °C for 4 h, brought to a pH of 7 by the addition of solid potassium carbonate, and decolourised by the addition of aqueous sodium metabisulphite. The organic layer was separated and the aqueous layer was washed with dichloromethane (2 x 100 ml). The combined organic extracts were dried ( $Na_2CO_3$ ), dichloromethane was removed *in vacuo* and the resulting residue was recrystallised from hexane to give colourless crystals.

Yield: 19.1 g (56%); mp 98-99 °C;  $^1H$ NMR, 400 MHz,  $CDCl_3$ ,  $\delta$ , ppm: 8.55 (s, 2H). KBr disc,  $\nu$   $cm^{-1}$ : 1516, 1375, 1228, 1132, **925, 747**

**4-benzyloxy-1-bromobenzene 36**

A mixture of 4-bromophenol **35** (20 g, 0.16 mol), benzyl chloride (25 g, 0.20 mol), potassium carbonate (55.3 g, 0.40 mol) and butanone (100 ml) was heated and stirred

under reflux for 20 h. The cooled mixture was filtered, subjected to evaporation *in vacuo* and the resulting residue was recrystallised from petroleum spirit (60-80 °C fraction) to give colourless crystals.

Yield: 27.5 g (65%); mp 60-61 °C;

<sup>1</sup>HNMR, 400 MHz, CDCl<sub>3</sub>, δ, ppm: 7.42-7.25 (7H, m), 6.77 (2H, d), 5.03 (2H,s);

IR, KBr disc, ν cm<sup>-1</sup>: 2893, 1584, 1487, 1249, 734

#### ***4-Benzyloxyphenylboronic acid 37***

*n*-Butyllithium (2 ml, 10 M in hexanes) was added dropwise to a stirred solution of compound **36** (5 g, 0.02 mol) in dry tetrahydrofuran (100 ml) at -78 °C. The resulting mixture was stirred for an hour at -78 °C and a solution of the trimethyl borate (4.2 g, 0.04 mol) in dry tetrahydrofuran (30 ml) was added dropwise. The mixture was then allowed to warm to room temperature and hydrochloric acid (10%) was added. The mixture was stirred for an additional hour, poured into water, and the product was isolated by extraction into ether (2 x 200 ml). The ethereal extracts were washed with water and dried (MgSO<sub>4</sub>). The ether was removed *in vacuo* to give a white solid.

Yield: 3.8 g (83%);

<sup>1</sup>HNMR, 400 MHz, CDCl<sub>3</sub>, δ, ppm: 7.75 (2H, d), 7.40 (5H, m), 6.98 (2H, d), 5.12 (2H, s); IR, KBr disc, ν cm<sup>-1</sup>: 3311, 1605, 1249, 1380

#### ***2-(4-Benzyloxyphenyl)-5-bromopyrimidine 38***

A solution of compound **37** (2.1 g, 9.2 mmol) in DME (10 ml) was added dropwise, under an atmosphere of nitrogen, to a degassed mixture of compound **34** (2.8 g, 10.1 mmol), tetrakis(triphenylphosphine)palladium (0) (270 mg, 0.23 mmol), DME (30 ml), and aqueous 2M sodium carbonate (30 ml). The mixture was heated under reflux for 16 h, water was added to the mixture and the resulting organic layer was separated. The aqueous layer was washed with ether (2 x 100 ml), and the combined extracts were washed with saturated brine (100 ml) and dried (MgSO<sub>4</sub>). The organic solvent was

removed *in vacuo* and the residue was re-crystallised from methanol to give colourless crystals.

Yield (1.6 g, 52%); mp 155 °C

<sup>1</sup>HNMR, 400 MHz, CDCl<sub>3</sub>, δ, ppm: 5.14 (2 H, s.), 7.06 (2 H, d.), 7.30-7.48 (5 H, m), 8.35 (2 H, d.) and 8.77 (2 H, s.); IR, KBr disc, ν cm<sup>-1</sup>: 1600, 1550, 1520, 1410, 1325, 1250, 1165, 1040, 1025, 1010

***2-(4-Benzyloxyphenyl)pyrimidine-5-carboxylic acid 39***

A degassed solution of compound **38** (6.0 g, 4.7 mmol) in THF (100 ml) was cooled to -100 °C and 1.6 M *n*-butyllithium (3.25 ml, 5.2 mmol) was added dropwise with stirring at such a rate that the temperature was maintained below -90 °C. The resulting mixture was stirred at approximately -95 °C for 1 h. The orange mixture was poured onto a vigorously stirred suspension of powdered dry ice in dry tetrahydrofuran and, after reaching room temperature, the resulting slurry was acidified with dilute sulphuric acid. The crude product was isolated by extraction into ether (2 x 100), washed with saturated brine (100 ml), dried (MgSO<sub>4</sub>) and the solvent was removed *in vacuo*. The isolated product was washed with light petroleum spirit (40-60 °C) and filtered to give a white powder.

Yield: 1.13 g (65%); mp ~300 °C;

<sup>1</sup>HNMR, 400 MHz, CDCl<sub>3</sub>+DMSO, δ, ppm: 5.17 (2H, s), 7.09 (2H, d), 7.3-7.47 (5H, m), 8.47 (2H, d), 9.25 (2H, s.); IR, KBr disc, ν cm<sup>-1</sup>: 3050 br, 1690, 1575, 1380, 1300, 1250, 1170, 1020 and 800

***(S)-1-Methylheptyl 2-(4-benzyloxyphenyl)pyrimidine-5-carboxylate 40***

DEAD (0.80 g, 4.4 mmol) was added dropwise to a solution of compound **39** (1.15 g, 3.7 mmol), (*R*)-(-)-2-octanol<sup>15</sup> (0.58 g, 4.4 mmol), triphenylphosphine (1.16g, 4.4 mmol) and dry tetrahydrofuran (50 ml). The mixture was stirred for 24 h, and

---

<sup>15</sup> In the synthesis of the racemic version of compound **76** the racemic modification of the 2-octanol was used in this step

tetrahydrofuran was removed *in vacuo*. The product was isolated by flash-chromatography over silica gel using dichloromethane as the eluent. The product was recrystallised from methanol to give colourless crystals.

Yield: 1.1 g (71%); mp 102.5 °C

<sup>1</sup>HNMR, 400 MHz, CDCl<sub>3</sub>, δ, ppm: 0.88 (3 H, t), 1.20-1.50 (11 H, m), 1.70 (2 H, m), 5.16 (2H, s), 5.20 (1H, sext), 7.09 (2H, d), 7.34-7.47 (5H, m), 8.47 (2H, d) and 9.25 (2H, s); IR, KBr disc, ν cm<sup>-1</sup>: 2660, 2560, **1680**, 1575, 1400, 1385, **1290**, **1250**, 1170

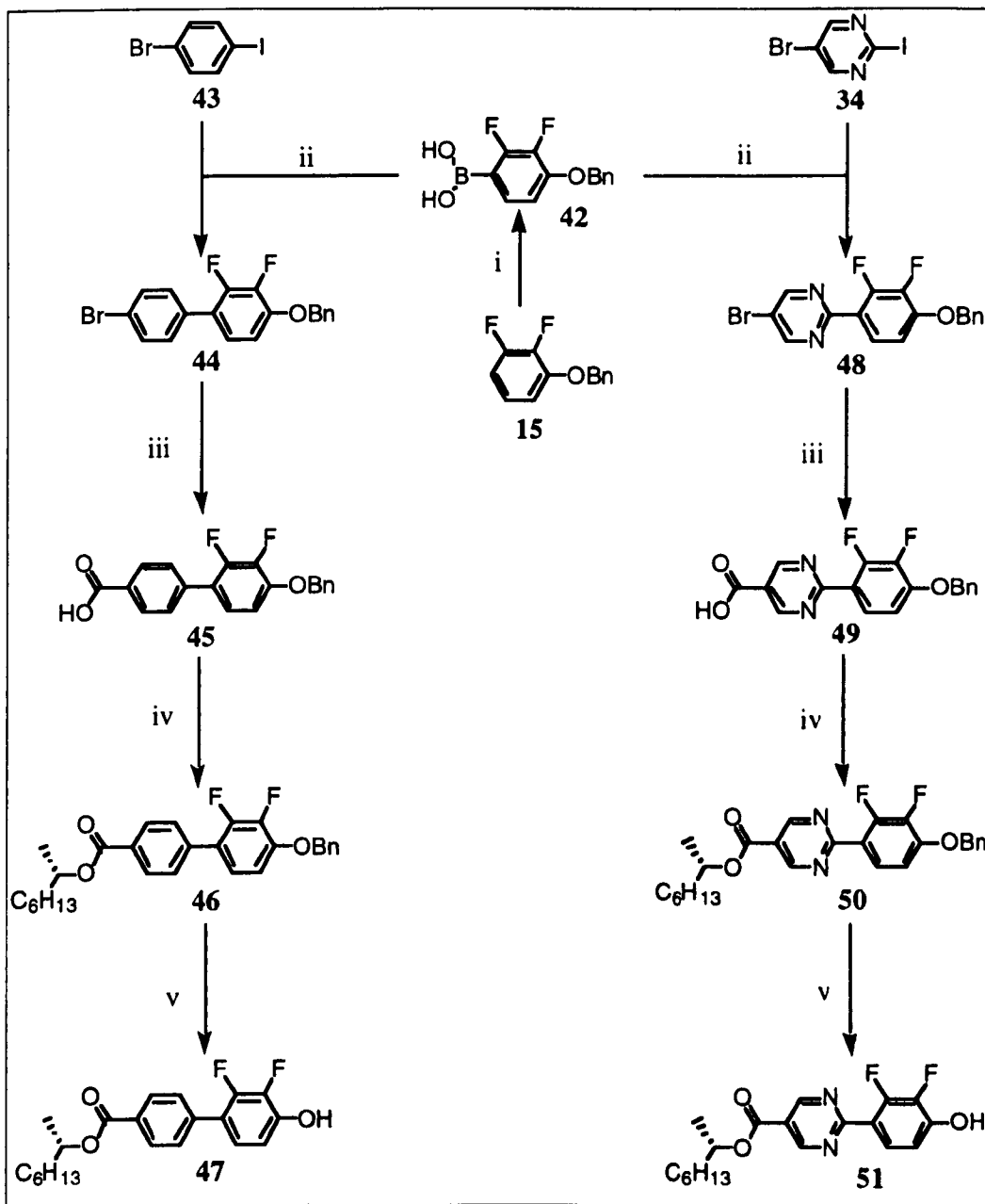
**(S)-1-Methylheptyl 2-(4-hydroxyphenyl)pyrimidine-5-carboxylate 41**

Compound **40** (1.0 g, 2.4 mmol) was deprotected by hydrogenolysis over 5% Pd/C in ethyl acetate (50 ml).

Yield: (0.7 g, 90%); mp 98.8 °C

<sup>1</sup>HNMR, 400 MHz, CDCl<sub>3</sub>, δ, ppm: 9.25 (2H, s), 8.45 (2H, d), 6.95 (2H, d), 5.20 (1H, sext), 1.59-1.81 (2H, m), 1.29-1.42 (11H, m), 0.88 (3H, t); IR, KBr disc, ν cm<sup>-1</sup>: **3440** br, 2920, **1670**, 1570, 1430, 1345, 1300, 1165 and 810; M<sup>+</sup> 588.

### 3.2.3.3 Preparation of (*S*)-1-methylheptyl 2,3-difluoro-4-hydroxybiphenyl-4'-carboxylate **47** and (*S*)-1-methylheptyl 2-(2,3-difluoro-4-hydroxyphenyl)pyrimidine-5-carboxylate **51**



**Scheme 5.5** Preparation of (*S*)-1-methylheptyl 4'-hydroxy-2',3'-difluorobiphenyl-4-carboxylate **47** and (*S*)-1-methylheptyl 2-(4'-hydroxy-2',3'-difluorophenyl)pyrimidine-5-carboxylate **51** i. a) BuLi, -78 °C, THF; b) B(OMe)<sub>3</sub>; c) H<sup>+</sup>. ii. Pd(OAc)<sub>2</sub>, DMSO, NaHCO<sub>3</sub>, water. iii. a) BuLi, -100 °C, THF. b) CO<sub>2</sub>. c) H<sup>+</sup>. iv. DEAD, PPh<sub>3</sub>, *R*-2-octanol v. Pd(C), H<sub>2</sub>, EtOAc

The synthetic pathways in the preparation of compounds **47** and **51** are outlined in the scheme 5.5. The synthetic steps were similar to those used in preparation of the 2-phenylpyrimidine compound **41**. The cross-coupling reaction of the bromo-iodo disubstituted arenes **43** and **34** with the boronic acid **42** using the conventional Suzuki protocol gave poor selectivity of cross-coupled product. To improve the yield of the target compounds the more active catalyst Pd(OAc)<sub>2</sub> [11] was used in the solvent mixture of DMSO-water. The conversion in synthesis of **44** and **48** was more than 90% within 10 minutes after addition of the catalyst.

#### ***4-benzyloxy-2,3-difluorophenylboronic acid 42***

To a vigorously stirred solution of **15** (21.6 g, 0.098 mol) in dried tetrahydrofuran cooled to -78 °C under a nitrogen atmosphere butyllithium solution in hexanes (2.5 M, 44 ml) was added over an hour. After additional stirring for 30 minutes a 50% solution of the trimethyl borate (20.4 g, 0.2 mol) in tetrahydrofuran was added dropwise. The mixture was allowed to reach a room temperature overnight and treated with a solution of hydrochloric acid (18%). The tetrahydrofuran was removed *in vacuo* and the product was extracted into ether, washed with water and dried (MgSO<sub>4</sub>). The solvent was removed *in vacuo*, the off-white solid was stirred for an hour in warm hexane and filtered to give a white powder.

Yield: 20.4 g (79%) Mp 150 °C

<sup>1</sup>HNMR, 400 MHz, DMSO, δ, ppm: 8.16 (2H, s), 7.50-7.25 (6H, m), 7.06 (1H, dt), 5.22 (2H, s). IR, KBr disc, ν cm<sup>-1</sup>: 3405, 1633, 1469, 1371, 1215, 899, 729 M<sup>+</sup>: 264

#### ***4-benzyloxy-4'-bromo-2,3-difluorobiphenyl 44***

Compound **42** (4.8 g, 0.018 mol), compound **43** (5 g, 0.018 mol) and NaHCO<sub>3</sub> (4 g, 0.048 mol) were mixed in water (150 ml) and stirred under nitrogen atmosphere. Dimethyl sulfoxide was added dropwise until all of the reagents had gone to the solution. After the addition of DMSO Pd(OAc)<sub>2</sub> (40 mg, 1 mol%) was added in one

portion and the mixture was heated to 80 °C for 1 h. TLC analysis revealed the completion of the reaction and the mixture was poured into water, acidified with HCl, extracted into ether and dried (MgSO<sub>4</sub>). After removal of the solvent the mixture was purified by the chromatography over silica using dichloromethane as the eluent.

Yield: 5.1 g, 71% Mp 145.5-146.5 °C

<sup>1</sup>HNMR: CDCl<sub>3</sub>, δ, ppm, 7.55 (d, 2H), 7.40 (m, 7H), 7.03 (dd, 1H), 6.84 (dd, 1H), 5.20 (s, 2H); IR: KBr disc, ν, cm<sup>-1</sup> 1639, 1495, 1472, 1297, 1195, 1066, 805. M<sup>+</sup> 374

#### ***4-benzyloxy-2,3-difluorobiphenyl-4'-carboxylic acid 45***

n-Butyllithium in hexanes (2.5 M solution, 6 ml) was added dropwise to the solution of **44** (5 g, 13.3 mmol) in 200 ml of tetrahydrofuran at -100 °C under nitrogen atmosphere. The resulting yellow suspension was stirred for 1 hour and poured onto slurry of solid carbon dioxide in tetrahydrofuran. After reaching ambient temperature the mixture was acidified by aq. solution of hydrochloric acid (18%), then the product was extracted into ethyl acetate, the resulting solution was washed with water and dried (MgSO<sub>4</sub>). After removal of solvent the yellow solid was washed with cold methanol and filtered to give an off-white solid.

Yield: 3.9 g (87%) mp >300 °C

<sup>1</sup>HNMR, 400 MHz, CDCl<sub>3</sub>, δ, ppm: 8.11 (d, 2H), 7.56 (d, 2H), 7.40 (m, 5H), 7.11 (dt, 1H), 6.89 (dt, 1H), 5.21 (s, 2H) IR, KBr, ν cm<sup>-1</sup>: 3444, 2939, 1700, 1637, 1292, 1068, 772, 729. M<sup>+</sup> 340

#### ***(S)-1-methylheptyl 4-benzyloxy-2,3-difluorobiphenyl-4'-carboxylate 46***

Diethylazodicarboxylate (2.2 g, 12.6 mmol) was added dropwise to the solution of the acid **45** (3.9 g, 11.5 mmol), *S*-(-)-2-octanol (1.6 g, 12.6 mmol) and triphenylphosphine (3.3 g, 12.6 mmol) in dry tetrahydrofuran. After stirring at room temperature under nitrogen atmosphere for 24 hours the tetrahydrofuran was removed *in vacuo*. The residue was washed with water, and the product extracted into ether and dried (MgSO<sub>4</sub>).

The product was purified by column chromatography on silica using dichloromethane as an eluent.

Yield: 3.3 g (64%) mp 88-89 °C

<sup>1</sup>HNMR, 400 MHz, CDCl<sub>3</sub>, δ, ppm: 8.09 (d, 2H), 7.56 (d, 2H), 7.41 (m, 5H), 7.10 (dd, 1H), 6.86 (dd, 1H), 5.21 (s, 2H), 5.18 (sec, 1H), 1.75 (m, 1H), 1.62 (m, 1H), 1.50-1.25 (m, 10H), 0.88 (t, 3H). IR, KBr, ν, cm<sup>-1</sup>: 2933, 1722, 1639, 1280, 1063, 771, 730, 708. M<sup>+</sup> 452

***(S)-1-methylheptyl 2,3-difluoro-4-hydroxybiphenyl-4'-carboxylate 47***

The benzyl ester **46** (3.2 g, 7.1 mmol) was cleaved by catalytic hydrogenation in the presence of Pd/C 10% in ethyl acetate. After reaction completion the catalyst was filtered off, the solvent removed *in vacuo* to give a colourless oil.

Yield: 2.5 g (97%)

<sup>1</sup>HNMR, 400 MHz, CDCl<sub>3</sub>, δ, ppm: 8.10 (d, 2H), 7.56 (dd, 2H), 7.12 (m, 1H), 6.88 (m, 1H), 5.33 (d, 1H), 5.17 (sx, 1H), 1.75-1.25 (m, 10H), 1.35 (d, 3H), 0.88 (t, 3H)

***2-(4-benzyloxy-2, 3-difluorophenyl)-5-bromopyrimidine 48***

The procedure was used as described for compound **44**. Amounts used: boronic acid **42** (3.7 g, 0.014 mol), compound **34** (4 g, 0.014 mol), NaHCO<sub>3</sub> ( 3.5 g, 0.042 mol), water (150 ml).

Yield: 2.9 g 55%. Mp 141-142 °C

<sup>1</sup>HNMR, 400 MHz, CDCl<sub>3</sub>, δ, ppm: 8.86 (2H, s), 7.81 (1H, m), 7.40 (5H, m), 6.88 (1H, dd), 5.24 (2H, s). IR, KBr disc, ν, cm<sup>-1</sup>: 1634, 1532, 1422, **1210**, 1090, 790, 730; M<sup>+</sup> 376

***2-(4-benzyloxy-2, 3-difluorophenyl)pyrimidine-5-carboxylic acid 49***

The procedure was used as described for compound **45**. Amounts used: compound **48** (3.7 g, 9.3 mmol), n-butyllithium (2.5 M in hexanes, 4.1 ml, 10.2 mmol), tetrahydrofuran 100ml.

Yield: 2.3g (72%)

<sup>1</sup>HNMR, 400 MHz, CDCl<sub>3</sub>, δ, ppm: 7.96 (dt, 1H), 7.42 (m, 5H), 6.94 (dd, 1H), 5.25 (s, 2H). IR, KBr disc, ν, cm<sup>-1</sup>: 3452, 1702, 1632, 1591, 1410, 1303, 1102, 795, 734. M<sup>+</sup> 342

**(S)-1-methylheptyl 2-(4-benzyloxy-2, 3-difluorophenyl)pyrimidine-5-carboxylate 50**

The procedure was used as described for compound **46**. Amounts used: compound **49** (2.3 g, 6.7 mmol), S-(-)-octanol (1 g, 8.0 mmol), triphenylphosphine (2.1 g, 8.0 mmol) diethylazodicarboxylate (1.4 g, 8.0 mmol), tetrahydrofuran 70 ml.

Yield: 2.2 g (73%) Mp 73-74 °C

<sup>1</sup>HNMR, 400 MHz, CDCl<sub>3</sub>, δ, ppm: 9.43 (s, 2H), 7.94 (dd, 1H), 7.39 (m, 5H), 6.90 (dt, 1H), 5.25 (s, 2H), 5.22 (sec, 1H), 1.76 (m, 1H), 1.63 (m, 1H), 1.50-1.25 (m, 11H), 0.88 (t, 3H). IR, KBr, ν, cm<sup>-1</sup>: 2935, 2846, 1720, 1630, 1594, 1289, 794, 729. M<sup>+</sup> 454

**(S)-1-methylheptyl 2-(2, 3-difluoro-4-hydroxyphenyl)pyrimidine-5-carboxylate 51**

The procedure was used as described for compound **47**. Amounts used: compound **50** (2.2 g, 4.84 mmol),

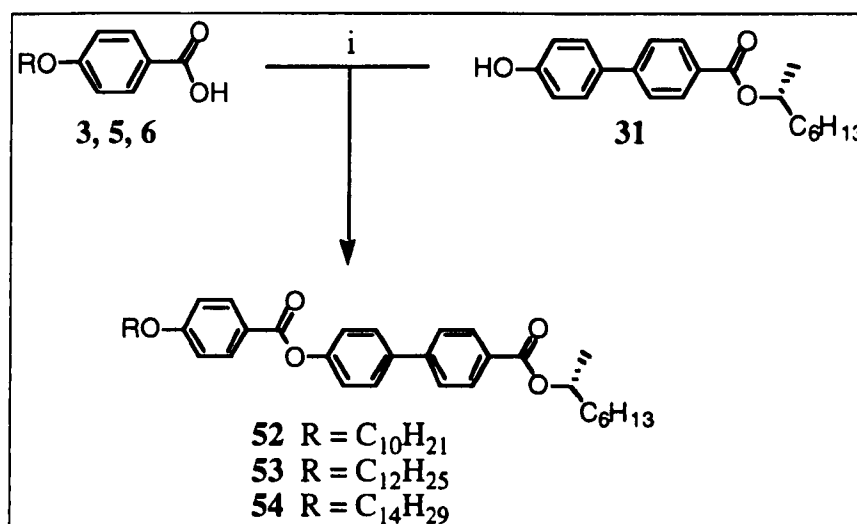
Yield: 1.3 g (76%); Mp 77-78 °C

<sup>1</sup>HNMR, 400 MHz, CDCl<sub>3</sub>, δ, ppm: 9.33 (s, 2H), 7.97 (m, 1H), 6.92 (m, 1H), 5.57 (s, 1H), 5.21 (sex, 1H), 1.75-1.25 (m, 10H), 1.38 (d, 3H), 0.88 (t, 3H); IR, KBr, ν, cm<sup>-1</sup>: 3200, 2931, 2860, 1733, 1632, 1593, 1290, 799; Mass M<sup>+</sup> 364

### 3.2.4 Preparation of final products

#### 3.2.4.1 Preparation of compounds of general structure 1: (R)-1-methylheptyl 4'-(4-*n*-alkoxybenzoyloxy)biphenyl-4-carboxylates 52-54 .

The final synthetic step in preparation of compounds of general structure 1 (see general scheme in section 2. Aims) is shown in the scheme 3.6. The esterification of alkoxybenzoic acids with intermediate 31 was achieved using dicyclohexylcarbodiimide (DCC) in the presence of dimethylaminopyridine (DMAP) [12].



**Scheme 3.6** Preparation of compounds of general structure 1: i. DCC, DMAP, DCM, rt.

The general method used in preparation of 4-*n*-alkoxy and 4-*n*-alk- $\omega$ -enoxyloxy substituted compounds of general structure 1 to 4 and 7 to 9 is described below:

To a solution of alkoxybenzoic acid (1 mol eq), 1-methylheptyl 4'-hydroxybiphenyl-4-carboxylate (1 mol eq), DMAP (0.1 mol eq) in the dichloromethane (40 ml), DCC (1 mol eq.) was added in small portions and the mixture was cooled down to 0 °C. The mixture was stirred for 24 h. The precipitate was filtered, the filtrate was concentrated and purified by flash-chromatography using dichloromethane as the eluent.

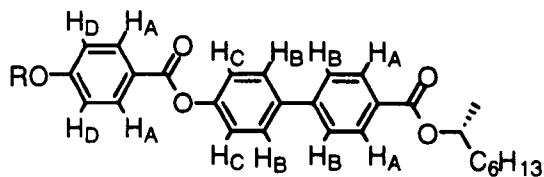


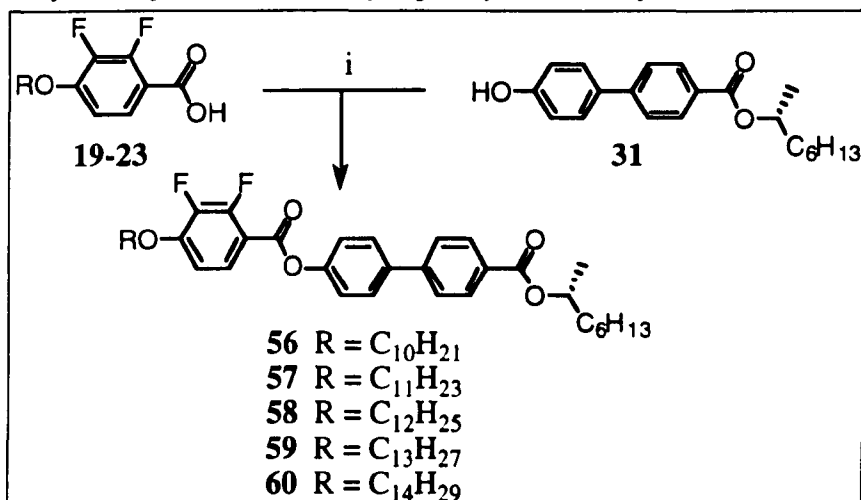
**Table 3.5** Data of  $^1\text{H}$ NMR spectroscopy for (*R*)-1-methylheptyl 4'-(4-alkoxybenzoyloxy) biphenyl-4-carboxylates **52-54**.

No	$C_n$	1HNMR, 400 MHz, $\text{CDCl}_3$ , $\delta$ , ppm								
		H aryl				-CH-	-CH <sub>2</sub> -		-CH <sub>3</sub>	
		4H <sub>A</sub> dd	4H <sub>B</sub> dd	2H <sub>C</sub> d	2H <sub>B</sub> d	1H, sec	O-CH <sub>2</sub> - t, 2H	-(CH <sub>2</sub> ) <sub>n</sub> - m	d, 3H	t, 6H
52	10	8.14	7.66	7.31	6.98	5.18	4.06	1.8-1.2 28H	1.35	0.88
53	12	8.14	7.66	7.30	6.98	5.18	4.05	1.8-1.3 30H	1.35	0.88
54	14	8.14	7.66	7.30	6.99	5.19	4.06	2.0-1.2 32H	1.36	0.89

**Table 3.6** Data of infrared spectroscopy, mass spectrometry, HPLC analysis preparative yields for (*R*)-1-methylheptyl 4'-(4-alkoxybenzoyloxy)biphenyl-4-carboxylates **52-54**

No	IR, KBr, $\nu$ , $\text{cm}^{-1}$			$M^+$	Purity, HPLC	%
	C=O	C=C <sub>Ar</sub>	C-H			
52	1735 1714	1609	2924 2859	586	100	51
53	1792 1718	1611	2926 2855	614	99.1	53
54	1735 1712	1608	2926 2858	642	99.6	43

### 3.2.4.2 Preparation of compounds of general structure 2: (R)-1-methylheptyl 4'-(4-alkoxy-2,3-difluorobenzoyloxy)biphenyl-4-carboxylates 56-60



Scheme 3.7 Preparation of compounds of general structure 2: i. DCC, DMAP, DCM, rt.

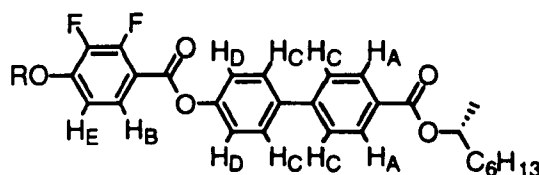


Table 3.7 Data of <sup>1</sup>H NMR spectroscopy for compounds of general structure 2

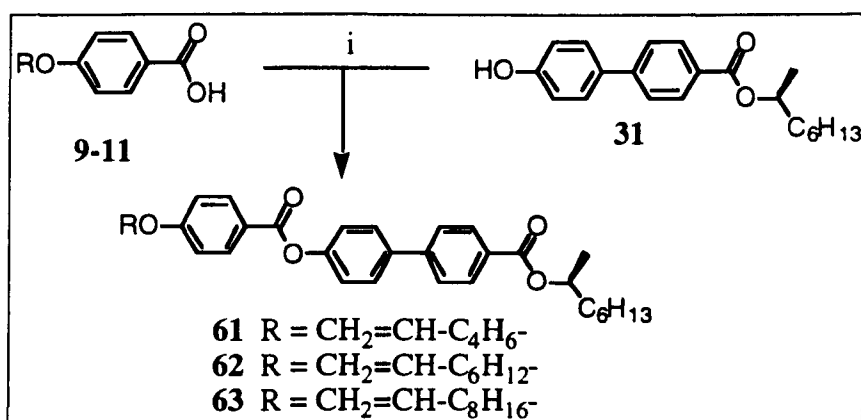
No	C <sub>n</sub>	1H NMR, 400 MHz, CD <sub>2</sub> Cl <sub>2</sub> , δ, ppm										
		H aryl					-CH-	-CH <sub>2</sub> -			CH <sub>3</sub>	
		2H <sub>A</sub> d	2H <sub>B</sub> m	2H <sub>C</sub> dd	2H <sub>D</sub> d	2H <sub>E</sub> m	1H, sex	O-CH <sub>2</sub> 2H, t	CH <sub>2</sub> -CH <sub>2</sub> 2H, quint	-CH <sub>2</sub> - nH, m	CH-CH <sub>3</sub> 3H, d	-CH <sub>3</sub> 6H, t
<b>56</b>	10	8.10	7.88	7.70	7.33	6.88	5.14	4.15	1.87	1.8-1.2 23H	1.35	0.89 0.88
<b>57</b>	11	8.10	7.87	7.70	7.32	6.88	5.14	4.15	1.87	1.8-1.2 25H	1.34	0.88
<b>58</b> <sub>16</sub>	12	8.11	7.86	7.66	7.32	6.83	5.18	4.14	1.87	1.8-1.2 27H	1.36	0.89 0.88
<b>59</b>	13	8.10	7.88	7.70	7.33	6.88	5.14	4.15	1.87	1.8-1.2 29H	1.37	0.88
<b>60</b> <sub>16</sub>	14	8.11	7.86	7.66	7.32	6.83	5.18	4.14	1.87	1.8-1.2 31H	1.36	0.88

Table 3.8 Data of infrared spectroscopy, mass spectrometry, HPLC analysis, optical rotation and preparative yields for compounds of general structure 2

No	IR, KBr, ν, cm <sup>-1</sup>			M <sup>+</sup>	[α] <sup>25</sup>	Purity, HPLC	%
	C=C <sub>Ar</sub>	C=O	C-H				
<b>56</b>	1634	1729, 1709	2926, 2857	623	-23.2	100	58
<b>57</b>	1633	1731, 1710	2928, 2855	637	-22.8	100	52
<b>58</b>	1640	1733, 1710	2923, 2856	650 M <sup>+</sup>	-22.3	100	36
<b>59</b>	1637	1734, 1715	2923, 2854	665	-22.3	100	54
<b>60</b>	1610	1734, 1712	2923, 2853	679	-20.1	99.2	50

<sup>16</sup> The spectra were recorded in CDCl<sub>3</sub>

### 3.2.4.3 Compounds of general structure 3: (S)-1-methylheptyl 4'-(4-alk- $\omega$ -enyloxy benzoyloxy)biphenyl-4-carboxylates 61-63



Scheme 3.8 Preparation of compounds of general structure 3: i. DCC, DMAP, DCM, rt.

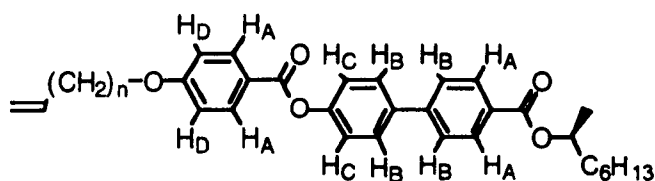


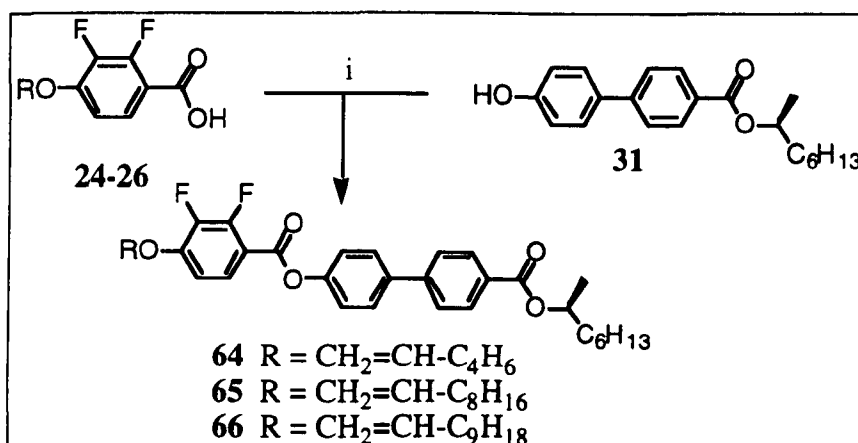
Table 3.9 Data of <sup>1</sup>HNMR spectroscopy for compounds of general structure 3

No	C <sub>n</sub>	1HNMR, 400 MHz, CDCl <sub>3</sub> , δ, ppm										
		H aryl				CH	-CH <sub>2</sub> -			-CH <sub>2</sub> =CH-		-CH <sub>3</sub>
		4H <sub>A</sub> dd	4H <sub>B</sub> dd	2H <sub>C</sub> d	2H <sub>D</sub> d	1H, sec	O-CH <sub>2</sub> t, 2H	(CH <sub>2</sub> ) <sub>n</sub> m, X H	=C-CH <sub>2</sub> q, 2H	CH <sub>2</sub> = M, 2H	=CH- dq, 1H	t, 3H d, 3H
61	4	8.16	7.66	7.31	6.98	5.18	4.07	1.9-1.2 14H	2.15	5.03	5.84	1.35 0.88
62	6	8.14	7.66	7.31	6.98	5.18	4.06	1.9-1.2 18H	2.08	4.99	5.82	1.36 0.88
63	8	8.14	7.67	7.31	6.98	5.18	4.05	1.9-1.2 22H	2.05	4.98	5.82	1.36 0.88

Table 3.10 Data of infrared spectroscopy, mass spectrometry, HPLC analysis, optical rotation and preparative yields for compounds of general structure 3

No	IR, KBr, v, cm <sup>-1</sup>				M+	[α] <sup>25</sup>	Purity, HPLC	%
	C=C <sub>Ar</sub>	C=O	C=C	C-H				
61	1609	1735 1720	1643	2936 2846	528	+25.3	99.1	75
62	1609	1725	1644	2930 2860		+23.3	100	82
63	1612	1735 1721	1645	2929 2855	584	+19.4	99.6	38

### 3.2.4.4 Preparation of compounds of general structure 4: (S)-1-methylheptyl 4'-(4-alk- $\omega$ -enyloxy-2,3-difluoro benzoyloxy)biphenyl-4-carboxylates 64-66



**Scheme 3.9** Preparation of compounds of general structure 4: i. DCC, DMAP, DCM, rt.

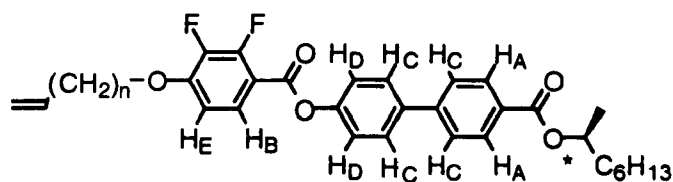


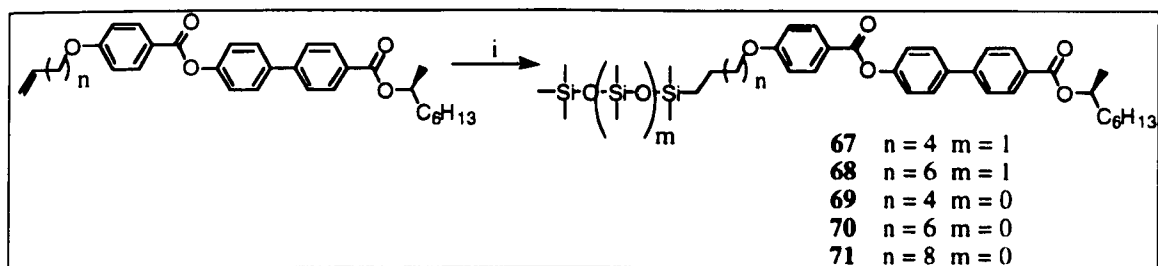
**Table 3.11** Data of <sup>1</sup>HNMR spectroscopy for compounds of general structure 4

No	C <sub>n</sub>	1HNMR, 400 MHz, CDCl <sub>3</sub> , $\delta$ , ppm										
		H aryl					CH	-CH <sub>2</sub> -		-CH <sub>2</sub> =CH-		-CH <sub>3</sub>
		4H <sub>A</sub> d	4H <sub>B</sub> m	2H <sub>C</sub> dd	2H <sub>D</sub> d	2H <sub>E</sub> m	1H, sec	O-CH <sub>2</sub> t, 2H	=C-CH <sub>2</sub> q, 2H	CH <sub>2</sub> = M, 2H	=CH- dq, 1H	t, 3H d, 3H
<b>64</b>	4	8.11	7.86	7.66	7.32	6.83	5.18	4.15	2.15	5.03	5.84	1.36 0.88
<b>65</b>	8	8.11	7.86	7.66	7.32	6.84	5.18	4.14	2.14	4.97	5.82	1.36 0.88
<b>66</b>	9	8.11	7.86	7.66	7.32	6.83	5.18	4.14	2.05	4.98	5.82	1.36 0.88

**Table 3.12** Data of infrared spectroscopy, mass spectrometry, HPLC analysis, optical rotation and preparative yields for compounds of general structure 4

No	IR, KBr, $\nu$ , cm <sup>-1</sup>				M+	[ $\alpha$ ] <sup>25</sup>	Purity, HPLC	%
	C=C <sub>Ar</sub>	C=O	C=C	C-H				
<b>64</b>	-	1718	1628	2932 2860	564	+23.5	100	75
<b>65</b>	-	1731 1708	1631	2930 2858	620	+21.0	100	82
<b>66</b>	-	1728 1708	1627	2933 2860	634	+19.7	99.7	38

**3.2.4.5 Preparation of compounds of general structure 5: (S)-1-methylheptyl 4'-{4-[ $\omega$ -(1,1,3,3,3-pentamethyldisiloxanyl)- or ( $\omega$ -1,1,3,3,5,5-heptamethyl)trisiloxanyloxy]benzoyloxy} biphenyl-4-carboxylates 67-71**



**Scheme 3.10** Preparation of compounds of general structure 5: Karstedt catalyst,

1,1,3,3,3-pentamethyldisiloxane or 1,1,3,3,5,5,5-heptamethyltrisiloxane, toluene, r. t.

The synthesis of compounds of general structure 5 is shown in the scheme 3.10. The catalytic hydrosilylation of the alkenes of general structure 2 was carried out as described in ref 14 using platinum divinyltetramethyldisiloxane<sup>17</sup> as the catalyst. The method is described below and also used for preparation of compounds of general structure 6 (see next section):

The solution of (*R*)-1-Methylheptyl 4'--(4''-*n*-alkenoxybenzoyloxy)biphenyl-4-carboxylate (55-57) (1 mol) and 1,1,1,2,2-pentamethyldisiloxane or 1,1,1,2,2,3,3-heptamethyltrisiloxane (1.2 mol) in toluene was stirred under nitrogen atmosphere at room temperature. 5 mg of platinum divinyltetramethyldisiloxane was added and the mixture was stirred for 24 hours. The toluene was removed *in vacuo* and the residue was purified by flash-chromatography using the mixture of ethyl acetate (20%) in dichloromethane.

<sup>17</sup> The platinum catalyst is known as Karstedt complex and is used in hydrosilylation of wide variety of alkene substrates [13].

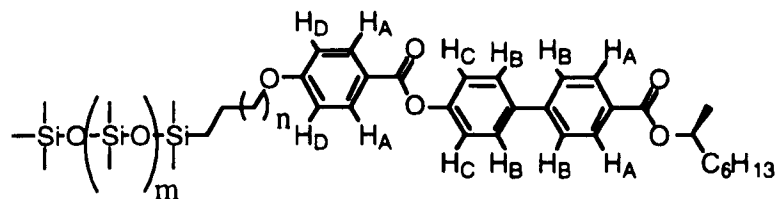


**Table 3.13** Data of  $^1\text{H}$ NMR spectroscopy for compounds of general structure 5

No	n	m	$^1\text{H}$ NMR, 400 MHz, $\text{CDCl}_3$ , $\delta$ , ppm										
			H aryl				CH	-CH <sub>2</sub> -			CH <sub>3</sub>		
			4H <sub>A</sub> dd	4H <sub>B</sub> dd	2H <sub>C</sub> d	2H <sub>D</sub> d	1H sec	O-CH <sub>2</sub> 2H, t	CH <sub>2</sub> m	Si-CH <sub>2</sub> 2H, t	Si-CH <sub>3</sub> nH, 3s	CH-CH <sub>3</sub> 3H, d	-CH <sub>3</sub> 3H, t
67	4	1	8.10	7.68	7.29	6.98	5.12	4.04	1.9-1.2 H	0.55	0.07-0.01 21H	1.32	0.86
68	6	1	8.14	7.66	7.30	6.98	5.18	4.05	1.9-1.2 H	0.54	0.09-0.01 21H	1.36	0.87
69	4	0	8.14	7.66	7.30	6.98	5.18	4.06	1.9-1.2 H	0.53	0.07-0.05 15H	1.36	0.88
70	6	0	8.08	7.60	7.24	6.92	5.11	3.99	1.9-1.2 H	0.48	0.05-0.00 15H	1.29	0.82
71	8	0	8.05	7.64	7.24	6.93	5.08	4.00	1.9-1.2 H	0.46	0-0.02 15H	1.28	0.82

**Table 3.14** Data of infrared spectroscopy, mass spectrometry, HPLC analysis, optical rotation and preparative yields for compounds of general structure 5

No	IR, KBr, $\nu$ , $\text{cm}^{-1}$				M <sup>+</sup>	[ $\alpha$ ] <sup>25</sup>	Purity, HPLC	%
	C=C <sub>Ar</sub>	C=O	C-Si	C-H				
67	1610	1734 1713	1073	2964 2864	425*	+21.1	96.1	20
68	1610	1734 1720	1057	2932 2862	453*	+17.7	95.9	65
69	1610	1735 1715	1067	2934 2863	351*	+19.3	99.4	50
70	1610	1736 1715	1062	2930 2861	379*	+18.6	99.6	44
71	1610	1736 1715	1074	2926 2858	407*	+17.8	100	35

**3.2.4.6 Preparation of compounds of general structure 6: (S)-1-methylheptyl 4'-[4-[ $\omega$ -(1,1,3,3,3-pentamethyldisiloxanyl)alkoxy]benzoyloxy]biphenyl-4-carboxylates 72-74**

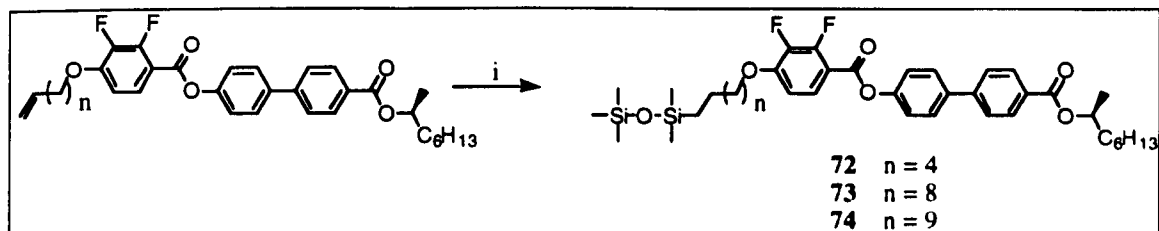


**Figure 3.11** Preparation of compounds of general structure 6: i. Karstedt catalyst, 1,1,3,3,3-pentamethyldisiloxane, toluene, r. t.

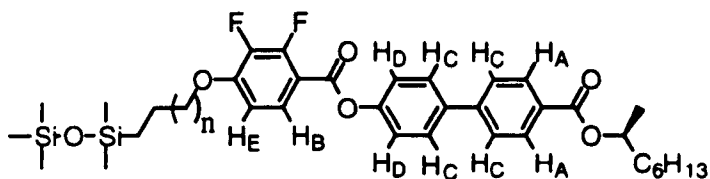


**Table 3.15** Data of <sup>1</sup>HNMR spectroscopy for compounds of general structure 6

No	n	1HNMR, 400 MHz, CD <sub>2</sub> Cl <sub>2</sub> , $\delta$ , ppm										
		H aryl					CH	-CH <sub>2</sub> -		CH <sub>3</sub>		
		2H <sub>A</sub> d	H <sub>B</sub> m	4H <sub>C</sub> dd	2H <sub>D</sub> d	H <sub>E</sub> m	1H sec	O-CH <sub>2</sub> 2H, t	Si-CH <sub>2</sub> 2H, t	Si-CH <sub>3</sub> s	CH-CH <sub>3</sub> 3H, d	-CH <sub>3</sub> 3H, t
72	6	8.10	7.88	7.70	7.33	6.89	5.15	4.15	0.54	.07 9H .05 6H	1.32	0.88
73 <sup>18</sup>	10	8.09	7.84	7.64	7.30	6.81	5.15	4.12	0.48	.04 9H .02 6H	1.33	0.86
74	11	8.10	7.88	7.70	7.32	6.88	5.15	4.15	0.52	.06 9H .04 6H	1.36	0.88

**Table 3.16** Data of infrared spectroscopy, mass spectrometry, HPLC analysis, optical rotation and preparative yields for compounds of general structure 6

No	IR, KBr, $\nu$ , cm <sup>-1</sup>				M <sup>+</sup>	[ $\alpha$ ] <sup>25</sup>	Purity, HPLC	%
	C=C <sub>Ar</sub>	C=O	C-Si	C-H				
72	1626	1736 1715	1082	2931 2861	712*	+15.7	99.6	20
73	1619	1736 1715	1062	2931 2860	646*	+20.4	100	65
74	1620	1740 1715	1066	2930 2860	457*	+17.3	99.1	50

<sup>18</sup> The spectrum was recorded in CDCl<sub>3</sub>



### 3.2.4.8 Preparation of compounds of general structure 8: (S)-1-methylheptyl 4'-(4-alkoxybenzoyloxy)-2', 3'-difluorobiphenyl-4-carboxylates 80-84

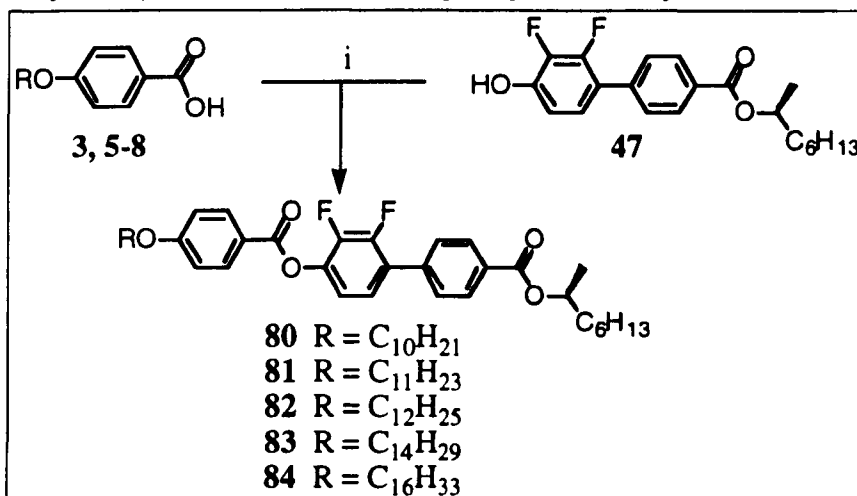


Figure 3.13 Preparation of compounds of general structure 8: i.DCC, DMAP, DCM, rt.

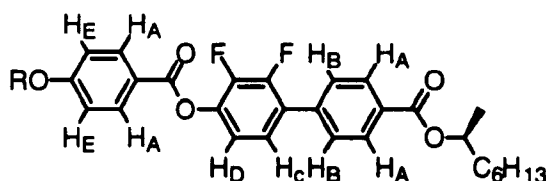


Table 3.19 Data of <sup>1</sup>HNMR spectroscopy for compounds of general structure 8

No	C <sub>n</sub>	1HNMR, 400 MHz, CDCl <sub>3</sub> , δ, ppm										
		H aryl					-CH-	-CH <sub>2</sub> -			CH <sub>3</sub>	
		2H <sub>A</sub> d+d	2H <sub>B</sub> d+d	H <sub>C</sub> m	H <sub>D</sub> M	2H <sub>E</sub> dd	1H, sex	O-CH <sub>2</sub> 2H, t	CH <sub>2</sub> -CH <sub>2</sub> 2H, quint	CH <sub>2</sub> nH, m	CH-CH <sub>3</sub> 3H, d	-CH <sub>3</sub> 6H, t
80	10	8.15	7.62	7.24	7.14	6.99	5.14	4.15	1.82	1.8-1.2 24H	1.36	0.89 0.88
81 <sup>19</sup>	11	8.14	7.65	7.30	7.18	7.02	5.15	4.07	1.81	1.8-1.2 26H	1.35	0.89 0.88
82 <sup>19</sup>	12	8.14	7.65	7.30	7.17	7.02	5.16	4.07	1.79	1.8-1.2 28H	1.35	0.89
83	14	8.15	7.62	-	7.14	6.99	5.18	4.06	1.82	1.8-1.2 32H	1.35	0.88
84 <sup>19</sup>	16	8.14	7.65	7.30	7.17	7.01	5.16	4.07	1.81	1.8-1.2 36H	1.35	0.89 0.88

Table 3.20 Data of infrared spectroscopy, mass spectrometry, HPLC analysis, optical rotation and preparative yields for compounds of general structure 8

No	IR, KBr, v, cm <sup>-1</sup>			M <sup>+</sup>	[α] <sup>25</sup>	Purity, HPLC	%
	C=C <sub>Ar</sub>	C=O	C-H				
80	1610	1733, 1709	2929, 2859	623	+18.4	100	61
81	1610	1733, 1718	2929, 2859	637	+17.6	99.2	69
82	1611	1733, 1711	2929, 2858	651	+19.9	99.4	59
83	1613	1751, 1720	2930, 2859	679*	+18.3	99.6	54
84	1611	1750, 1719	2927, 2857	707	+17.6	99.4	48

<sup>19</sup> The spectrum was recorded in CD<sub>2</sub>Cl<sub>2</sub>

### 3.2.4.9 Preparation of compounds of general structure 9: (S)-1-methylheptyl 2-[4-(4-alkoxybenzoyloxy)-2,3-difluorophenyl] pyrimidine-5-carboxylates 85-88

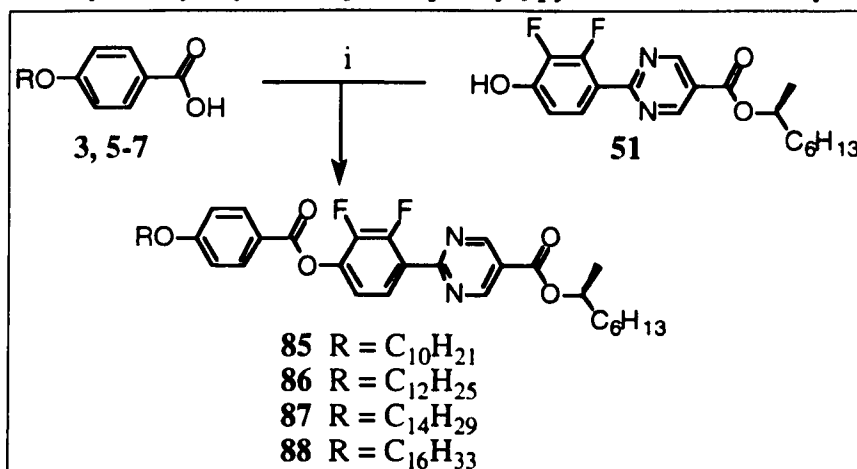


Figure 3.14 Preparation of compounds of general structure 9: i – DCC, DMAP, CH<sub>2</sub>Cl<sub>2</sub>

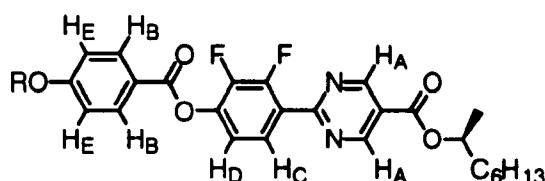


Table 3.21 Data of <sup>1</sup>HNMR spectroscopy for compounds of general structure 9

No	C <sub>n</sub>	<sup>1</sup> HNMR, 400 MHz, CDCl <sub>3</sub> , δ, ppm										
		H aryl					-CH-	-CH <sub>2</sub> -			CH <sub>3</sub>	
		2H <sub>A</sub> s	2H <sub>B</sub> d	H <sub>C</sub> m	H <sub>D</sub> m	2H <sub>E</sub> dd	1H, sex	O-CH <sub>2</sub> 2H, t	CH <sub>2</sub> -CH <sub>2</sub> 2H, quint	CH <sub>2</sub> nH, m	CH-CH <sub>3</sub> 3H, d	-CH <sub>3</sub> 6H, t
<b>85</b>	10	9.38	8.16	8.05	7.21	6.99	5.23	4.06	1.81	1.8-1.2 24H	1.39	0.89
<b>86</b>	12	9.38	8.16	8.05	7.22	6.99	5.23	4.06	1.83	1.8-1.2 28H	1.39	0.89 0.88
<b>87</b>	14	9.38	8.16	8.05	7.22	6.99	5.23	4.06	1.83	1.8-1.2 32H	1.39	0.89 0.88
<b>88</b>	16	9.38	8.16	8.05	7.22	6.99	5.23	4.06	1.83	1.8-1.2 36H	1.35	0.89 0.88

Table 3.22 Data of infrared spectroscopy, mass spectrometry, HPLC analysis, optical rotation and preparative yields for compounds of general structure 9

No	IR, KBr, ν, cm <sup>-1</sup>			M	[α] <sub>D</sub> <sup>25</sup>	Purity, HPLC	%
	C=C <sub>Ar</sub>	C=O	C-H				
<b>85</b>	1610	1740 1717	2936 2860	625	+18.6	99.5	44
<b>86</b>	1610	1745 1722	2932 2860	652	+18.0	99.6	37
<b>87</b>	1611	1745 1722	2928 2860	512	+16.1	99.3	49
<b>88</b>	1609	1743 1718	2926 2858	579	+15.9	99.1	62

**References (Section 3)**

1. DR Coulson, *Inorganic Synthesis*, 1972, **13**, 121
2. CRC Handbook of Physics and Chemistry, 1988, ed. Priest, R.C., CRC Press, Boca Raton, 68th Edition.
3. H Feuer and J Hooz in "Patai: The Chemistry of the Ether Linkage", New York: Interscience, 446
4. GW Gray, B Jones, *J Chem Soc*, 1953, 4179
5. SM Kelly, R Buchecker, *Helv. Chim. Acta*, 1988, **71**, 461
6. SM Kelly, *Helv. Chim. Acta*, 1989, **72**, 594
7. MB Smith, "Organic Synthesis, McGraw-Hill, 1994
8. JW Goodby, SJ Patel and E Chin, *J Mat Chem*, 1992, **2**, 197
9. JW Goodby, M Hird, R Lewis, K Toyne, *J.Chem.Soc.Chem.Commun.* 1996, **24**, 2719
10. N Miyaura and A Suzuki, *Chem Rev*, 1995, **95**, 2457
11. TJ Wallow and BM Novak, *J Org Chem*, 1997, **62**, 7170
12. J March, "Advanced Organic Chemistry", 3<sup>rd</sup> ed, McGraw-Hill, 1985
13. MA Brook, "Silicon in Organic, Organometallic, and Polymer Chemistry, John Willey & Sons, Inc, 2000, p.404
14. GH Mehl, JW Goodby, *Chem Commun*, 1999, 13

## 4 Results and discussion

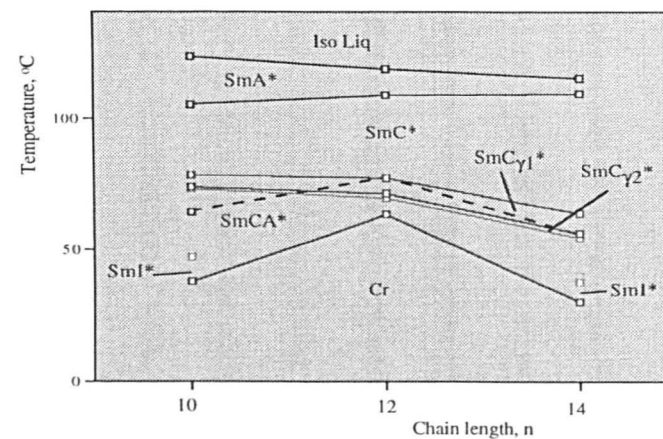
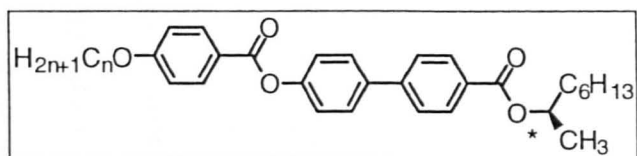
### Stability of the smectic C phases as a function of molecular structure

#### 4.1 Aromatic cores based on the biphenyl fragment

##### 4.1.1 Compounds of general structure 1: *(R)*-1-Methylheptyl 4'-(4-*n*-alkoxybenzoyloxy) biphenyl-4-carboxylates, 52-54

The structure of *(R)*-1-Methylheptyl 4'-(4-*n*-alkoxybenzoyloxy)biphenyl-4-carboxylates **52-54** incorporates the 4-benzoyloxybiphenyl system, an example of the aromatic core that favours an extensive ferroelectric and antiferroelectric behaviour in mesomorphic state. All of the members of the series **1** are pure smectogens with nematic and frustrated blue and TGB phases being completely suppressed from their phase sequences. The smectic polymorphism is similar to that of MHPOBC and includes SmA\*, SmC\*, SmC<sub>F11</sub>\*, SmC<sub>F12</sub>\*, SmC<sub>A</sub>\* and SmI\* phases (figure 4.1). The ferroelectric smectic C\* phase dominates the phase sequences over broad temperature ranges. It remains enantiotropic regardless of the size of the non-chiral alkyl chain and, generally, the phase stability increases with elongation of the chain at the expense of the high temperature smectic A\* phase. In contrast, the antiferroelectric smectic C\* phase is less pronounced and in most cases remains monotropic. Even if it appears on heating its temperature interval is significantly shorter than during the cooling cycle. The hysteresis in the phase transition temperatures of the antiferroelectric phases (on heating and cooling) indicates that the phase transitions are not conventional liquid crystal transition, which are driven by a change in "lattice-type" structure [1]. The SmC<sub>A</sub>\* phase is preceded with two modifications of the ferroelectric phase, which emerge over narrow temperature intervals, thereby preventing direct SmC\*-SmC<sub>A</sub>\* phase transitions. Their appearance is thought to be a direct consequence of the competition between synclinic and anticlinic ordering as described in the introduction.

**Figure 4.1** Mesomorphic properties of (R)-1-methylheptyl 4'-(4-n-alkoxybenzoyloxy)biphenyl-4-carboxylates, **52-54**, compounds of general structure **1**



No	n	T, °C / ΔH, kJ mol <sup>-1</sup>									
		Mp	SmI*	SmC <sub>A</sub> *	SmC <sub>FII</sub> *	Sm <sub>FII2</sub> *	SmC*	SmA*	Iso Liq	Cr	
52	10	• 64.5 [24.9]	(•) 47.1 [-3.7]	• 73.0 [-]	• 73.6 [-]	• 78.7 [-0.02]	• 105.4 [-0.18]	• 123.6 [-5.1]	•	38.1 [-0.1]	
53	12	• 77.3 [46.5]	-	(•) 69.8 [-]	• 71.2 [-]	(•) 77.2 [-0.02]	• 108.7 [-0.28]	• 118.9 [-5.0]	•	63.4 [-43.9]	
54	14	• 55.5 [40.0]	(•) 37.5 [-3.5]	(•) 54.8 [-]	• 56.2 [-]	• 64 [-]	• 109.3 [-0.3]	• 115.4 [-4.5]	•	29.9 [-17.6]	

First order phase transitions between the isotropic liquid and the smectic A\* phase as well as the melting and recrystallisation transitions were detected by the DSC method (figure 4.2). The SmA\*-SmC\* and SmC<sub>A</sub>\*-SmI\* transitions were also “visible” in the DSC curves due to their weak first-order character [2]. The enthalpy values of the SmA\*-SmC\* transitions were approximately ten times smaller than typical values of first-order Iso Liq – SmA phase transition [3]. For compound **52** it was found that a minor discontinuity is also attained at the transitions from SmC\* phase to FI phase and subsequent SmC<sub>A</sub>\* phase, giving rise to small peaks in the DSC curve (figure 4.2). However, in most cases the enthalpies of the second-order transitions between the smectic C modifications were too small to measure and therefore the phase identification was carried out using polarizing microscopy.

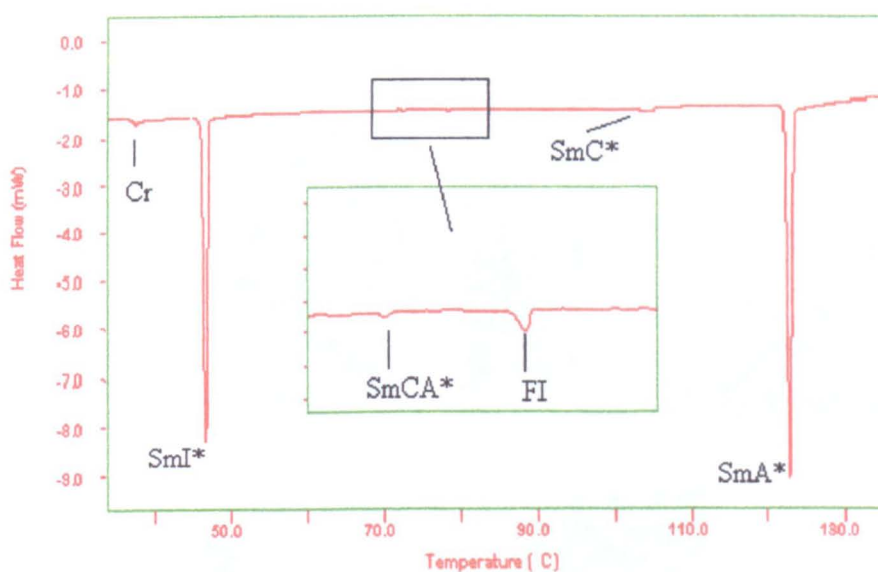


**Figure 4.2:** DSC cooling trace for compound **52**. Scanning rate 10 °/min

In the microscopy preparations the types of liquid-crystalline phases were assigned by comparing their textures to reference sources (see for example [4]). Thus, for compound **54**, the smectic A phase was characterised via its clear focal-conic domains and the extinct homeotropic region when the material was observed between cross-polarizers

(figure 4.3a). At the transition to the smectic C\* phase, the focal-conic fans appeared broken and at some areas banded as a result of stabilisation of the molecular tilt and helix formation. At the same time, the homeotropic region turned dark blue (figure 4.3b) showing the formation of the helical structure. Small domains of the *schlieren* texture were also observed in uncovered droplets of the material. In the vicinity of the  $\text{SmC}_{\text{F12}}^*$  phase, the homeotropically aligned region exhibited *schlieren* domains which became very mobile with disordered fluctuations observed throughout the sample.

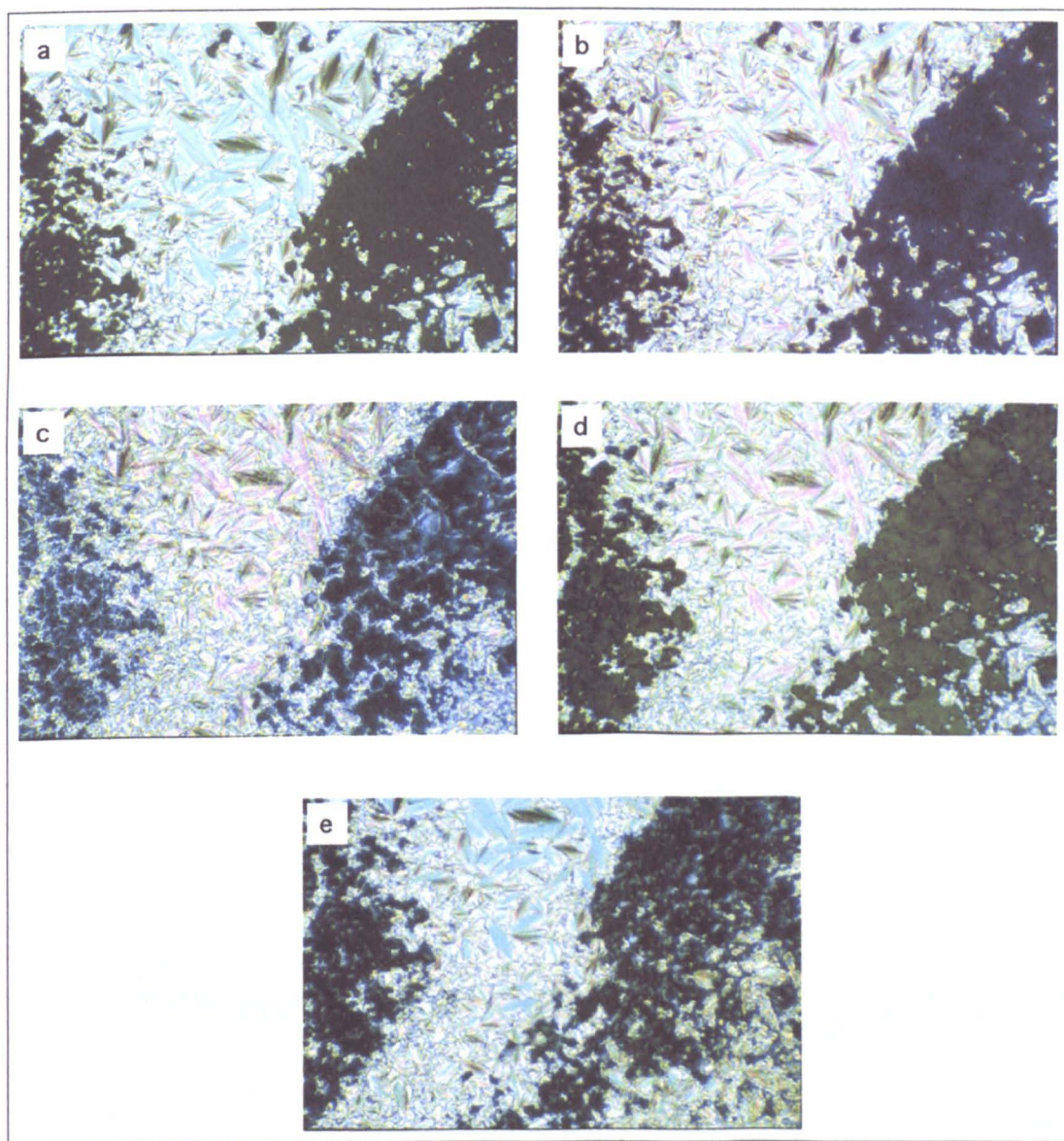


**Figure 4.3:** Textures of compound **54**. a)  $\text{SmA}^*$ , 111 °C; b)  $\text{SmC}^*$  phase, 104 °C; c)  $\text{SmC}_{\text{F12}}^*$  phase, 56.5 °C; d)  $\text{SmC}_A^*$  phase, 52.2 °C; e)  $\text{SmI}^*$  phase, 34 °C

On cooling the characteristic *schlieren* pattern gradually developed over all homeotropic region and the fluctuations diminished (figure 4.3c). At the transition to the  $\text{SmC}_{\text{F12}}^*$  phase another wave of fluctuations reconstructed the samples appearance and with a further temperature decrease the green coloured domain of the antiferroelectric phase started growing in the homeotropically aligned region of the specimen (figure 4.3d). The focal-conic fans cleared as a result of the formation of the alternating molecular tilt in smectic layers. Remarkably, the direction of the helix that was formed in the smectic  $\text{C}^*$  phase changed its sign to the opposite in the antiferroelectric phase.

The antiferroelectric properties of the  $\text{SmC}_{\text{A}}^*$  phase were studied in detail through electric field measurements using the triangular wave method [5]. In the ferroelectric smectic  $\text{C}^*$  phase, molecular reorientation from one uniform state to another produces an electric current, which flows between the surfaces when the external electric field passes a zero point. As a result, one sharp peak is usually observed in the current-time trace (figure 4.4a), and the value of the spontaneous polarization is calculated from the area under this peak in voltage-time coordinates. In turn, tristate switching in the antiferroelectric phase involves two independent molecular reorientations giving rise to two electric currents.

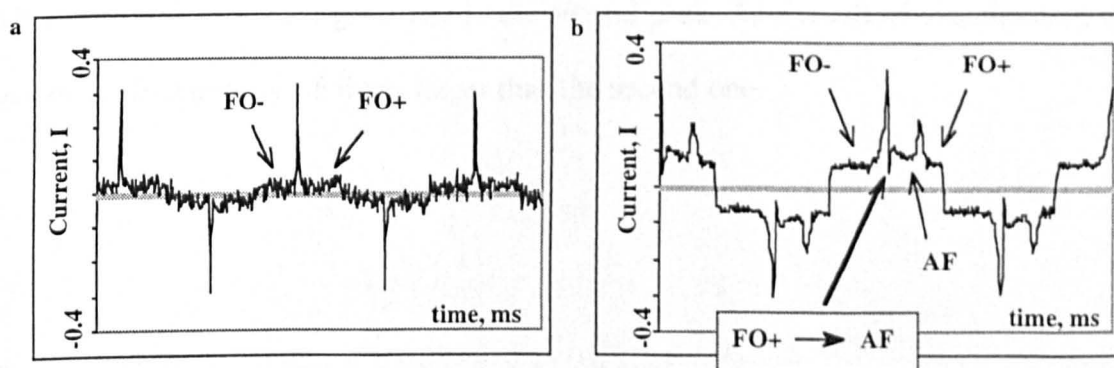


**Figure 4.4:** The current-time traces recorded for compound **53**: a)  $\text{SmC}^*$  phase, 78 °C, electric field 10 Hz, 20 VPP. b)  $\text{SmC}_{\text{A}}^*$  phase, 68 °C, electric field 10 Hz, 20 VPP.

When the external electric field alternates slowly, the two broad peaks will appear on the current time trace. The first peak originates from the quick reorientation of the molecular dipoles at the transition from the **FO(-)** state to the **AF** state. A subsequent transition from the **AF** to the **FO(+)** state gives rise to a second peak in the current-time trace [6].

For compound **53** two switching peaks were clearly observed in the temperature range of the antiferroelectric phase (figure 4.4b), thereby confirming that the switching in this phase proceeds *via* three states. However, the shapes and sizes of two signals were noticeably different. This is because the lowest frequency value of the electric field (5 Hz) that allowed signal capturing with minimum level of noise was still too high to provide a slow rate of alteration of the electric field. As a result, driven by a fast changing electric field the transition from the **FO-** state proceeds directly to the **FO+** overshooting the **AF** state. Moving around the smectic **C\*** cone the molecules gain enough “acceleration” to switch from one side of the cone to another when **E** changes from a negative value to zero. Then, with an electric field passing a zero point and moving towards a positive maximum the material relaxes from the **FO+** to the **AF** state giving rise to the backward current peak (figure 4.4b) [6]. Following reorientation from **AF** state to the **FO-** state gives rise to the second peak. As a result of overshooting the size of the first peak is 1.5 times larger than the second one.

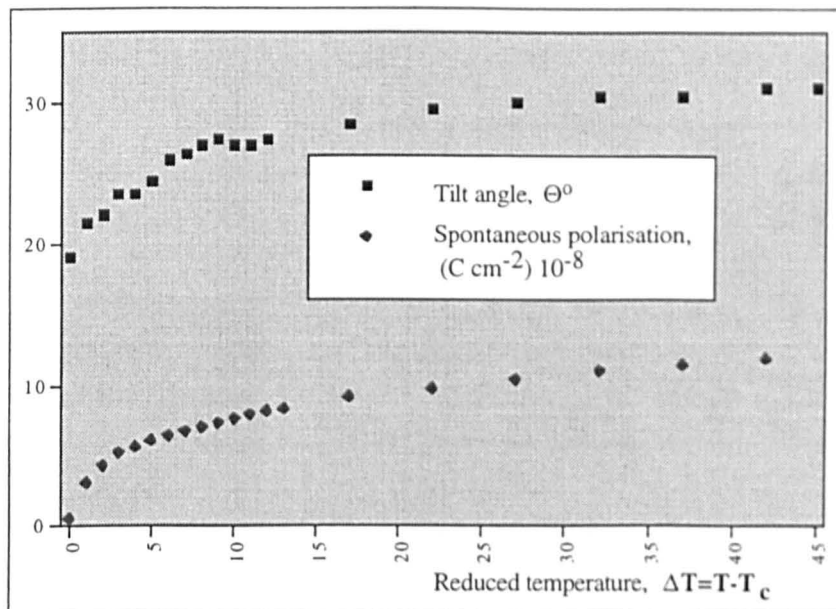


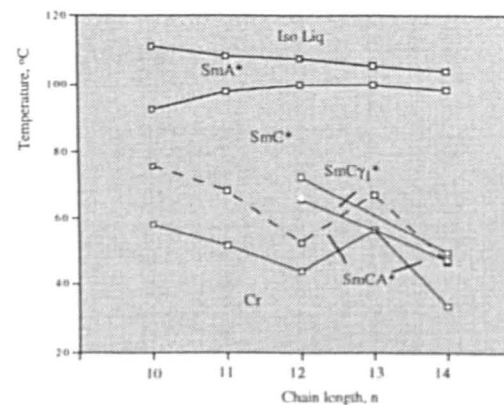
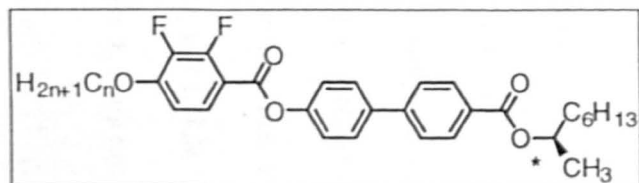
**Figure 4.5:** The spontaneous polarization and optical tilt angle as a function of reduced temperature recorded for compound **53**. Applied electric field 20 Hz, 20 VPP

In general, all three compounds of general structure **1** possess quite a high value of the “apparent” spontaneous polarization, *ca.* 100 nC cm<sup>-2</sup> (compound **53**) in the temperature region of the antiferroelectric phase. It can be seen from figure 4.5 that the magnitude of the spontaneous polarization grows continuously with decreasing temperature from the Curie point (SmA\*-SmC\* transition) and disappears in the SmI\* phase because the electric field was too small to switch this higher ordered state. The optical tilt angle has a different temperature dependence, at Curie temperature it has a zero value and it reaches 25 degrees in the antiferroelectric phase (figure 4.5).

### Summary:

The antiferroelectric SmCA\* phase was observed for all members of the series **1**. In most cases, the phase is monotropic and appears only during the cooling cycle. Thus, the molecular core employed is more favourable for formation of the ferroelectric smectic C\* phase, which is the most pronounced mesophase in the series. These results are in keeping with those previously reported for these materials [7].

**Figure 4.6:** Mesomorphic properties of (R)-1-methylheptyl 4'-(4-alkoxy-2,3-difluorobenzoyloxy)biphenyl-4-carboxylates, **56-60**, compounds of general structure **2**



No	n	T, °C / [ $\Delta H$ , kJ mol <sup>-1</sup> ]									
		Mp	SmC <sub>A</sub> *	Sm <sub>FI1</sub> *	Sm <sub>FI2</sub> *	SmC*	SmA*	TGBA	Iso	Cr	
56	10	• 75.5 [31.3]	-	-	-	• 92.9 [-0.1]	•	•	• 111.1 [-4.2]	• 58.2 [-28.9]	
57	11	• 68.4 [29.4]	-	-	-	• 97.7 [-0.27]	•	•	• 108.3 [-3.9]	• 51.5 [-27.1]	
58	12	• 52.5 [38.1]	• 65.8 [-0.01]	• 66.4 [-]	• 72.2 [-]	• 99.8 [-0.28]	•	•	• 107.3 [-4.0]	• 44.3 [-36.9]	
59	13	• 67.2 [48.1]	-	-	-	• 99.71 [-0.29]	•	•	• 105.6 [-3.9]	• 56.3 [-45.3]	
60	14	• 46.7 [42.6]	• 47.1 [-]	-	• 49.7 [-]	• 98.4 [-0.38]	•	•	• 103.9 [-4.0]	• 33.6 [-31.1]	

#### 4.1.2 Compounds of general structure 2: *(R)*-1-methylheptyl 4'-(4-alkoxy-2,3-difluorobenzoyloxy)biphenyl-4-carboxylates, 56-60

The general structure of compounds of general structure **2** includes two ortho-fluorine substituents attached to the outer ring of the 4-benzoyloxybiphenyl core which was used in series **1** as the parent system for comparative studies (see figure 4.6). This structural modification greatly affected the magnitude of the transverse molecular dipole as a consequence of the introduction of fluorine atoms, which possess high electronegativity. As predicted in the MacMillan's model of the smectic C phase, strengthening the lateral dipole should improve stability of the molecular tilt in smectic layers. However, in the series **2** the stability of the tilted smectic phases was found almost unchanged when the transition temperatures are compared to those of the type **1** materials. For instance, the temperature interval of the SmC\* phase for C14 homologues **54** and **60** is roughly the same and extends over 50 °C.

Lateral fluorine substituents, however, promote formation of the TGBA phase, which was observed over a narrow temperature interval (less than a half of a degree) for all of the homologues synthesised. At the low temperature end of the phase sequences enantiotropic ferroelectric and antiferroelectric SmC\* phases were exhibited by the C12 and C14 homologues (compounds **58** and **60**). There is an odd-even effect that suppresses the antiferroelectric and frustrated sub-phases for odd members of homologue series. For even numbers the optimal chain length, which favours the SmC<sub>A</sub>\* phase, is 12. The C10 homologue, which exhibited the broadest antiferroelectric phase in series **1**, does not possess smectic sub-phases at all.

The microscopy studies were carried out as described for compounds of general structure **1**. It was difficult to observe the transition from the SmA\* to the SmC\* phase

in the homeotropic region because the pitch length in the smectic C\* phase was very short and therefore both phases appeared optically extinct between cross-polarizers. In free-standing preparations it was possible to distinguish between textures of the SmC\* and SmA\* phases (figure 4.7) as the white lines associated with the *schlieren* texture were clearly seen on the edge of the film in the SmC\* phase.

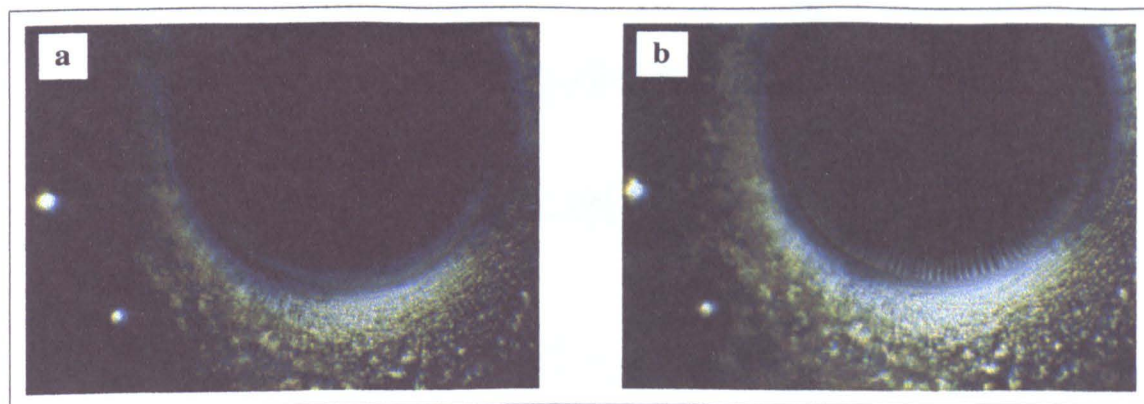


**Figure 4.7:** Photomicrographs of the free-standing films made for compound **57** a) SmA\*, 104.0 °C; b) SmC\*, 90.0 °C

The textures of the ferroelectric and antiferroelectric phases are shown in the figure 4.8 for compound **58**. The homeotropic regions were covered with a fluctuating *schlieren* domain in the SmC<sub>FI2</sub>\* phase, which became more fluid and colourful in the SmC<sub>FI1</sub>\* phase. In the SmC<sub>A</sub>\* phase the *schlieren* texture was replaced with a network of blue domains.

Compounds of general structure **2** possess a large value of the spontaneous polarization, which in the antiferroelectric phase reached an apparent value of *ca.* 160 nC cm<sup>-2</sup> (compound **57**). This is about 30 % higher than corresponding value determined for members of the series **1**. The magnitude of the apparent tilt angle grew with reducing temperature and varied between 32 and 33 degrees for long-chain homologues.

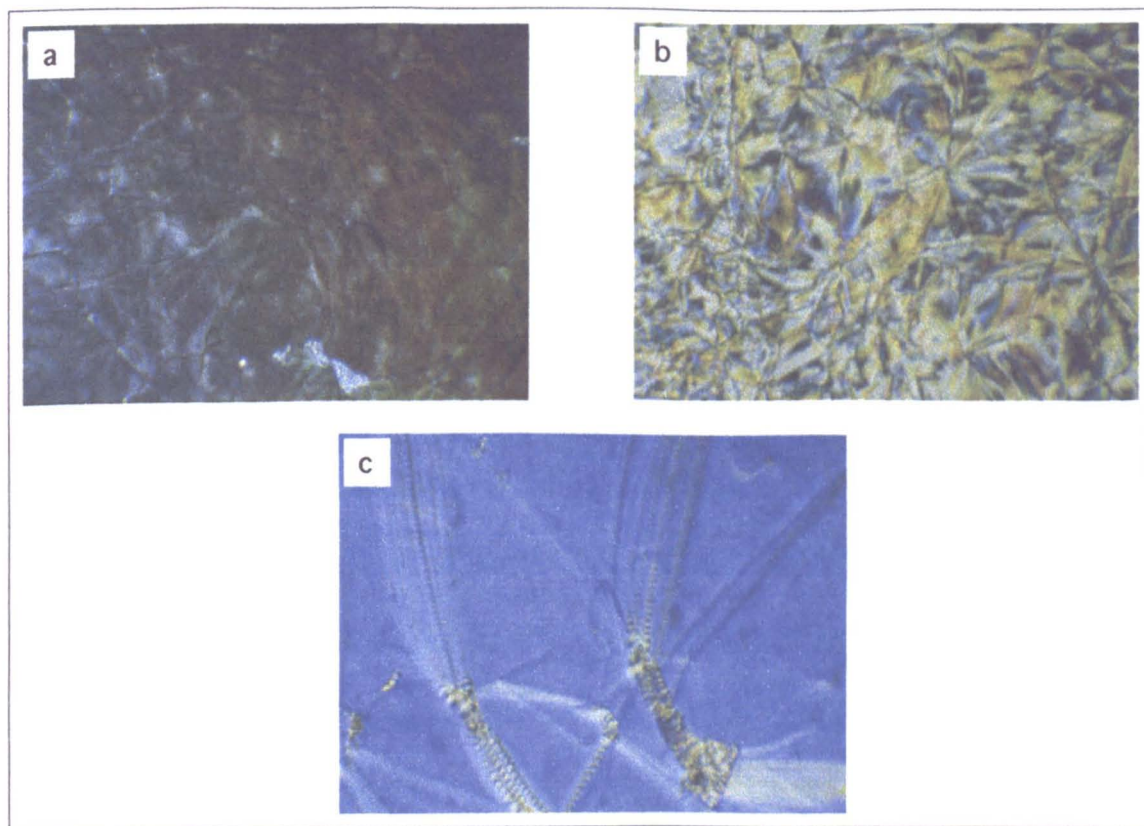
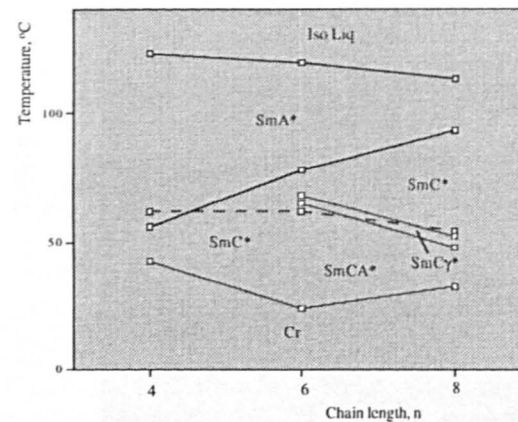
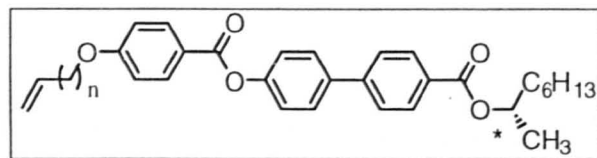


**Figure 4.8:** Textures for compound **58** a)  $\text{SmC}_{\text{F12}}^*$ , 70 °C; b)  $\text{SmC}_{\text{F11}}^*$ , 66 °C; c)  $\text{SmC}_{\text{A}}^*$ , 64 °C

### Summary:

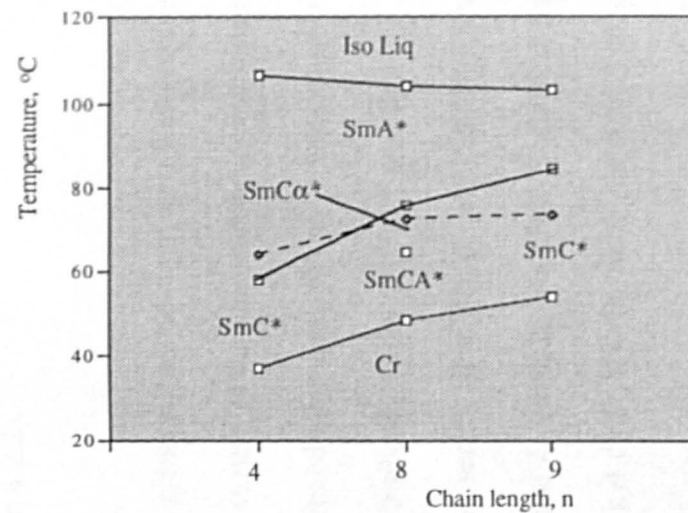
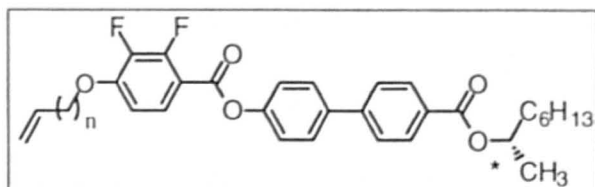
With two fluorine substituents introduced into molecular structure the stability of the antiferroelectric  $\text{SmC}_{\text{A}}^*$  phase was slightly improved. It became enantiotropic for even homologues of the series **2**, however the width of the phase interval remained unaffected and, as in series **1**, did not exceed 30 °C.

**Figure 4.9:** Characterization of mesomorphic behaviour of (*S*)-1-methylheptyl 4'-(4-*n*-alkenyloxybenzoyloxy) biphenyl-4-carboxylates, **61-63**, compounds of general structure **3**



No	n	T, °C / [ $\Delta H$ , kJ mol <sup>-1</sup> ]						
		Mp	SmC <sub>A</sub> *	Sm <sub>FII</sub> *	SmC*	SmA*	Iso	Cr
<b>61</b>	4	• 61.4 [16.2]	–	–	(•) 55.7 [-0.13]	• 123 [-4.6]	• 42.6	
<b>62</b>	6	• 61.5 [19.4]	• 64.8 [-]	• 67.6	• 77.9 [-0.11]	• 119.6 [-4.4]	• 23.7	
<b>63</b>	8	• 54.1 [33.1]	(• 47.7 [-0.014]	(•) 51.8 [-]	• 93.2 [-0.28]	• 113.4 [-4.8]	• 32.2 [-4.74]	

**Figure 4.10:** Characterisation of mesomorphic behaviour of (S)-1-methylheptyl 4'-(4-n-alkenyloxybenzoyloxy) biphenyl-4-carboxylates, **64-66**, compounds of general structure **4**



No	n	T, °C / [ $\Delta H$ , kJ mol <sup>-1</sup> ]								
		Mp	SmC <sub>A</sub> *	SmC <sub><math>\alpha</math></sub> *	SmC*	SmA*	Iso Liq	Cr		
<b>64</b>	4	• 64.1 [21.0]	-	-	(•) 58.0 [-0.14]	• 107 [-4.04]	• 107 [-4.04]	• 37 [-16.4]		
<b>65</b>	8	• 72.6 [35.5]	(•) 64.6 [-]	• 75.9 [-0.08]	-	• 104.1 [-4.40]	• 48.7 [-32.6]			
<b>66</b>	9	• 73.4 [31.6]	-	-	(•) 84.6 [-0.19]	• 103.5 [-4.42]	• 54.1 [-28.9]			

## 4.2 Introduction of the terminal double bond/siloxane unit into the non-chiral alkyl chain

### 4.2.1 Compounds of general structure 3, (*S*)-1-methylheptyl 4'-(4-alk- $\omega$ -enyloxy benzoyloxy)biphenyl-4-carboxylates 61-63, and general structure 4, (*S*)-1-methylheptyl 4'-(4-alk- $\omega$ -enyloxy-2,3-difluorobenzoyloxy) biphenyl-4-carboxylates 64-66

The stability of a particular type of smectic C\* sub-phase is believed to be driven by the interlayer correlation and its relative strength [8]. One of the ways to alter these interlayer interactions is to introduce a rich electron substituent at the terminus of the liquid crystalline molecule. In this way, one could achieve a complete domination of the synclitic ordering of the smectic layers over anticlinic ordering and *vice versa*.

The effect of a terminal double bond attached to the non-chiral alkyl chain of the parent structures **1** and the difluorobenzoate compounds of general structure **2** was first investigated in this work. The double bond was subsequently replaced with a silyloxy chain of different lengths (see section 4.2.2).

In both series of alkenes **3** and **4** the phase sequences appeared less diverse (see figures 9 and 10) in comparison to the wide variety of the smectic phases exhibited by the alkyl analogues. The presence of the terminal double bond did not appear to favour formation of the TGB and related frustrated sub-phases. Also, the SmI\* and SmC<sub>F1</sub>\* phases were not exhibited by these homologous series. The SmA\* and SmC\* phases followed similar trends to those in series **1** and **2**. Namely, the SmA\* phase thermal stability deteriorated with increase of the alkyl chain length while the SmC\* phase gradually became more stable.

In most cases, the antiferroelectric  $\text{SmC}_A^*$  phase was observed only during cooling cycles. The phase was preceded with the  $\text{SmC}_{FI}^*$  phase which prevented a direct  $\text{SmC}^*-\text{SmC}_A^*$  phase transition. For the difluorobenzoate compound **65** the  $\text{SmC}^*$  phase was replaced with a non-commensurate  $\text{SmC}_\alpha^*$  phase [9], which underwent a direct transition to a  $\text{SmC}_A^*$  phase without mediation of ferri phases. The structure of  $\text{SmC}_\alpha^*$  phase still needs to be clarified. As discussed in the introduction, this phase appears to exhibit ferroelectric properties at the higher temperatures and becomes antiferroelectric near the phase transition to the  $\text{SmC}_A^*$  phase.

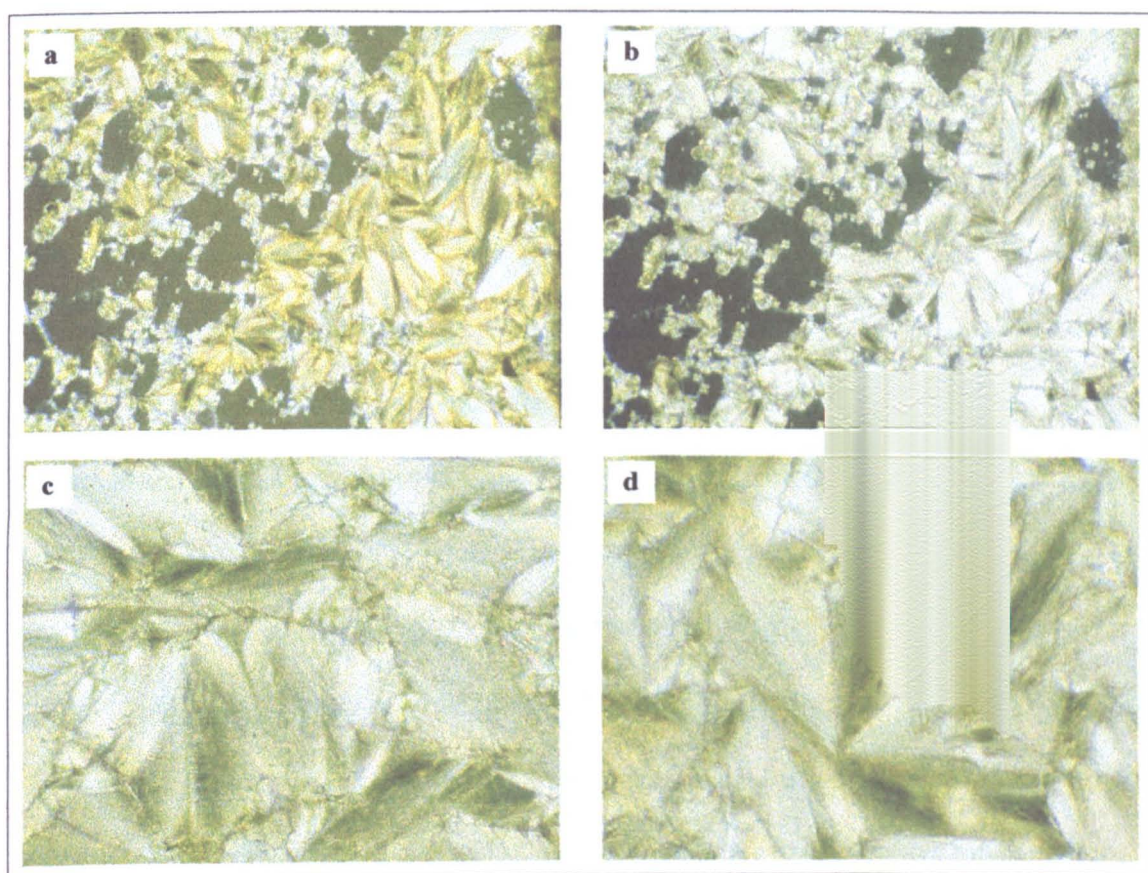


**Figure 4.11:** Textures of the smectic phases observed compound **65**. a)  $\text{SmC}_\alpha^*$ , 67 °C; b)  $\text{SmC}_A^*$  phase, 62.7 °C and for compound **63** c)  $\text{SmC}_{FI}^*$ , 47.9 °C; d)  $\text{SmC}_A^*$  phase, 45.2 °C

When observed in the polarizing microscope, the  $\text{SmC}_\alpha^*$  phase showed a characteristic pattern of the focal-conic fans [10], which was easily distinguished from the focal-

conics of the  $\text{SmC}^*$  phase (figure 4.11a) through an unusual bright-orange colour of the edges of the fans. In the  $\text{SmC}_A^*$  phase the colour disappeared giving rise to a focal-conic pattern which was similar to the texture of the antiferroelectric phase observed for compounds of general structure **1**, see figure 4.11b. In free-standing film preparations the *schlieren* texture of the  $\text{SmC}_A^*$  phase exhibited several two-brush defect that was clearly visible in the central parts of the film (compound **62**, figure 4.16). Appearance of the two-brush dispirations signifies the presence of alternating molecular tilt direction in the smectic layers and is regarded as a classical defect characteristically found in *schlieren* textures of the  $\text{SmC}_A^*$  phase [11].

The texture of the ferroelectric  $\text{SmC}_{\text{FII}}^*$  phase was also composed of focal-conic domains. As shown in the figure 4.11c, the broken fans of the smectic  $\text{C}^*$  phase became covered with narrow lines manifesting the transition to the  $\text{SmC}_{\text{FII}}^*$ . At the transition to the antiferroelectric phase the focal-conic defects appeared clearer due to the alternating layer structure giving an apparent director perpendicular to the layers (figure 4.11d).

Additional evidence for the properties of the ferroelectric and antiferroelectric of the  $\text{SmC}^*$  and  $\text{SmC}_A^*$  phases was obtained through the studies of the electrooptical response of compound **62**. In the smectic  $\text{C}^*$  phase the voltage function of transmittance had the shape of a hysteresis loop. The loop split into two smaller hystereses in the antiferroelectric smectic  $\text{C}_A^*$  phase indicating appearance of the third state during the field-induced switching. The antiferroelectric double hysteresis can be converted back into the single loop when the frequency of the applied field becomes too high and there is not enough time for relaxation to occur back to the antiferroelectric state.

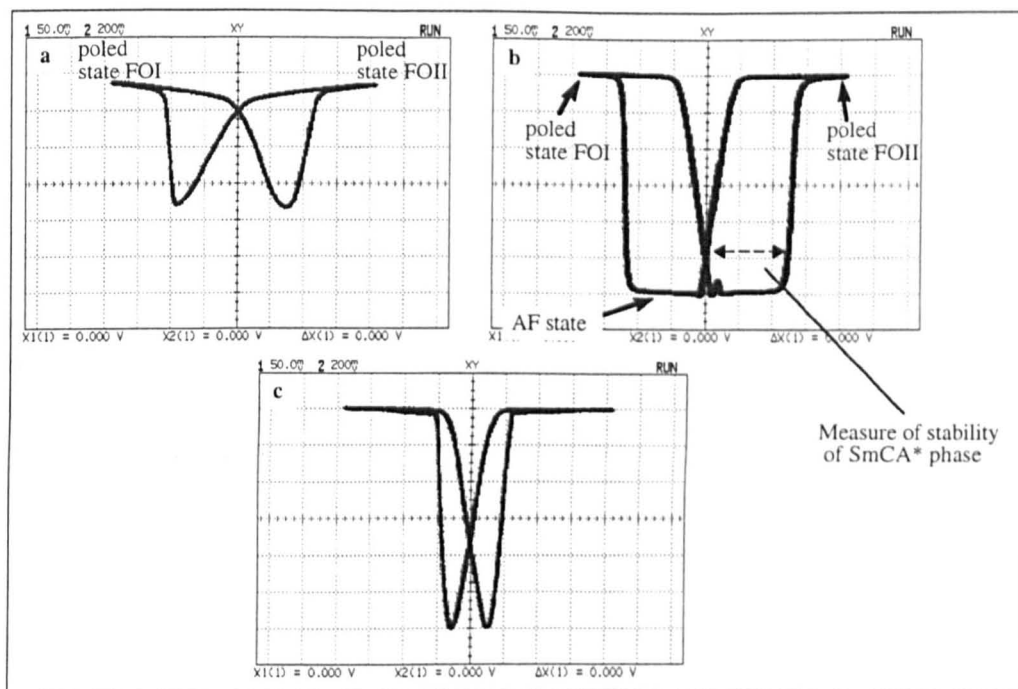


**Figure 4.12:** The voltage-optical transmittance curves recorded for compound **62**. (here and on the following diagrams the level of transmittance is shown along the y-axis) a) SmC\* phase, 88 °C, 2Hz, 2 VPP; b) SmC<sub>A</sub>\* phase, 44 °C, 20 mHz, 2VPP; d) SmC<sub>A</sub>\* phase, 44 °C, 2 Hz, 2VPP. The orientation of the cell was set such that the layer normal of the smectic C\* phase was parallel to the top polariser. As a result both ferroelectric states had a similar level of transmittance and the hysteresis loops appeared folded up into “W”-shaped curves.

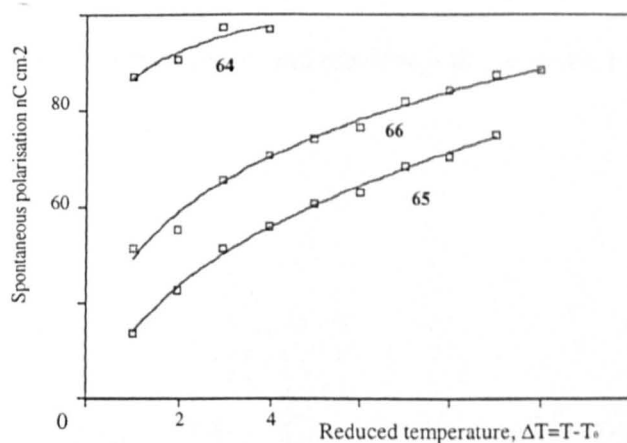


**Figure 4.13:** The spontaneous polarization of ferroelectric phase plotted as a function of the reduced temperature from the Curie point for compounds of general structure **4**, at 20 Hz, 2 VPP.

A more detailed discussion of the electrooptical behaviour of compound **62** can be found later in chapter 5.

The values of the spontaneous polarization for the alkene types **3** and **4** were estimated as being slightly lower than those determined for compounds **1** and **2**. The temperature dependency of the spontaneous polarization is described by the equation:

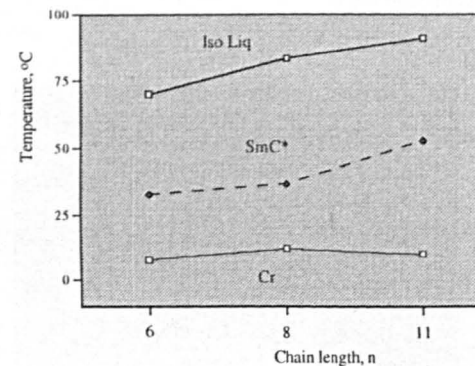
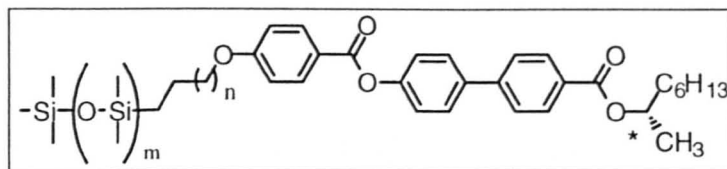
$$P_s(T) = P_{s_0}(T_c - T)^\alpha$$

with experimentally determined values of  $\alpha$  varying from 0.1 to 0.4 for different homologues, however, the values found are far smaller than the theoretically predicted value of 0.5 derived from Landau theory [12].

### **Summary:**

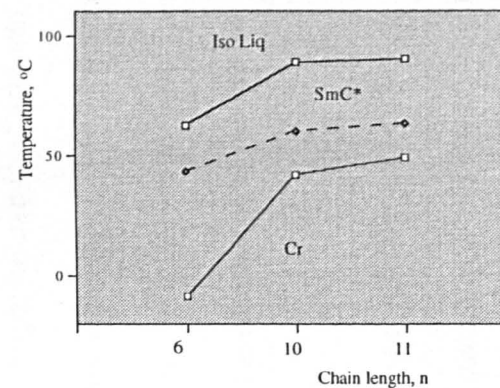
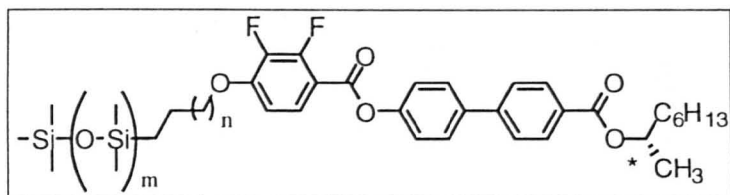
The alkenyl compounds of general structure **3** and **4** show both ferroelectric and antiferroelectric smectic C phases. The synclinic order of the smectic layers is more favourable than the anticlinic ordering. The  $\text{SmC}_A^*$  phase remains monotropic for the majority of the homologues. The liquid crystal polymorphism is greatly reduced as a result of the introduction of the terminal double bond (types **3** and **4**) into materials of general structure **1** and **2**. Furthermore, the tendency to form the frustrated and smectic hexagonal phases was suppressed.

**Figure 4.14:** Mesomorphic properties of (S)-1-methylheptyl 4'-[4-[ $\omega$ -(1,1,3,3,3-pentamethyldisiloxanyl)- or -( $\omega$ -1,1,3,3,5,5-heptamethyl)trisiloxanyl alkoxy]benzoyloxy]biphenyl-4-carboxylates, 67-71, compounds of general structure 5



No	n	m	Mp	C*	Iso Liq	Cr
<b>67</b>	4	2	• 32.7	• 50.9 [-3.1]	•	-4 [-7.3]
<b>68</b>	6	2	• 28.2 [14.4]	• 69.3 [-3.2]	•	6.3 [-11.6]
<b>69</b>	4	1	• 32.3 [20.9]	• 70.3 [-5.8]	•	7.7 [-14.6]
<b>70</b>	6	1	• 36.4 [17.8]	• 83.3 [-4.2]	•	12.2 [-11.5]
<b>71</b>	9	1	• 52.7 [41.8]	• 91.1 [-4.48]	•	9.9 [-18.9]

**Figure 4.15:** Mesomorphic properties of (S)-1-methylheptyl 4'-[4-[ω-(1,1,3,3,3-pentamethylsilyloxy)alkoxy-2,3-difluoro]benzoyloxy]biphenyl-4-carboxylates, **72-74**, compounds of general structure **6**



No	m	n	T, °C [ $\Delta H$ , KJ mol <sup>-1</sup> ]					
			Mp	SmC*	Iso Liq	Cr		
<b>72</b>	1	4	•	43.4 [33.2]	•	63.2 [-3.38]	•	-8.9 [-9.13]
<b>73</b>	1	8	•	60.3 [23.5]	•	88.7 [-3.37]	•	42.6 [-20.7]
<b>74</b>	1	9	•	63.5 [23.4]	•	90.4 [-2.45]	•	49.4 [-21.3]

**4.2.2** Compounds of general structure 5 *(S)-1-methylheptyl 4'-{4-[ $\omega$ -(1,1,3,3,3-pentamethylsilyloxy)alkoxy-2,3-difluoro]benzoyloxy}biphenyl-4-carboxylates* 67-71 and general structure 6 *(S)-1-methylheptyl 4'-{4-[ $\omega$ -(1,1,3,3,3-pentamethylsilyloxy)alkoxy-2,3-difluoro]benzoyloxy}biphenyl-4-carboxylates* 72-74

As described in the introduction, one way to control anticlinic versus synclinic ordering in the smectic C phase formed by bimesogen molecules is through the introduction of a siloxane chain as the bridging group. When the bridge contains an even number of siloxane units the synclinic smectic C phase is formed. Conversely, the chain with an odd number of silicon atoms stabilises the anticlinic ordering.

It was anticipated that a similar mechanism could be used to stabilise a derived type of ordering in the smectic C phase in monomesogen compounds which have a siloxane unit attached to the terminal position in the non-chiral chain. Several highly polar silicon-oxygen bonds are thus concentrated in one part of molecule which should make the molecular architecture that of a pseudo amphiphile with pronounced polar and non-polar parts separated by the alkyl chain. Thus, the siloxane chains of molecules in the neighbouring smectic layers might be expected to form polar aggregates at the layer interface. As a result, the molecules might be expected to be arranged in a bilayered structure. This ordering would be expected to have synclinic or anticlinic properties depending on the number of the siloxane units introduced.

To investigate the effect of the siloxane end-group on mesomorphic behaviour the terminal double bond of the structures **3** and **4** was substituted with di- and tri-siloxane chains yielding two new series **5** and **6** (figures 4.14 and 4.15). There were two major consequences of this structural modification. First, a significant depression in phase transition temperatures was observed for all of the homologues synthesised. The decrease in the isotropization temperature observed for the siloxane materials was as

much as 40 °C to 50 °C when compared to the alkenes and alkyl analogues respectively (see for example **69**, **63** and **52**). This large drop in transition temperatures is driven by the siloxane fragments that group together in the mesomorphic state and, therefore, increase the relative stability of a smectic C layered structure at low temperatures. It also facilitates a supercooling that in the case of 2,3-difluorobenzoate compound **72** extends over 52 °C reaching almost -10 °C before crystallisation/glassification sets in.

The second consequence of the inclusion of the siloxane chain in the molecular structure was that the phase sequences were reduced to possessing one liquid crystalline phase, which in all cases was the smectic C\* phase. Its stability remained unaffected by the length of either siloxane or alkyl chain unless the total number of atoms exceeded 14. In this case, an increase in both the clearing and melting points was observed.

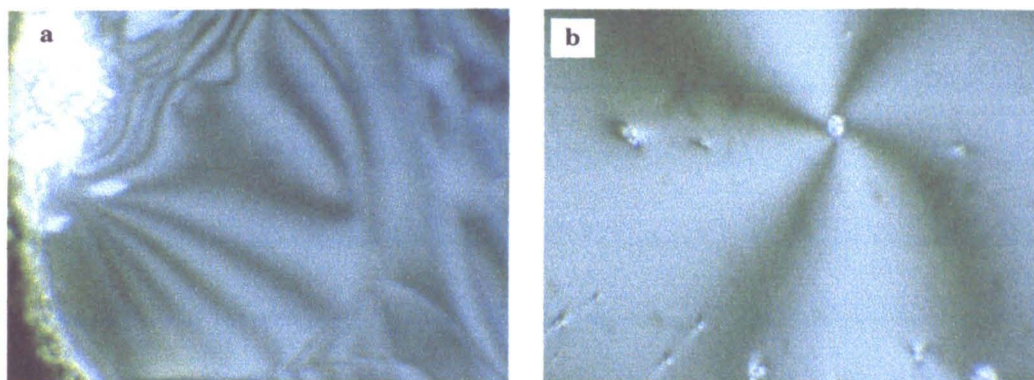


**Figure 4.16:** Two and four-brush defects observed in the *schlieren* textures: a) compound **62**, SmCA\* phase, 54.2 °C; b) compound **68**, SmC\* phase, 72.0 °C

The antiferroelectric phase was not found for any of the homologues in series **5** or **6**. The odd-even stability effect of the siloxane chain observed for the bimesogen materials seemed not to be applicable for the mono-substituted siloxane compounds, synclinic smectic C\* ordering was preferred for both odd and even numbers of the siloxane units in the chain.

The smectic C\* phase was identified with a help of a free-standing preparation. Only four-brush defects were found in the *schlieren* texture (figure 4.16b). Broken focal-conic domains were also observed in the samples prepared in thin electrooptical cells. In switching studies rather high magnitudes of the optical tilt angles in the smectic layers were found. The experimental measurements found that for all of the siloxane materials synthesised the tilt angle is ca. 45°.

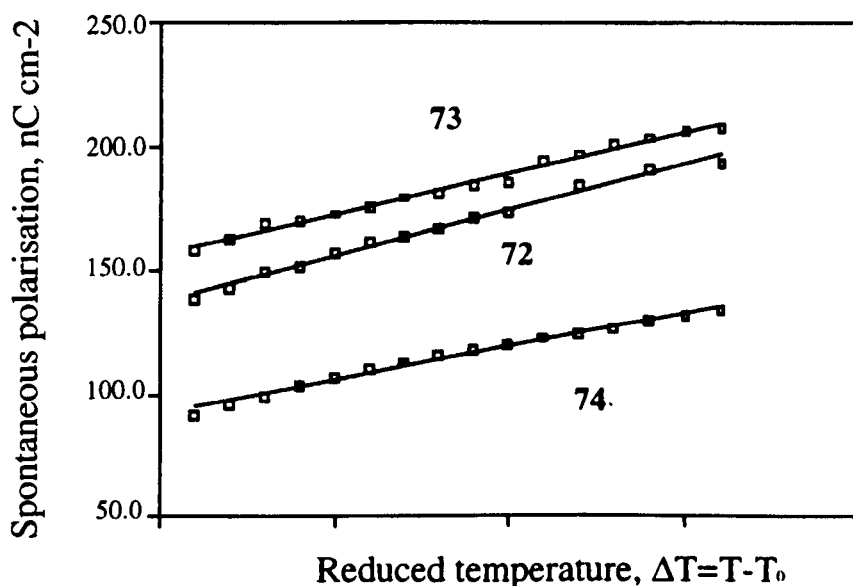


**Figure 4.17:** The spontaneous polarization plotted as a function of the reduced temperature from the Curie point for compounds of general structure 6. Applied field: 20 Hz, 2 VPP.

The spontaneous polarization was almost two times higher than the corresponding value in the alkene analogues and reached values over 200 nC cm<sup>-2</sup>. The magnitude of Ps undergoes a smooth growth with the decrease in temperature, see figure 4.17. Interestingly, the behaviour of the temperature dependency was linear and not quadratic with all three data sets fitted to a sample formula

$$Ps(T) = aT + b$$

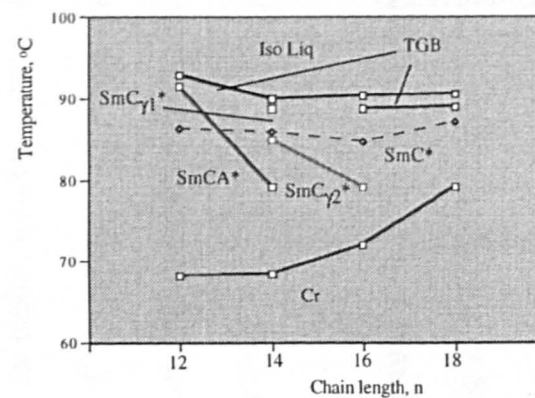
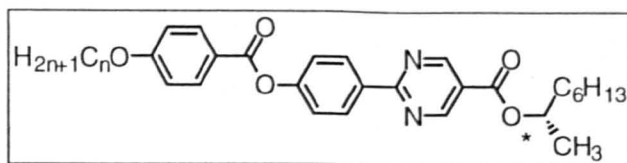
where the coefficient  $a$  is  $0.032 \pm 0.005$  and  $b$  is  $1.243 \pm 0.32$  (in absolute units).

As a result of the direct Iso Liq - SmC\* transition the spontaneous polarization varies discontinuously from zero to a finite value and remains constant over the whole temperature interval of the smectic C\* phase.

**Summary:**

The siloxane compounds of general structure **5** and **6** show a distinct tendency to form synclitic SmC\* phases. The stability of the phase remains unaffected with variation of the length of either siloxane or non-chiral alkyl chain. High values of the tilt angle and spontaneous polarization are likely to be a result of assembly of the siloxane fragments giving rise to improved molecular ordering in layers. The electrooptical effects, which originate from exceptionally high values of the tilt angle are described in chapter 5.

**Figure 4.18:** Mesomorphic properties of (*S*)-1-methylheptyl 2-[4-(4-alkoxybenzoyloxy)phenyl]pyrimidine-5-carboxylates, **75-79**, compounds of general structure **7**



No	n	T, °C / DH, kJ mol <sup>-1</sup>									
		Mp	SmC <sub>A</sub> *	SmC <sub>F11</sub> *	SmC <sub>F12</sub> *	SmC*	TGBC <sub>A</sub>	TGBC	BP	Iso Liq	Cr
<b>75</b>	10	• 110 [-]	-	-	-	-	-	-	-	-	• 110 [-]
<b>76</b>	12	• 86.4 [50.1]	• 91.6 [-0.22]	-	-	-	• 93.0 [0.87]	-	-	-	• 68.3 [28.8]
<b>77</b>	14	• 86.0 [43.3]	(• 79.3 [-0.01]	• 85.0 [-]	• 88.7 [-1.60]	-	-	• 90.0 [-]	• 90.4 [-]	• 68.5 [39.3]	
<b>78</b>	16	• 84.7 [43.7]	-	(• 79.2 [-0.03]	-	• 88.7 [-1.04]	-	• 90.4 [-]	-	• 72.1 [40.0]	
<b>79</b>	18	• 87.2 [46.4]	-	-	-	• 88.9 [-1.30]	-	• 90.5 [-]	-	• 87.2 [46.4]	

### 4.3 Modifications of the central part of the aromatic core

#### 4.3.1 Compounds of general structure 7: *(S)*-1-methylheptyl 2-[4-(4-alkoxybenzoyloxy)phenyl] pyrimidine-5-carboxylates 75-79

The structural modifications described in the previous sections were aimed at alternating the interlayer correlation in the smectic phase and to leave the lateral molecular interactions within each layer relatively unaffected. Furthermore, it was essential to investigate the role played by polar and steric interactions spreading laterally between molecules, and how these might stabilise the smectic C\* and smectic C<sub>A</sub>\* phases. As the fluorine atoms introduced at the outer phenyl ring of structures 2 did not produce any significant change of the mesomorphic behaviour, it was hypothesised that the strength of the lateral interactions associated with the fluorine atoms are mainly dependent on the structure of the central part of molecular core.

In order to develop the ideas of quadrupolar coupling further the phenyl ring in the biphenyl fragment of structures 1 was substituted with a pyrimidine cycle to increase the longitudinal component of molecular dipole. Resulting series of *(R)*-1-methylheptyl 2'-(4''-*n*-dodecyloxybenzoyloxyphenyl) pyrimidine-5-carboxylates, 7, thus represent a new family of aromatic heterocyclic compounds, which were found to exhibit a peculiar combination of the mesomorphic properties.

Across the homologue series the mesomorphic behaviour changed dramatically. The C<sub>10</sub> homologue 75 did not exhibit liquid crystalline properties at all, whereas the C<sub>12</sub> homologue 76 showed a broad antiferroelectric SmC<sub>A</sub>\* phase. A TGB phase was discovered at the transition of the antiferroelectric smectic phase to the isotropic liquid. This material was the subject of the detailed studies, which are reported separately in a chapter 5. The temperature interval of the SmC<sub>A</sub>\* phase became shorter with elongation

of the alkyl chain and for the C16 homologue **78** it was absent. Conversely, the stability of the smectic C\* phase underwent an opposite trend; the phase was most stable for the members with longer alkoxy chains. In the intermediate region of the diagram in figure 4.18 (compounds **77** and **78**) ferrielectric smectic sub-phases were found either above the SmC<sub>A</sub>\* or below the SmC\* phase on cooling. Consequently, there was no compound in the series that exhibited both synclinic and anticlinic smectic C\* phases. The stability of one type of the smectic layer ordering over another (synclinic or anticlinic) could be simply controlled by the length of the non-chiral alkyl chain. Ferrielectric frustrated phases were stabilised for the C14 and C16 homologues, in the manner similar to the mechanism proposed for the temperature induced SmC\*-SmC<sub>A</sub>\* transition [13]. The medium chain length is favourable for the formation of both SmC\* and SmC<sub>A</sub>\* phases over the same temperature interval. The only energetically allowed solution of the co-existence of both synclinic and anticlinic ordering in smectic layers is thus realised through the introduction of frustrated ferrielectric structures.

Presence of the rich electron 2-phenylpyrimidine ring system in the core of the structures of materials in series **7** destabilises the orthogonal SmA\* phase and, instead, favours the formation of various TGB phases at the high temperature region of the phase sequences. In most cases, the type of the TGB phase observed was determined by the smectic phase lying at lower temperature. Thus, the antiferroelectric TGBC<sub>A</sub>\* phase was observed for compound **76** above the SmC<sub>A</sub>\* phase. The next homologue in the series, compound **77**, exhibited a TGBC\* phase over a short temperature range, even though the low temperature phase was of the ferrielectric type. It is likely that a 3-layer periodicity of the ferrielectric I phase was not compatible with the TGB helix and, as a result, a homogeneous direction of the molecular tilt was forced to occur within the

smectic blocks. The TGBC phase was also observed for the other longer chain homologues **78** and **79**.

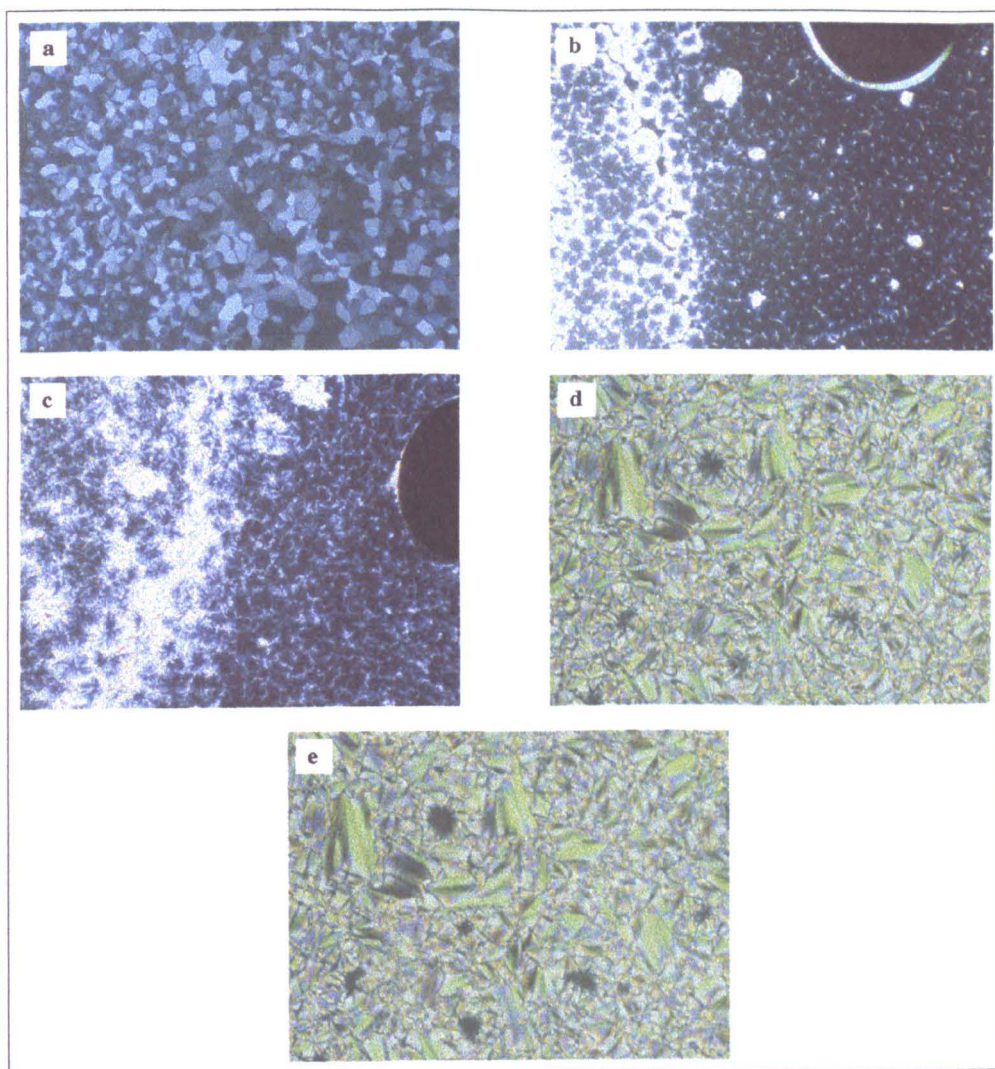


**Figure 4.19:** The textures observed for compound **77**: a) BP, 90.2 °C; b) TGBC phase, 90 °C; c) SmC<sub>FI2</sub>\* phase, 88 °C; d) SmC<sub>FI1</sub>\* phase, 85.0 °C; e) SmC<sub>A</sub>\* phase, 79 °C. (the photographs were taken from different areas of the sample preparation for clarification of the textural appearances)

The blue phases were another type of chirality-induced frustrated phases stabilised by materials of general structure **7**. The phase was observed for compound **77** above the TGBC phase on heating. As the chiral nematic phase was not present in the phase sequence, a direct BP-TGB phase transition took place thereby raising speculation that

the smectic ordering may be retained in the double twist cylinder of the blue phase, i.e. a layered blue phase (see section 3.3.2 for more discussion on the layered blue phases). The blue phase exhibited a typical mosaic texture (figure 4.19a). At the transition to the TGBC phase the highly birefringent domains were observed growing at the air-liquid crystal interface. The mosaics disappeared giving rise to a black homeotropic texture, which transformed into a very fluid *schlieren* texture in the  $\text{SmC}_{\text{F12}}^*$  phase (figure 4.19b and c). In the focal-conic region the  $\text{SmC}_{\text{F11}}^*$  phase was easily recognised via its strip fans texture which was very similar to the texture of the  $\text{SmC}_{\text{F11}}^*$  phase observed for compound **63**. With decreasing temperature the lines vanished and the typical focal-conic texture of the antiferroelectric  $\text{SmC}_{\text{A}}^*$  phase was formed (figure 4.19e).

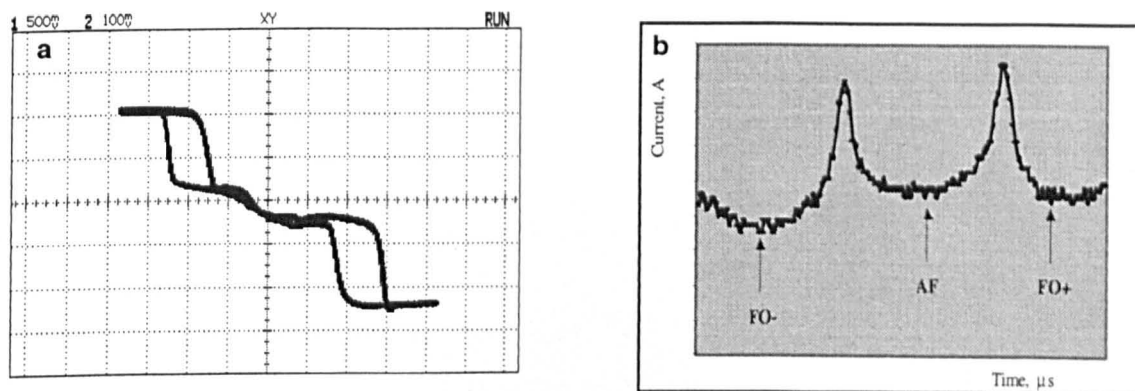


**Figure 4.20:** The electrooptic behaviour of the compounds of general structure **5**: a) compound **77** – the voltage-transmittance curve in the  $\text{SmC}_{\text{A}}^*$  phase (78 °C), applied field: 1 Hz, 1 VPP; b) compound **76** – the current-time trace recorder in the  $\text{SmC}_{\text{A}}^*$  phase (88 °C), applied field: 10 Hz, 2 VPP

Tristate switching in the antiferroelectric  $\text{SmC}_{\text{A}}^*$  phase of compounds **76** and **77** was fully characterised through triangular wave electric field studies. In current-time traces the spontaneous polarization was composed of two broad peaks (see figure 4.20b) corresponding to switching between the ferroelectric and the antiferroelectric states. The

electrooptic response was typical for tristate switching with a double hysteresis loop being observed for a wide range of frequencies (figure 4.20a).

**Summary:**

Introduction of the pyrimidine heterocyclic ring into the aromatic core of the parent structures **1** favoured a rich liquid-crystalline polymorphism including different types of the frustrated phases. The antiferroelectric and ferroelectric phases were found at the opposite ends of the homologue series with ferroelectric sub-phases being dominant for the intermediate members of the series.

**4.3.2** Compounds of general structure 8: *(S)*-1-methylheptyl 4'-(4-alkoxybenzoyloxy)-2',3'-difluorobiphenyl-4-carboxylates 80-84 and general structure 9 *(S)*-1-methylheptyl 2-[4-(4-alkoxybenzoyloxy)-2,3-difluoro phenyl] pyrimidine-5-carboxylates 85-88

An effective means of stabilising either synclinic or anticlinic ordering in the smectic C\* phase was found when two lateral fluorine substituents were introduced into the central part of the aromatic core. Two new series **8** and **9** were derived from the compounds of general structure **1** and **7** when fluorine substituents were attached to the adjacent ortho-positions in the biphenyl and 2-phenylpyrimidine units respectively (figures 4.22 and 4.23). This study allowed us to compare two systems where one had essentially strong lateral dipoles with another, which had both longitudinal as well as lateral dipoles, thereby allowing the effect of dipolar and quadrupolar coupling on synclinic or anticlinic ordering to be studied.

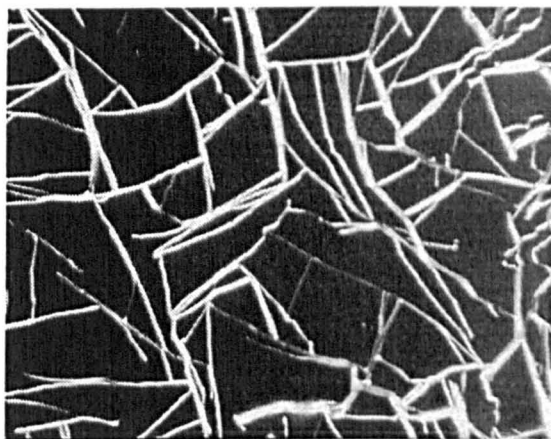
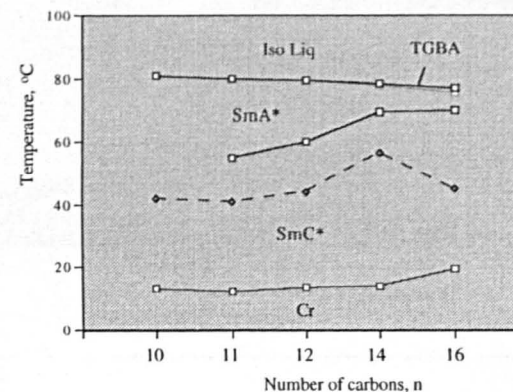
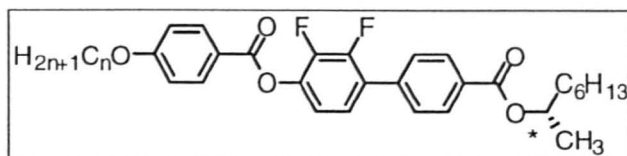


**Figure 4.21:** The texture of the TGBA phase observed for compound **84** at 76.8 °C

Each series favoured a particular type of the smectic C phase. Series **8** showed a broad smectic C\* phase with only the SmA\* phase appearing at the higher temperatures. For long alkyl chains (starting from compound **82**) the TGBA\* phase was stable over short temperature interval manifesting an increasing tendency of the molecules to form a

Figure 4.22: Mesomorphic properties of (S)-1-methylheptyl 4'-(4-alkoxybenzoyloxy)-2',3'-difluorobiphenyl-4-carboxylates, **80-84**, compounds of

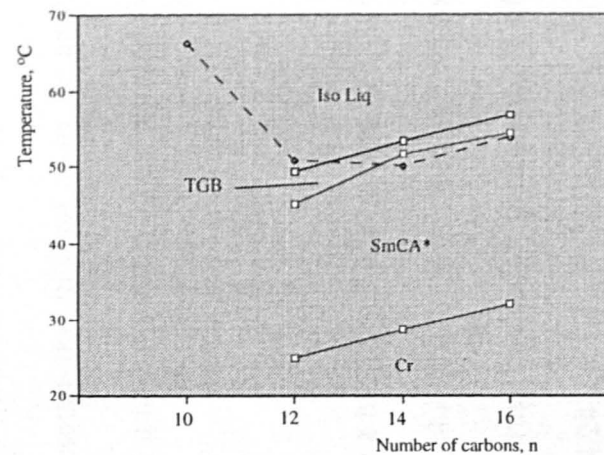
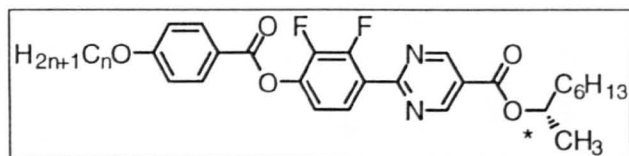
general structure **8**



No	n	T, °C / [ $\Delta H$ , kJ mol <sup>-1</sup> ]								
		Mp	SmC*	SmA*	TGB	Iso Liq	Cr			
<b>80</b>	10	42	—	•	81	—	•	13.1		
		[59.2]			[-11.2]			[-38.3]		
<b>81</b>	11	41.2	•	54.8	•	79.8	—	•	12.4	
		[56.5]		[-]	[-9.6]			[-22.7]		
<b>82</b>	12	43.9	•	59.8	•	79.5	•	79.7	•	13.9
		[49.5]		[-0.45]	[-]		[-11.3]		[-50.1]	
<b>83</b>	14	56.4	•	69.2	•	78.1	•	78.6	•	14
		[82.9]		[-0.16]	[-]		[-11.2]		[-50.8]	
<b>84</b>	16	45.1	•	69.8	•	75.6	•	77.0	•	19.5
		[78.4]		[-0.24]	[-]		[-10.5]		[-60.3]	

**Figure 4.23:** Mesomorphic properties of (*S*)-1-methylheptyl 2-[4-(4-alkoxybenzoyloxy)-2,3-difluorophenyl] pyrimidine-5-carboxyates, **85-88**,

compounds of general structure **9**



No	n	T, °C / [ΔH, kJ mol <sup>-1</sup> ]					
		Mp	SmC <sub>A</sub> *	BP	Iso Liq	Cr	
<b>85</b>	10	66.2 [56.7]	-	-	•		
<b>86</b>	12	50.9 [67.1]	(•	45.4 [-0.55]	•)	47 [-]	~25 [-]
<b>87</b>	14	50.1 [43.5]	(•)	48.2 [-]	•	53.3 [-]	28.7 [-47.1]
<b>88</b>	16	53.8 [65.0]	•	54.4 [-]	•	57.0 [-]	32.2 [-31.8]

cholesteric-like helix. The temperature range of the phase became broader when the alkyl chain was elongated. For compound **84** the temperature range of the TGB phase was wide enough for the typical filamentary pattern to be observed in the microscope, see figure 4.21. The filaments disappeared in the SmA\* phase giving rise to an optically extinct homeotropic texture.

The ferroelectric smectic C\* phase was stable over broad temperatures for all of the members in the series **8** with the temperature range of the phase extending to below room temperature as a result of the supercooling. Despite presence of the fluorine substitutes, which are known to decrease transition temperatures, the melting points in the series **8** were similar to those found for series **1**.

*(S)*-1-methylheptyl 2-[4-(4-alkoxybenzoyloxy)-2,3-difluorophenyl] pyrimidine-5-carboxylates, **9** exhibit the antiferroelectric SmC<sub>A</sub>\* phase but no ferroelectric phases were found. In the absence of any of the other smectic C\* phases the SmC<sub>A</sub>\* phase remains stable over 20 °C. It should be noted, that in most cases the antiferroelectric phase is monotropic and its stability at ambient temperatures resulted from a large supercooling.

Apart from the SmC<sub>A</sub>\* phase there were a number of blue phases, which existed over unusually wide temperature ranges. The blue phases were observed on cooling in the DSC, with the thermographs showing small enthalpy peaks for all of the liquid crystalline members of the series (figure 4.24).

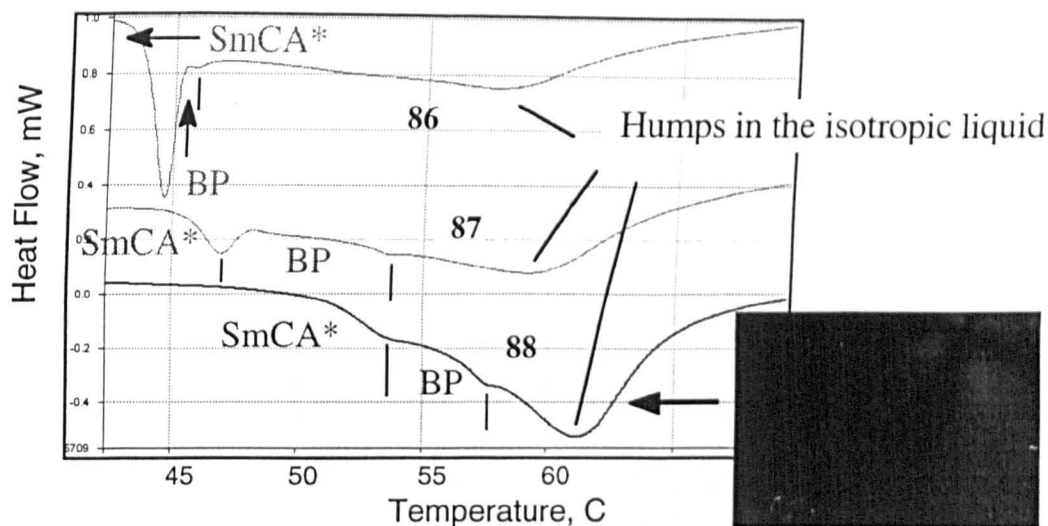


**Figure 4.24:** DSC cooling traces recorded for compounds of general structure **9**<sup>20</sup>. The scan rate: 10 °min<sup>-1</sup>.

Although a broad peak for this transition was observed in the DSC, it is not clear if the peak corresponds to a real phase transition or represents a partial, chirality-induced ordering in the isotropic liquid. Nevertheless, when observed in the optical microscope, uncovered droplets of compound **88** exhibited four-brush defects in the vicinity of the transition to the mesomorphic state (figure 4.24). The defects were not involved in any movement and disappeared when the transition to the blue phase occurred.

A remarkable feature of the blue phase of compounds of general structure **9** is that it is not followed on cooling by a chiral nematic phase. In this respect, it is similar to the blue phase found for compound **77** (section 3.3.5) that underwent a direct transition to the TGBC phase. The absence of a chiral nematic phase before the transition into the layered phases implies that the structure of the blue phase may also have a quasy-layered ordering. Thus, we can speculate on existence of the smectic-like blue phases, which should feature blocks of the smectic layers involved in a double twist cylinder

<sup>20</sup> The photomicrograph in figure 4.24 shows the appearance of a sample of compound **88** in the isotropic liquid at the vicinity to the phase transition to the mesomorphic state.

structuring. It was also interesting to speculate that blue phases of the compounds of general structure **9** would also have an anticlinic arrangement of the molecules within proposed layers.

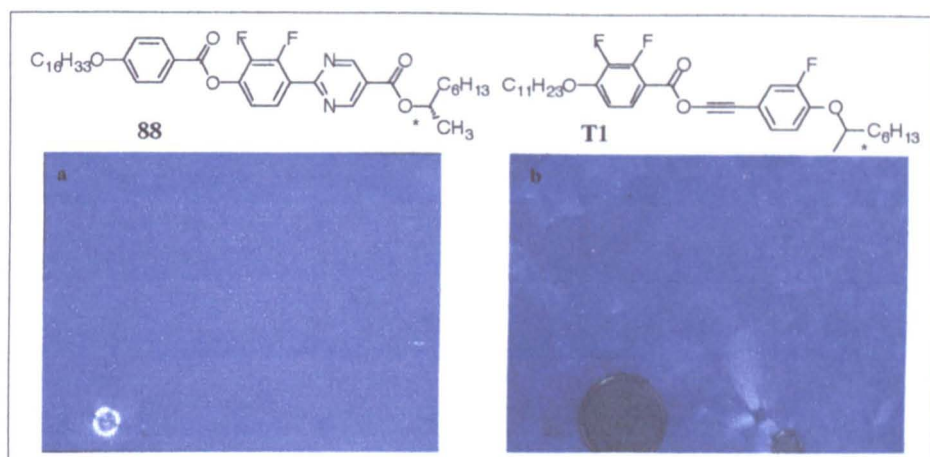


**Figure 4.25:** Textures of the blue phases a) compound **88** a) 55.7 °C; b) compound (R)-4-[3-fluoro-4-(1-methylheptyloxy)phenylethynyl]-phenyl 2,3-difluoro-4-undecyloxy benzoate, **T1**, 112.0 °C

In order to provide a reference source for typical textures of the blue phase, compound 4-[3-fluoro-4-(1-methylheptyloxy)phenylethynyl]-phenyl 2,3-difluoro-4-undecyloxy benzoate **T1** was synthesised according to the methods described in ref 14. A rich sequence of the frustrated phases exhibited by this compound included blue phase and two types of the TGB phases: TGBA and TGBC. In figure 4.25, the texture of the blue phase of tolane **T1** is compared to the blue phase of **88**. It can be seen clearly that a mosaic pattern is only visible in the texture of **T1**. A defect-free texture of the blue phase in the photomicrograph on the left indicates that the phase structure is unique and different from the conventional “nematic-like” blue phase.

### Summary :

It was shown that stability of the ferroelectric and antiferroelectric smectic C\* phases may be controlled *via* structural design of the aromatic core. In series **8** the difluorobiphenyl unit favours the SmC\* phase, which becomes stable upon transition

correlation lengths present so that the interlayer correlation  $\xi_{\parallel}$  (see figure 5.3) is only spread over several layers. As a consequence, there is no long-range interaction, which could keep the direction of the molecular tilt uniform from layer to layer in the presence of an external force that induces randomisation [7].

The driving force for such “randomisation” may be provided by weak cell surface interactions. If the surface polar interactions are only strong enough to keep the molecules in a planar orientation (i.e. a homogeneous cell where the alignment layer consists of a relatively non-polar polymer) the molecules may tilt randomly in the plane to the right or left. The size of the opposite tilt domains is assumed to be smaller than wavelength of visible light. Therefore, the random state appears uniform when observed in a polarizing microscope [7].

The effect of the surfaces was thoroughly investigated in the recent studies of the two-component Mitsui mixture [8] (figure 5.4).

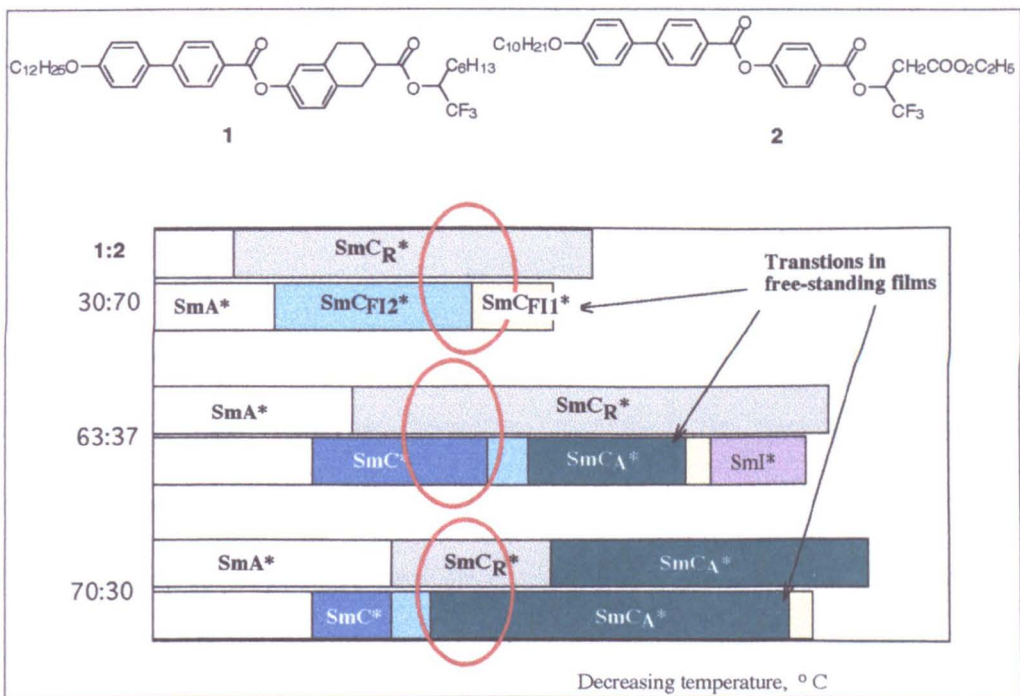


**Figure 5.4:** The components of the Mitsui mixture and transition temperatures found in a free-standing film and in a planar thin cell.

from the orthogonal SmA\* phase and exists until recrystallisation takes place. In turn, the antiferroelectric phase is stabilised by the 2-phenylpyrimidine core of series **9** with all of the other modifications of the smectic C\* phase having been suppressed.

### 4.3.3 References (section 4)

1. JW Goodby, personal communications
2. MA Anisiomov, VP Voronov, AO Kulkov, F Kholmurodov, *J Phys (France)*, 1985, **46**, 2157
3. J Thoen in "Phase Transitions in Liquid Crystals" ed. S Martellucci and AN Chester, New York: Plenum, 1992
4. GW Gray and JW Goodby, "Smectic liquid crystals: Textures and Structures", Philadelphia: Leonard Hill, 1984
5. K Miyasto, S Abe, H Takazoe, A Fukuda and E Kuze, *Jpn J Appl Phys*, 1983, **22**, L661
6. A Fukuda in "Handbook of Liquid Crystals", ed D Demus, J Goodby, GW Gray, H-W Spiess, V Vill, Wiley-VCH, 1998, Vol 2B
7. JW Goodby, SJ Patel and E Chin, *J Mat Chem*, 1992, **2**, 197
8. T Matsumoto, A Fukuda, M Johno, Y Motoyama, T Yui, S Seomun and M Yamashita, *J Mat Chem*, 1999, **9**, 2051
9. K Hiraoka, A Taguchi, Y Ouchi, H Takazoe, A Fukuda, *Jpn J Appl Phys*, 1990, **29**, L103
10. L Seung-Eun, PhD Thesis, the University of Hull, 1998
11. Y Takanishi, H Takazoe, A Fukuda, H Komura and J Watanabe, *J Mater Chem*, 1992, **1**, 71
12. JW Goodby in *Ferroelectric Liquid Crystals* ed. JW Goodby et al. 1991, Gordon and Breach Science Publishers p 194
13. A Fukuda and T Matsumoto, *Mol Cryst Liq Cryst*, 1999, **328**, 1
14. HT Nguyen, A Bouchta, L Navailles, P Barois, N Isaert, RJ Twieg, A Maaroufi, C Destrade, *J Phys II (France)*, 1992, **2**, 1889

## **5 V-shaped electrooptical response in the smectic C\* phase**

### **5.1 Theoretical description of the problem**

Tristate switching in liquid crystals under the application of an AC electric field as discussed in previous chapter, appears to be a unique property of the antiferroelectric smectic C phase. Its technological potential was realised in the creation of a new type of the display device [1]. For this device to become of commercial importance, however, there is a need of improvement in its switching characteristics. In particular, the presence of pretransitional effects [2] and poor alignment of materials in the cell substantially reduces the contrast and transmission of the “off” and “on” states and, consequently, there is often poor device performance.

Extensive studies on the physical properties of antiferroelectric materials, as well as the fast-growing number of new compounds being prepared over the last decade, have resulted in the discovery of some rather promising effects in antiferroelectric systems which have accelerated the commercialisation process of tristate liquid crystal devices [3, 4].

One effect studied was the V-shape electrooptical response, which was observed in 1996 by Japanese scientists [5]. In these studies a mixture of three liquid crystal materials (figure 5.1) was placed to a thin cell with planar surface alignment. The cell was placed between crossed polarizers with the lower polarizer set parallel to the smectic layer normal. Under the application of an electric field the optical response observed over a broad temperature range was hysteresis-free with a sharp change of transmission. The switching which produced such a V-shape response was designated as a thresholdless antiferroelectric response.

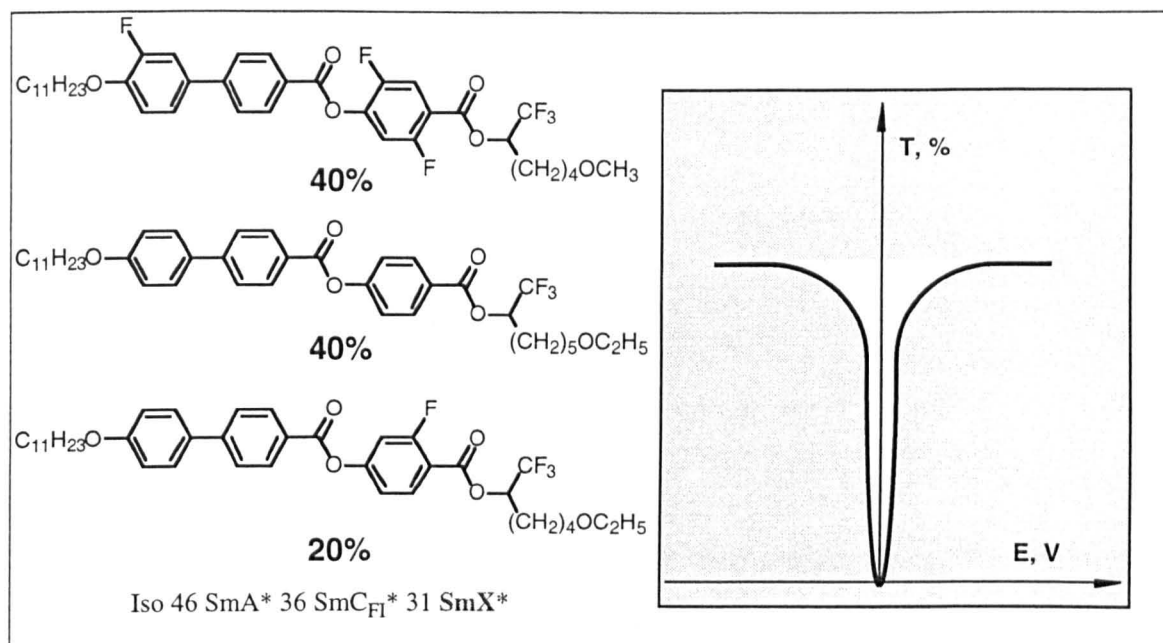


**Figure 5.1** Chemical structures and concentration (in weight percent) of the components in the Tokyo mixture, which exhibits a V-shape optical response

The V-shaped descriptor is possibly more controversial than the oxymoron “liquid crystals”. Nevertheless, as well as the latter perfectly describes properties of the mesomorphic state, the former is the most appropriate term for V-shape switching, provided that the phase is indeed antiferroelectric. The main characteristics of V-shape switching are:

1. The presence of a third state during the dynamic switching in a planar oriented thin cell. The state occurs at zero field and when the cell is placed between crossed polarisers with the lower polarizer being parallel to the layer normal almost complete extinction of light can be achieved (figure 5.1).
2. The absence of a hysteresis loop and a narrow shape of V indicates that switching between third state and uniform ferroelectric states is thresholdless.

V-shape switching appears to be an extremely attractive effect, which can produce grey-scale with high contrast. Such a device has been manufactured by Casio [1] even though

there is still no complete understanding of the molecular processes at the heart of the phenomenon. It remains a subject of a major scientific discussion – in what state is the liquid crystal at the very tip of V.

In order to explain the molecular dynamics during thresholdless switching it was first assumed that switching from one ferroelectric uniform state to another involves passage through a third state, which is different from the conventional antiferroelectric state where the molecules tilt in opposite directions in adjacent layers [4]. Instead, it was believed that a random distribution of the molecular azimuthal angle on passing from one layer to the next might be preferred at zero electric field. In other words, at zero volts there may be a new type of a smectic tilted phase which would have a Langevin response [5] to an external electric field. At any finite value of the applied field the random structure becomes unstable due to  $\mathbf{Ps}\cdot\mathbf{E}$  coupling and a thresholdless reorientation of the molecules in all of the layers occurs, resulting in a transition to the either of the switched ferroelectric states (figure 5.2).

The main disagreement with this “random” model is the fact that in experiments the phase which was found to exhibit V-shape switching also was found to be strongly chiral with a helix of short pitch [6]. It is unlikely that a strongly helical phase has a random distribution of the azimuthal angle in neighbouring layers. Nevertheless, it was also found that in some temperature regions the pitch of the helix diverges and sometimes to very large values. It can be argued that for these temperatures there is a large anisotropy of the molecular

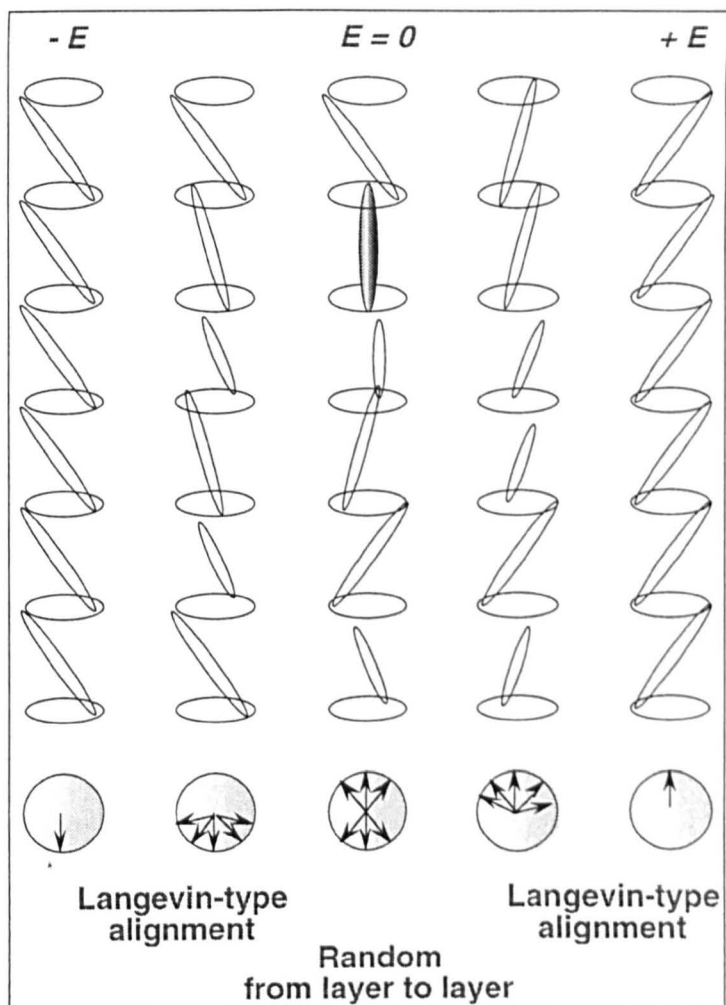


**Figure 5.2** The structure of the “random” smectic C phase shown at zero field.

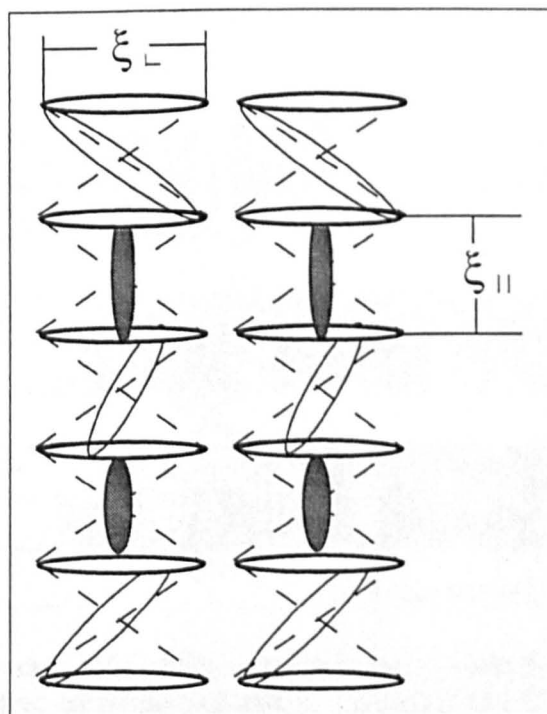


**Figure 5.3** Schematic representation of inter- and intra layer correlation lengths.

Compounds **1** and **2** were mixed in different proportions and the mesomorphic behaviour in various regions of the phase diagram was examined by two different techniques. When the mixture samples were spread in a free-standing film, experiments using conoscopy under the application of an electric field detected six tilted phases including  $\text{SmC}_A^*$ ,  $\text{SmC}^*$ ,  $\text{SmC}_{\text{FI}}^*$  and  $\text{SmI}^*$  phases. On the other hand, in the thin planar cell only two phases could be distinguished judging by textural appearances. In one of them designated a  $\text{SmC}_R^*$  phase V-shape switching was observed over a wide range of frequencies under the application of a triangular field. As shown in figure 5.4, a V-shaped response occurs in temperature region circled by the red line. Remarkably, in all three mixtures in figure 5.4 this region lies in the vicinity of a phase transition to the ferrielectric sub-phases, which were found in free-standing films.

The existence of the intermediary ferrielectric structures at the transition from the ferroelectric phase to the antiferroelectric phase is believed to result from the energy competition between synclinic and anticlinic ordering (see section 1.2) [9]. At certain temperatures both organisations are energetically possible, thereby producing a frustrated ferrielectric structure. Near to the transition from the ferroelectric phase to the ferrielectric phase the correlations between the smectic layers are thought to be substantially weakened. As a consequence, the molecules may tilt to the right or left<sup>21</sup> when sandwiched between two substrates resulting in the formation of the microsize domains, as mentioned previously. Transmission of plane-polarized light through such a structure would be at a fairly low level. Thus, the V-shape optical response to the electric field occurs naturally, as there is no threshold for a field driven transition to a bright uniform ferroelectric state.

---

<sup>21</sup> This description of the ferrielectric phases relies on the Ising model discussed in the section. The model only allows discontinuous variation of the azimuthal angle from 0 to  $\pi$  excluding the possibilities of any other tilt direction but to the right or left.

When moving to the left from the red circle area shown in figure 5.4 the V-shape curve is replaced by a W-shape ferroelectric response as a result of an increased stability of the smectic C phase. On the other side of the circle, at the transition from the ferrielectric phase to the antiferroelectric phase a double hysteresis loop response dominates. Thus, V-shape switching can only be realised in the small temperature region around the ferrielectric phases where the interlayer correlation is significantly weakened.

In general, a characteristic of the optical response curve is greatly affected by the temperature and the frequency of the applied electric field [10]. A temperature decrease tends to stabilise a V-shape curve and also lower the level of transmission in the field off state. In similar fashion, a W hysteresis can be avoided at low frequencies though some anomalies are observed when the frequency is too low. This will be discussed in more detail in the results section of this chapter.

In the discussion of the “random” model, recent electrooptical studies on the switching dynamics in surface-stabilised cell [11] are worth mentioning. Experimental results show that the molecules move in a collective fashion from a uniform switched state to the dark zero-field state during the V-shaped switching. It is apparent that collective molecular motion excludes any possibilities for randomisation of the phase structure. Nevertheless, the random phase model still remains workable assuming that the molecular rearrangement during the switching will only occur in the domains where the spontaneous polarization opposes the direction of the electric field. The other half of the domains will remain unchanged, so the collective motion of the molecules is not in contradiction with the proposed domain structure. Still, such a phase has not been yet confirmed experimentally at any temperatures in Tokyo or Mitsui mixtures.

It was originally assumed that the phase exhibiting a V-shape optical response is of the antiferroelectric type. Indeed, a hysteresis-free response was observed independently in the antiferroelectric smectic  $C^*$  phase exhibited by individual liquid crystalline compounds [12]. Detailed studies were reported on frequency induced transformations of double hysteresis loops into single V-shaped switching curves [13].

The SmX phase of the Tokyo mixture, see figure 5.1, however, was recently shown to be a ferroelectric smectic  $C^*$  phase [14]. This raised the speculation that the V-shape response is a property of dynamical processes occurring during the switching under the application of an applied electric field in surface-stabilized ferroelectric cells.

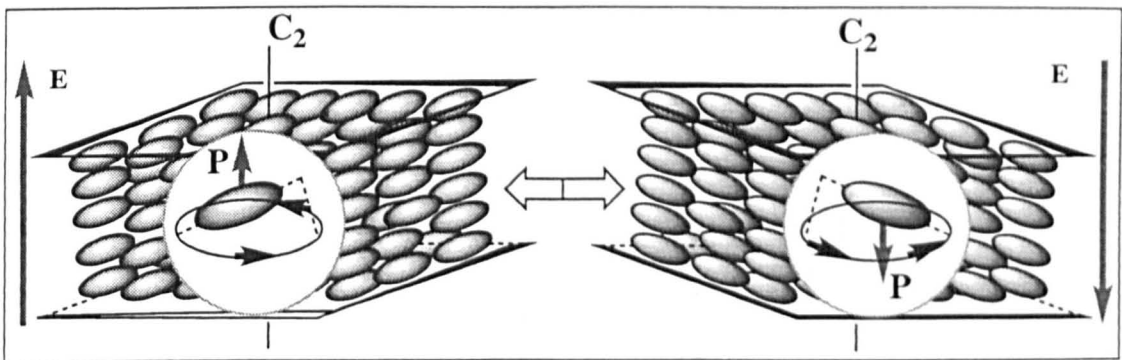


**Figure 5.5:** Molecular reorientation under the application of an electric field in the geometry of the surface-stabilised smectic  $C^*$  phase.

In a surface stabilised geometry the molecules in the smectic layers are oriented parallel to the substrates and may adopt one of the uniform tilted orientations (figure 5.5), with the layer polarizations pointing in the same direction either up or down. Switching the field to another direction will cause a molecular reorientation to the opposite tilted state and a reversal of the polarization. Placed between crossed polarisers with the optic axis in one state being parallel to the plane of incoming light the cell gives no transmission. The intensity of light passing through the analyser when the molecules are switched to the other state is described by the equation [15]:

$$I = I_0 \sin^2 2\theta \sin^2 \frac{\pi d \Delta n}{\lambda} \quad (1)$$

where  $\theta$  is an angle between the modulator optic axis and the plane of incoming light,  $d$  – cell thickness,  $\Delta n$  – birefringence,  $\lambda$  – the wavelength. According to this equation there will be a maximum transmission in the switched state if the tilt angle  $\theta$  is  $22.5^\circ$  (the cone angle is  $45^\circ$ ) and the cell acts as a half-wave retardation plate ( $\pi d \Delta n = (2n+1)\pi$ ), thereby rotating the plane of light to further  $45^\circ$  degrees.

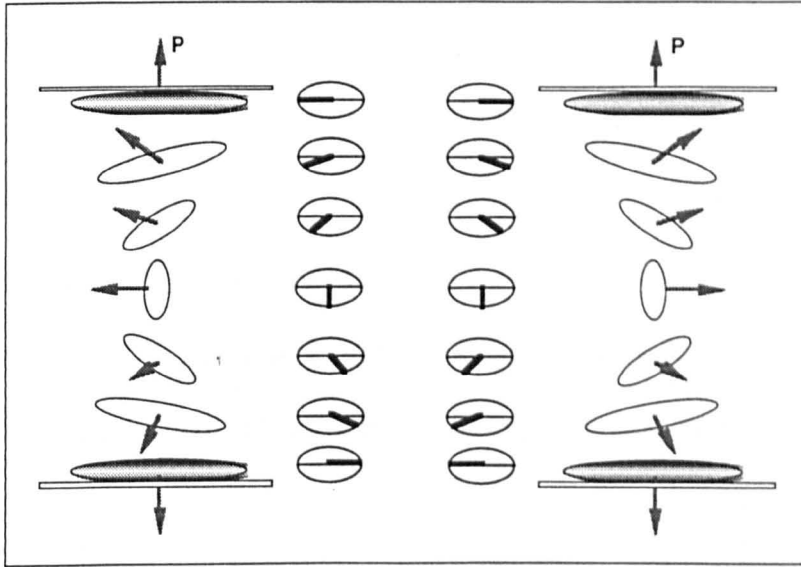


**Figure 5.6:** Proposed model for the twist state found in the surface-stabilised smectic  $C^*$  phase, in the absence of an electric field.

In the absence of an electric field the liquid crystal relaxes to its ground state which is preferred between two surfaces. Generally, formation of domains corresponding to both tilted directions is observed. In addition, so-called twisted structures, which arise due to the competition between various physical forces exerted on the molecules in the cell, are randomly present in the bulk [16, 17]. The possible structures of the twisted state in the surface-stabilised geometry are shown in figure 5.6 [17].

The twisted nature of the relaxed state may be understood in terms of an equilibrium between the various contributions to the total energy of the liquid crystal sandwiched between two surfaces. In the absence of an electric field and provided that the

spontaneous polarization of the material is small, the energy consists of two terms only: a nematic-like elastic and polar, non-polar surface interactions [18]:

$$E = E_{el}(k_1, k_2, k_3) - W_n - W_p \quad (2)$$

where  $k_1$ ,  $k_2$  and  $k_3$  are the splay, twist and bend elastic constants and where  $W_n$  and  $W_p$  represent the non-polar and polar surface energy terms. The bulk nematic energy is lowest when the director field is uniform. The surface polar and non-polar energies are both minimal when the molecules are parallel to the surface and the polar term will be further reduced when the polarization vector at the surface is directed out of the cell. As a result, in the bulk twist and bend deformations disappear, and the splay contribution to the elastic energy dominates. In contrast, the surfaces make the twist and bend contributions play a significant role. Bringing the surfaces closer together the splay deformation is expelled from the bulk, and more twisted and bent structures are realised giving rise to the uniform twist of the director passing from one surface to another.

Each state, depicted in figure 5.6, corresponds to one of the uniform ferroelectric states and will dominate dynamic process at zero field during the switching when the molecules are reoriented by an electric field. Switching to and from the twisted state was first utilised by Patel in a liquid crystal light modulator with a high tilt (about 45°) smectic C\* material [19]. A good contrast ratio was achieved in a cell with surface rubbing directions being at 90° to one another. Optically, the twisted smectic structure appears similar to the twisted nematic structure, as the optical eigenmodes of the sample are linearly polarized when the Mauguin condition  $\Delta n d \gg \lambda$  is satisfied [20]. Therefore, linearly polarized light passing through such a structure rotates through an angle equal to the twist in the structure. When light enters the 90° twisted smectic modulator the polarization plane is rotated by 90 degrees, and the cell appears light between cross polarizers.

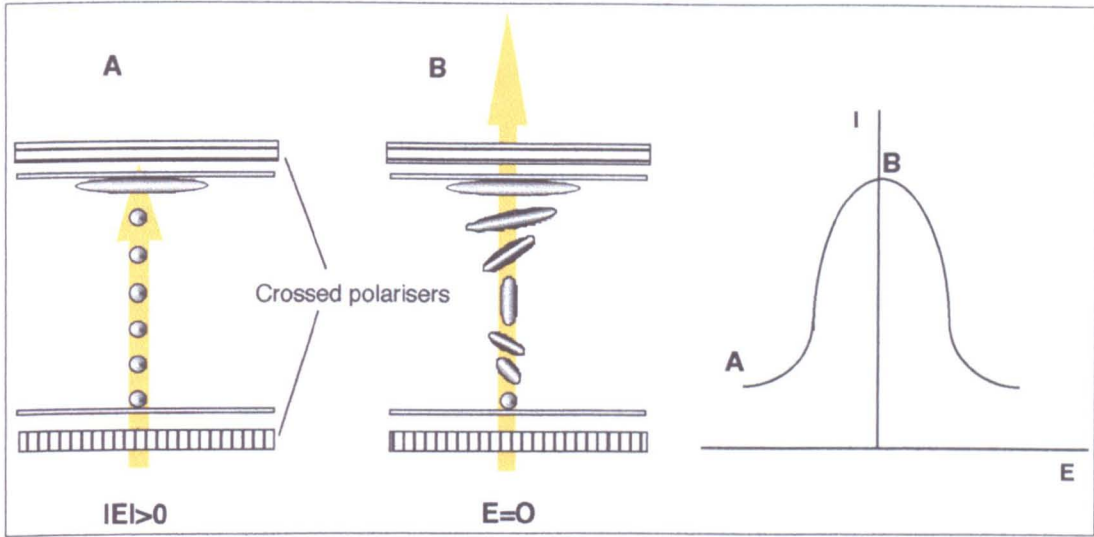


**Figure 5.7** Patel twisted device and the transmittance curve between parallel polarizers.

When an electric field is applied, one of the uniform states is produced with the director being at  $90^\circ$  to the incoming light. No light passes through the second polarizer and the cell becomes dark, see figure 5.7. Unwinding the helix only slightly will result in elliptical eigenmodes being produced and a portion of the initially linearly polarized light will be transmitted. Thus, distortion of the helical structure by an electric field controls the contrast between the “on” and “off” states thereby producing grey scale operation. The switching does not require reorientation of the molecules at the surfaces of the cell, therefore such a device operates at a substantially faster speed compared to the bistable ferroelectric device.

It can be seen in figure 5.7, that the transmittance curve of the twisted device is reminiscent of the letter V though rather broader [18]. The energy of the dynamic process in the presence of an electric field includes two more terms, apart from the elastic and surface contributions mentioned earlier, because the presence of the electric field results in coupling with the spontaneous polarization and dielectric constant. Hence, the equation of motion becomes as follows [22]:

$$E = E_{el}(k_1, k_2, k_3) - W_p - W_n - PE \sin \varphi - \Delta \epsilon \epsilon_0 E^2 \quad (3)$$

These four contributions determine the profile of the director motion in the cell. Optical changes due to this motion are described by the corresponding transmittance-voltage curve, the shape of which will be strongly affected by shifting the balance between the various energies. For example, the broad curve shown in the figure 5.6 can be greatly narrowed by varying the strength of the surfaces [18], and consequently the contribution of the surface interactions to the total energy. In the presence of an electric field the polar surface energy and the ferroelectric torque compete with each other in the region of the surface. Depending on the direction of the electric field the director near to the surface will be rotated by the ferroelectric torque acting against the polar anchoring energy at one surface and amplifying it at another. Therefore, there will be different speeds in the unwinding of the helix at the two surfaces resulting in a broad transmission change. In order to make it sharper (or more V-shape) the surface energy is required to be decreased, however, it still needs to have a significant contribution to induce a formation of a twisted structure.

A large negative dielectric anisotropy has similar effects. The dielectric torque, included in equation 3, is the driving force in the transition between the “on” and “off” states in a nematic twisted cell. It acts similarly in a ferroelectric smectic C\* material, however, until now its contribution was considered negligible [22]. If a material possesses a large positive dielectric anisotropy, the dielectric coupling will counteract the ferroelectric torque resulting in slow helix unwinding and a broad transmission curve. It becomes more V-shaped when  $\Delta\epsilon$  diminishes, and for large negative values a high optical contrast ratio can be easily attained.

Thus, the twisted structures found in surface stabilised ferroelectric liquid crystals can be used to create a nematic-like device that, under certain conditions, may exhibit a V-

shaped optical response. Apparently, the contrast ratio of such device, even if all the necessary parameters were optimised would be greatly reduced by formation of two opposite types of twisted states that have different optical properties [17]. Also, in experiments, complete transmission or extinction of light (depending on the orientation of the analyser) was not achieved in the 90° twist smectic C\* device as the Mauguin condition could not be fully satisfied and plane polarized light was not produced by the twisted structure.

Nevertheless, if one accepts that the SmX\* phase in the Tokyo mixture is a ferroelectric smectic C\* phase, a V-shape form of the transmittance-voltage dependence at certain frequencies can be explained by the formation of twisted states during dynamic switching in the surface-stabilised geometry. To explain almost complete light extinction when the system transforms into the twisted state, the model of a polarized-stabilised kink (PSK) [14] was introduced for which some basic ideas are summarised below.

In the absence of an electric field, the state with a splay-bend deformation of the polarization field<sup>22</sup> is associated with a polarization charge density  $\rho_p = -\nabla \cdot \mathbf{P}$  and thereby with the additional electrostatic energy  $\sim (\nabla \cdot \mathbf{P})^2$  [14].

---

<sup>22</sup> The twist-bend deformation of the director field discussed before will be accompanied by the splay-bend deformation of the polarization field. For this reason the twisted state sometimes is called splayed state stressing that it is the polarization is the main subject of the investigation.

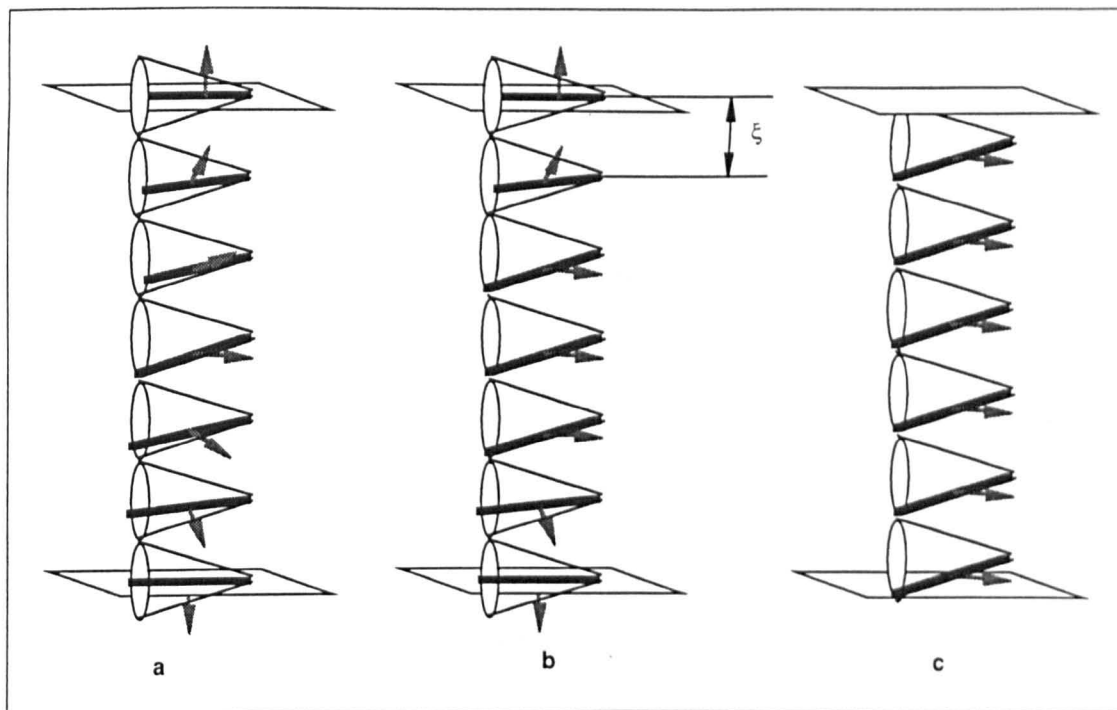


**Figure 5.8** The PSK model and director deformations during changing of the electric field from zero to the finite value.

For low spontaneous polarization materials the electrostatic energy is relatively small compared to the other terms in equation 3. However, in the case of a material with a large magnitude of spontaneous polarization, the electrostatic contribution becomes significant, and, as a result, the system has to rearrange itself in order to reduce this contribution. In other words, the system produces an electric field with negative charges being in bulk where the polarization vectors are parallel to the layer plane, and the positive charges are concentrated in the vicinity of the surfaces, see figure 5.8. The field and the energy associated with this arrangement can be expelled if the twist deformation (and negative charge) is moved to the surfaces thereby giving rise to a uniform polarization (and the director) alignment in the bulk. Consequently, there will be a twisted domain (polarization-stabilised kink) near each surface, the thickness of which can be described as a result of minimisation of the electrostatic energy and the orientational elastic energy:

$$\xi_p = \sqrt{\epsilon K / P^2} \quad (4)$$

where  $\epsilon$  is the dielectric constant of the liquid crystal. Polarization charge effects become important when the size of the polarization stabilised kink  $\xi_p < d$  - the thickness of the cell. In this case, a nearly uniform molecular arrangement in the bulk will be produced and thus, good optical extinction between cross-polarisers is achieved [21]. When the electric field is changed the molecules move continuously to one of the uniform “up” or “down” states producing a thresholdless electrooptical response.

It should be noted that thresholdless switching was observed in Tokyo mixture both in the SmX\* phase (which is believed here to be a normal smectic C\* phase) and in the truly antiferroelectric phase. The detailed analysis of the switching reveals that the ground state in the absence of an electric field is indeed antiferroelectric. However, after application of the electric field and bringing all of the molecules into the uniform ferroelectric state, the switching starts to proceed through the splayed state stabilised by the polarization charge.

Thus, the PSK model provides a simple explanation of thresholdless switching assuming that the liquid crystal phase shows such a response in a surface-stabilised ferroelectric smectic C phase. One problem of this model is based on the fact that simple calculations show that the size of PSK domain will be small enough for a spontaneous polarization of  $10 \text{ nC cm}^{-2}$  to produce V-shaped switching behaviour. In reality, however, V-shape switching starts to be realised for the materials with spontaneous polarization of order of  $100 \text{ nC cm}^{-2}$ . This contradiction was explained by the presence of ionic impurities in the low  $P_s$  materials, which screen out the polarization charges and reduce the “stiffening effect”. It is argued that ferroelectric materials, which were subjected to extreme purification should exhibit V-shape

switching even though their polarization values are considerably smaller than those shown in the recent experimental studies.

Another more serious contradiction of the model appears when one considers the values of the surface torques which should be present in order to maintain the PSK domains near surfaces [21]. The torque is given as:

$$\tau_{PSK} \sim K / \xi_P = (KP^2 / \epsilon)^{1/2} \quad (5)$$

For the materials with a spontaneous polarization of greater than 100 nC cm<sup>-2</sup>, this torque will be of an order of magnitude higher than typical polar and non-polar surface interactions can provide. Hence, for the PSK state to be realised the polarization should be less than 20 nC cm<sup>-2</sup>. This clearly contradicts the experimental data on which the whole model of PSK initially relied.

The problem was resolved by introducing the concept of insulating layers, which separate the polarization charge from the bulk of liquid crystal. As a result, the surface polar energy contribution may be excluded from the equation of the total energy and the orientation of the director (**n**) and the polarization from surface to surface is driven purely by elastic contributions. As mentioned above this contribution is at a minimum when the director **n** is parallel to the surfaces. The resulting uniform state will respond to an electric field in a continuous way so that the bulk polarization rotates as a block. In fact, this conclusion seems to have experimental support as a V-shape response was observed both in the bulk and near to the surfaces [21].

In general, omitting the details of the phenomenological description of the polarization stabilised states, both the PSK and the insulating layer models explicitly demonstrate that the high magnitude of the spontaneous polarization plays a crucial role in the

stabilisation and uniformity of the zero field state which material adopts in a surface stabilised cell.

Summarising this discussion, it should be said that the explanation of complete light extinction during V-shape switching could be derived via three different approaches:

1. Partial randomisation of the azimuthal angle in the smectic layers caused by surface interactions and weak interlayer correlations.
2. Formation of a twisted state.
3. Realisation of a uniform zero-field state due to the high magnitude of the material's spontaneous polarization.

Bearing these comments in mind, results on the electrooptical responses of the various materials prepared will now be discussed.

## 5.2 Results of the electrooptical studies in selected homologues of compounds of general structure 1-9

As discussed in the previous device and engineering section, V shaped switching in a surface stabilised cell was found to be critically dependant on three factors; (i) temperature, (ii) frequency of the applied electric field and (iii) the polarity of the surfaces. It was also noted that materials which produce thresholdless switching possess relative high values of the spontaneous polarization, i.e. more than  $100 \text{ nC cm}^{-2}$ . However, there seems to be a lack of data on the role of chemical structure in the ability of a liquid crystalline material to produce a thresholdless optical response.

In order to investigate voltage-transmittance characteristics as a function of the chemical structure, a set of electrooptical experiments were performed for several liquid crystals synthesised during the course of the project. The compounds selected for study possess the most stable ferroelectric or antiferroelectric  $\text{SmC}^*$  phases in their respective homologous series. The measurements were taken in thin (*ca.* 2 or 5  $\mu\text{m}$ ) planar aligned cells by applying a triangular electric field and varying the orientation of the cell between two cross polarizers in a transmitted light microscope. The transmittance as a function of the electric field was recorded at different frequencies, voltages and temperatures for each of the compounds (see figures below)<sup>23</sup>.

Firstly, a V-shape response was simulated for compound **53** (figure 5.9). Its rich mesomorphic behaviour is reminiscent to the phase morphology of the Tokyo mixture. The phase sequence includes  $\text{SmA}^*$ ,  $\text{SmC}^*$ ,  $\text{SmC}_{\text{FI}}^*$  and  $\text{SmC}_{\text{A}}^*$  phases. The spontaneous polarization gradually increases from  $30 \text{ nC cm}^{-2}$  at the  $\text{SmA}^*$ - $\text{SmC}^*$  transition and reaches a value of above  $140 \text{ nC cm}^{-2}$  near to the antiferroelectric phase.

---

<sup>23</sup> It was assumed that the materials under investigation possess a long pitch helical structure in the smectic  $\text{C}^*$  phases. It was also believed that in thin planar cell the surface-stabilised geometry is realised with the helix remaining unwound after application of an electric field.

This value is fairly similar to the estimated spontaneous polarization for the **SmX** phase of the Tokyo mixture [4].

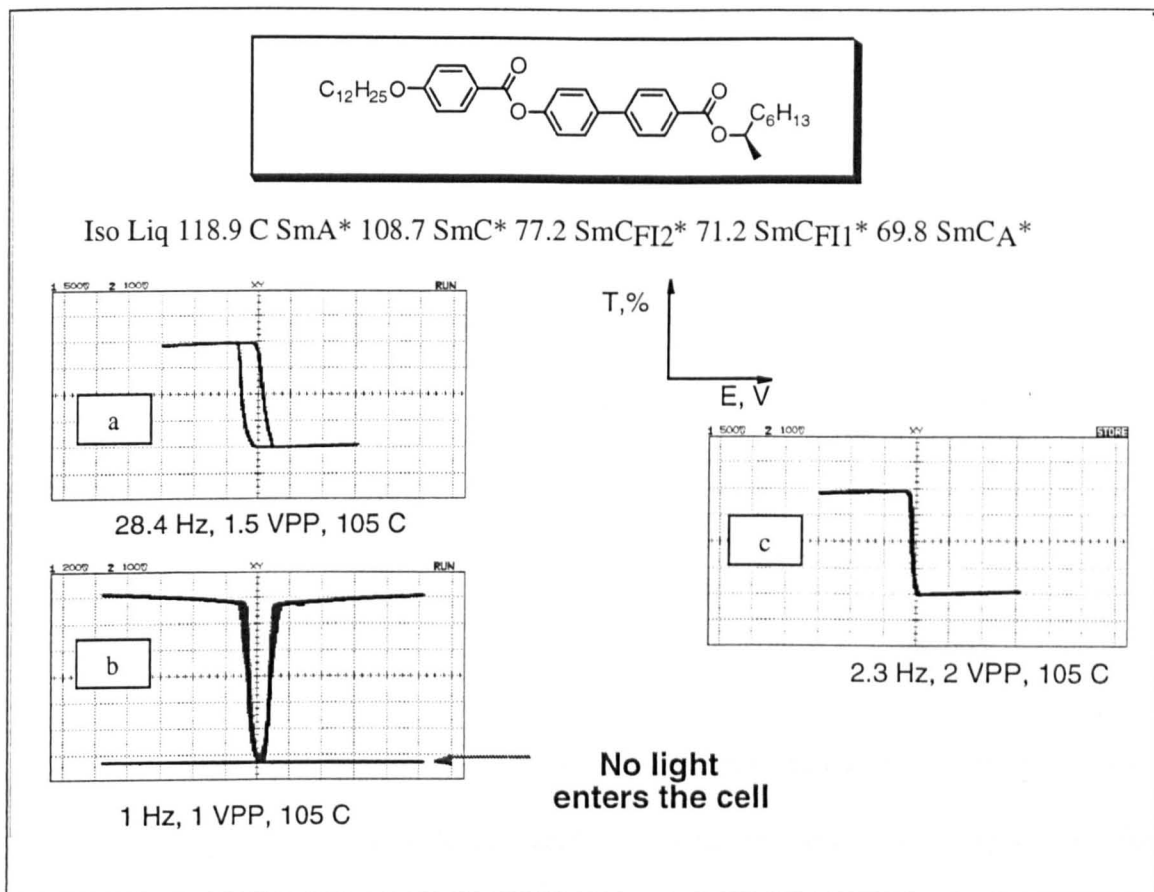


**Figure 5.9:** Voltage-transmission curves recorded for compound **53** at various fields. Here and in the following diagrams the relative level of transmission is shown along y-axis.

The electrooptical response showed a normal ferroelectric hysteresis at the frequencies above 5 Hz (figure 5.9a). Decreasing the frequency resulted in the hysteresis loop shrinking into a thin line (figure 5.9b). It can be seen in figure 5.9 that the slope of the line is steep because a sharp change in transmission occurs between two switched states. When the orientation of the cell was changed so the axis of the polarizer was set parallel to the smectic layer normal a V-shaped response was obtained (figure 5.9c). The shape of the curve remained unchanged for a relatively broad range of frequencies. However, below a certain value the hysteresis loop reappeared.

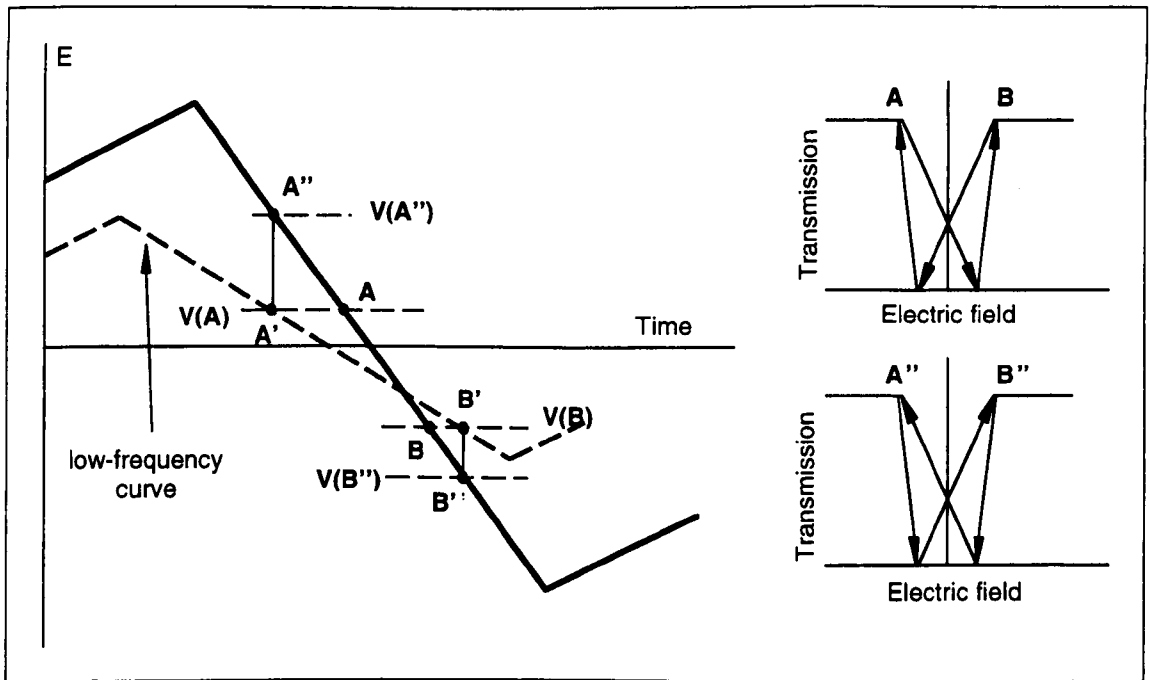


**Figure 5.10:** Schematic diagram explaining reappearance of hysteresis loop at low frequency of an external electric field

This effect can be explained in terms of the distribution of space charge in the surface-stabilised cell [10]. When an external field  $E_{ext}$  is applied to the liquid crystal cell the layer spontaneous polarization is aligned along the field direction, thereby generating opposite surface charges, which produce an electric field  $E_{sur}$ . Since  $E_{sur}$  is smaller than  $E_{ext}$ , positive and negative ions in the bulk move in opposite directions creating the ionic field  $E_{ion}$ , which opposes  $E_{ext}$ . If the frequency of the external field is high enough, the charges do not have time to move far away from each other and generate a substantial  $E_{ion}$  before the external field changes sign. Thus, a normal hysteresis response is produced as switching starts at point **A** and is completed at **B** (figure 5.10). When the frequency is low, the mobility of ions increases so that  $E_{ion}$  has a significantly high contribution and, thus a negative electric field exists when the external field is zero. Therefore, the switching actually starts at **A'** and finishes at **B'** (**A''** and **B''** on the black curve). If  $|A''| > |B''|$  the abnormal hysteresis takes place, and when  $|A''| = |B''|$  a hysteresis-free V-shape response is produced.

As shown in the figure 5.9, when the V-shape curve is stabilised, complete extinction of light was observed at the tip of the V. The bottom line in diagram 10c corresponds to zero transmission when no light passes through the cell. Thus, all the features of the switching described for the Tokyo and Mitsui mixtures can be simulated in the ferroelectric smectic C\* phase. It should be noted that the voltage-transmission curves depicted in the figure 5.9 were recorded at a temperature close to the smectic A\*-smectic C\* phase transition. At these temperatures if any type of randomisation of molecular tilt is induced by the surfaces at the tip of the V, it cannot be a result of the competition between synclinic and anticlinic ordering as suggested by the random model. The antiferroelectric and intermediate sub-phases appear 40° below the temperature point where the V-shaped switching is observed and therefore such sub-phases cannot affect the thermodynamic stability of the smectic C\* ordering.

However, the temperature still appears to be an important factor in the stabilisation of the intermediary switching state, as demonstrated for compound **58**. A V-shaped curve was observed in the smectic C\* phase using the method described above for compound **53**, but only at higher frequencies (see figure 5.11). At 90 °C, just a few degrees below the second-order smectic A\*- smectic C\* phase transition the dark state does not correspond to zero transmission. However, the transmittance level decreases with temperature and at 74 °C complete extinction is observed.

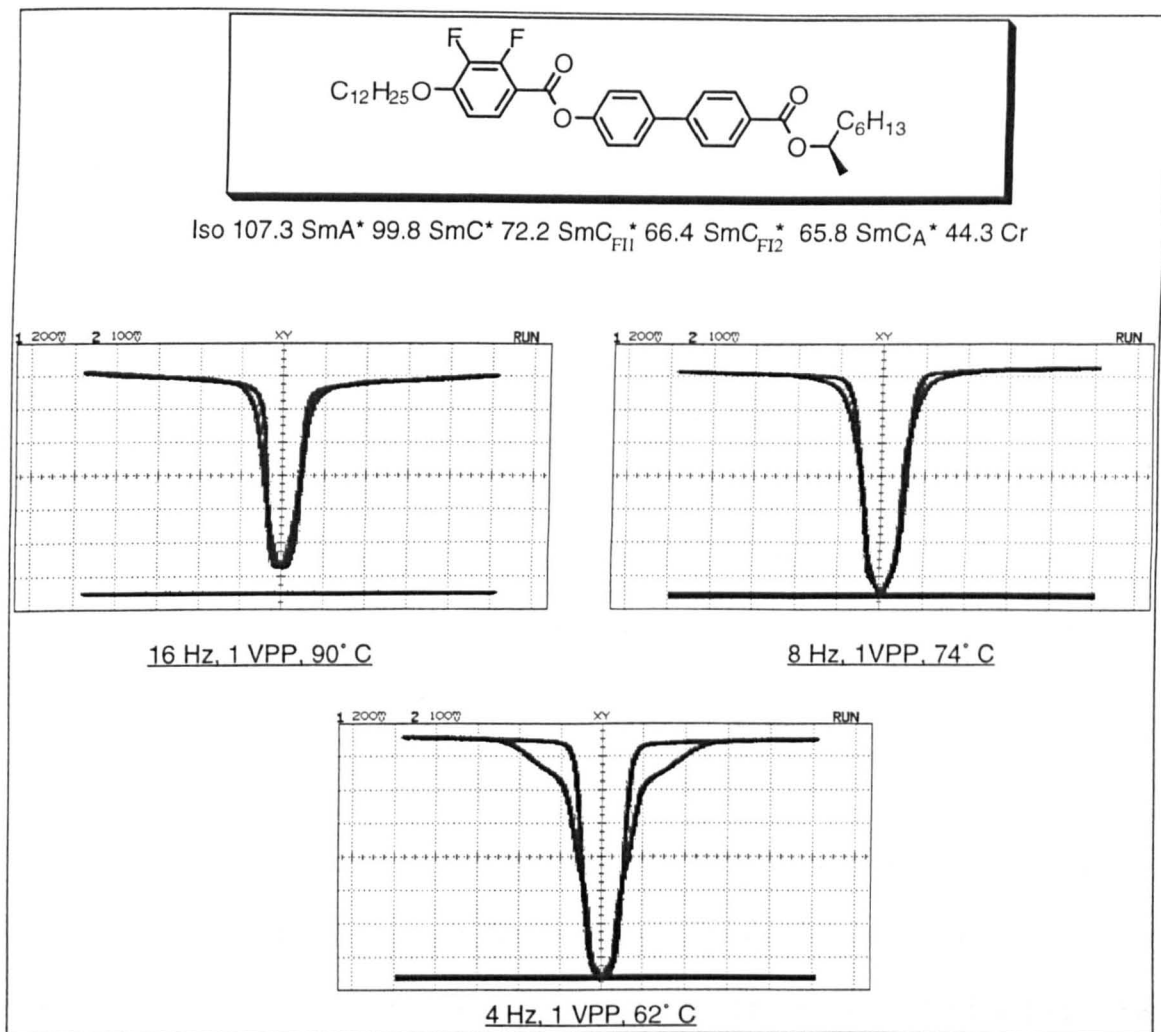


**Figure 5.11:** Voltage-transmission curves recorded for compound **58** at various electric fields

If one takes into account the PSK model, the temperature dependence of the transmission can be explained in terms of the high value of the spontaneous polarization at lower temperatures. According to the well-known result related to the Landau expansion for a second order phase transition [22], the spontaneous polarization as a secondary order parameter undergoes gradual growth with the reduced temperature from the Curie point:

$$\theta = \left(\frac{\alpha}{b}\right)^{1/2} (T_c - T)^{1/2}$$

$$P = \frac{1}{2} P_0 \sin 2\theta \quad (6)$$

where  $\alpha$  and  $\beta$  are the coefficients of the first two terms of the expansion.

The spontaneous polarization of the compound **58** increases from approximately 76 nC cm<sup>-2</sup> at 90 °C to 101 nC cm<sup>-2</sup> at 74 °C. Such an increase in the value of  $P_s$  would seem to be enough to transform a twisted structure at zero field to a uniform polarization stabilised state which dominates the material between the two surfaces. As a result, the level of transmittance drops to zero. The PSK model may well describe the properties observed, however it should also be remembered that the materials possess a very short pitch of the helix in the SmC\* phase, and thus heli-electric effects cannot be ruled out.

Attempts were also made to simulate V-shape curves of the voltage-transmittance function in the smectic C\* phases of siloxane materials **70** and **71**. These compounds (like all of the other siloxane compounds prepared in this project) exhibit first-order transitions from the isotropic liquid to the smectic C\* phase. The corresponding value of the tilt angle in the smectic C\* phase, which is just slightly lower than 45°, does not change with temperature. The spontaneous polarization reaches 110 nC cm<sup>-2</sup> in the vicinity of the phase transition, and it monotonically increases with decreasing temperature to approximately 200 nC cm<sup>-2</sup>.

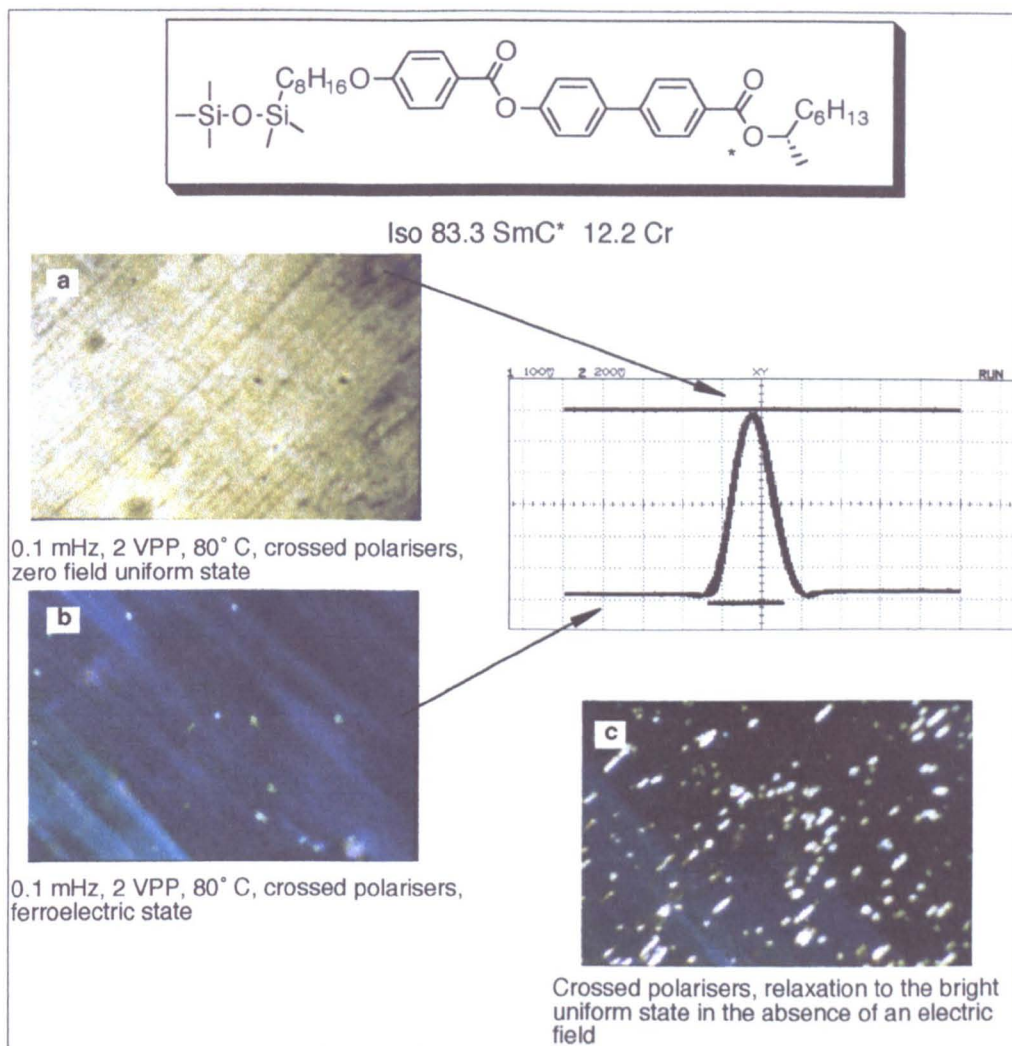


**Figure 5.12:** Compound 71. Photomicrographs show appearance of the zero-field state (a) and the uniform ferroelectric state (b) during the switching in 5  $\mu\text{m}$  cell, relaxation to a bright state with no field applied (c)

In this case, the V-shaped switching was not affected by the temperature, and could be observed throughout the whole temperature range of the phase, with a small hysteresis being a function of the frequency of applied field. The V-shaped curve appears to be turned up side down as the plane of the incoming light was set parallel to the director in one of the ferroelectric states. When the molecules are in this state, light travels with a polarization direction parallel to the principal molecular axis, so complete light modulation is achieved. As a result, the cell appears dark. At the second uniform state

the molecules are switched along the smectic cone to the opposite tilt positions. The dark texture is observed again, as this time the polarization plane is perpendicular to the optic axis of the material. It can be seen in the figure that the light extinction is not complete for these states because the tilt angle is slightly less than  $45^\circ$

In the configuration described, the third zero-field state occurs when molecules reached central position on the smectic cone which is at  $45^\circ$  to the plane of incident light. The photomicrographs taken of compound **71** (figure 5.12) show the difference in appearance of the uniform dark state and bright zero field state. The height of the transmission curve reaches almost the maximum value as shown in the figure. When the electric field is switched off the material slowly relaxes to the bright ground state (figure 5.12).

Similar electrooptical behaviour was observed for compound **70**. It was found that even if the polarizers are set parallel to each other the transmission value does not reach a minimum level as indicated by the bottom line in figure 5.13b and remains at rather high level. The absence of mirror symmetry between the transmission curves recorded for parallel and crossed polarizers originates from the non-linear polarization eigenmodes. The results explicitly show that there is no uniformity achieved in the field-off state. Instead, a twisted structure seems to be a possibility for these compounds in the absence of an electric field, because the Mauguin condition is not fully satisfied as the incoming plane polarized light is not fully rotated by the twisted structure and emerges elliptically polarized.

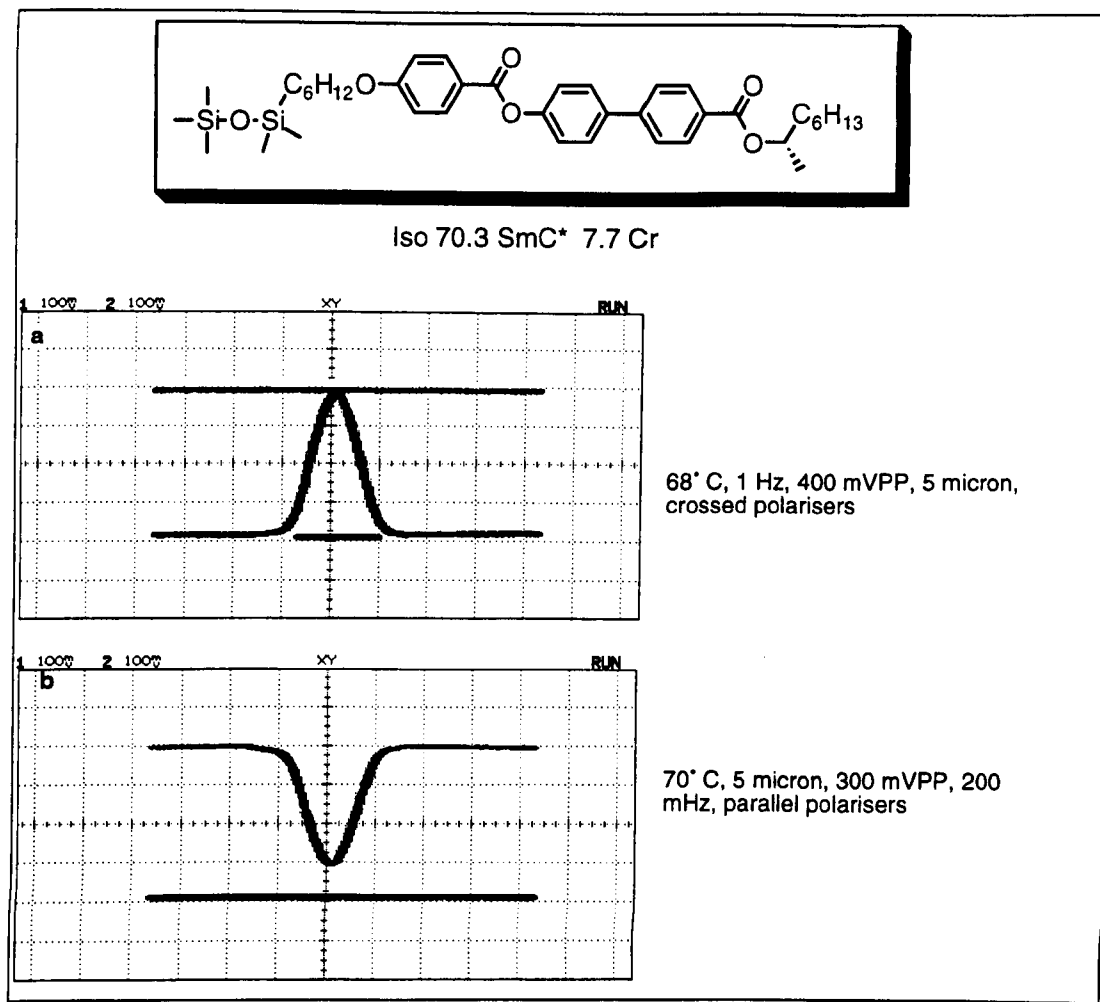


**Figure 5.13:** Voltage-transmission curves recorded for compound **70** between cross- (a) and parallel (b) polarizers

Comparing the results obtained for compounds **53**, **58**, **70** and **71** shows that in the surface stabilised geometry there is competition between twisted and uniform, polarization stabilised states. Assuming that the spontaneous polarization plays an important role in stabilisation of the uniform state there seems to be a critical value for a particular material above which the twisted structure transforms into the uniform state. For example, such transformations occur for compound **58** only at low temperatures where the spontaneous polarization has a substantially high value. However they do not take place for compounds **70** and **71** despite the fact that the spontaneous polarizations are almost double those of compounds **53** and **58**. A twisted structure dominates at all values in the polarization-temperature function. Thus, the critical value of the

spontaneous polarization is not universal, and is determined by the properties of material.

Any modification to the chemical structure, which *amplifies the intermolecular interactions* at the same time will reduce the chances of the uniform state being stabilized at zero field. In the case of compound **58**, two fluorine atoms laterally attached to one phenyl fragment of the parent structure **53**, serve as additional sites for interactions between neighbouring molecules within a layer. Similarly, the siloxane chains of compound **70** greatly increase the interlayer interactions. While the former can be overcome by a temperature driven increase in the spontaneous polarization, the latter remains fairly strong and can not be counteracted by the electrostatic torque even if the torque is induced by an exceptionally strong spontaneous polarization.

This hypothesis is supported by the results obtained for compound **62**. The only difference in its chemical structure from compound **53** is the terminal double bond attached to the non-chiral chain. The spontaneous polarization is also roughly the same, approximately  $80 \text{ nC cm}^{-2}$ . The compound possesses a broad antiferroelectric phase, for which the electrooptical response was observed and compared to the results for the ferroelectric phase. In order to include the surface effect in the discussion, the material was investigated when placed in two planar cells of different thickness (2 and 5  $\mu\text{m}$ ).

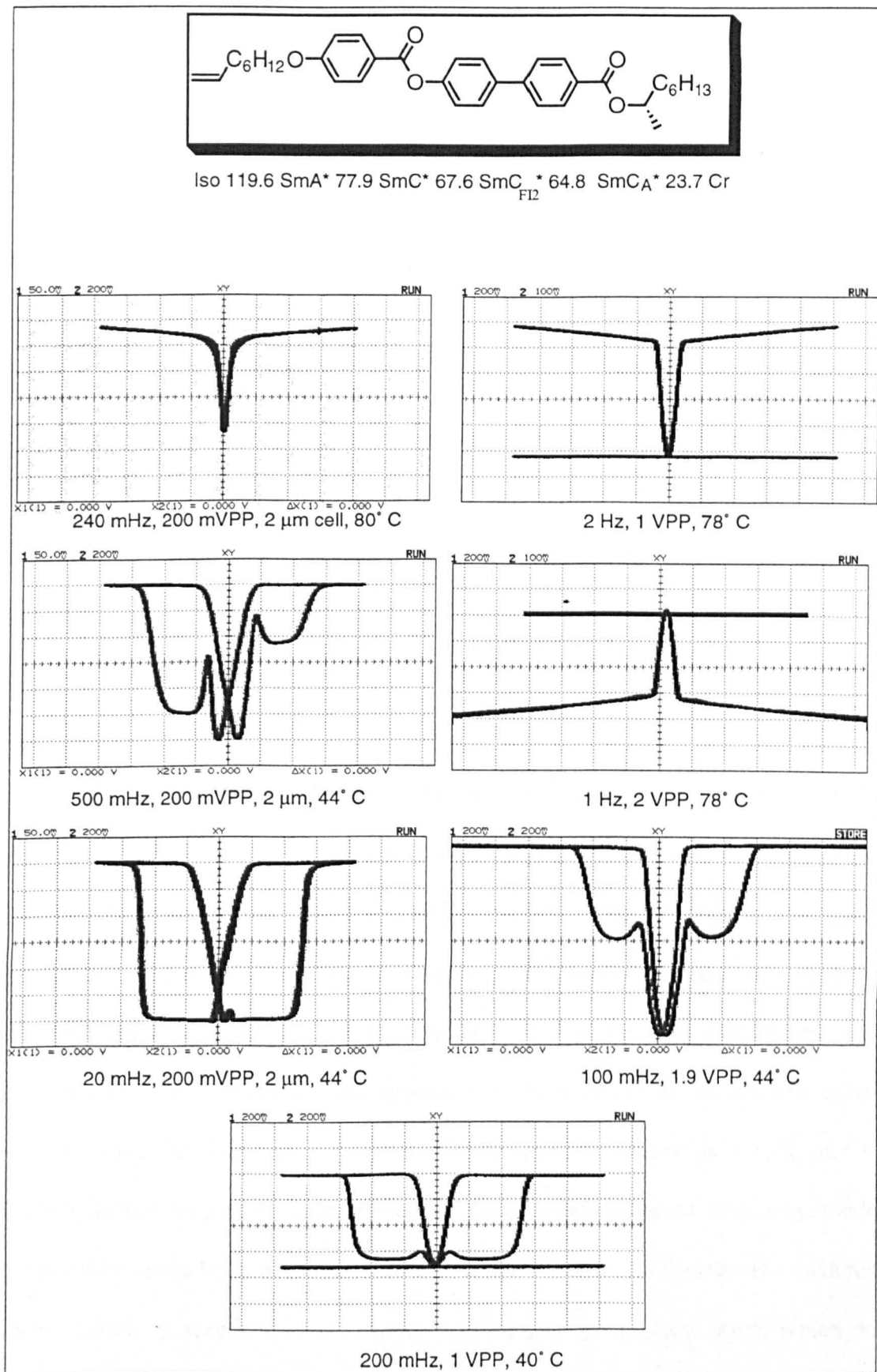


**Figure 5.14:** Voltage-transmission curves for compound **62**. Cell thickness is 5 μm unless stated.

In fact it was found that for narrow cell gaps at least, the cell thickness does not affect either the width of the V shape [21] nor the general trends in the material's response to the electric field. In both cells a typical W-shape ferroelectric response was produced at 80 °C when a high frequency field was applied. This response was converted into a V-shaped line at 240 mHz in a 2  $\mu\text{m}$  plate separation and at 2 Hz in cell with a gap of 5  $\mu\text{m}$ .

It can be seen in figure 5.14, complete extinction of light was achieved between cross-polarizers, however, between parallel polarizers the cell transmission reaches maximum and an almost symmetrical inversion of the V-shaped response is observed. It is most likely that a uniform structure is fully realised here with the plane of polarization of the incoming light being parallel to the optical axis of the material in the zero field state.

At 44 °C in the antiferroelectric phase a double hysteresis loop was observed when the frequency was low enough for the material to relax into the antiferroelectric ground state. As shown in figure 5.14, the double hysteresis loop transforms into typical ferroelectric hysteresis loop at high frequencies, an effect which has been described previously for antiferroelectric liquid crystals [23]. For the intermediate frequency range, where antiferroelectric state appears transitory during switching, the optical response curve exhibits features of both ferroelectric W-shaped switching and the double hysteresis loop of the antiferroelectric phase. By adjusting the frequency, the W-shaped curve could be transformed into a V-shaped line at which point the switching process clearly proceeds via four states. Surprisingly, the uniform state, which was formed at the tip of "V" in the ferroelectric phase is, however, still present in the antiferroelectric phase. As reflected by a voltage-transmission curve (figure 5.14), the molecular reorientation from the ferroelectric state occurs via the so-called uniform

"structure", where complete extinction of light was observed and then relaxes back to the antiferroelectric ground state. The hypothetical model for the molecular reorientation obtained during this process is depicted in figure 5.15.

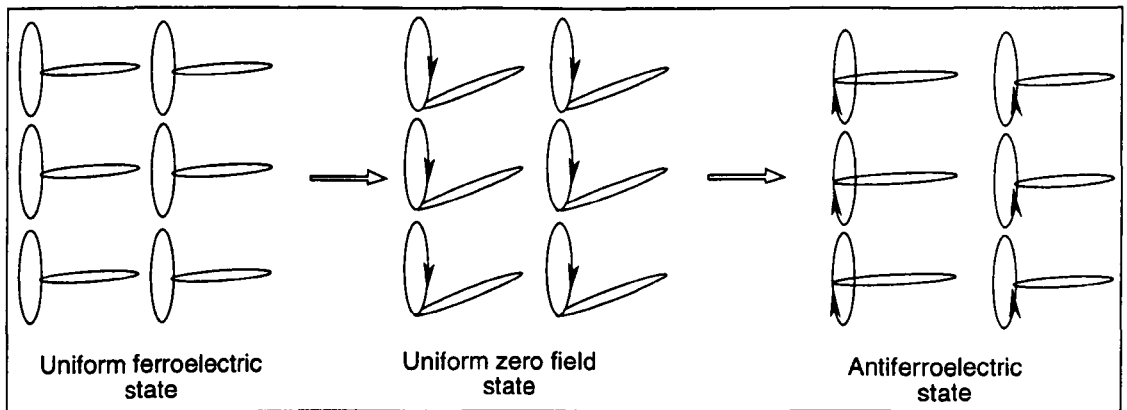


**Figure 5.15:** Possible molecular reorientation during tristate switching of an antiferroelectric phase in a surface-stabilised geometry at low frequencies of an external electric field.

Remarkably, the tip of V-shaped switching curve still corresponds to zero field, thereby allowing the speculation that, at least during the dynamic switching process, the polarization stabilised uniform structure is thermodynamically more stable than the antiferroelectric state in surface-stabilised geometries. The differences in textural appearance of the antiferroelectric and uniform zero-field states are shown in figure 5.16.

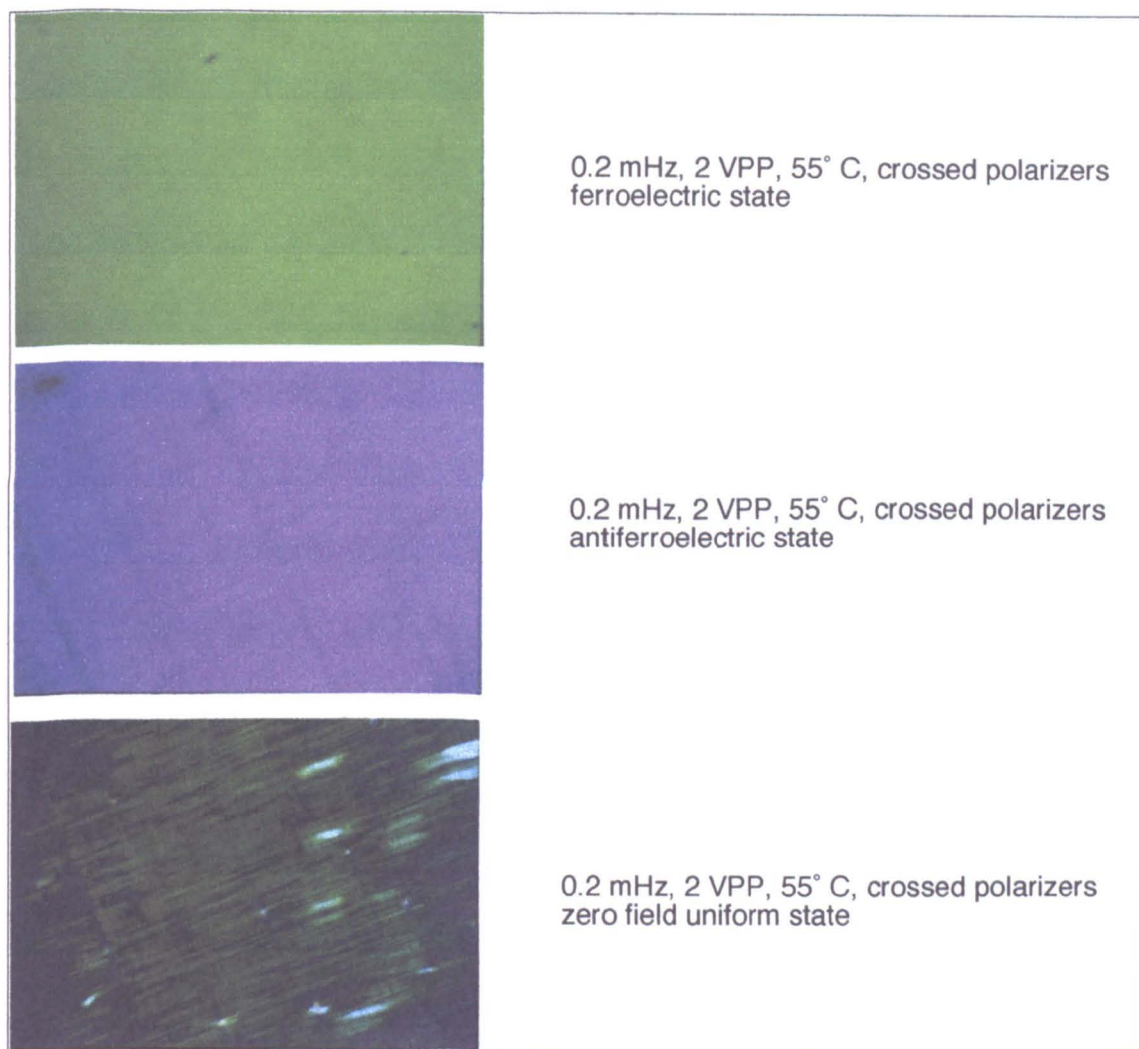


**Figure 5.16** Photomicrographs taken for compound **62** while switching under the application of a low-frequency electric field

These results were also reproduced for compound **88**, which does not exhibit a ferroelectric phase and is instead just antiferroelectric. The ferroelectric hysteresis loops appearing at high frequencies could not be collapsed to give a single line response because the switching *via* the antiferroelectric state dominates over a wide range of frequencies resulting in a mixed V-shaped and double hysteresis curve (figure 5.17). Again, the zero-field state has the lowest transmission as shown in figures 5.17, however, it does not give a completely dark state with total extinction of light. In this case, the two fluorine atoms attached to the aromatic core are likely to play similar role as those described for compound **58**, i.e. opposing the electrostatic torque due to the

high spontaneous polarization. As a result the field-off state is likely to be represented by a twisted structure.

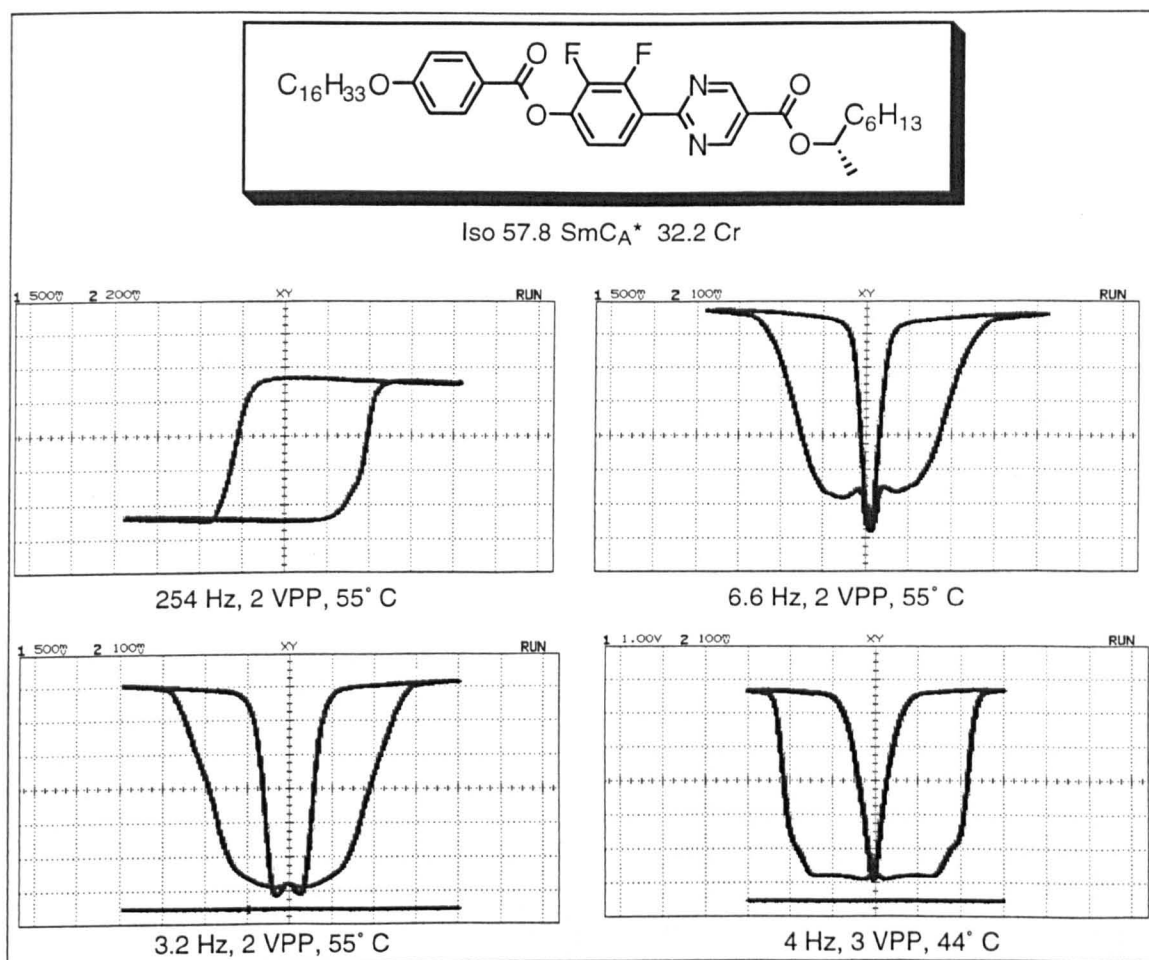


**Figure 5.17:** Voltage-transmission curves recorded for compound 88

In conclusion for the results obtained on the various materials studied several observations and property-structure activities may be drawn:

1. The V-shape electrooptical response is a property of the material placed in the surface-stabilised geometry, and can be observed for switching in ferroelectric smectic C\* phase.
2. At the tip of V-shaped switching curve, the uniform polarization stabilised structure is likely to be formed according to the mechanism described by models of the polarization stabilised kink (PSK) and insulating layer structures.
3. The stability of the uniform state is greatly affected by the chemical structure of the material. Functional groups introduced to the molecular core and chains may reduce

the polarization effect thereby resulting in domination by the twisted state. In such cases, the V-shaped switching curve can still be observed, however, the transmission at the tip of V does not become zero. An exception is twisted structure formed by high tilt materials.

**References (section 5)**

1. A Fukuda, in "Handbook of Liquid Crystals", ed D Demus, J Goodby, GW Gray, H-W Speiss, V Vill, Willey-VCH, VCH, 1998, Vol 2B
2. A Fukuda, *Proc Asia Display'95*, Hamamatsu, 61
3. P Rudquist, K D'have, ST Lagerwall, R Dabrowski, Presented at the 18<sup>th</sup> ILCC, Sendai, Book of Abstracts, 2000, p. 23
4. S Inui, N Iimura, T Suzuki, H Iwane, K Miyachi, Y Takanishi and A Fukuda, *J Mat Chem*, 1996, **6**, 671
5. RJ Coelho, "Physics of Dielectrics for the Engineer", Oxford: Elsevier, 1979
6. Ch Bahr and D Fliegner, *Phys Rev Lett*, 1993, **70**, 1842
7. T Matsumoto, A Fukuda, M Johno, Y Motoyama, T Yui, S Seomun and M Yamashita, *J Mat Chem*, 1999, **9**, 2051
8. SS Seomun, T Gouda, Y Takanishi, K Ishikawa and H Takazoe, *Liq Cryst*, 1999, **26**, 151
9. K Itoh, M Kabe, Y Takanishi, k Ishikawa, H Takazoe and A Fukuda, *J Mat Chem*, 1997, **7**, 407
10. ADL Chandani, Y Cui, SS Seomun, Y Takanishi, K Ishikawa and H Takazoe, *Liq Cryst*, 1999, **26**, 167
11. JS Patel and SW Suh, *J Kor Phys Soc*, 1998, **32**, S1048
12. SL Wu and WJ Hsieh, *Chem of Mat*; 1999; **11**, 852
13. SS Seomun, Y Takanishi, k Ishikawa, H Takazoe and A Fukuda, *Jap J App Phys*, 1997, **36**, 3586
14. P Rudquist, JPF Lagerwall, M Buivudas, F Gouda, ST Lagerwall, DA Coleman, S Bardon, T Bellini, DR Link, G Natale, MA Glaser, DM Walba, MD Wand, XH Chen, *J Mat Chem*, 1999, **9**, 1257
15. JS Patel, JW Goodby, *Opt Eng*, 1987, **26**, 5, 373

16. H Takazoe, Y Ouchi, K Ishikawa and A Fukuda, *Mol Cryst Liq Cryst*, 1986, **139**, 27
17. Y Ouchi, H Takazoe and A Fukuda, *Jap J App Phys*, 1987, **26**, 1
18. SW Suh, JH Lee, YJ Kim, SS Park and SD Lee, *Ferroelectrics*, 1996, **179**, 181
19. JS Patel, *Appl Phys Lett*, 1992 **60**, 280
20. JC Khoo and ST Woo, "Optics and Non-linear Optics of Liquid Crystals",  
Singapore: World Scientific, 1993
21. NA Clark, D Coleman and JE Maclennan, *Liq Cryst*, 2000, **27**, 985
22. ST Lagerwall in "Handbook of Liquid Crystals", ed D Demus, J Goodby, GW Gray,  
H-W Speiss, V Vill, Willey-VCH, VCH, 1998, Vol 2B, 552
23. LM Blinov, "Physics of Liquid Crystals", Willey-VCH, 1999

## 6 Twist grain boundary phase with local antiferroelectric structure

### 6.1 Introduction

It was demonstrated in chapter 3 that the antiferroelectric  $\text{SmC}_A^*$  phase is often accompanied by a number of sub-phases and frustrated structures. Among the latter, the family of TGB (Twist Grain Boundary) phases captures special interest, because it appears in a wide range of natural phenomena [1].

The prediction [2, 3] and discovery of the twist grain boundary (TGB) smectic  $A^*$  phase in the (*S* or *R*)-1-methylheptyl 4'-(4-alkoxyphenylpropionoyloxy)biphenyl-4-carboxylates, **I** [1, 4] led to the unification of phase transitions in liquid crystals with those found for superconductors. Apart from the unification of these two dissimilar physical phenomena, TGB phases have been found to be common in the field of self-organising systems with such frustrated phases mediating phase transitions from either the isotropic liquid or the chiral nematic phase to the smectic state [5, 6, 7].

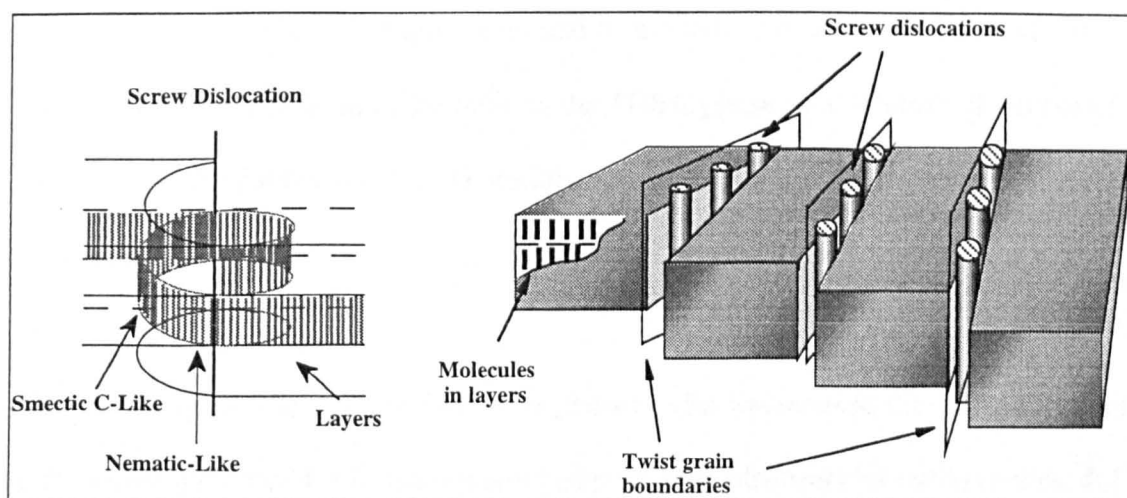


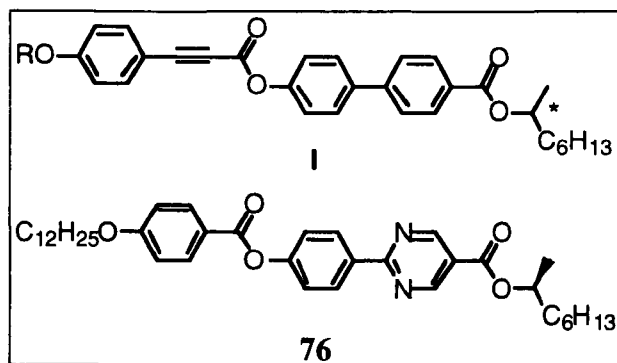
**Figure 6.1** Schematic representation of the TGBA\* phase and a screw dislocation

The structure of the TGB phase features blocks of a smectic phase rotated in the same sense with respect to one another by a small angle, thereby producing a helical structure in the direction of the planes of the layers (figure 6.1). The rotation of the smectic

blocks relative to each other is due to a periodic lattice of screw dislocations being formed perpendicular to the layers. These twisted defects represent a complex molecular organisation (figure 6.1) and penetrate the smectic structure similarly to the periodic array of a magnetic field in the **II** superconductors [8].

Over the past ten years a number of TGB phases have been identified and characterised. Generally the structures of TGB phases have been found to be based on the structures of the smectic phases that they either replace or which they form upon cooling. Frustrated equivalents of the smectic  $A^*$  and  $C^*$  phases have been found with both having variants that are dependent on the commensurability or incommensurability of the number of sheets of screw dislocations with respect to the pitch of the phase [9, 10], i.e. a rational or irrational number per  $360^\circ$  twist of the helix. For the TGBC modification a number of sub-phases have been discovered which are dependent on; (i) the presence (TGBC\*) or expulsion (TGBC) of the local heli-axis of the smectic  $C^*$  phase which is oriented perpendicular to the layers of molecules and to the heli-axis of the TGB phase; (ii) the inversion of the handedness of the helix in the TGBC phase as a function of temperature [11]; and (iii) the formation of a 2D modulated structure in the TGB phase with respect to the tilt [12].

It is interesting to note that the first TGB phases to be found were discovered in the (*S* or *R*)-1-methylheptyl 4'-(4-alkoxyphenylpropioloyloxy)biphenyl-4-carboxylates, **I** [1, 4]. In fact it appears that TGB phases often occur in conjunction with other frustrated phases such as Blue Phases, for example. Although, through the medium of chirality the unification of superconductors with liquid crystals appears to have been achieved [2, 3], it also seems that chirality dependent frustrations unify a variety of structures of mesophases that exhibit non-linear physical properties [13].



This chapter gives account of the studies of the liquid crystal properties of compound **76**, (*S*)-1-methylheptyl 2-[4-(4-dodecyloxybenzoyloxy)phenyl] pyrimidine-5-carboxylate, and its racemic modification synthesised in the course of this programme. Through miscibility studies, investigations of defect textures, differential scanning calorimetry, and electrical field studies, it was concluded that this material exhibits the novel antiferroelectric TGBC\*<sub>A</sub> mesophase.

## 6.2 Transition Temperatures

The transition temperatures, and the associated enthalpies for each phase transition, for (*S*)-1-methylheptyl 2-[4-(4-dodecyloxybenzoyloxy)phenyl]pyrimidine-5-carboxylate **76** are described in the following section and include a TGB phase which undergoes direct transition to the  $SmC_A^*$  phase on cooling. To clarify the origins and structure of this particular TGB phase, the racemic modification of compound **76** was synthesised accordingly, and liquid crystalline properties of both materials were determined by thermal polarized microscopy and differential scanning calorimetry, see Table 6.1.

<b>S-isomer</b>				
Iso – TGBC <sub>A</sub> *	TGBC <sub>A</sub> * - SmC <sub>A</sub> *	SmC <sub>A</sub> * - Cryst	Mp	
93 [-0.87]	91.6 [-0.22]	68.3 [-28.8]	86.4	
<b>Racemate</b>				
Iso – SmA	SmA - SmC	SmC - SmC <sub>Alt</sub>	SmC <sub>Alt</sub> - Cryst	Mp
96 [-9.12]	90.5 [-]*	89.2 [-]*	43.6 [-34.8]	72.6 [75.6]

**Table 6.1** Phase transition temperatures and enthalpies found for compound **76** and its racemic modification. \* - enthalpy was too small to measure.

Firstly, it should be noted that the purities of both materials were evaluated and found to be better than 99.5%. Therefore it should be emphasised that differences in the transition temperatures between the enantiomer and its racemate are real, as are differences in phase sequences and phase types. Thus the differences are associated with the effects of chirality on the system. For example, the isotropization temperature for the racemate is higher than that for the enantiomer, whereas the transition to a tilted smectic phase is lower. Furthermore, the racemate and the enantiomer do not exhibit the same number of liquid crystal phases or the same phase sequences, but nevertheless the

racemate exhibits smectic phases on cooling from the isotropic liquid and therefore it is highly unlikely that the chiral variant would exhibit a chiral nematic phase. Thus the high temperature phase of the enantiomer is expected to be smectic.

### 6.3 Differential Scanning Calorimetry

Figure 6.2 shows the cooling scans for both the racemic modification and the (*S*)-enantiomer. For the racemate (dotted line) the smectic A phase forms first on cooling from the isotropic liquid at 96 °C. On further cooling a smectic C phase is formed at 90.5 °C, but as the transition is second order it is detected only as a baseline step in the DSC. As the temperature is lowered a weak first order transition is found for the synclincic smectic C to anticlinic smectic C<sub>alt</sub> phase at 89.2 °C.

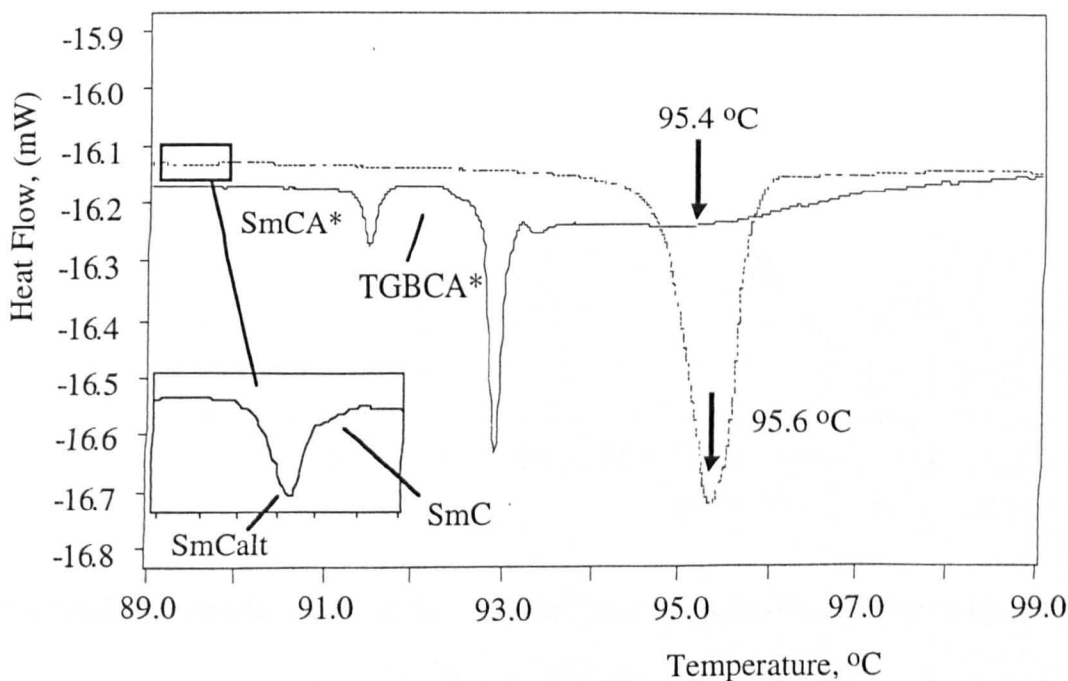


**Figure 6.2** Differential scanning thermographs obtained on cooling for the (*S*)-enantiomer, **76** (solid lines) and its racemic modification (dotted lines), the scan rate was 2 °C min<sup>-1</sup>.

The enantiomer, solid line in Figure 6.2, shows strong pretransitional effects in the isotropic liquid just before the transition to the TGB phase. At a scan rate of 10 °C min<sup>-1</sup>

these effects become more pronounced as shown in Figure 6.3. A distinct depression appears which has a minimum at roughly the same temperature as the smectic A phase is formed from the isotropic liquid for the racemate. Transitional effects in the isotropic liquid are typical for systems that are about to form TGB phases and are associated with entangled or disentangled flux phases, *i.e.* the amorphous liquid has some long range order associated with it [15]. The transition to the TGB phase is *strongly first order*, but the associated enthalpy is much lower than that obtained for the clearing point of the racemate. However, the enthalpy for the isotropic liquid to smectic A transition is approximately equal to the sum of the enthalpies associated with the pretransitional effect in the liquid and the isotropic liquid to TGB phase of the enantiomer [1, 4].

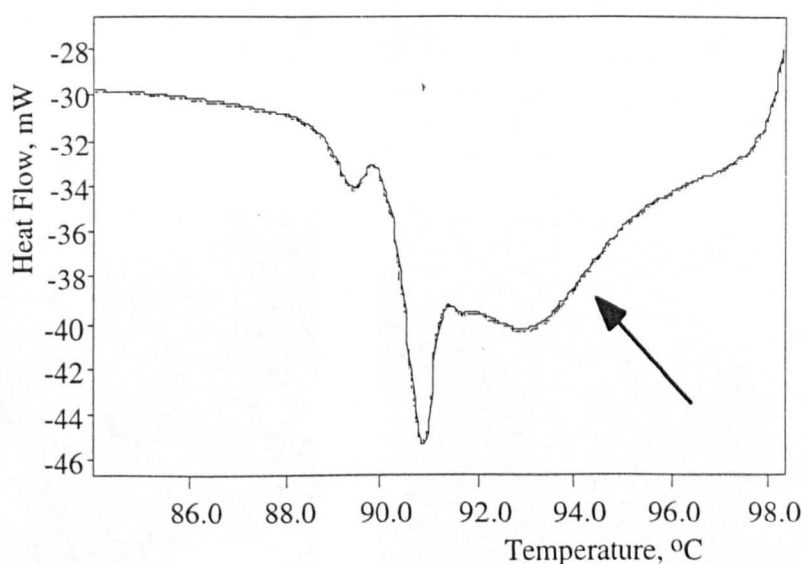


**Figure 6.3** Differential scanning thermograph (enlargement) obtained on cooling for the (*S*)-enantiomer, **76**, the scan rate was  $10\text{ }^{\circ}\text{C min}^{-1}$ .

### Defect Textures

Homogenous, homeotropic, uncovered droplets, and free-standing film specimens of the chiral compound **76** were examined by thermal polarized light microscopy. The phase first formed from the isotropic liquid was iridescent and clearly helical. The phase did not exhibit either a focal-conic, platelet or *schlieren* defect texture, and was

not typical of a TGBA\* or TGBC/C\* phase. Figure 6.4a shows an uncovered film of the phase supported on cleaned glass. An apparent *schlieren* texture is observed, but on closer examination this texture shows some features associated with a focal-conic pattern. At lower temperatures the transition to and from the smectic C\*A phase was characterised with the formation of filaments typical of a TGB phase, see figure 6.4c [14].

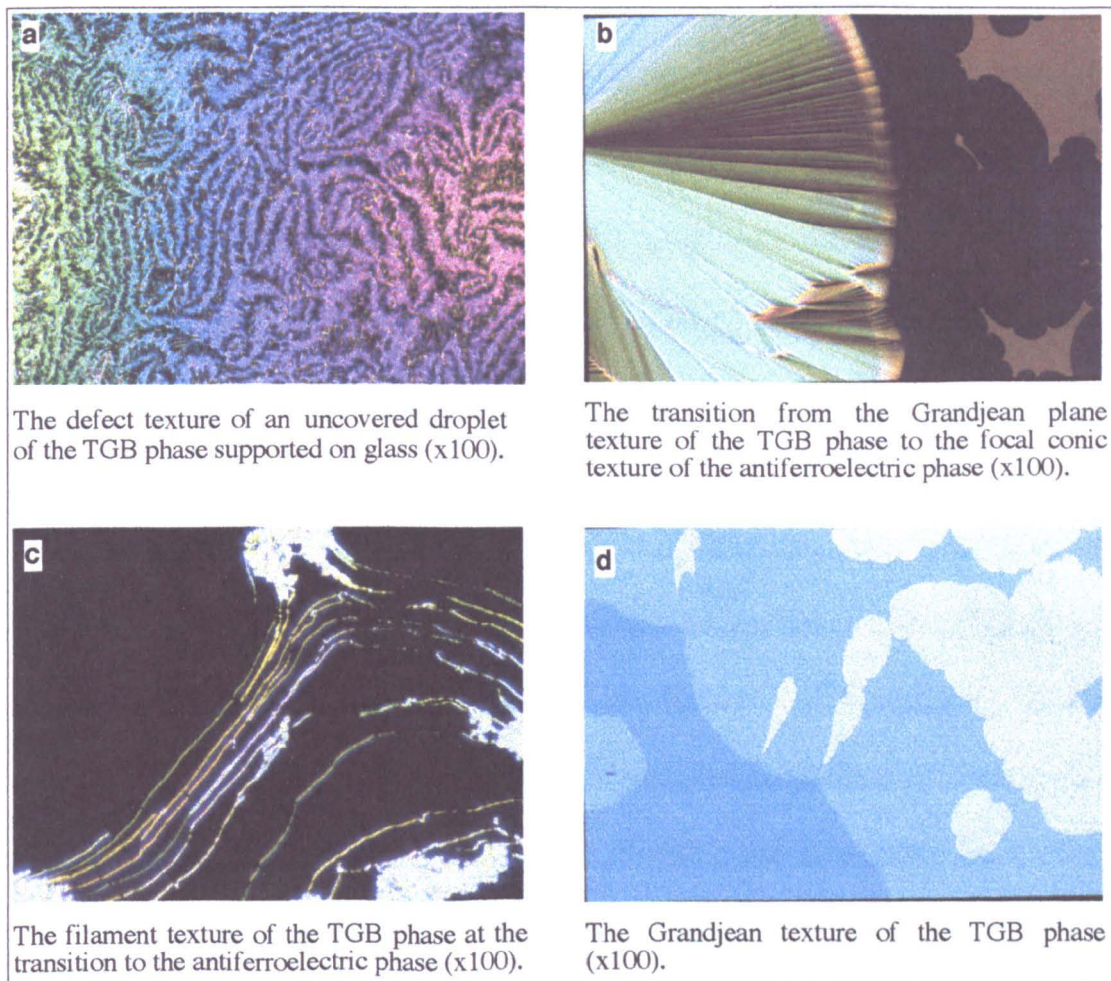


**Figure 6.4** Various textures observed for compound 76

A Grandjean planar texture, typical of a helical phase was obtained in a homogeneously aligned cell with a *ca.* 5  $\mu\text{m}$  spacing that had been antiparallel-buffed, see figure 6.4d. The platelet areas are associated with domains that have differing numbers of twists of the helical macrostructure associated with them. The fact that the heli-axis is normal to

the glass substrates of the cell indicates that the twist is in the direction of the planes of the layers, *i.e.* typical of a TGB phase.

The presence of filaments and a heli-axis in the plane of the layers confirm that the phase formed first on cooling the isotropic liquid of the racemate is a twist grain boundary phase, however, the lack of a characteristic texture suggested that the phase was not of the type characterised so far.

Figure 6.4b shows a transition from the Grandjean texture of the TGB phase to the focal-conic texture of the antiferroelectric smectic C\*<sub>A</sub> phase. The formation of a homogeneous focal-conic texture from a planar Grandjean texture indicates movement of the optic axis through 90° and confirms that the heli-axis is in the planes of the layers in the TGB phase.

Comparing the results obtained for the racemic modification with those for the (*S*)-enantiomer yields some interesting and contrasting observations. The mesophase formed first on cooling the isotropic liquid of the racemic modification exhibits a focal-conic texture that is characterised by its elliptical and hyperbolic lines of optical discontinuity, and a homeotropic optically extinct texture. The presence of these defect textures characterises the mesophase as smectic A. Subsequent cooling leads to the homeotropic areas becoming *schlieren* (see figure 6.5a), and the focal-conic domains becoming broken, both of these textures are characteristic of the formation of a smectic C phase. As the temperature is lowered there is the formation of a third phase, again characterised by the presence of a *schlieren* texture (see figure 6.5b), but this time the focal-conic domains are not as broken as they were in the smectic C phase. These observations are in keeping with the third phase being an *anticlinic* smectic C<sub>Alt</sub> phase,

where the tilt directions of the molecules alternate on passing from one layer to the next, *ie* the tilt direction rotates through an angle of  $180^\circ$  on passing from one layer to another. Thus the racemate appears to exhibit a SmA, SmC, SmC<sub>Alt</sub> phase sequence, whereas the (*S*)-enantiomer exhibits a TGB and SmC<sub>A</sub>\* sequence.

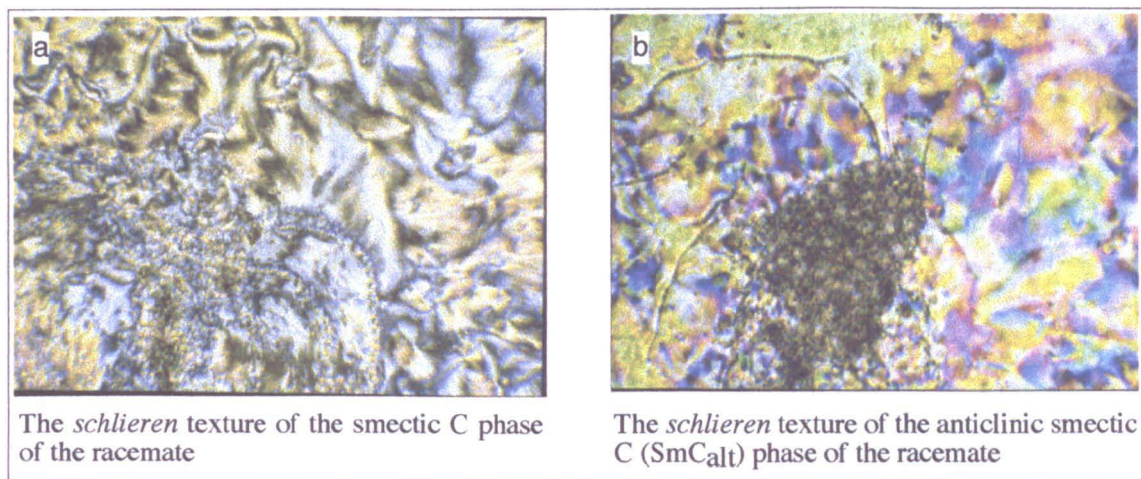


**Figure 6.5** Textures observed for racemic modification of compound **76**

The effect of increasing the optical purity of the system is to suppress the formation of the smectic A\* and smectic C\* phases to the benefit of the antiferroelectric SmC\* phase and the introduction of a frustrated TGB phase. This clearly demonstrates that the phase transitions and the transition temperatures are chirality dependent. The effects of chirality on the phase transitions are equally clearly demonstrated by calorimetry.

### 6.5 Miscibility Studies

A miscibility phase diagram was constructed for binary mixtures of the racemate and the (*S*)-enantiomer **76** thereby giving the phase transition temperatures as a function of optical purity. Binary mixtures were prepared by weighing out each of the components onto a glass slide, heating them until they were in their liquid states, then mixing them with a spatula tip and placing a cover-slip over the resulting liquid. The transition temperatures for each binary mixture were then determined by thermal polarized light microscopy.

Figure 6.6 shows the transition temperatures of the various binary mixtures as a function of concentration. It can be seen that as the optical purity is increased the smectic A\* and smectic C\* phases are suppressed, and the antiferroelectric smectic C\* phase becomes relatively stabilised. Part of the way across the phase diagram, at about 75% of the racemate in the mixture, a TGB phase is introduced. The defect textures exhibited by this TGB phase are indicative of it being a TGBA\* modification (figure 6.6) [1, 4].

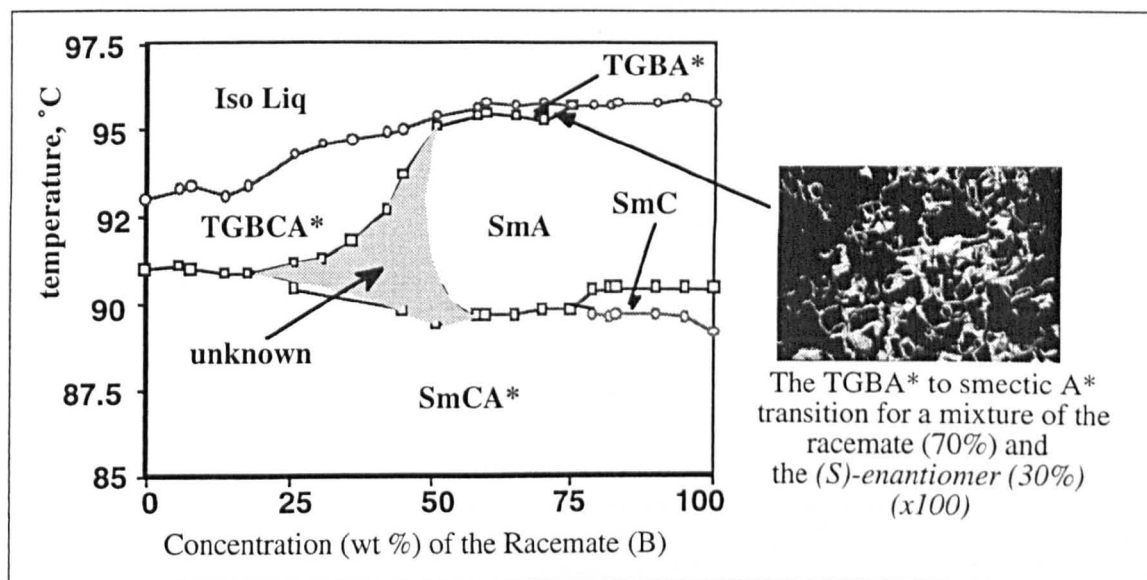


**Figure 6.6** Binary phase diagram, as a function of concentration (wt %) and temperature (°C), between the (*S*)-enantiomer, **76**, A and its racemate, B.

It can also be seen from Figure 6.6 that the temperature range of the TGB phase widens considerably when the (*S*)-enantiomer is in an excess of greater than 50%. Electrical field studies indicate that at this point the nature of the TGB phase changes from TGBA\* to TGBCA\*. However, no phase transition from one TGB phase to the other was detected, which might be due to the sharpness of the cross-over from one modification to the other.

## 6.6 Electrical Field Studies

The spontaneous polarization in the antiferroelectric phase of compound **76** was determined, as a function of the reduced temperature from the Curie point, using the triangular wave techniques described earlier. It should be noted that the measurement of the spontaneous polarization in an antiferroelectric phase is an artefact of the current flow reversal for switching between the two ferroelectric fully switched states, *i.e.* it is the sum over the double hysteresis loop.

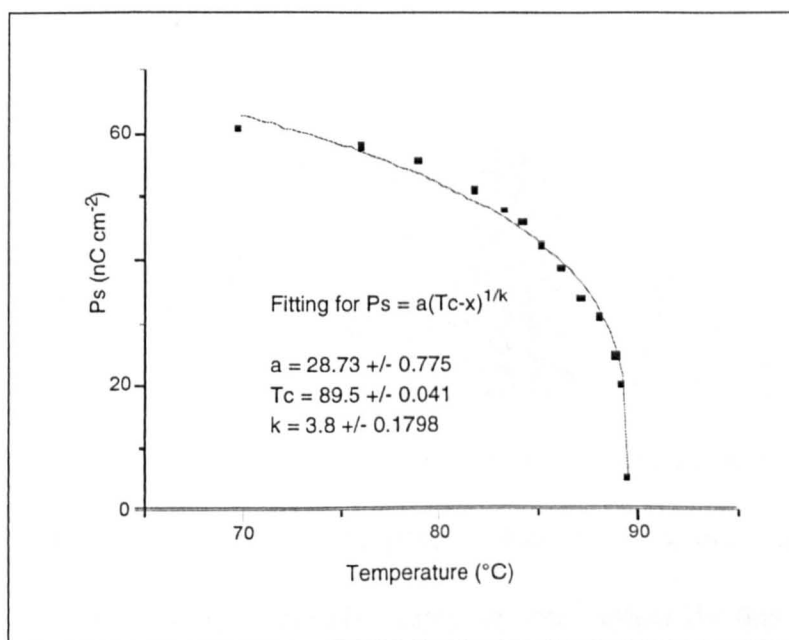


**Figure 6.7** The spontaneous polarization ( $\text{nC cm}^{-2}$ ) measured as a function of the reduced ( $\Delta T = T - T_C$ ) temperature for compound **76**.

Figure 6.7 shows that the polarization rises from a low value at the Curie point to give a saturated value of approximately  $60 \text{ nC cm}^{-2}$  at a reduced temperature of  $20 \text{ }^\circ\text{C}$ . Thus, for an antiferroelectric material with a structure based on the 1-methylheptyl moiety the spontaneous polarization is relatively low.

Examination of the current flow as a function of temperature and time, see Figure 6.8, shows that as the material is switched from one stable ferroelectric state to the other two

separate events occur which correspond to switching from one ferroelectric state to the antiferroelectric state and on to the other ferroelectric state.

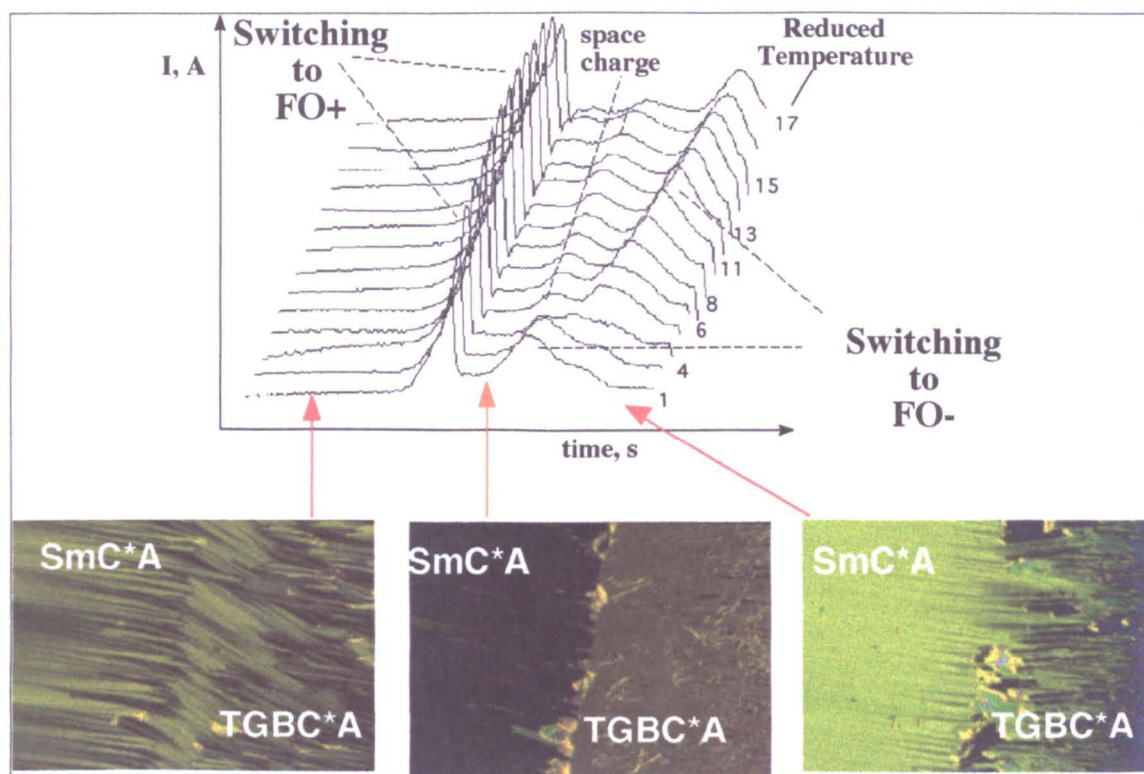


**Figure 6.8** The time (s) current trace as a function of the reduced temperature ( $\Delta T = T - T_C$ ) from the TGB to antiferroelectric phase transition using the triangular wave method. The movement of space charge is clearly seen and isolated by this technique.

As the temperature is reduced so the antiferroelectric state becomes more stable, which is probably reflected in a higher viscosity. At the transition to the TGB phase there is no appreciable change in the switching process indicating that the phase formed from the TGB phase on cooling is indeed antiferroelectric, thereby confirming the observations made from the miscibility studies, *i.e.* that compound **76** does not exhibit either a smectic A\* or smectic C\* phase which correspond to the achiral phases of the racemate.

During the switching processes samples of compound **76** were observed in the microscope. The photomicrographs in figure 6.8 show remarkable behaviour at the TGB to antiferroelectric phase transition under the application of the external electric

field. In the three plates the antiferroelectric phase is on the right-hand side and the TGB phase on the left. As the field is reversed the dark stable ferroelectric state (picture on the left) passes through an intermediary stable state corresponding to the antiferroelectric phase, photograph in the middle, before reaching the second stable, light ferroelectric state, shown in the picture on the right. The TGB phase can also be seen to follow the same switching pattern indicating that it too has a bulk antiferroelectric structure.

It is also interesting to note the events that take place prior to, and during, the switching of the TGB phase. When the cell is filled from the isotropic liquid the homogeneous alignment causes the formation of a helical macrostructure, associated with the TGB phase, perpendicular to the glass substrates. As the field is applied the helix unwinds to give a bookshelf-like geometry, as the field is increased a helix, associated with an antiferroelectric phase, now forms perpendicular to the layers and parallel to the planes of the glass substrates. Increasing the field induces this phase to unwind to give a stable unwound antiferroelectric phase, which as the field is increased gives way to a stable switched ferroelectric phase.

### **The model**

We have shown via a number of techniques that (*S*)-1-methylheptyl 2-[4-(4'-dodecyloxybenzoyloxy)phenyl]-pyrimidine-5-carboxylate, **76**, exhibits a TGB - antiferroelectric smectic  $C_A^*$  phase sequence on cooling from the isotropic liquid. The character and structure of the TGB phase is interesting because the phase shows three state switching and novel defect textures which indicate that it has a local antiferroelectric structure. This means that the mesophase will be composed of a layered structure that will be punctuated with a lattice of screw dislocations. The screw

dislocations will induce a twist of sheets or blocks of the phase about an axis parallel to the layers of the phase. Between the screw dislocations the molecules will be tilted in layers with the tilt directions rotating through  $180^\circ$  on passing from one layer to the next, as in an antiferroelectric phase. A cartoon of the proposed structure of this new and interesting state of matter is shown in Figure 6.9.

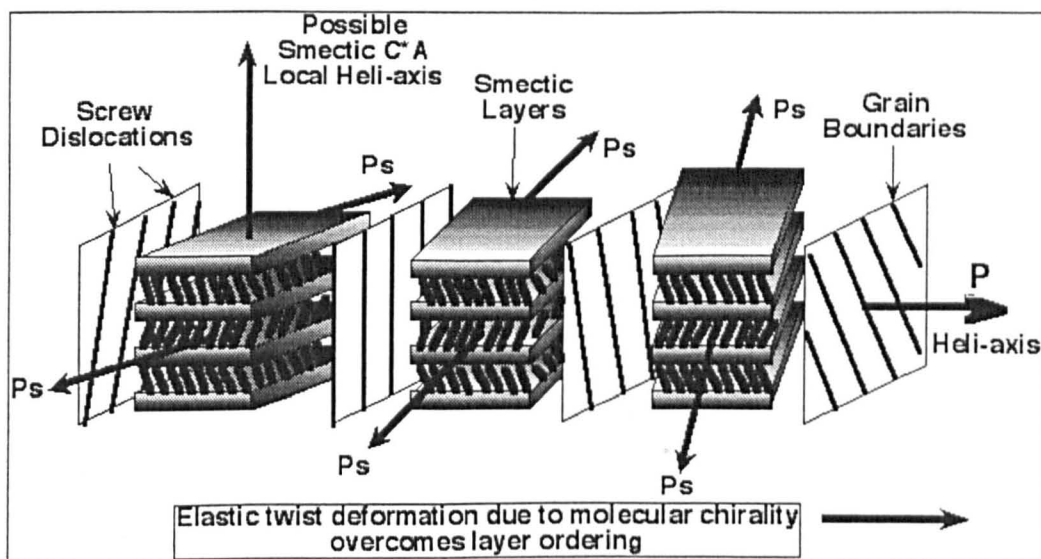


**Figure 6.9** Proposed structure of the TGB phase with local antiferroelectric structure

This model has two possible variations, one where the interlayer twist of the normal antiferroelectric phase is expelled to the dislocations in the TGB phase, and one where there is a twist perpendicular to the layers and to the in-plane heli-axis of the TGB phase. For the situation where the interlayer twist is expelled to the screw dislocations, the polarization vector can lie either perpendicular or parallel to the heli-axis. The way in which the helix of the TGB phase reorients in the electrical field studies suggests that the polarization vector is probably perpendicular to the in-plane twist, much as it is in the TGBC phase [16, 17]. Though the recent studies on the issue may prove otherwise [18]. Finally we note that the commensurability/incommensurability of the in-plane twist cannot be gauged from these studies. Further investigations using x-ray diffraction may be able to elucidate these possibilities.

## 6.8 References (section 6)

1. JW Goodby, MA Waugh, SM Stein, E Chin, R Pindak and JS Patel, *Nature*, 1989, **337**, 449.
2. P de Gennes, *Sol State Commun*, 1972, **10**, 753.
3. SR Renn and TC Lubensky, *Phys Rev A*, 1988, **38**, 2132.
4. JW Goodby, MA Waugh, SM Stein, E Chin, R Pindak and JS Patel, *J Am Chem Soc*, 1989, **111**, 8119.
5. AJ Slaney and JW Goodby, *J Mater Chem*, 1991, **1**, 5.
6. AJ Slaney and JW Goodby, *Liq Cryst*, 1991, **9**, 849.
7. A Bouchta, HT Nguyen, MF Achard, F Hordouin, C Destrade, RJ Tweig, A Maaroufi and N Isaert, *Liq Cryst*, 1992, **12**, 575.
8. AC Rose-Innes and EH Rhoderick, "Introduction to Superconductivity", Oxford: Pergamon, 1969
9. G Strajer, R Pindak, MA Waugh, JW Goodby and JS Patel, *Phys Rev Lett*, 1990, **64**, 1545.
10. L Navailles, P Barois and HT Nguyen, *Phys Rev Lett*, 1993, **71**, 545; L Navailles, R. Pindak, P Barois and HT Nguyen, *Phys Rev Lett*, 1995, **74**, 5224; L Navailles, P Barois and HT Nguyen, *Phys Rev Lett*, 1994, **72**, 1300.
11. K Takatoh, AGM Lamb and JW Goodby, unpublished results.
12. PA Pramod, R Pratibha and NV Madhusudana, *Current Sci*, 1997, **73**, 761.
13. JW Goodby, I Nishiyama, AJ Slaney, CJ Booth and KJ Toyne, *Liq Cryst*, 1993, **14**, 37.
14. JM Gilli and Kamayé, *Liq Cryst*, 1992, **12**, 545.
15. JW Goodby, DA Dunmur and PJ Collings, *Liq Cryst*, 1995, **19**, 703.
16. SR Renn and TC Lubensky, *Mol Cryst Liq Cryst*, 1991, **209**, 349; SR Renn, *Phys Rev A*, 1992, **45**, 953.
17. M Petit, P Barois and HT Nguyen, *Europhys Lett*, 1996, **36**, 185.
18. JG Meier, P Rudquist, AS Petrenko, JW Goodby and ST Lagerwall, *Liq Cryst*, 2002, **29**, 17

## 7 Conclusions

During the last decade the families of tilted smectic phases were significantly extended by discovery of the antiferroelectric and similar SmC type phases. Most of these phases are of practical interest because they show unique optical behaviour under the application of electric fields. Their speed of switching allows them to be used in advanced liquid crystal display technologies. Potential applications as well as theoretical studies of antiferroelectricity in liquid crystals set a high demand for preparation of new materials.

The objective of this work was to investigate the effect of the structural modifications in series of chiral 1-methylheptyl 4'-(4-n-alkyloxybenzoyloxy)biphenyl-4-carboxylates, on the thermal stability of the smectic C\* phases, especially the antiferroelectric SmC<sub>A</sub>\* phase, and other chirality induced frustrated phases. Nine new homologous series of chiral liquid crystalline compounds were synthesised. Their mesomorphic properties were studied through the differential scanning calorimetry method, textural observations in optical microscope, and the triangular wave field method. The stability of the antiferroelectric SmC<sub>A</sub>\* phase was evaluated in different series of compounds and conclusions were made regarding the structure-mesomorphic property relations.

For selected homologues the phenomenon of the V-shaped electrooptical switching was observed at low frequency fields. It was shown that the V-shaped response could be simulated in the surface-stabilised geometry in the ferroelectric SmC\* phase for any material that was prepared in the course of this work. Based on the extensive analysis of the literature data the model for molecular re-orientation during the V-shaped response in a thin homogeneous alignment was proposed.

One of the homologues in series of (*S*)-1-methylheptyl 2-[4-(4-*n*-alkyloxybenzoyloxy phenyl) pyrimidine-5-carboxylates was found to exhibit the new type of the Twist Grain Boundary (TGB) phase. Through miscibility studies, investigation of defect textures, differential scanning calorimetry and electrical field studies it was concluded that (*S*)-1-methylheptyl 2-[4-(4-dodecyloxybenzoyloxyphenyl) pyrimidine-5-carboxylate exhibits an antiferroelectric twist grain boundary TGBC<sub>A</sub>\* phase.